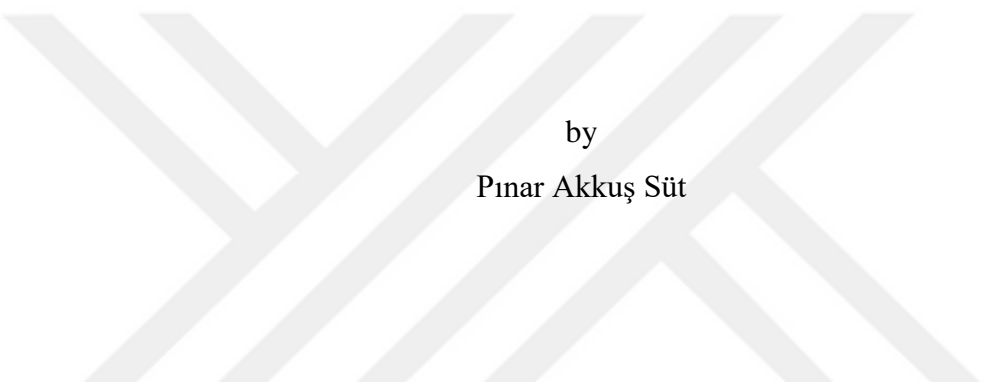DEVELOPMENT OF DNA ORIGAMI BASED NANOCARRIERS

by
Pınar Akkuş Süt

Submitted to Graduate School of Natural and Applied Sciences
in Partial Fulfillment of the Requirements
for the Degree of Doctor of Philosophy in
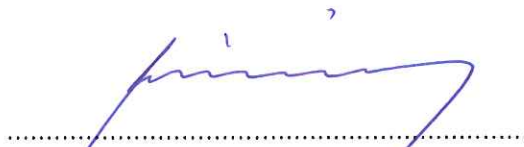Biotechnology

Yeditepe University
2018

DEVELOPMENT OF DNA ORIGAMI BASED NANOCARRIERS

APPROVED BY:

Prof. Dr. Mustafa Çulha ....
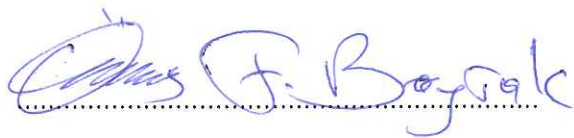(Thesis Supervisor)

Assoc. Prof. Dr. Bunyemin Çoşut ....

Assoc. Prof. Dr. Kaan Keçeci ....

Assoc. Prof. Dr. Ömer Faruk Bayrak ....

Assist. Prof. Dr. Andrew Harvey ....

DATE OF APPROVAL: ..../..../2018

ACKNOWLEDGEMENTS

I would like to express my deepest respect and gratitude to my supervisor Prof. Mustafa Çulha for his material and spiritual supports with his guidance. He is my second chance who revived me and provided to work on better conditions in my academic life.

I would like to express my gratitude to Şaban Kalay and his esteemed wife, Betül, who provided to meet with Prof. Dr. Mustafa Çulha and made a great contribution in the beginning of the new part of my life.

Andrew Harvey and Omer Faruk Bayrak, two precious members of the thesis monitoring jury... I would like to thank Andrew Harvey and Ömer Faruk Bayrak for their contributions during my thesis.

I would like to thank people who contributed my theoretical and experimental scientific progress throughout this process.

I would like to acknowledge TUBITAK for financial support during my PhD study.

My family, which is the only real thing I will not doubt of sincerity and love ...

ABSTRACT

DEVELOPMENT OF DNA ORIGAMI BASED NANOCARRIERS

Deoxyribonucleic acid (DNA), a biomacromolecule that contains genetic information, can be used as a building material to construct novel structures by taking advantage of the specific pairing property between its bases. This field, called DNA nanotechnology, refers to the preparation of variety of functional materials at nanoscale by using the structural properties of DNA. In this thesis, it was aimed to develop a new DNA based nanovehicle, DNA tile, which can be used in the treatment of cancer and similar diseases, using the DNA nanotechnology concept. DNA tile structure was designed to have sticky sequences that can be hybridized to their complementary sequences. Prepared DNA structure was characterized using agarose gel electrophoresis, atomic force microscopy (AFM) and dynamic light scattering (DLS) analyses. The complementary oligonucleotides were functionalized with targeting molecules including lactose, folic acid, and RGD peptide to allow enhanced the cellular uptake of DNA tile. The DNA tile structure synthesized by the DNA origami approach was used for the drug and gene delivery applications using different cell lines. Doxorubicin, chemotherapy drug, was loaded into the DNA tile efficiently. The cellular uptake of nonfunctionalized and functionalized DNA tiles with targeting agents was compared and it was found that targeting molecules greatly increased the cellular uptake of DNA tiles. The greatest uptake effect was seen with lactose modification. Breast cancer cell line, which expresses luciferase, was prepared and used in gene silencing studies. The DNA tile containing the morpholino sequence, which was designed for specific to mRNA of firefly luciferase to silence the luciferase expression, was prepared. It was found that the transferred morpholino decreased the expression level of luciferase indicating that DNA tile successfully delivered the morpholino into the cells. Lactose was found to be more effective as a targeting molecule for the delivery of studied therapeutics. The results obtained from *in vitro* studies have shown that DNA tile structures are suitable nano-structures for the transport of drugs and possibly other therapeutics.

ÖZET

DNA ORİGAMİ TABANLI NANOTAŞIYICILARIN GELİŞTİRİLMESİ

Genetik bilginin saklandığı biyomakromolekül olan deoksiribonükleik asit, bazları arasındaki spesifik eşleşme özelliğinden faydalanılarak, bir yapı malzemesi olarak yeni yapıların tasarlanması ve hazırlanmasında kullanılabilmektedir. DNA nanoteknoloji olarak isimlendirilen bu alan, DNA'nın yapısal özelliklerinin kullanılmasıyla nano ölçekte birçok fonksiyonel malzeme ve yapının hazırlanmasını ifade etmektedir. Bu tez çalışmasında DNA nanoteknoloji kullanılarak kanser ve benzeri hastalıkların tedavisinde kullanılabilecek yeni bir nanotaşıyıcı sistemin, DNA karo yapısının geliştirilmesi amaçlanmıştır. DNA karo yapıları, kendilerine eşlenik oligonükleotidlerle hibritleşebilecek yapışkan uç dizilimlerine sahip olacak şekilde tasarlanmıştır. Eşlenik oligonükleotidler seçimli moleküler hedefleme ve hücresel alıma imkan veren laktoz, folik asit ve RGD peptit gibi moleküller kullanılarak işlevselleştirilmiştir. Hazırlanan DNA karo yapısı agaroz jel elektroforezi, atomik güç mikroskopu ve dinamik ışık saçılması kullanılarak karakterize edilmiştir. DNA origami yaklaşımıyla sentezlenen DNA yapılarının, ilaç taşınması ile gen susturma uygulamalarındaki kullanımı farklı hücre hatlarının kullanımıyla araştırılmıştır. Kemoterapi uygulamalarında yaygın olarak kullanılan doksorubisin, DNA karo yapısına interkalasyon ile etkin bir şekilde yüklenmiştir. Hedefleme araçlarıyla işlevselleştirilmemiş ve işlevselleştirilmiş ilaç yüklü DNA karo yapılarının hücresel alımları kıyaslanmıştır. Hedefleme moleküllerinin DNA karo yapılarının hücresel alımını büyük ölçüde arttırdığı ve en büyük etkiyi laktozun sağladığı gözlenmiştir. Gen susturma çalışmalarında kullanılması planlanan lusiferaz eksprese eden hücre hattı hazırlanmıştır. Lusiferaz anlatımını susturmak için tasarlanan lusiferaz mRNA'sına spesifik antisens morfolino dizisi içeren DNA tile yapısı hazırlanarak, lusiferaz proteininin anlatımı üzerine etkisi araştırılmış ve morfolino içeren işlevselleştirilmiş DNA karo yapısının morfolinoyu hücre içine taşıdığı ve lusiferaz anlatımını azalttığı gözlenmiştir. Hedefleme molekülleri içerisinde laktozun yine gen susturmada daha etkili olduğu bulunmuştur. *In vitro* çalışmalardan elde edilen sonuçlar, DNA karo yapılarının ilaç vb terapötiklerin taşınması için uygun nano yapılar olduğunu ortaya koymuştur.

TABLE OF CONTENTS

LIST OF FIGURES

LIST OF TABLES

LIST OF SYMBOLS/ABBREVIATIONS

mg	Milligram
ml	Milliliter
nm	Nanometer
AFM	Atomic force microscopy
DCC	N',N'-dicyclohexyl carbodiimide
DMEM	Dulbecco's modified Eagle medium
DMSO	Dimethyl sulfoxide
DNA	Deoxyribonucleic acid
DNA tile-Dox	Doxorubicin loaded DNA tile
DNA tile-Dox-Fol	Folic acid modified doxorubicin loaded DNA tile
DNA tile-Dox-Glu	Glucose modified doxorubicin loaded DNA tile
DNA tile-Dox-Lac	Lactose modified doxorubicin loaded DNA tile
DNA tile-Dox-Mal	Maltose modified doxorubicin loaded DNA tile
DNA tile-Dox-Man	Mannose modified doxorubicin loaded DNA tile
DNA tile-Dox-RGD	RGD peptide modified doxorubicin loaded DNA tile
Dox	Doxorubicin
EDTA	Ethylenediaminetetraacetic acid
5(6)-FAM	5(6)-carboxyfluorescein
FBS	Fetal bovine serum
FR-positive	Folate receptor positive
FT-IR	Fourier transmission infrared spectroscopy
FS	Forward scatter
GAPDH	Glyceraldehyde-3-Phosphate Dehydrogenase
MALDI-TOF MS	Matrix-assisted laser desorption (MALDI) time-offlight (TOF) mass spectrometry (MS)
MOPS	3-(N-morpholino)propanesulfonic acid
NHS	N-hydroxysuccinimide
PBS	Phosphate buffered saline
PI	Propidium Iodide

RGD	Arginine-glycine-aspartic acid
SS	Side scatter
SDS	Sodium dodecyl sulfate
T	Thymine
TAE/Mg^{2+}	Trizma base-acetic acid-ethylenediaminetetraacetic acid/magnesium acetate
TBS	Tris-buffered saline
TBS-T	Tris-buffered saline, 0.1 per cent Tween 20

1. INTRODUCTION

Drug delivery can be defined as the mechanism of administration of therapeutic agents to the body, in order to achieve a therapeutic effect in humans or other organisms. Consumption of plant roots and leaves were primitive drug intake patterns, which were approaches lacking consistency and equivalency as very basic requirements. Since the end of the 18th century, the development of different delivery mechanisms as tablets, capsules, etc. has allowed the dose control of therapeutics and these mechanisms provided that the therapeutics can show the same effects continuously. The modern pharmaceutical industry, which began with the discovery of vaccines, has continued to grow with the discovery of penicillin and the isolation of therapeutic substances from natural sources.

Today, advances in medicine and pharmacy have been improving the quality of human life. Biotechnological developments create new possibilities for the treatment of diseases. New drugs and drug carrier systems have been tried to be developed and these show opportunities for efficient therapy applications. In this sense, new materials have been developed as drug delivery vehicles and the nanotechnology concept tremendously contributes to this field. Nanomaterials are extensively used in these applications as drug delivery vehicles due to their extraordinary properties. Drug delivery systems comprising the use of different nanoparticles are shown in Figure 1.1 [1].
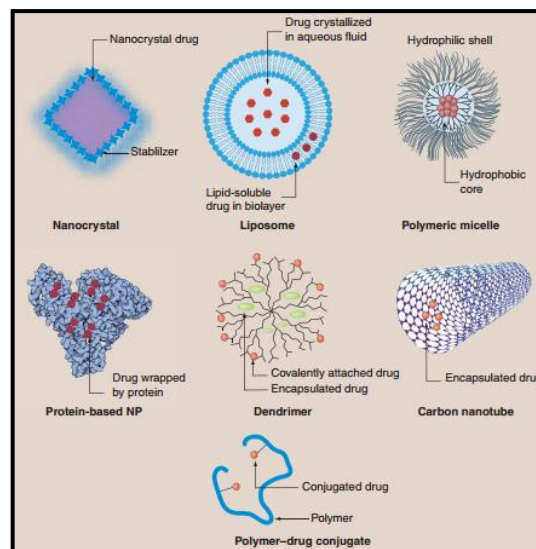
Figure 1.1. Drug delivery systems involving the use of nanoparticles [1]

For cancer treatment different nanomaterials including dendrimers, liposomes, metallic nanoparticles, etc. are being currently investigated for their use. Many of these studies, which include the nanoparticle usage with chemotherapeutics, have been revealed for the treatment of several cancers including melanoma, breast cancer, etc. Commercial nano-based drug formulations that are successful in clinical trials, and approved by the FDA, are also available [2-9]. However, some studies have reported that nanomaterials, which are intensively explored for their use in therapy applications, show some biocompatibility problems. They can affect cellular metabolisms, induce oxidative stress conditions, and cause nutrient depletion due to the absorption of nutrients and proteins.

When these adverse conditions are taken into account, biomacromolecule-based structures have begun to be studied as alternative structures in developing drug delivery applications. Especially deoxyribonucleic acid (DNA) based systems present biocompatibility, biodegradability, and non-toxic features and these properties make them good candidates for biotechnological applications. In this thesis, a DNA based drug delivery system was prepared and the efficiency of this system as a drug and gene delivery vehicle was investigated under *in vitro* conditions.

2. THEORETICAL BACKGROUND

2.1. STRUCTURE AND PROPERTIES OF DNA

DNA is a biomacromolecule containing genetic information fundamental for vital events, which occur in living organisms. The information contained in DNA is stored in the nucleotide sequence of the structure. The building units of the DNA molecule are four different nucleotides, separated by the difference in the nitrogenous organic bases they contain. Each nucleotide consists of a five-carbon sugar, a nitrogenous organic base, and phosphate groups. DNA molecule composed of two long polynucleotide chains containing these four types of nucleotides (Figure 2.1). Hydrogen bonds between the DNA bases, located in different strands, stabilize these two polynucleotide chains together [10].
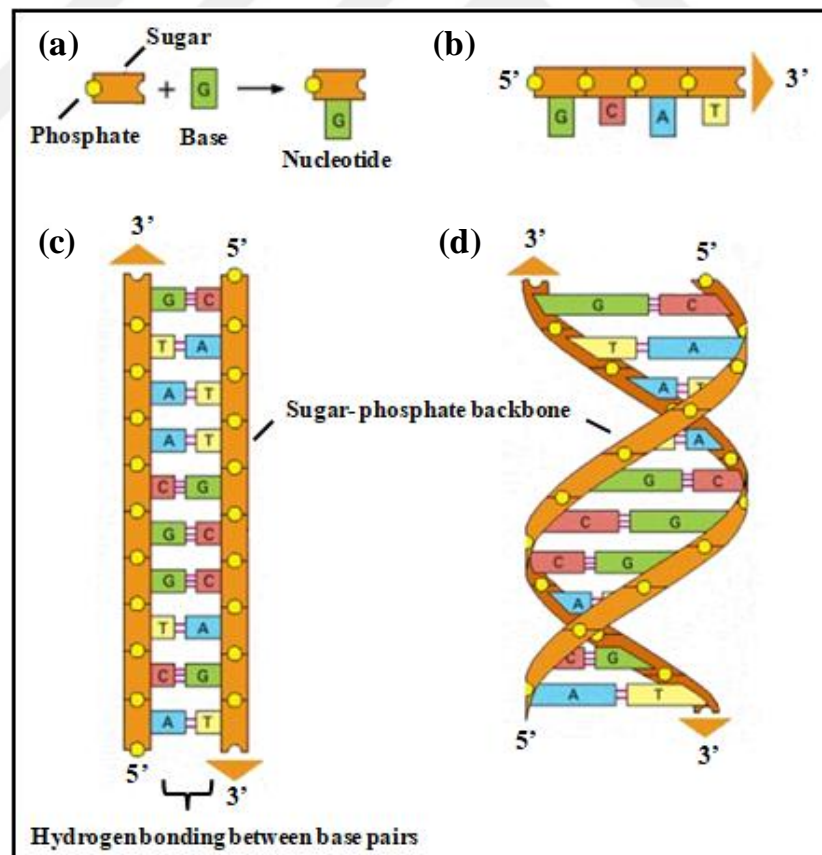
Figure 2.1. Structure of DNA. (a) Components of the DNA structure, (b) DNA strand, (c) arrangement of the polynucleotide chains, and (d) helix formation [10].

When hydrogen bonds form between the bases of two polynucleotide chains, a purine base always pairs with a pyrimidine base. While adenine matches with thymine, guanine matches with cytosine. The three-dimensional double helix structure of DNA originates from these two polynucleotide chains.

DNA, a highly biocompatible molecule, has the flexibility and rigidity that can easily be adjusted depending on the base pairs it contains. Single-stranded DNA chains are highly flexible, while short double-stranded ones have a rigid structure. It is not possible to construct complex nanostructures using linear DNA strands alone. Special structures can be formed when the single and double-stranded DNA chains are used together. DNA molecules have the ability to be modified at different points.

Adenine-thymine and guanine-cytosine Watson-Crick hydrogen bonding allows the programming of artificial DNAs [11]. In this sense, DNA nanotechnology, is a new technology that aims for the preparation of new nanostructures through DNA hybridization. DNA material science, which is related to structural DNA nanotechnology is a rapidly developing research area. Using DNA and its structural features, many functionalized materials and structures at nanoscale can be prepared. Thus, DNA is introduced as a building material into materials science.

2.2. DNA NANOTECHOLOGY AND DNA ORIGAMI APPROACH

DNA origami approach, which was pioneered by Paul Rothemund, allows for the preparation of many 2D and 3D DNA constructs [12, 13]. In fact, the foundations of this approach extend back to the work of Nadrian Seeman in the 1980s. Nadrian Seeman, who was inspired by the Holliday junction, suggested that different DNA constructs could be generated using the immobile branched junction DNA motifs. He created various DNA constructs such as cube, pentagonal dodecahedron using DNA motifs, for instance, double and triple crossover [14-17]. The Holliday junction structure, a guiding spirit of Seeman, and DNA motifs used in the construction of different DNA structures are shown in Figure 2.2.
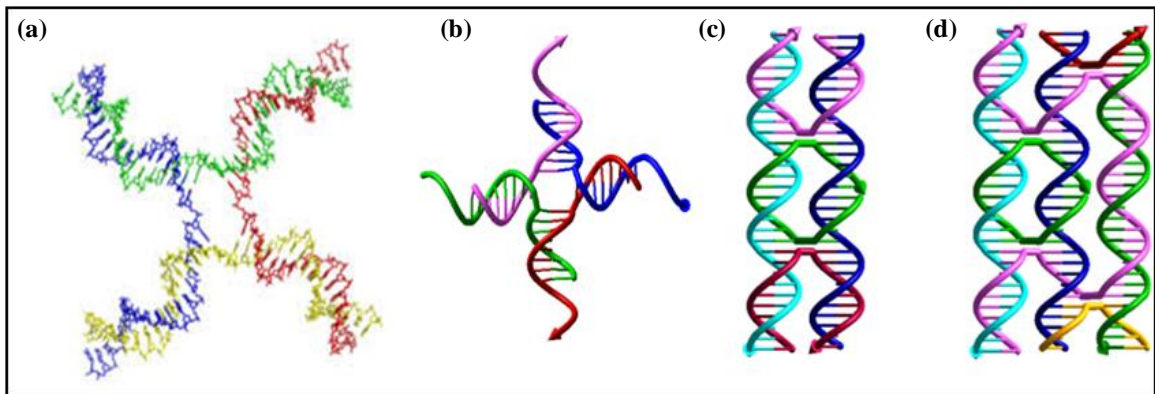
Figure 2.2. Holliday junction structure (a) and DNA motifs used in the construction of different DNA structures (b) sticky end containing four-arm junction, (**c**) double crossover, and (d) triple crossover [18].

Day by day, this approach gained importance and complex structures which are synthesized using this approach have been increased [19]. The first 2D DNA structure was designed by Winfree et al. using DNA tiles [20]. In 1999, the first discrete 3D structures were reported by Seeman [21].

Until the work of Paul Rothemund, DNA tiles and other motifs such as DNA triangles have been used for the preparation of DNA nanostructures. The studies, which could be regarded as the earliest examples of pre-Rothemund DNA origami techniques, were carried out by Yan et.al and Shih et al in 2003 and 2004 [22, 23]. In the first study, Yan et. al. reported the formation of nano-arrays using long scaffolds and short helper chains [23]. In the second study performed by Shih et.al., the formation of an octahedron DNA structure using a few small DNA chains and a heavy DNA chain was reported [22].

The DNA origami technique, which was inspired from the Japanese paper folding art origami and forming of desired shaped and sized DNA structures through the folding of long M13 viral single-stranded DNA with the help of short helper DNA strands, was performed firstly by Paul W.K. Rothemund in 2006 [13]. The formation of DNA origami and the best known examples of this approach are shown in Figure 2.3. In his first studies, Rothemund created the most known samples of origami technique such as smiley faces, stars, triangles and squares [13].
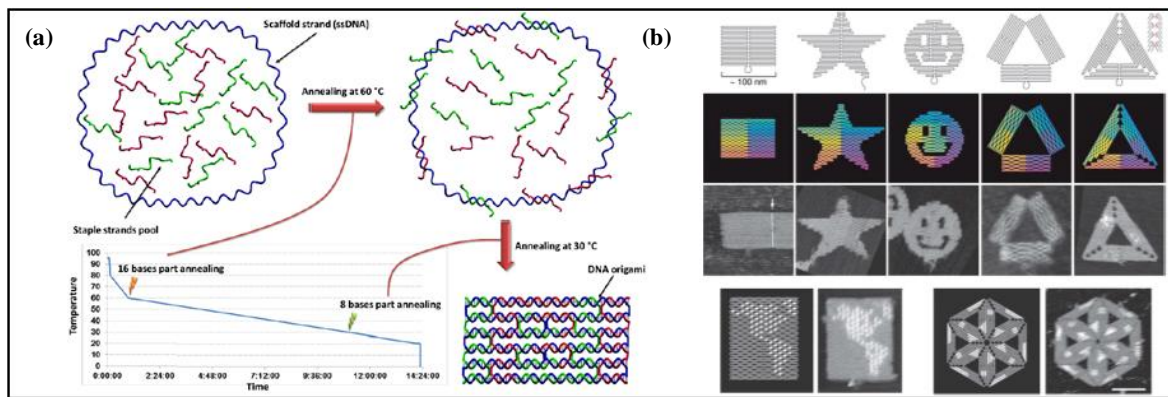
Figure 2.3. Formation of DNA origami (a) and the best known examples of DNA origami approach (b) developed by Rothemund [13, 18].

Rothemund achieved the desired constructs using small complementary DNA strands and the M13 bacteriophage genome in an appropriate buffer solution. Construction of more complex 3D structures such as tetrahedron [24], prisms [25], three-dimensional DNA box with openable lid structure [26] was realized soon afterwards.

2.3. PREPARATION OF DNA ORIGAMI STRUCTURES

DNA nanostructures can be constructed using a variety of methods such as a scaffolded approach and a multi-stranded approach. [27, 28]. An older tile-based approach is preferred for smaller and simpler structures, and repeated tile-like units are also used for the formation of desired structure. The application of the scaffolded approach is more accurate in the formation of larger and more complex structures.

In the multi-stranded approach, using short-oligonucleotides, which are complementary to each other at various points, can hybridize and hybridization provides the creation of desired DNA structure. The oligonucleotides used in equivalent stoichiometry in a buffer solution, previously heated and then cooled slowly, and the desired DNA structure can be formed. This approach has disadvantages due to the low percentage of product yield depending on the experimental error, the necessity of extra purification steps, the limited occurrence of the structures that can be obtained and the necessity of providing well-adjusted oligonucleotide concentrations [27].

In a scaffolded approach [13], several short-oligonucleotides, which are complementary to a scaffold strain at various points, hybridize to the scaffold strain and hybridization provides the creation of the desired DNA structure. Hybridization of the oligonucleotides gives form to the scaffold strain. This method has advantages such as high product yield, elimination of purification steps, product formation in a shorter time, and the ability to handle complex structures [28]. There is also a single stranded approach in which only a single scaffold chain is used. The approaches used in DNA origami preparation are shown in Figure 2.4.
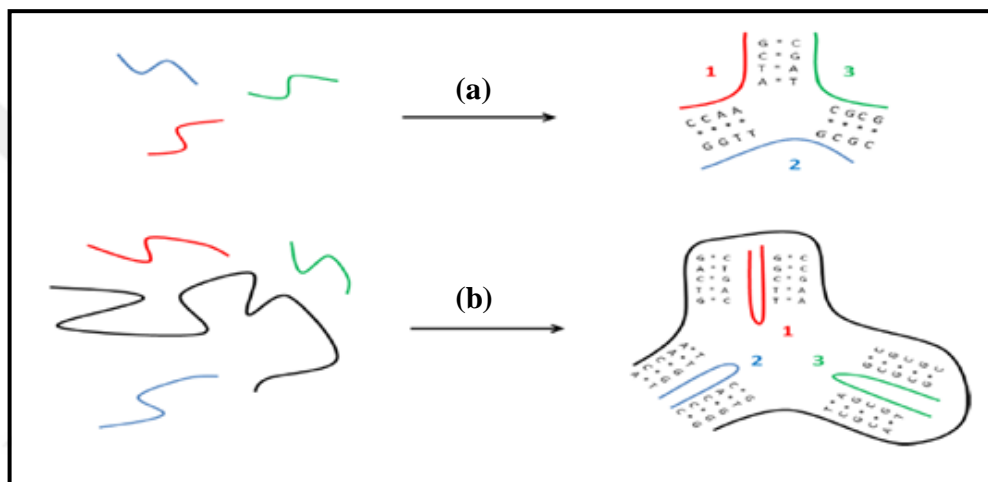
Figure 2.4. The approaches used in DNA origami preparation. (a) Multi stranded approach and (b) Scaffolded approach [27, 28].

A variety of the computer aided design tools are used to design DNA based structures and to determine the manufacturability of the designed structures. Web servers such as NUPACK [29] and MFOLD [30] and computer programs such as SEQUIN [31], UNIQUIMER-3D [32] and TIAMAT [33] serve for this purpose. Open-source software CADNAno is also one of the most preferred software because of the facilities providing to the user [34].

2.4. APPLICATIONS OF DNA ORIGAMI STRUCTURES

A DNA origami approach has been used in many different areas such as arrangement of various molecules and nanoparticles , chemo and biosensors, drug delivery systems and the preparation of nano-sized robots and carrier structures [35-44]. A DNA origami approach

is also widely used in the arrangement of organic and inorganic molecules. The idea of nanoparticle arrangement using DNA was first demonstrated by the work of Mirkin [35] and Alivisatos [44]. In the study of Mirkin, the alignment of the 13 nm diameter gold nanoparticles was carried out using oligonucleotides in a controlled manner [35]. It has been shown that different numbers of gold nanocrystals could be arranged in any desired manner by utilizing the base-pairing feature of oligonucleotides in the study of Alivisatos [44]. In the arrangement of multi-component populations of SWNT, a reactangular DNA origami was used as a template [45]. A triangular DNA origami structure, which contains sticky ends at certain points, was used for the sequential arrangement of gold nanoparticles [36]. The arrangement of 20 nm diameter AgNPs modified with ps-po chimeric DNA strands on the triangular DNA origami structure was performed in the work of Pal. [46]. The hierarchical alignment of metal nanoparticles, quantum dots, and organic dyes have also been carried out using a DNA origami approach, similar to planet-satellite organization [37]. A summary of arrangement of nanoparticles and organic dyes via DNA origami structures are demonstrated in Figure 2.5.
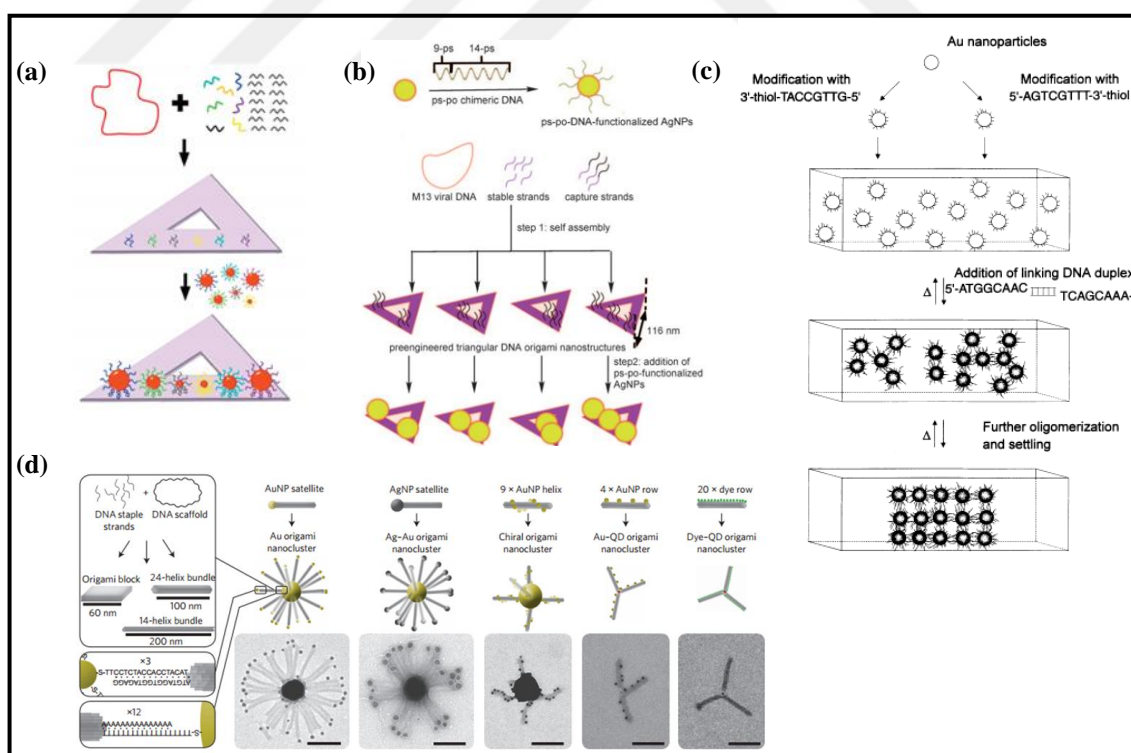
Figure 2.5. Arrangement of materials by DNA origami structures. Assembly of gold nanoparticles AuNPs (a and d), silver nanoparticles (b), and (c) metal nanoparticles, quantum dots, and organic dyes [35-38].

Beside nanoparticles, DNA origami can serve as a template for the organization of other type molecules such as streptavidin [39], proteins [40], etc. Triangular nucleic acid probes, which designed for the RNA hybridization and acted as a macroscopic DNA chip, are one of the first uses of DNA origami [39].

Nanostructures synthesized by DNA origami approach find use in drug delivery systems. The nanopill structure with DNA aptamer lock structure that can be opened in the presence of suitable antigen is one of the first examples of the DNA origami approach in drug delivery systems [47]. The use of DNA origami structures in the form of tube and triangle for the delivery of doxorubicin was studied in breast cancer cells [43]. These constructs displayed an increase in drug toxicity and helped to overcome the drug resistance in drug-resistant MCF-7 cells. Daunorubicin, an anthracycline drug such as doxorubicin, was loaded onto rod-shaped DNA origami structure and efficiency of this system on leukemia cells, which display multidrug resistance, was investigated [42]. The results of the study showed that the drug-loaded system was taken effectively into the cells and the efficiency of the drug was increased. It has been shown that DNA origami tube constructs coated with CpG oligodeoxynucleotides, which are promising molecules for immunotherapy applications, generated more immunoreactivity than the treatment performed using lipofectamine, conventional carrier system [48].

In the studies where metal nanoparticles were incorporated into the DNA origami structure, constructs with promising in terms of theranostic could be obtained. In the study of gold nanorod-DNA origami association, DNA molecules assumed the carrier role for the therapeutic molecule and the AuNPs took on different tasks at the same time. While the use of gold nanoparticles increased the cellular uptake and antitumor activity, they also enabled the cellular imaging and photo thermal therapy of tumor cells [49].

Recently, 3D DNA origami structures like containers have been reported for several researchers. The closed tehrahedron shaped container [24], DNA box with a controllable lid [26], and 3D box [50] shaped origami structures have been done (Figure 2.6). In future, these 3D origami structures will be used delivery systems for transport and release of different cargos [51].
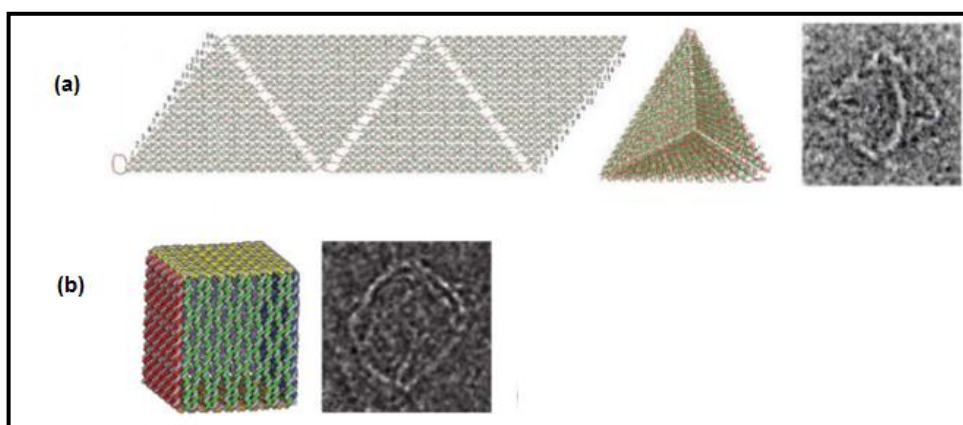
Figure 2.6. 3D DNA origami structures. (a) Tetrahedron shaped DNA origami structure, and (b) DNA origami box with a controllable lid [26, 52].

In addition to drug delivery and nanoparticle arrangements, DNA-based nanostructures were used in sensing and examining of biomolecular interactions [53-56]. The platforms prepared with DNA-based nanostructures were also used in the determination of single nucleotide polymorphism [57-60]. DNA nanoconstructs designed to exhibit conformational changes depending on the pH of the environment has also been reported [61]. It is also known that single-helix thick DNA origami tube structure was used to contribute to NMR analysis of the membrane proteins, which performed for the structure determination [62].

2.5. IMPORTANCE OF TARGETING

Properties of a drug carrier, delivery device and targeting way are critical factors for developing drug delivery systems. It is expected that an ideal drug delivery system should be non-toxic, biocompatible, stable *in vivo* and *in vitro*, allow controlled drug release, be easily prepared, and be cheap. Furthermore, the selective and specific recognition of target cells is one of the most important features expected from such a system. Targeted systems refer to systems that enable the localization of the therapeutics to the target site and limit activities of the therapeutics outside the target regions [63]. Targeting improves the treatment efficiency, decrease the side effects of drugs, and increase the quality of patient's life. The use of antibodies, growth factors, etc. molecules as targeting agents is being studied intensively in order to improve the activities of drug delivery systems [64-67]. The

target structures are generally cell proliferation markers overexpressed on tumor cell surface [68].

The idea of a targeted drug delivery system was put forward by Paul Ehrlich, a German biochemist who received the Nobel Prize in 1908, and introduced the "magic bullet" concept into the literature. In his first study, Paul Ehrlich was inspired by the selective activity of the drug "Salvarsan" used in the treatment of syphilis [69].

Active and passive targeting are two main targeting strategies applied in drug delivery systems [70] (Figure 2.7). There are also physical targeting methods that allow the drug-loaded carrier system to reach the desired site depending on the change of environmental factors such as temperature, pH, electric field and ionic strength. Acidic environment exhibited by tumor cells also contributes to the development of different strategies for providing the selectivity of the drug carrier system [71-73]. Applications such as intraperitoneal and intravesical injections that allow the therapeutic agent to be administered directly to cancer cells without systemic circulation are also a passive targeting strategy.
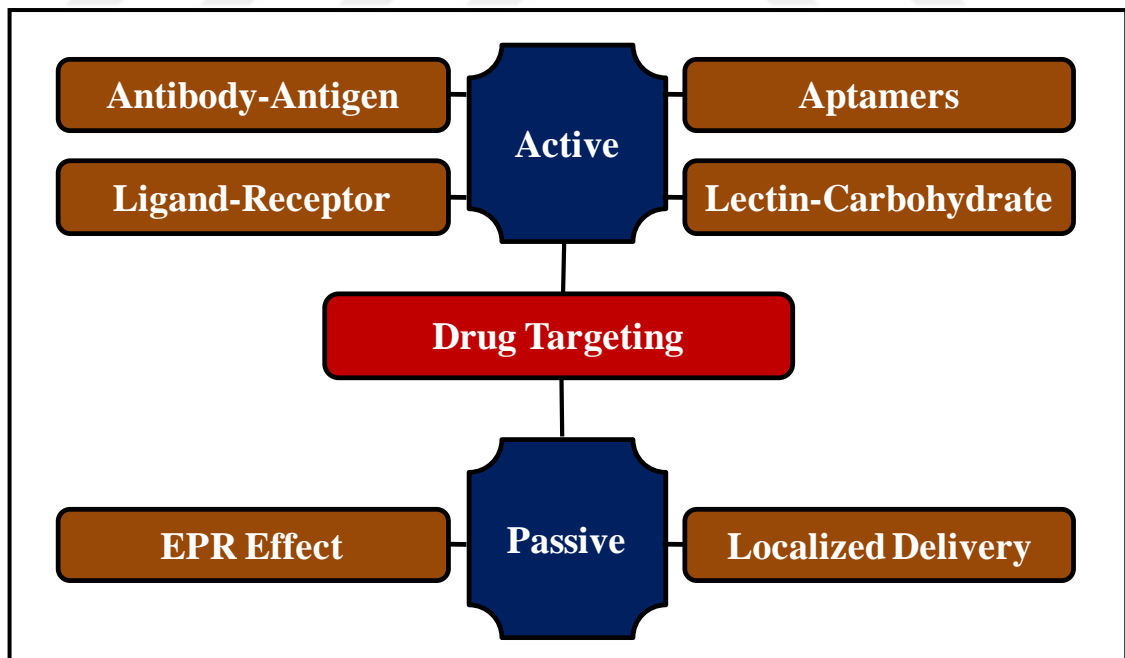
Figure 2.7. Drug targeting strategies

2.5.1. Passive Targeting

Drug delivery systems, which target metabolic circulation, are defined as passive transport systems. The targeting of the drug takes place through organism response to the physicochemical properties of the drugs and drug delivery systems. Passive targeting benefits from the anatomical differences of healthy and diseased cells [74]. Nanoparticles used in treatments tend to accumulate at tumor sites through leaking vasculature and attenuated lymphatics. Nanoparticle accumulation in tumor tissue region due to leaky vasculature is shown in Figure 2.8. This type targeting is also called as enhanced permeability and retention effect (EPR) based targeting [75, 76]. Nanoparticles accumulate in ranging from 100 nm to 2 μm in the environment of tumor angiogenesis, reducing systemic toxicity and allowing toxic effects to be seen only in the tumor site. Anticancer drugs do not have such an advantage alone.
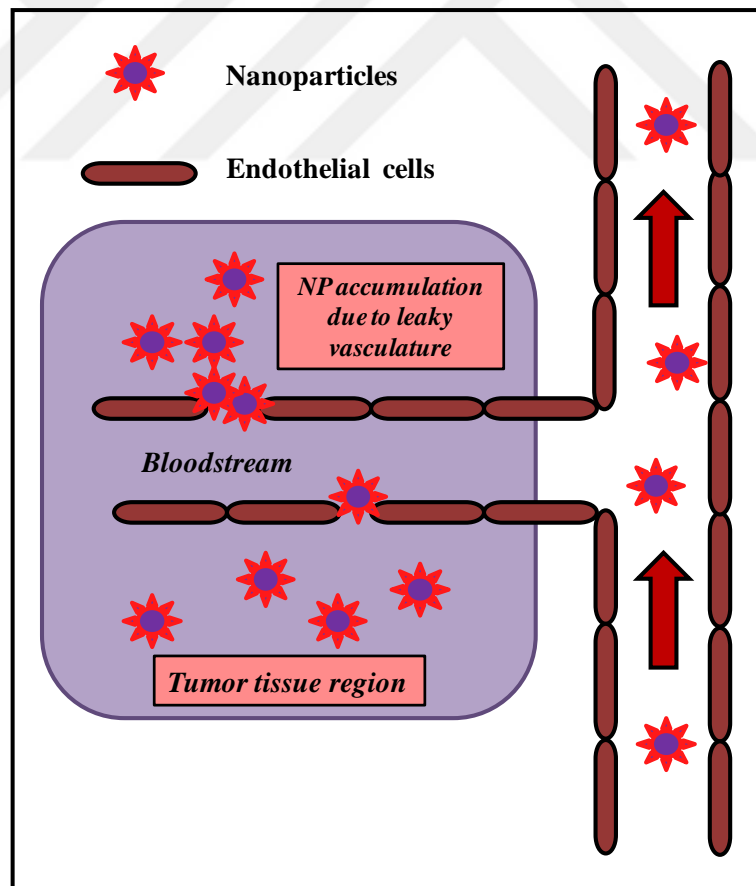
Figure 2.8. Nanoparticle accumulation in tumor tissue region due to leaky vasculature [77]

2.5.2. Active Targeting

In active targeting strategy, the drug carrier is conjugated with specific molecules such as aptamers [78], antibodies [79-83], peptides [84-89], etc. and targeting is achieved by the interactions provided through these ligands. Organs, cancer cells and cell organelles can be targeted in this type targeting and these methods are named as first order, second order and third order targeting applications, respectively. As mentioned above, strategies, which developed by taking into account tumor environment conditions, and specific molecules are used in active targeting. Transferrin-like proteins [90], glycosaminoglycan molecules such as hyaluronic acid [91-93] have been used as targeting agents in many studies from molecular imaging applications to gene silencing applications. Active tumor targeting using targeting molecules is shown schematically in Figure 2.9.
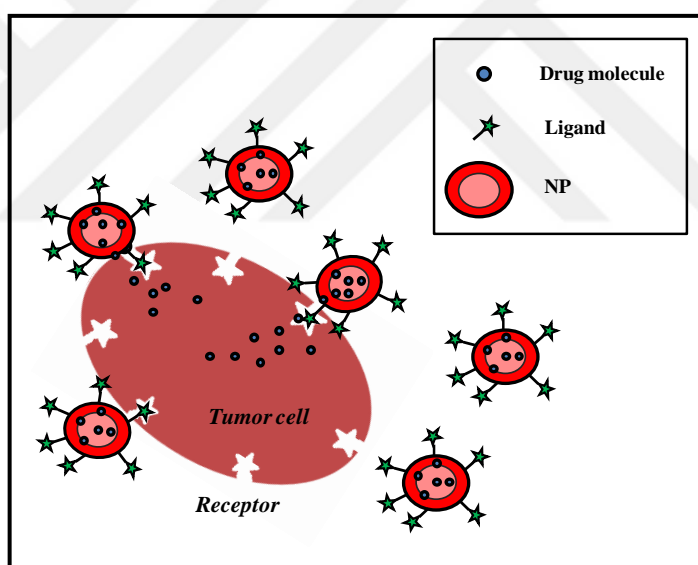
Figure 2.9. Active tumor targeting with ligand-NP complex

2.5.2.1. Folic acid-based Targeting

Targeting folate receptors, which are highly expressed in many cancer cells such as ovarian, brain and breast cancer is one of the important strategies that are used in many studies and tested for efficacy [64, 94-98]. Folate receptors, which are more expressed in cancer cells than healthy cells, can be targeted by the use of folic acid ligand, which is an inexpensive molecule that does not cause unwanted side effects in the organism [99]. Folic

acid-containing carrier systems are taken into the cell through receptor-mediated endocytosis [100]. Folic acid mediated cellular uptake takes place as shown in Figure 2.10.

Folate-based targeting is used to selectively transport many therapeutic molecules including antisense oligonucleotides [101-104], imaging agents [105], gene delivery vectors [106-111], and chemotherapeutics [112-114] to target cancer cells.

Folic acid can be conjugated by applying EDC/NHS chemistry to protein like molecules due to the presence of readily activatable carboxyl groups [115]. It can be bound directly to the drug carrier system as well as to the therapeutic molecule for targeting [104]. Although direct attachment of folic acid to drug molecules is considered as a good strategy, the fact that drug molecules have mostly hydrophobic character limits the targeting activity. The use of molecules having a hydrophilic character between the therapeutic molecule and folic acid as linking agents makes a significant contribution to targeting efficiency [116].
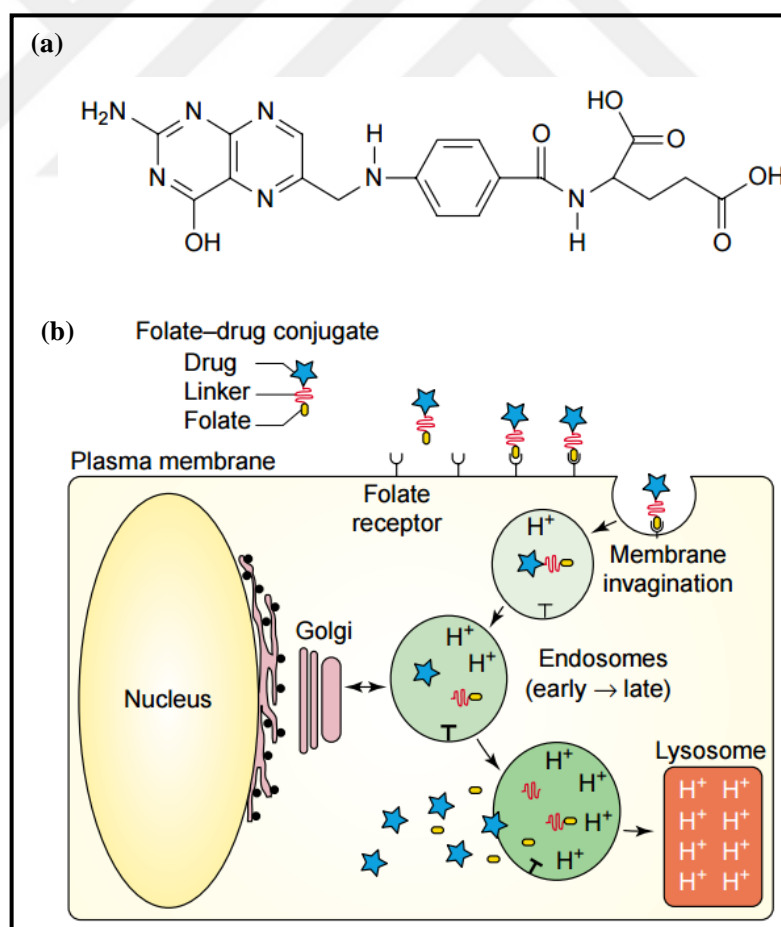
Figure 2.10. Molecule formula of folic acid (a) and schematic representation of folate mediated endocytosis (b) [117].

As in the case of vinblastine, conjugates of this anticancer drug with folic acid, EC-145 and EC-0225, can be given as an example of increasing the targeting activity (Figure 2.11). It should be noted that when preparing the drug-folic acid conjugate, the affinity of the folic acid receptor should be maintained [116].
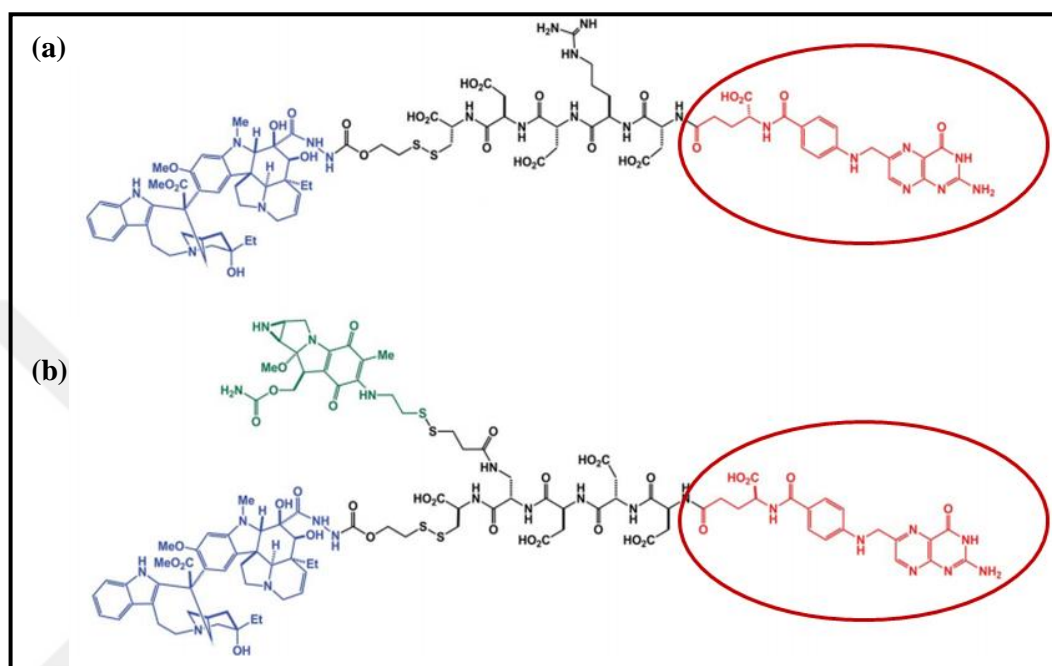
Figure 2.11. Folic acid containing anticancer agents. Vinblastine-derived microtubule polymerization inhibitor molecules (a) EC-145 [118] and (b) EC-0225[119].

Momordin herbal toxin and bacterial exotoxin are among the first therapeutic molecules reported to be effectively taken up by folate mediated endocytosis in tumor cells expressing the folate receptor [120, 121]. The toxin formulations containing folic acid have been reported to have higher tumor killing activity in FR-positive cancer cells such as HeLa cells [121, 122]. It has been reported that folate-mediated targeting in cells such as KB and HeLa contributes to the cellular uptake and selectivity of drug delivery systems [123].

There are also studies in which the activity of cationic liposomes in gene delivery applications is enhanced by the use of folate ligands [96, 103, 111]. The increased cellular uptake and accessibility to tumor site for the polymeric nanoparticles modified with folic acid have been reported in breast cancer cells [115].

It has been emphasized that magnetite nanoparticles coated with folic acid showed higher uptake and localization in tumor cells when used in imaging in breast cancer cells [124]. PEG nanoparticles synthesized by solvent evaporation and modified with folic acid have been reported to exhibit an enhanced therapeutic effect in FR-positive cells [125]. In the folic acid-based targeting applications, targeting activity can be hindered by some factors such as the amount of endogenous folate in the organism, size of the delivery vehicle and the low expression level of folate receptors in patients [96].

2.5.2.2. RGD peptide-based Targeting

$\alpha v \beta 3$ integrins are class of angiogenesis-associated targets for proteins which harboring RGD sequence. These are highly expressed receptors on neovascular endothelial cells [68, 126]. The use of imaging agents and drug molecules in the treatment of cancer by targeting the $\alpha v \beta 3$ integrin has been reported in many studies. The most common method for targeting the $\alpha v \beta 3$ integrins is using peptides and nonpeptide mimetics which include RGD sequence [127, 128]. Targeting activities of linear and cyclic RGD sequences are frequently studied [65, 129-134].

2.5.2.3. Carbohydrate-based Targeting

German scientist Otto Warburg has shown that cancer cells have much more glucose consumption than other cell. It has been reported that the rates of aerobic glycolysis in cancer cells are also quite high [135, 136]. Today, this inference by Warburg is called the "Warburg effect" and considered one of the most important features of cancer [137].

A variety of strategies have been developed using Warburg effect to fight cancer. Inhibition of metabolic enzymes with various molecules [138, 139] and the selective targeting of cancer cells by glycoconjugation have been extensively revealed.

Glycoconjugation strategy originates from the extensive use of radiolabeled glucose analog, 2-deoxy-2-(^{18}F)fluoro-D-glucose, in the visualization of tumors and metastases through high glucose uptake rate [140, 141]. The detection of tumor sites using radio labeled glucose analog with PET imaging is demonstrated in Figure 2.12.
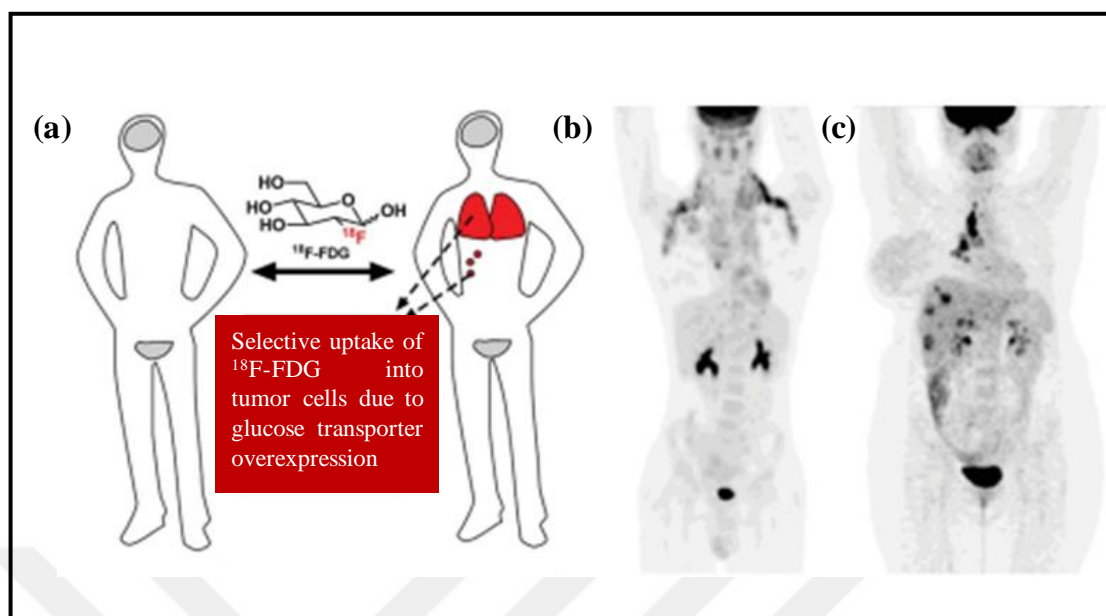
Figure 2.12. Positron emission tomography (PET) imaging using radiolabeled glucose analog 2-deoxy-2-(18F)fluoro-D-glucose. (a) Healthy patient, (b) metastatic Hodgkin's lymphoma patient's PET scan and (c) metastatic breast cancer patient's PET scan [141, 142].

The glycotargeting aim with the use carbohydrate or lectin molecules as targeting agents is to increase the efficacy of a drug delivery system. When the carrier system is modified using lectin molecules, cell glycoproteins or glycolipids are targeted [143]. Similarly, lectin proteins are targeted by the addition of carbohydrate molecules to the carrier system.

Targeting agents can be used in the modification of carrier molecules as well as conjugation with a therapeutic agent. As mentioned in the folic acid targeting part, carbohydrate molecules can be conjugated directly to a drug molecule.

The carbohydrate conjugated drug molecules prepared in this way are shown in Figure 2.13. 1-D-galactose-conjugated docetaxel [143, 144], 2-D-glucose-conjugated paclitaxel [145], 6-D-gluctose-conjugated chlorambucil [146], 6-D-gluctose-conjugated methane sulfonate[147], Peracetylated 2-fluorodeoxyglucose-conjugated chlorambucil [148, 149], and D-threoside-conjugated chlorambucil [150] are the examples of carbohydrate conjugated drugs.
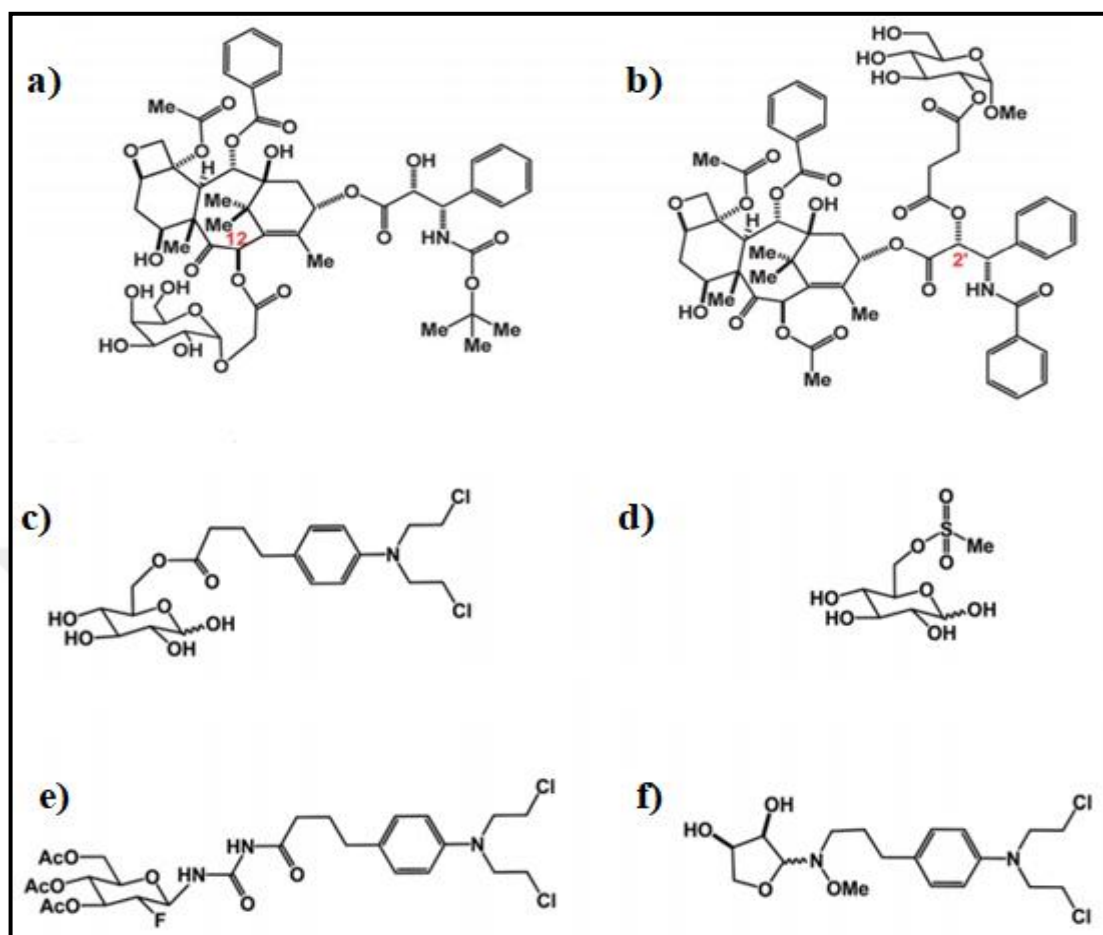
Figure 2.13. Carbohydrate-conjugated drugs. (a) 1-D-galactose-conjugated docetaxel [144, 145], (b) 2-D-glucose-conjugated paclitaxel [146], (c) 6-D-gluctose-conjugated chlorambucil [147], (d) 6-D-gluctose-conjugated methane sulfonate[148], (e) Peracetylated 2-fluorodeoxyglucose-conjugated chlorambucil [149, 150], and (f) D-threoside-conjugated chlorambucil [151].

2.5.2.4. Nucleic acid and Antisense Oligonucleotide Delivery and Glycotargeting Strategies

In recent years, nucleic acids have been used as a part of a drug delivery system as a therapeutic unit or carrier. DNA structures, assembled using DNA base-pairing, were used to construct nanostructures for the delivery of pharmaceuticals and antisense oligonucleotides. However, their difficulty to pass the cellular membrane due to their highly charged nature decrease their applicability as carrier structures in these applications.

The facilitated cellular uptake of the nucleic acids, which are generally taken by the cells through different mechanisms such as adsorptive endocytosis, can be provided by using various chemicals or applying mechanical and electrical stimuli. Cationic lipids such as Lipofectamine[TM], dendrimers calcium phosphate and cationic peptides are widely used for nucleic acid delivery [152-159]. The transport of nucleic acid structures can also be achieved by applying electroporation or particle bombardment [160-164].

In recent years, the utility of interactions between lectins and glycans for targeting and delivery gained importance and were named as glycotargeting for the nucleic acid delivery [165]. A carbohydrate moiety recognized by the lectins on cell surfaces is incorporated into the constructed nucleic acid structure. The presence of such a moiety allows the uptake of nucleic acids through receptor-mediated endocytosis.

The carbohydrate molecule can be interact non-covalently with nucleic acid constructs, as well as it can be incorporated directly or via a carrier structure. Oligonucleotides can be functionalized with carbohydrates by the formation of covalent bonds between sugar molecules and nitrogenous DNA bases. Positively charged polypeptides, which are frequently used to deliver nucleic acids, can be glycosylated with various carbohydrate molecules [166]. Polysaccharides such as chitosan and schizophyllan can also be modified by sugar molecules recognized by lectins and their uses in gene transfer applications has been reported [167-169]. As in the case of the schizophyllan, which protects single chain DNA from nuclease attack, does not produce immune response and allows long circulation, polysaccharide molecules have been used for the direct delivery of antisense oligonucleotides.

2.6. CANCER THERAPY

Cancer is one of the biggest causes of death in worldwide. Cancer whose frequency of sightings is increasing day by day, has been treated with surgery, radiotherapy and chemotherapy applications. Chemotherapy applications come to the forefront from these methods in the treatment of advanced stage cancer. In chemotherapy treatments, the therapeutic agent should be given to the patient in high doses to ensure that the obtaining desired final concentration in target tissues or cells. While the development of new agents in treatment applications, which will increase the survival chances of patients, is targeted,

the presence of biological barriers, which impede the transport of drugs to target sites, significant side effects, and physiological effects arise from undesirable non-target effects are important issues must be overcome effectively. The side effects such as neurotoxicity and cardio toxicity observed in healthy cells and the formation of resistance against therapeutics cause the disease to worsen. Thus, there is a special demand for the therapies including new drugs, drug delivery systems, which overcome these problems and increase the effectiveness of chemotherapeutic agents providing targeting of cancer cells and being less toxic to healthy cells.

2.6.1. Doxorubicin

Cancer drugs are classified according to their functions and compositions. There are alkylating agents that prevent further proliferation of cancer cells and directly damage DNA. Antimetabolites interacting with DNA and RNA synthesis, replaces with building blocks to prevent DNA replication and transcription. Anthracyclines, which interact with enzymes responsible for DNA replication to influence the cell cycle process, are also important cancer drugs [170, 171]. Doxorubicin (Dox) is an anthracycline-type chemical approved by the FDA, which can be used alone or in combination with other agents for the treatment of many cancer types. In 1970s, it was extracted from *Streptomyces* peucetius var. caesius. It is generally used for the treatment of breast cancer. The molecular formula of Dox, which generally triggers the apoptotic cell death in cancer cells, and the types of cancers treated with doxorubicin are shown in Figure 2.14 [172-175].
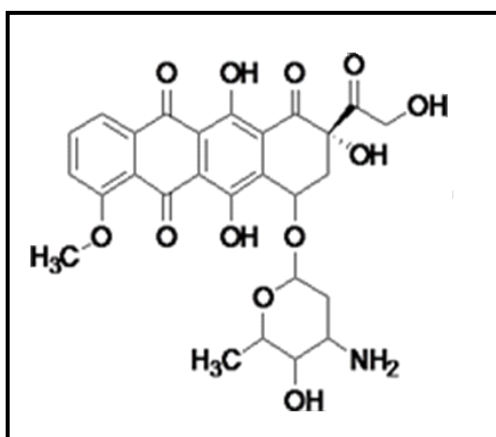
Figure 2.14. The structure of Dox [176].

2.6.2. Mechanism of Dox

Dox is taken by passive diffusion to the cells and the major metabolite is doxorubicinol. When Dox is administered intravenously, the distribution half-life is approximately 3-5 minutes and this indicates that the rapid cellular uptake. The Dox half-life in the tissue is quite slow compared to cellular uptake and varies from 24 to 36 hours [177]. It is approximately 50 times more abundant in the nuclear parts of the cell than cytoplasm and mostly accumulated in cell nuclei.

Antitumor activity of Dox arises from events such as DNA intercalation, topoisomerase II inhibition, free radical formation. The entrance of various molecules into the planar deoxyribonucleic acid bases is defined as intercalation. Due to their chemical nature and size, polycyclic, aromatic and planar molecules are suitable for placement between DNA base pairs interact via intercalation with DNA. Compounds such as ethidium bromide, proflavine, and doxorubicin have the ability to intercalate, and some of these molecules are used in the treatment of cancer.

Intercalation was first introduced by Leonard Lerman [178]. In Lerman's study, the interaction between DNA and several polycyclic aromatic compounds such as acridine and proflavine was investigated and he observed the changes such as unwinding of DNA and extension of the deoxyribose-phosphate backbone applying X-Ray diffraction [178].

Dox leads to apoptosis through caspase activation and mitochondrial membrane potential deterioration [172, 179]. Beside cancer cells, Dox also affects other cells and shows side effects on healthy cells [180].

Dox interacts with DNA through intercalation (Figure 2.15) and inhibits macromolecular biosynthesis [181, 182]. Topoisomerase 2b was reported as cardiotoxicity mediator induced by Dox in rats. In replication process, DNA strands are uncoiled by topoisomerase 2b [183, 184].
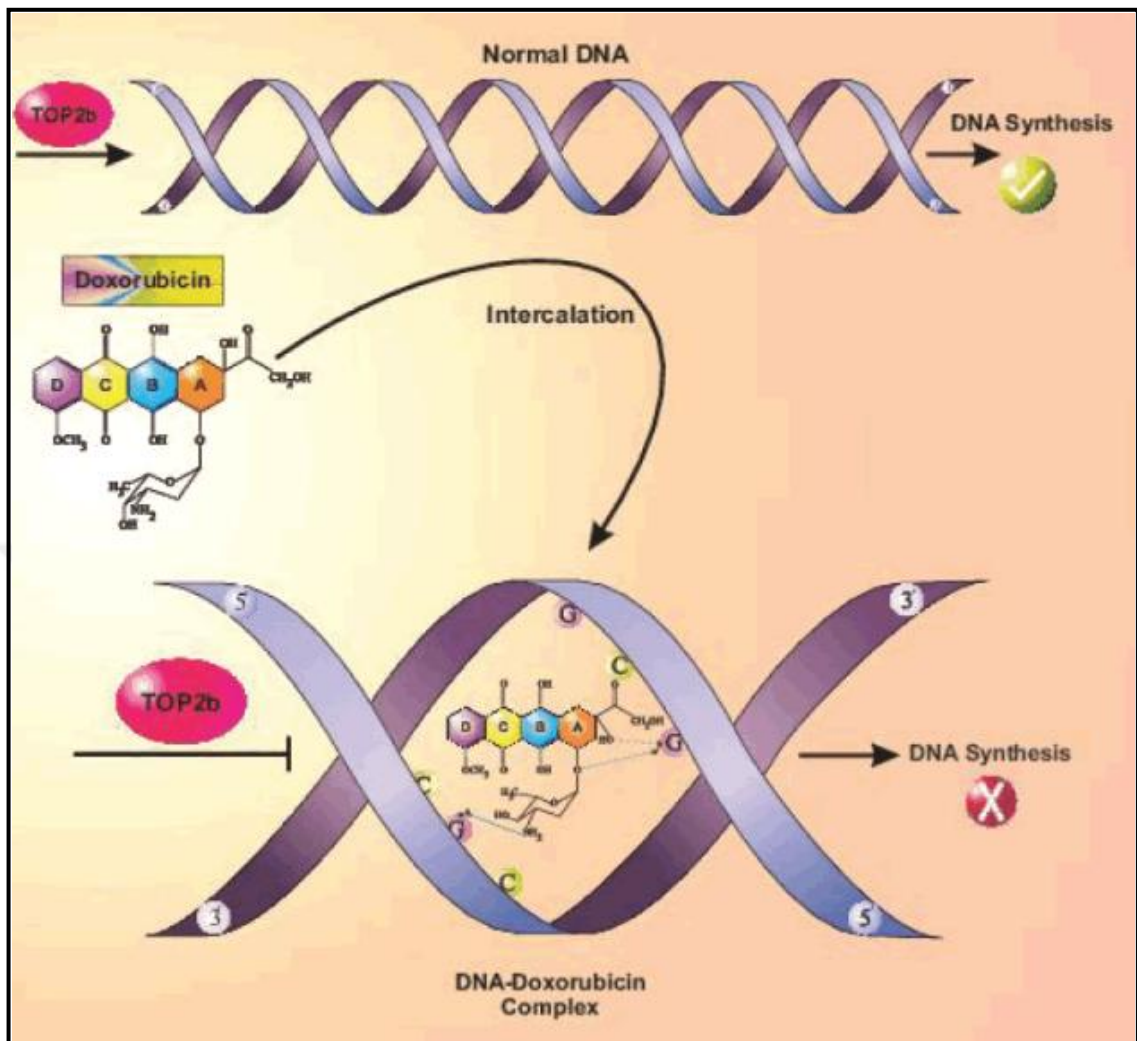
Figure 2.15. Intercalation of Dox [185]

Failure to repair DNA damage induces apoptosis and cell growth is hindered in the G1 and G2 phases. Antiproliferative effect of doxorubicin comes out together with cytotoxicity by binding of Dox to molecular targets like topoisomerase I and II enzymes, causes the DNA damage [186]. In cardiomyocytes, the activation of P53 and apoptotic pathways have been reported due to Dox induced cardio toxicity [187]. Production of Dox-induced ROS arises from the reduction of expression levels of Top2b dependent antioxidant enzymes [188].

Dox-induced apoptosis has an important role in the appearance of cardiotoxicity, which is the most important side effect of Dox. The cardiotoxicity occurs by the formation of superoxide and free radicals (Figure 2.16).
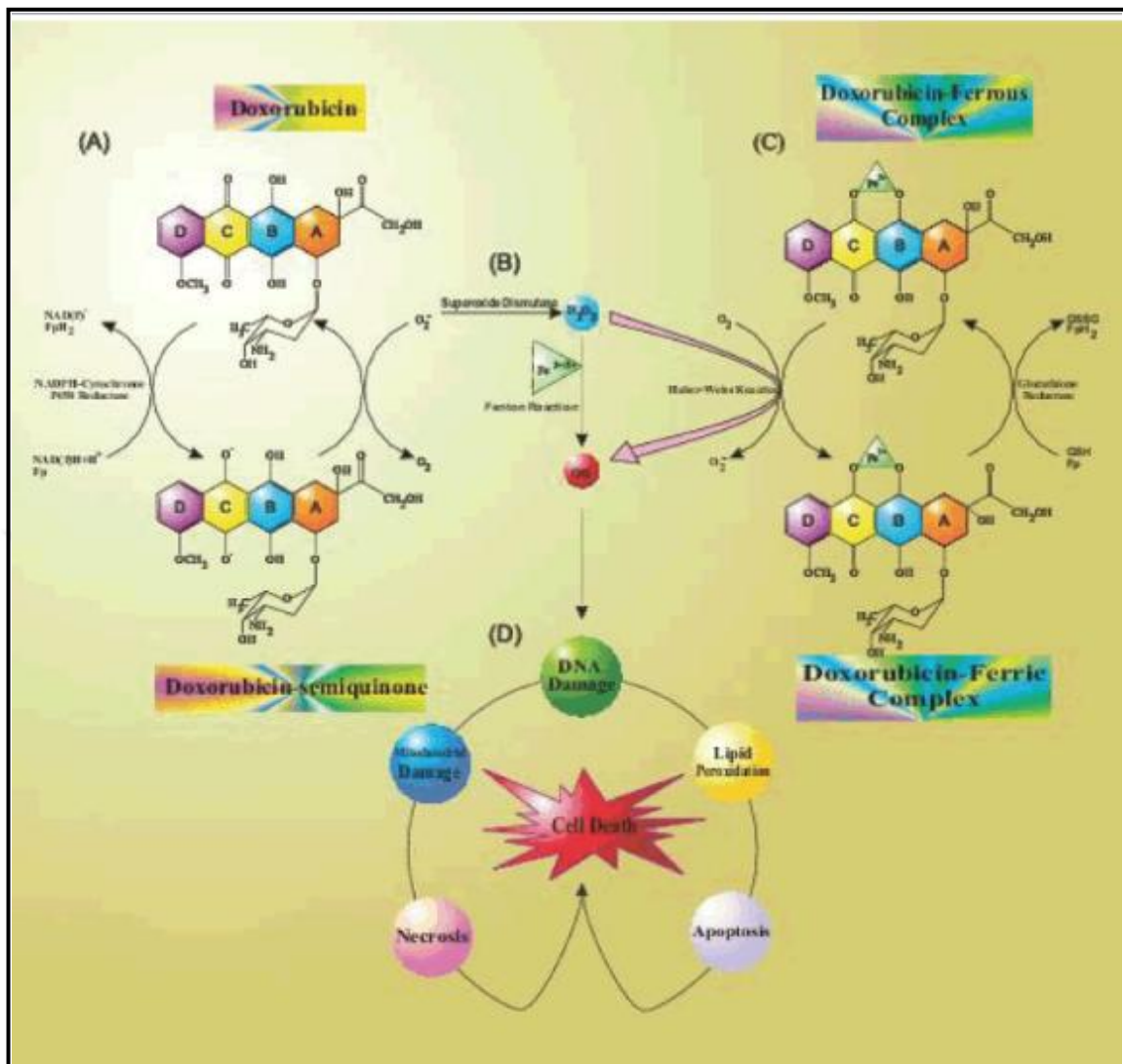
Figure 2.16. Dox-induced oxidative stress [185]

Dox performs free radical formation in two ways. The non-enzymatic method uses iron while the respiratory chain of mitochondria is involved in the enzymatic pathway [189, 190]. This situation is related to the generation of reactive oxygen species (ROS) due to Dox redox activity. When Dox is oxidized to the non-stabilized semiquinone and then returned to the Dox structure, the process leads to the release of reactive oxygen species which results in events such as membrane damage, oxidative stress and DNA damage with lipid peroxidation [191]. The reaction begins with the loss of one electron of Dox and the formation of the Dox semiquinone radical is produced via reduced NADPH-cytochrome P450 reductase. In normoxic conditions, unpaired electron is transferred to oxygen form superoxide radicals. The semiquinone radical forms complex with iron [192-195]. Flavoproteins cause the reduction of sem radicals by taking electrons from the cofactor

molecule and converting them to Dox. These cyclic redox reactions are important because they cause the formation of many superoxide radicals even at very low concentration of Dox [196].

Reactive nitrogen species are also the cause of the occurrence of Dox-induced cardiotoxicity. Binding of Dox to the reductase part of endothelial nitric oxide synthase results in an increase in the amount of superoxide [197].

Dox leads to reduction of activities cardiac enzymes such as catalase and glutathione-S-transferase. Because the amount of antioxidant in heart tissue is lower than in other places, the free radicals will have a high potential to cause damage to the heart [198].

The Dox-induced mitochondrial damage is induced by the respiratory chain defect, which allows continuous generation of free radicals, and mitochondrial damage triggers apoptosis by causing cytochrome C release. Binding of proteins in electron transport chain with cardiolipin, which founds in the mitochondrial membrane, is necessary for the achieving functions of these enzymes effectively. The interest of Dox with cardiolipin leads to the production of more superoxide molecules. This type of effect of Dox also affects other membrane proteins, causing mitochondrial activity to weaken [199].

Dox initiates the activation of apoptose-inducing AMP-activated protein kinase-dependent molecular signals to affect the Bcl-2/Bax apoptosis pathway. The change in Bcl-2/Bax ratio induces apoptosis with downstream activations of different caspases [170].

2.6.3. Therapeutic Forms and Delivery Systems of Doxorubicin

When chemotherapy drugs are administered, they cause toxicity and undesirable side effects that affect all cells in patients. Therefore, drug delivery systems have been developed to reduce the toxicity of these drugs and limit their activities outside the tumor area. The use of nanoparticles for drugs with toxic side effects such as Dox has been extensively investigated and some of the improved nanoparticle-based formulations have been also marketed.

Table 2.1. The liposome based Dox products

Liposome-based Dox formulations	Particle type	Application status	Ref.
Doxil	PEGylated liposome	approved and in use	[200-202]
Lipo-dox	PEGylated liposome	approved and in use	[203]
Myocet	Liposome	approved and in use	[200, 201, 204]
Thermodox	PEGylated liposome	In clinical trial	[205, 206]

Improved liposomal drug delivery systems that can stay in the circulation for a long time and prevent the drug escape are promising for such drugs. PEG coated liposomal formulations of Dox are commercially available. In Table 2.1, liposome based Dox products that are in use and at the clinical trial stage are shown.

Designed in the form of a PEGylated nanoliposome, Doxil, is the first FDA approved nano-drug. In this formulation, circulation time of drug was enhanced and avoidance of RES was achieved. It targets cancer cells passively due to the EPR effect and the release of Dox occurs when the cancer cells are reached [207].

The evidence of EPR effect induced by passive targeting in humans was first demonstrated by Gabizon et al. [208]. The Dox levels in biopsy specimens, which were taken after Dox and Doxil treatments, from patients were compared and shown in Figure 2.17. Accumulation of Doxil in human tumors was supported by fluorescence microscopy analyses of biopsy specimens [209].
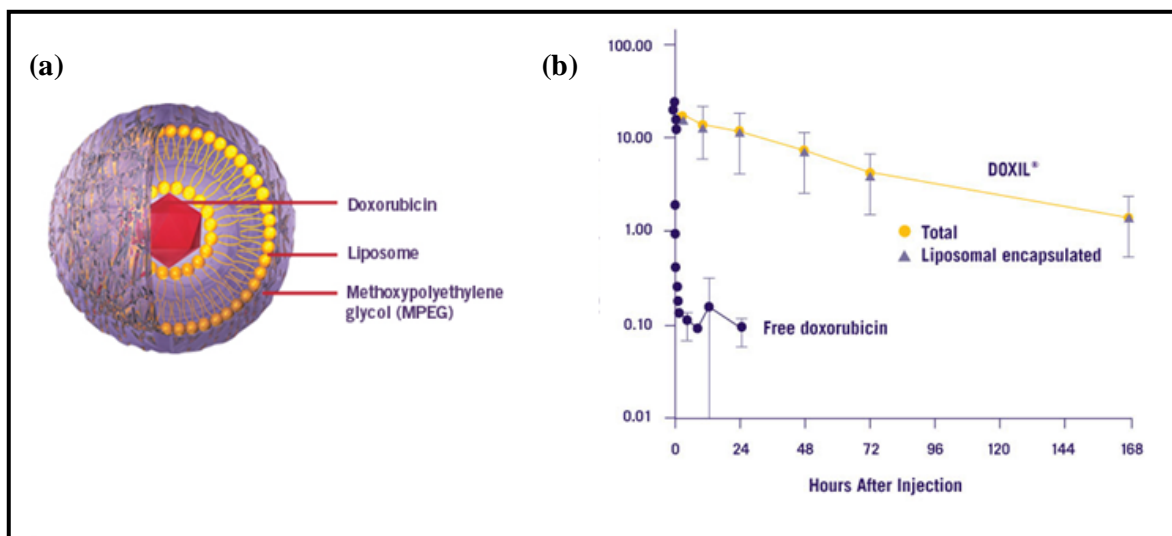
Figure 2.17. The schematic representation of (a) Doxil (a) and (b) plasma Dox levels of patients [208]

Many studies have been reported on the delivery of Dox using chitosan nanoparticles, which allow controlled drug release and are noted for their biocompatibility. In vitro study by Janes et al, dextran coupled chitosan nanoparticles were found to exhibit high anti-tumor activity on human melanoma cells and murine colorectal carcinoma cells [210].

The use of hydrogel-based systems in bone tumors has also been reported for Dox. In mice, the biodegrable chitosan/dipotassium orthophosphate hydrogel formulation was applied and it was seen that necrosis was not observed at the injection site and controlled release of the drug lowered the toxicity of the drug [211].

The use of Dox, which is conjugated with dextran to eliminate undesirable side effects, has been investigated in Mitra et al.'s work by encapsulating it into chitosan nanoparticles and results showed that the system was more efficacious for disease treatment compared to free Dox [212]. Iron oxide nanoparticles coated with chitosan showed high anticancer effect on resistant MCF-7 breast cancer cells [213].

In the study performed on human lung carcinoma cells, the use of star-shaped poly lactic glycolic acid (PLGA)-vitamin E nanoparticles in the transport of Dox has been investigated and increasing antitumor effect with higher cellular uptake was observed. [214]. Dox loaded nanoformulations are given in Figure 2.18.
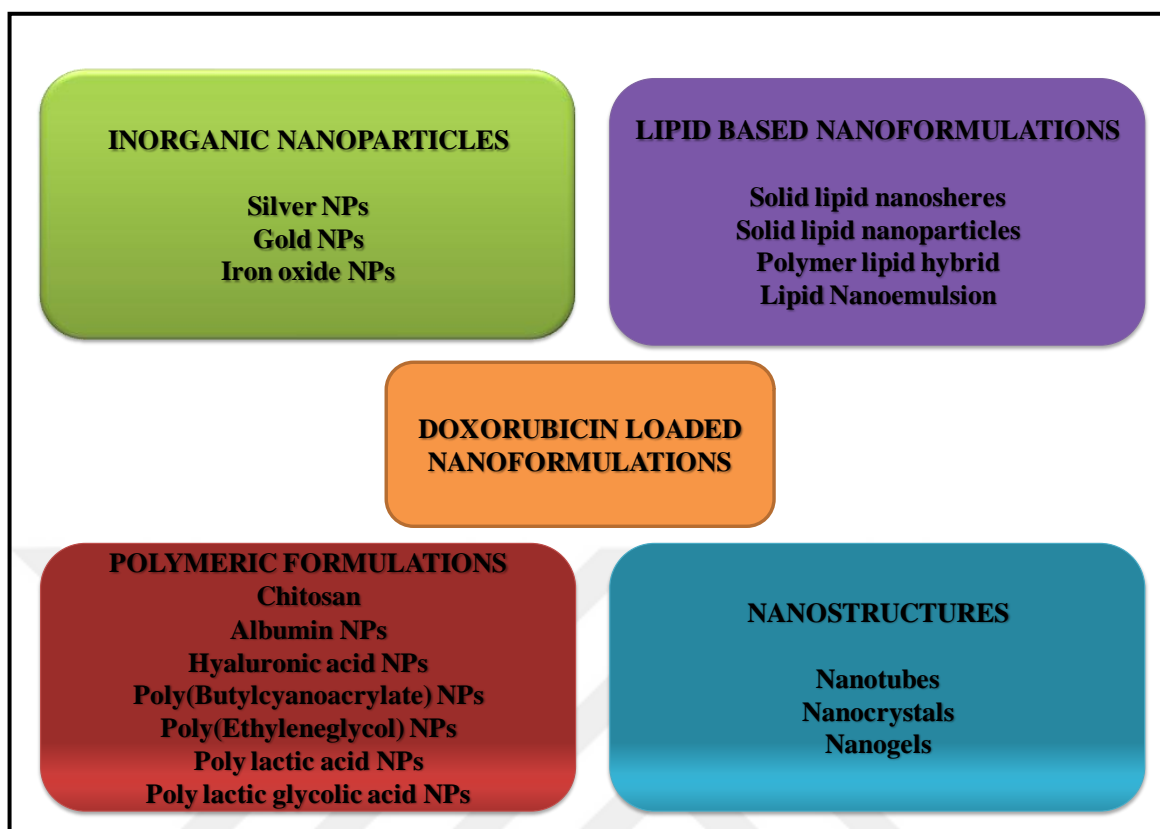
Figure 2.18. Dox loaded nanoformulations [215]

2.7.   GENE SILENCING AND MORPHOLINOS

2.7.1.   Gene Silencing

Since the discovery of the genetic material DNA, removal or mutation of genes has been extensively studied for the elucidation of gene functions in cellular events. Silencing of genes after transcription to determine their functions and stopping genetic activity leading to undesirable outcomes is an important approach for the treatment of diseases such as cancer. In antisense or gene knockdown mechanism, the expression of selected genes is inhibited by agents through Watson-Crick base pairing mechanism. These agents are named as antisense or gene knockdown agents. Phosphorothioate-linked DNAs (S-DNA), short interfering RNAs (siRNA), and morpholinos are three major classes (Figure 2.19) of gene knock down agents [216].
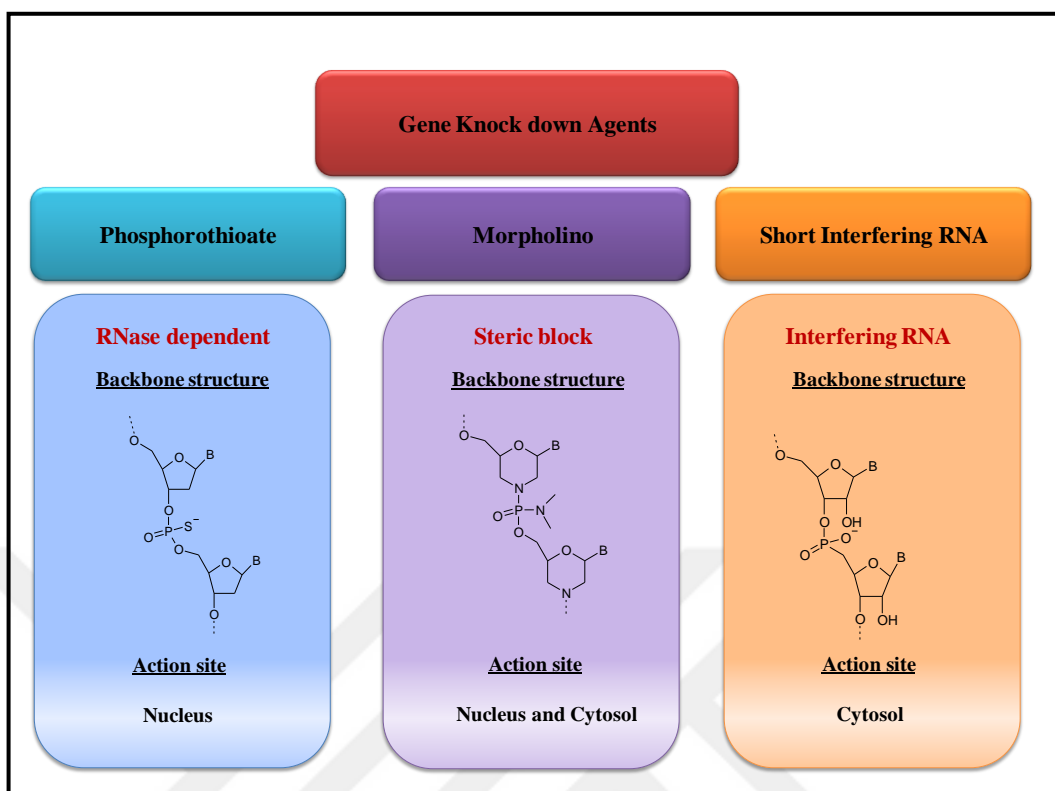
Figure 2.19. Structural types of gene knock down agents [216]

The development of such antisense oligo structures has began at the end of 1960 [217-220]. Inhibition of pathogen replication using synthetic oligonucleotides through antisense mechanism is the first report of antisense technology and is was reported by Zamecnik and Stephensen in 1978 [218]. In this report, Rous sarcoma virus RNA has been targeted using a tridecamer oligodeoxyribonucleotide. The tridecamer oligonucleotide prevent the replication through blocking protein translation [218, 221, 222]. This study and further studies showed that the usage of complementary antisense oligonucleotides can be promising therapeutic way to obtain gene-specific knockdown.

The gene knockdown agents should have high sequence specificity and also lack off-target effects. The sequence selectivity means that ability to block only the target RNA without blocking other RNA's in cell environment.

The antisense agent's high sequence specificity means that antisense oligo knocks down the only target RNA in the cell; low sequence specificity of antisense oligo means that antisense oligo knocks down the function of target RNA with other non-targeted RNAs in the cell [216].

The off-target effects of antisense oligos are results of the interactions of intracellular proteins, cell surface proteins and extracellular surface proteins with antisense agents through different mechanism than base-pairing [216].

2.7.2. Structure and Mechanism of Morpholinos

Morpholino oligomers contain six membered morpholino rings instead of five membered sugar ring and non-ionic phosphodiamidate inter subunit linkages instead of phosphate inter subunit linkages (Figure 2.20).
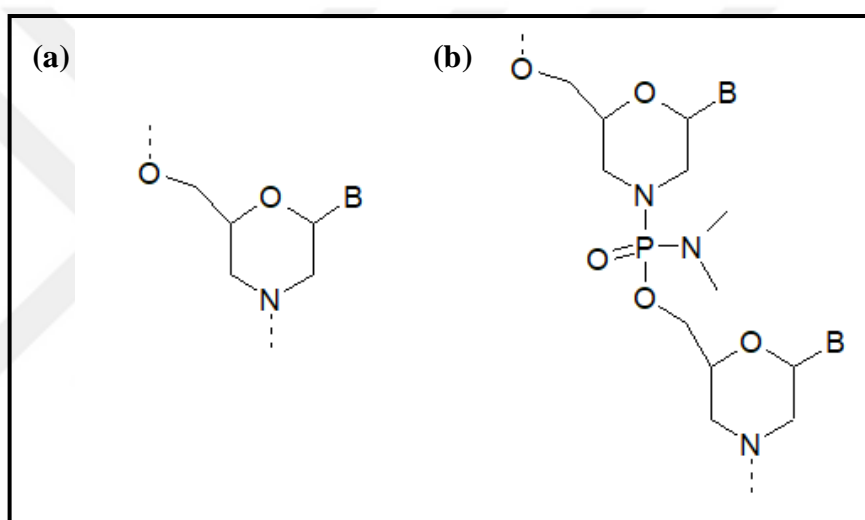
Figure 2.20. Morpholine ring (a) and Morpholino backbone structure (b).

The chemical structure of morpholinos provides advantages such as stability in biological environments, resistance to enzymatic degradation attacks, etc.[223]. It is known that morpholinos, which have a high solubility in aqueous solution, shows high affinity to target RNA sequences [224, 225]. Because of morpholinos' unnatural structures, they don't interact with proteins. Their non-ionic phosphorodiamidate inter subunit linkages (lack of backbone charge) provide simple and efficient delivery into the cells by endocytosis assisted delivery reagent [226].

 To exhibit activity, the minimum number of bases of the morpholino sequence should be about 14-15 bases [227]. Minimum inhibitory length means that the minimum length of a antisense oligo which match with the target RNA to show it's inhibition function. High targeting efficiency is result of morpholinos high affinity properties towards their target

RNA sequences and extended lenghts. Morpholino oligomers are design to block the translation of mRNA into protein [224]. Morpholino sequences are also used to inhibit splicing of pre-mRNA [228] (Figure 2.21).

DNA

mRNA

Morpholino oligomer hybridizes to RNA sequence

Protein translation is blocked
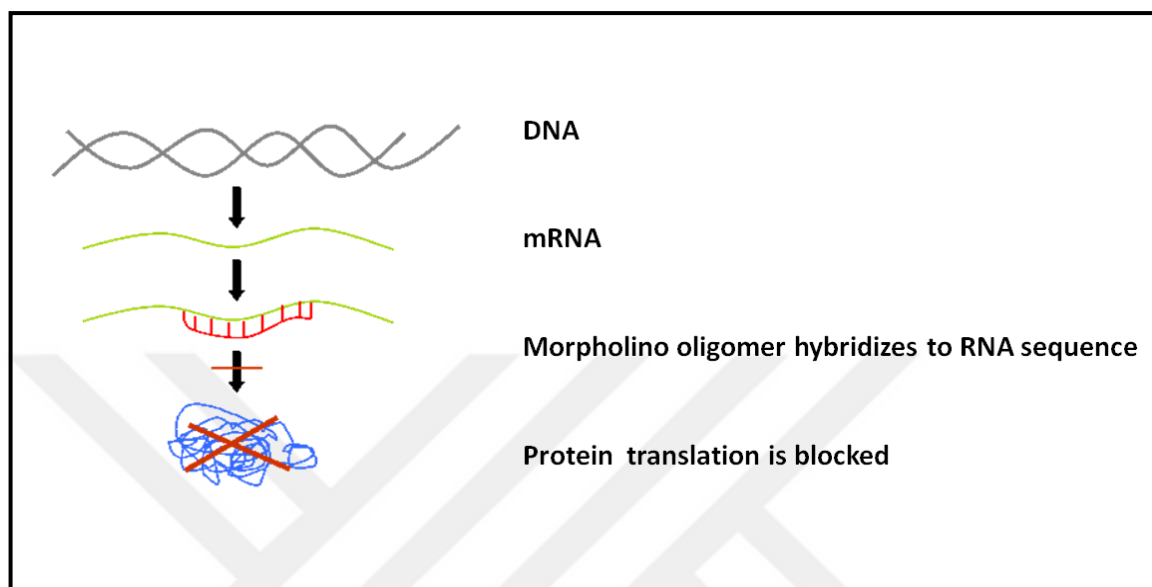
Figure 2.21. Blocking through morpholino oligomer

2.7.3. Luciferase

The luciferase enzymes present in organisms, exhibiting bioluminescence, are responsible for the catalysis of light-producing chemical processes [229]. North American firefly luciferase isolated from *Photinus pyralis* is one of the most studied enzymes. [230].

Luciferase molecular weight is 62 kDa and the production of light by luciferase reaction is dependent on the presence of ATP, oxygen, and luciferin substrates [229]. Fireflies except *P.pyralis* emit light at different wavelengths from 582 to 552 nm [231], while *P. pyralis* emits yellow-green light at 560 nm [232].

Different luciferase enzymes emit light at different wavelengths using the same reaction compounds depending on their protein structure [231]. The reaction scheme of the firefly luciferase is shown in Figure 2.22.
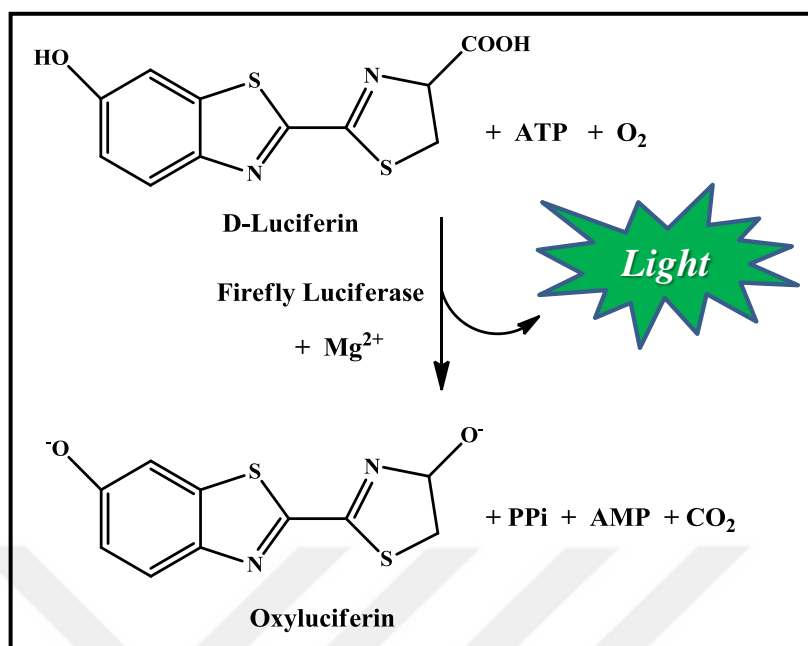
Figure 2.22. Reaction of Firefly luciferase

2.8. AIM OF THE STUDY

The aim of this study is to prepare DNA tile nano-carrier systems, which can be used as drug and gene delivery systems, and investigating their efficiency *in vitro* conditions. Several agents can be bind into DNA tile structure via hybridization of complementary modified oligonucleotides to form multifunctional DNA based nanocarrier system. Maintaining the basic tile structure, a new carrier system can be designed for every purpose (therapy, targeting, etc.).

In this thesis, lactose, folic acid, and RGD modified oligonucleotides will be hybridized to DNA tile structures. These molecules are used as targeting agents to provide efficient targeting of cancer cells. The well-known chemotherapy drug, doxorubicin will be used for killing the cancer cells. Therapy and targeting are aimed and carried out simultaneously with this system. The requirements to form a multifunctional nanocarrier system and the efficiency of this newly prepared system will be investigated. At the same time gene silencing experiments will be conducted to test the approach. For this purpose, luciferase expressed cells will be used and silencing of the luciferase gene will be studied as a model for gene silencing *in vitro.*

3. MATERIALS AND METHODS

3.1.   CHEMICALS AND REAGENTS

Magnesium acetate and folic acid were purchased from Applichem (Darmstadt, Germany). RGD peptide and agarose were purchased from Sigma (St. Louis, Mo. USA). Boric acid and ethidium bromide were purchased from Fisher Scientific. Sodium cyanoborohydride was purchased from Acros. Trizma base, acetic acid, cytochalasin B, and hydrochloric acid (Sigma-Aldrich, Germany), N,N'-dicyclohexyl carbodiimide (DCC), and *N*-Hydroxysuccinimide (NHS) were purchased from Sigma-Aldrich (Darmstadt, Germany). Ethylenediaminetetraacetic acid was purchased from Bio Basic (Markham, Canada). Doxorubicin (Dox) was purchased from Biotang (Lexingtan, USA). Sodium dodecyl sulfate (SDS) was purchased from Bio Basic Inc. (Canada). Lactose monohydrate and sodium azide (NaN_3) were purchased from Merck. Glucose was purchased from Riedel-de Haen.

3.2.   CELL LINES, CELL CULTURE MEDIA AND CHEMICALS

The MDA-MB-231 and BT-474 cells are breast cancer cells. MCF-7 cells are breast cancer cells. The A549 cells are adenocarcinomic human alveolar basal epithelial cells. The HeLa cells are cervical cancer cells. LNCaP cells are androgen-sensitive human prostate adenocarcinoma cells. The DU145 cells are human prostate cancer cells and PNT1A cells are healthy human prostate cells. The cell lines were purchased from the American Type Culture Collection. (ATCC).

Dulbecco's modified Eagle medium (1X DMEM, 4.5g/L D-Glucose, L-glutamine, sodium pyruvate; Gibco,USA), fetal bovine serum (FBS, Gibco, UK), HyClone™ phosphate buffered saline (10 X PBS, Gibco, USA), Pen-Strep (10,000 Units/ml penicillin, 10,000 µg/ml streptomycin; Gibco, USA), L-glutamine (200 mM, Gibco, UK), 0.25 per cent trypsin-EDTA (1X, Gibco, UK), sodium pyruvate (100 mM, Gibco, USA), dimethyl sulfoxide (DMSO, Sigma-Aldrich, USA), propidium iodide solution (PI, 1.0 mg/ml in water; Sigma-Aldrich, USA) Ribonuclease A (Sigma-Aldrich, USA), ethanol (Sigma-

Aldrich, USA), and 2-propanol (Sigma-Aldrich ,USA) were used for the cell culture experiments. RIPA buffer was obtained from Santa Cruz Biotechnology (USA). Goat anti-firefly luciferase antibody was purchased from Abcam (USA). All oligonucleotides (Oligo), used in DNA tile formation, were purchased from Alpha DNA (Montreal, Canada) and listed in Table 3.1.

Table 3.1. Oligonucleotide sequences used in DNA tile formation

Sequence Code	Base sequences of oligonucleotides (5'to 3')
Oligo 1	AGG CAC CAT CGT AGG AAA ATC TGC GTC AGC TCT CCG TAC ACC AGT GCT TCC ATG CGA AGT AAA ACG TTC CGA TCA CCA ACG GAG TAA AAC GAT CTA ACT GAT AAC TAG CAC CTC TGC TCA CGT GAG GAG TAA AAC TTG CC
Oligo 2	ATA CCG GAG GCT TCC TGT ACG GAG AGC TGA CGC AGA CCT ACG ATG GAC ACG CCG
Oligo 3	ATG CAA CCT GCC TGG CAA GAC TCC TCA CGT GAG CAG AGG ACT ACT CAT CCG TTA
Oligo 4	TTT CCG ACT GAG CCC TGC TAG TTA TCA GTT AGA TCG ACT CCG TTG GAC GAA CAG
Oligo 5	ATA GCG CCT GAT CGG AAC GAC TTC GCA TGG AAG CAC TGG ACC GTT CTA CCG ATT
Oligo 6	CTCGCAATCGGTAGAACGGTGGAAGCCTCCGGTATGCATG
Oligo 7	AAA AAA AAA ACG GCG TGT GGT TGC ATA AAA AAA AAA
Oligo 8	CGC TAT AAC GGA TGA GTA GTG GGC TCA GTC GGA AAG AGCA
Oligo 9	AAA AAA AAA ACT GTT CGT GGC GCT ATA AAA AAA AAA
Oligo 10	AAA AAA GGG TCG CGG TAA TCC TGT ACG GAG AGC TGA CGC AGA CCT ACG AAT GGC GCT GGG AAA AAA
Oligo 11	AAA AAA GGG TCG CGG TAA GGC AAG ACT CCT CAC GTG AGC AGA GGA CTA ATG GCG CTG GGA AAA AAG GGT CGC GGT AAG ATG GGT GAG CT
Oligo 12	AAA AAA GGG TCG CGG TAA CCC TGC TAG TTA TCA GTT AGA TCG ACT CCG AAT GGC GCT GGG AAA AAA
Oligo 13	AAA AAA GGG TCG CGG TAA CGG AAC GAC TTC GCA TGG AAG CAC TGG ACC AAT GGC GCT GGG AAA AAA
Oligo 14	CCC AGC GCC ATT CTA CCC ACT CGA

3.3. METHODS

3.3.1. Folding of DNA Tile Structures

DNA tile structure was formed using long scaffold strand (140 bases) and the short staple strands (36-54 bases). The tile formation was carried out in hybridization buffer TAE/Mg^{2+}. Oligonucleotide mixture was placed in a water bath heated to 95 °C and then the temperature of the water bath was expected to decrease to the room temperature within 24 hours. Oligonucleotides used in tile formation are given in Table 3.1. The oligonucleotides used to construct DNA tile structures, which were designed for the delivery of drug and antisense oligonucleotide, are given below. The DNA tile to be used for the doxorubicin delivery was generated using oligonucleotides 1-9. The tile to be used for the morpholino delivery was constructed using oligonucleotides 10-14 and oligonucleotide 1.

3.3.2. Characterization of DNA Tiles

3.3.2.1. *Agarose Gel Electrophoresis*

Agarose gel electrophoresis was applied to monitor the tile formation. The samples taken from the hybridization mixtures were loaded into 2 per cent agarose gel. Agarose gel was prepared by dissolving in the TAE buffer solution. The DNA tile structure formed by hybridization of oligonucleotide sequences to each other was monitored using a gel imaging system (Bio-Rad, USA).

3.3.2.2. *Dynamic Light Scattering (DLS)*

Dynamic light scattering measurements of DNA tile structures were carried out using a Zetasizer nano-ZS from Instruments (Malvern, UK). Measurements were performed at room temperature with a 173° scattering angle using 4 mW He-Ne laser conditions and repeated three times.

3.3.2.3. *Atomic Force Microscopy (AFM)*

DNA tile formation was monitored with AFM (Park Systems XE 100). DNA tile sample was dropped on freshly cleaved mica surface and dried samples were analyzed in non-contact mode with silicium tips at room temperature. An image-processing program XEI was used for the examining of AFM images.

3.3.3. Stability of DNA Tiles

The stability analysis of DNA tile structures was performed in cell medium. The tile structures were incubated in DMEM medium supplemented with 10 per cent FBS (fetal bovine serum), 100 unit/mL penicillin, and 100 μg/mL streptomycin solutions at 37 °C under 5 per cent CO_2 atmosphere. The stability of DNA tile structure was verified by agarose gel electrophoresis. Incubation samples were loaded into the agarose gel and run for 1 hour at 80 V. After running, agarose gel image was recorded by a gel imaging system.

3.3.4. Modification of Oligonucleotides

3.3.4.1. *Synthesis of Lactose Modified Oligonucleotide*

Carbohydrate modification of the amine-modified oligonucleotides was accomplished by applying the reductive amination procedure [233]. The reaction was carried out in the borate buffer solution in the presence of 20 mM lactose, 50 μM 5'-aminohexyloligonucleotide and 250 mM sodium cyanoborohydride in a single step for 18 hours at 60 °C. After the reaction, an ultracentrifuge column (MW 3000 Da) was used to remove unreacted chemicals. Centrifugation was carried out 3 times for 45 minutes at 3800 rpm at room temperature. The samples loaded to 2 per cent agarose gel were run at 60 volts for 90 minutes.

3.3.4.2. Synthesis of Folic acid Modified Oligonucleotide

Folic acid binding to 5'-aminohexyloligonucleotide was performed by applying the dicyclohexylcarbodiimide (DCC)/N-hydroxysuccinimide (NHS) chemistry. Activation of the carboxyl group of the folic acid was carried out in dimethylsulfoxide (DMSO) for 18 hours with stirring. After incubation, the side product of the activation reaction, DCU was removed by filtration and reaction mixture was added to the diethyl ether. The orange-yellow precipitate was filtered off and allowed to dry under vacuum and then reacted with 5'-aminohexyloligonucleotide. After the reaction, an ultracentrifuge column (MW 3000 Da) was used to remove unreacted chemicals and DMSO. Centrifugation was carried out for 45 minutes at 3800 rpm at room temperature.

3.3.4.3. Synthesis of RGD Modified Oligonucleotide

To RGD binding to oligonucleotide, carboxyl group of RGD peptide was activated. Activation was performed in DMSO for 18 hours with stirring After incubation, the side product of the activation reaction, DCU, was removed by filtration and reaction mixture was added to the diethyl ether. The orange-yellow precipitate was filtered off and allowed to dry under vacuum and then reacted with 5'-aminohexyloligonucleotide. After the reaction, an ultracentrifuge column (MW 3000 Da) was used to remove unreacted chemicals and DMSO. Centrifugation was carried out for 45 minutes at 3800 rpm at room temperature.

3.3.4.4. Synthesis of FAM Modified Oligonucleotides

FAM (25 mg) was incubated with 1-Ethyl-3-(3-dimethylaminopropyl)carbodiimide (EDC, 14 mg/mL) in dimethylsulfoxide (DMSO) for 4 hours. After 4.5 hour incubation, 15,5 mg EDC and 5'-amine-modified oligonucleotide (50 µM) was added into the reaction mixture and incubated for 18 hours at room temperature. After incubation, the reaction mixture was centrifuged with centrifugal filter (MWCO 3000) at 3500 rpm to remove DMSO and the chemicals except oligonucleotides.

3.3.5. Characterization of The Modified Oligonucleotides

Characterization studies of the modified oligonucleotides were carried out using the agarose gel electrophoresis, FT-IR and MALDI-TOF MS analysis.

3.3.5.1. Agarose Gel Electrophoresis

Agarose gel electrophoresis was performed to visualize the reaction products. The samples taken from the reaction mixtures were loaded to 2 per cent agarose gel which was prepared by dissolving in the TAE buffer solution. The products of the modification reactions were monitored using a gel imaging system (Bio-Rad, USA).

3.3.5.2. MALDI-TOF MS Analysis

MALDI-TOF MS analysis was also performed for the characterization of oligonucleotide modification reactions. 2,5-dihydroxybenzoic acid (DHB), α-cyano-4-hydroxycinnamic acid (CHCA), sinapinic acid (SA), and 3-Hydroxypicolinic acid (3-HPA) matrices were used for the analysis. In previous measurements, Bruker Daltonics Microflex mass spectrometer (Bremen, Germany) was used and mass spectra of the modified oligonucleotides were acquired in linear modes with average of 250 shots on a instrument, which equipped with a nitrogen UV-Laser operating at 337 nm. MALDI matrices and samples to be analyzed were dissolved in appropriate solvents and mixed together. For subsequent measurements, MALDI Synapt G2-Si High Definition Mass Spectrometry (Waters) was tried for the characterization of modified oligonucleotides.

3.3.5.3. FT-IR

Lyophilized modified oligonucleotide samples were also analyzed using a FT-IR instrument (Thermo NICOLET IS50, Massachusetts, USA) in attenuated total reflectance (ATR) mode.

3.3.6. Hybridization of The Modified Oligonucleotides to DNA Tile

The oligonucleotides modified with targeting agents were hybridized to the sticky ends of DNA tile in TAE/Mg^{2+} hybridization buffer with shaking at room temperature overnight.

3.3.7. Dox Intercalation to The DNA Tile

Dox intercalation was achieved by mixing Dox with DNA tile at room temperature overnight. The Dox-DNA tile complex formed during the incubation was centrifuged at the end of the incubation and obtained as red pellet. At the end of centrifugation, the remaining free Dox without binding was determined by reading the supernatant absorbance at 480 nm. After the removal of the supernatant, the Dox-DNA tile pellet was stored at +4 °C for later use. The red Dox-DNA tile pellet s were dissolved in the cell medium when used in the experiment.

3.3.8. Loading Efficiency of Dox

To calculate optimum Dox loading level, Dox solutions with different concentrations were prepared and incubated with DNA tile origami structure. Dox standart solutions were prepared from 2 mM Dox stock solution. Experiments were performed in triplicate.

3.3.9. Cell Culture Maintenance

MCF-7, HeLa, DU145, MDA-MB-231, PNT1A and A549 cells were cultured in Dulbecco's Modified Eagle's medium (with 4500 mg/L glucose, DMEM-HG) supplemented with 10 per cent FBS, 100 unit/mL penicillin, and 100 μg/mL streptomycin solutions. All the cells were cultured in 25 or 75 cm^2 flasks to ~ 80 per cent confluency and incubated at 37 $^\circ$C under 5 per cent CO_2 atmosphere. LNCaP cells are cultured in RPMI-1640 medium supplemented with 10 per cent FBS at 37 °C under 5 per cent CO_2 atmosphere.

When the cells reached 80 per cent confluency, they were continued by passaging. First, culture medium was removed and the cell layer was washed with 1XPBS solution. After washing with 1XPBS solution, 0.25 per cent trypsin (w/v) - 0.53 mM EDTA was added to the flask and waited until the cell layer was detached at 37 °C under 5 per cent CO_2 atmosphere. Trypsin activity was terminated by the addition of the cell medium. Cell suspension was transferred to the centrifuge tube and the cells were collected with centrifugation at 1500 rpm for 5 minutes at room temperature. After centrifugation, trypsin containing supernatant was removed and the cells were dispersed in fresh cell medium. Aliquot of the cell suspension were added into the culture flask and cells were incubated at 37 °C under 5 per cent CO_2 atmosphere.

3.3.10. Cytotoxicity Assay

The cytotoxicity analysis was performed applying WST-1 assay according to manufacturer's instructions. Analysis was carried out by the incubation of the cells cultured at a density of 10.000 cells per well with DNA tile and free Dox samples. After 24 hours incubation, cell medium was removed and WST-1 reagent (10 µL) containing fresh cell medium was added to the cells. Cells were incubated for 1 hour at 37 °C in a humidified atmosphere under 5 per cent CO_2. At the end of incubation, the absorbance values of the control and treatment samples at 450 nm were measured using a microplate reader (BIO-TEK ELX800, USA). KCjunior software (Winooski, VT) was used for the data analysis.

3.3.11. Cellular Uptake of The DNA Tiles

3.3.11.1. Cellular Internalization of DNA Tile

The cellular internalization of DNA tile structures were investigated using 5(6)-carboxyfluorescein (FAM) dye. BT-474 cells were seeded onto cover slips at the density of 150.000 cells/slip. After the 24-hours of the attachment, cells were incubated with free doxorubicin, 5(6)-FAM, 5(6)-FAM-DNA tile and 5(6)-FAM-Dox-DNA tile structures for 24 hours at 37 °C and 5 per cent CO_2. After the incubation, cells were washed with 10 per cent PBS solution three times and fixation was performed with 2 per cent

paraformaldehyde solution at 4°C for 30 minutes, than the treated cells were visualized using a confocal laser scanning microscope (Leica).

3.3.11.2. Fluorescence Spectroscopy

Cellular uptake of Dox was determined using fluorescence spectroscopy. At a density of 200,000 seeded cells were incubated with free drug and drug loaded modified / unmodified DNA tile samples (2 μM final Dox concentration). At the end of the incubation, the cell media were removed and the cells were washed with PBS. The cells were harvested and harvested cells were incubated at 4 °C for 15 minutes with lysis buffer. Quantities of Dox contents in PBS-added cell lysates were determined at 480 nm excitation wavelength using fluorescence spectroscopy.

3.3.11.3. Flow Cytometry

Levels of Dox in cells were also examined using flow cytometry. Cells were seeded into the 6 well plates at the density of 100.000 cells/well. At a density of 100,000 seeded cells were incubated with free Dox and Dox loaded modified/unmodified DNA tile samples (2 μM final doxorubicin concentration). After incubation, the cell media were removed and the cells were washed with PBS. The cells were harvested and harvested cells were resuspended in PBS solution. FACSCalibur flow cytometer (BD BIOScience, 342975, USA) was used for the analyses.

3.3.11.4. Confocal Microscopy

Intracellular localization of Dox in cells treated with Dox samples (2 μM final Dox concentration) was monitored using confocal microscopy. Cells in the coverslips (100,000 cells/slip) incubated with Dox samples were examined using confocal laser scanning microscope (Leica) after fixation.

3.3.12. Internalization Experiments with Inhibitors

Investigation of uptake way of the DNA tile structures was investigated using sodium azide (NaN$_3$, 3 mg/ml), chlorpromazine (15 µg/mL), nocadazole (50 µg/mL), cytochalasin B (1 µg/mL) and carbohydrate-based inhibitors (0.2 M). Cells were seeded in 6-well plates at a density of 100.000 cells/well and incubated with FBS free cell medium containing inhibitors for 30 minutes at 37°C in a 5 per cent CO$_2$ atmosphere. After treatment with inhibitors, old cell medium was removed and cells were incubated with fresh cell medium containing doxorubicin samples for two hours at 37°C in a 5 per cent CO$_2$ atmosphere. After incubation, doxorubicin levels of cells were determined using fluorescence spectroscopy as described in section 3.3.11.2.

3.3.13. Cell Cycle Analysis

U87 and HeLa cells were seeded in a 6-well plates at a density of 50.000 cells and incubated at 37 °C in humidifed atmosphere under 5 per cent CO$_2$ for 24 hours. After the cell attachment, cells were incubated with the Dox loaded DNA tile structures (with/without modifications) in DMEM High glucose (4.5 g/L) medium for 24 hours. At the end of incubation, cell medium was removed and cell layers were rinsed with 1X Phosphate-buffered saline (PBS) solution. 2-3 ml of trypsin-EDTA solution was added and waited until the cell layer was dispersed (5 minutes at 37 °C). Trypsin activity was terminated by the addition of the growth medium of the cells. The detached cells were transferred to the centrifuge tubes and cells were collected with centrifugation at 1500 rpm for 5 minutes at room temperature. Cells were washed with 1XPBS solution and centrifuged at 1500 rpm for 5 minutes. After centrifugation, cell pellet was re-suspended in 300 µL PBS solution and placed on ice. 700 µL ethanol was added to the each micro centrifuge tube and gently mixed. Cells were incubated at -20 °C for two hours. After incubation, cells were centrifuged and supernatant was removed. Cells were incubated with RNAse (100 µg/ml) solution for 1 hour and centrifuged at 2200 rpm for 5 minutes at + 4 °C. Propidium iodide staining was carried out for 15 minutes and flow cytometric analysis of the cell cycle process was performed.

3.3.14. Western Blot Analysis

Luciferase expressing MDA-MB-231 cells were seeded in a 6-well plates at a density of 150.000 cells and incubated at 37 °C in humidified atmosphere under 5 per cent CO_2 for 24 hours. After the cell attachment, cells were incubated with the morpholino containing DNA tile structures in FBS free DMEM High glucose (4.5 g/L) medium for 4 hours. At the end of incubation, DMEM high glucose medium containing FBS (10 per cent) was added to the cells and cells were incubated at 37 °C in humidifed atmosphere under 5 per cent CO_2 for 48 hours. After incubation, cells were washed with 1XPBS solution and centrifuged at 1500 rpm for 5 minutes. After centrifugation, cells were dissolved in RIPA buffer containing protease inhibitors and centrifuged at 14000 rpm for 10 minutes to obtain cell lysate. Supernatants were transferred to the new microcentrifuge tubes and protein contents of the cells were determined using Bradford assay [234]. Cell lysate samples containing 35 µg protein were run on SDS-PAGE to monitor luciferase expression levels of the samples. After running on SDS-PAGE, proteins were transferred to PVDF membranes and incubated with blocking solution, which contains 3 per cent BSA in TBS-T buffer. Blocking was performed at room temperature for 1 hour and then membrane was incubated with the anti-Firefly Luciferase antibody (abcam, ab181640) in TBS-T at 4 °C overnight. GAPDH expression levels of the samples were used as controls for the proper protein loading. The western blotting images were taken using a ChemiDoc MP imaging system (BioRad, USA).

3.3.15. Preparation of The Luciferase Expressing Cell Line

3.3.15.1. Transformation of The pGL4.10.[luc2] Vector into The E.coli DH5α Cells and Amplification of The pGL4.10.[luc2] Vector

Amplification of the pGL4.10.[luc2] vector purchased commercially, was performed by transformation into *E. coli* vector DH5α cells. The competent DH5α *E.coli* cells were thawed on ice and incubated with pGL4.10.[luc2] vector for 30 minutes. After incubation, cells were incubated at 42 °Cin water bath for 45 seconds and then put again on ice. Cells were shaken in the incubator at 37 °C at 180 rpm for an hour with addition of 200 µL of

LB medium. At the end of the incubation, bacterial cells were cultivated on LB agar petri dishes and incubated at 37 °C for 18 hours. After overnight growth on 1.5 per cent agar with 100 µg ampicillin/mL, colonies were picked out and grown in Luria-Bertani medium (LB, 10 g/L peptone, 5 g/L yeast extract, and 10 g/L sodium chloride) with 100 µg ampicillin/mL. The next day, single colonies, taken from ampicillin LB agar dishes, were amplified in LB medium in the shaking incubator at 180 rpm at 37 °C for 18 hours. After cultivation, cells were collected by centrifugation at 10000 rpm (+4 °C). pGL4.10.[luc2] vector was isolated from the collected cell pellets using the Invitrogen PureLink Quick Plasmid Miniprep isolation kit accordance with the manufacturer's instructions.

3.3.15.2. Amplification of The pLenti-Bi-cistronic Vector

E.coli DH5α cells which were taken from -20 °C stock and containing pLenti-Bi cistronic vector were amplified in LB medium at 37 °C at 180 rpm. After cultivation, cells were collected by centrifugation at 10000 rpm (+4 °C). pLenti-Bi-cistronic vector was isolated from the collected cell pellets using Invitrogen PureLink Quick Plasmid Miniprep isolation kit accordance with the manufacturer's instructions.

3.3.15.3. Amplification of The CMV VSV-G and Delta VPR Plasmids

CMV VSV-G packaging and Delta VPR envelope plasmids were amplified following the procedure given in section 2.10.2.

3.3.15.4. Digestion of The pLenti-Bi-cistronic and pGL4.10.[luc2] Vectors

Plasmids pLenti-Bi-cistronic (2 µg) and pGL4.10.[luc2] (2 µg) were digested using BamHI (NEB, 1 µL) ve KpnI (NEB, 1 µL) restriction endonuclease enzymes in CutSmart buffer (NEB, 10 µL). Digestion reactions were performed at 37°C for an hour with 100 µL final volume. The digestion products of the pLenti-Bi-cistronic and pGL4.10.[luc2] vectors were separated by gel electrophoresis on 1% agarose.

3.3.15.5. *Recovery of The Digestion Products of The pLenti-Bi-cistronic and pGL4.10.[luc2] Vectors*

Digestion products of pLenti-Bi-cistronic and pGL4.10.[luc2] cut from the agarose gel and purified according to manufacturer's instructions using the Invitrogen PureLink Quick Gel Extraction kit.

3.3.15.6. *Ligation of The Digestion Products*

After the vector and insert DNA have been prepared for ligation, 1:1, 1:3, and 1:5 vector:insert DNA ratios in order to find the optimum ratio were tested. The ligation of digested bands were performed in 20 µL final volume using T4 DNA ligase (1 µL), pLenti-Bi-cistronic vector (3 µL), pGL4.10.[luc2] vector (1.2, 3.6, and 6 µL; varying amounts of insert), ligation buffer (2 µL), and deionized water (nuclease free) at 22 °C for 18 hours. At the end of incubation, mixtures of ligation reactions were stopped by incubating at 65 °C for 10 minutes. Ligation mixtures in various vector:insert ratios were transformed into *E.coli* DH5α as indicated in section 3.3.15.1.1. After transformation, bacterial cells were cultivated on LB agar petri dishes (1.5 per cent agar with 30 µg kanamycin/mL) and incubated at 37 °C for 18 hours. The next day, the success of the ligations was observed by formation of colonies on LB agar petri dishes (1.5 per cent agar with 30 µg kanamycin/mL).

3.3.15.7. *Amplification of The pLenti-Bi-cistronic-[luc2] Ligation Vector*

The single colonies, taken from LB agar dishes (1.5 per cent agar with 30 µg kanamycin/mL), were amplified in LB medium in the shaking incubator at 180 rpm at 37 °C for 18 hours. After cultivation, cells were collected by centrifugation at 10000 rpm (+4 °C). pLenti-Bi-cistronic-[luc2] vector was isolated from the collected cell pellets using the Invitrogen PureLink Quick Plasmid Miniprep isolation kit accordance with the manufacturer's instructions.

3.3.15.8. Lentivirus Transfection and Infection Method

pLenti-bicistronic-[luc2] vector containing the gene sequence coding for the expression of luciferase was transfected into HEK293T cells using the triple plasmid packaging system. Transfection was performed using packaging plasmid (Delta VP), envelope plasmid (VSV-G), $CaCl_2$ (2 M), and 2xHBS (Hepes Buffer Saline) buffer solution. Transfection was supplemented with sodium butyrate and viral constructs were collected in the following days. The viral structures filtered with 45 µM filter and stored at -80 °C. The viral structures which were stored in -80 ° C were concentrated by centrifugation at 24,000 rpm for 2 hours at 4 °C. The virus structures were giving the LNCaP and MDA-MB-231 cells containing polybrene (4 mg/ml) in 6 well plates and cultured under the humidified atmosphere (37°C, 5 per cent CO_2) for 24 hours. Antibiotic selection was performed by addition of puromycin (1 mg/ml) to the cells after two days. Two weeks after the addition of puromycin, antibiotic selection was completed. After the antibiotic selection, cells were grown to the next passage and cultured.

4. RESULTS AND DISCUSSION

4.1. FORMATION AND CHARACTERIZATION OF DNA TILE

DNA origami structures are constructed using a variety of methods such as the scaffolded or multistranded approach, as mentioned earlier in Section 2.3 [27, 28]. In the DNA origami approach revealed by Rothemund, a long single-stranded viral DNA is used as a scaffold strain and the formation of DNA origami structures in the desired shape and size has been accomplished through the folding of the long scaffold strain with the aid of multiple short helper chains [13]. To prepare large and complex origami structures, the scaffolded approach, which allows the desired structures to be constructed with high efficiency, is generally preferred [28].

The construction of DNA origami structures is generally carried out applying the slowly cooling method in specific hybridization buffers. This method also called thermal annealing is often preferred for the successful folding of DNA origami structures [235]. In the slowly cooling process, the oligonucleotides that will form the origami structure are added to the hybridization solution at specific concentrations and the hybridization mixture containing oligonucleotides is heated to 95 °C and then slowly cooled to reach the designed structure with the minimum energy configuration [235]. During this process the oligonucleotides find the complementary sequence, annealing occurs, and the structure desired to be formed is folded into the most stable shape.

The buffer solution system used is also important for the origami formation. TAE buffer solution containing Mg^{2+} (TAE-Mg^{2+}) is frequently used as a hybridization solution for the origami formation. The hybridization efficiency for an optimized structure can be achieved by changing the concentrations of the buffer components. Mg^{2+} ions are added into the hybridization buffer solution to mask electrostatic charges between neighboring double strands [19]. If a buffer system is not suitable, deformations may occur in the targeted structure leading to the loss of integrity of the structure completely.

In this thesis, a DNA nanostructure in the form of a tile, which can be used for the transport of drugs and other therapeutics, was built by the scaffolded approach applying the

slowly cooling procedure in the TAE-Mg^{2+} buffer solution. The DNA tile structure to be prepared consists of nine oligonucleotides, which are complementary to each other at various points and composed of 36 to 140 bases. The arrangement of these oligonucleotides to form the DNA tile is shown in Figure 4.1.
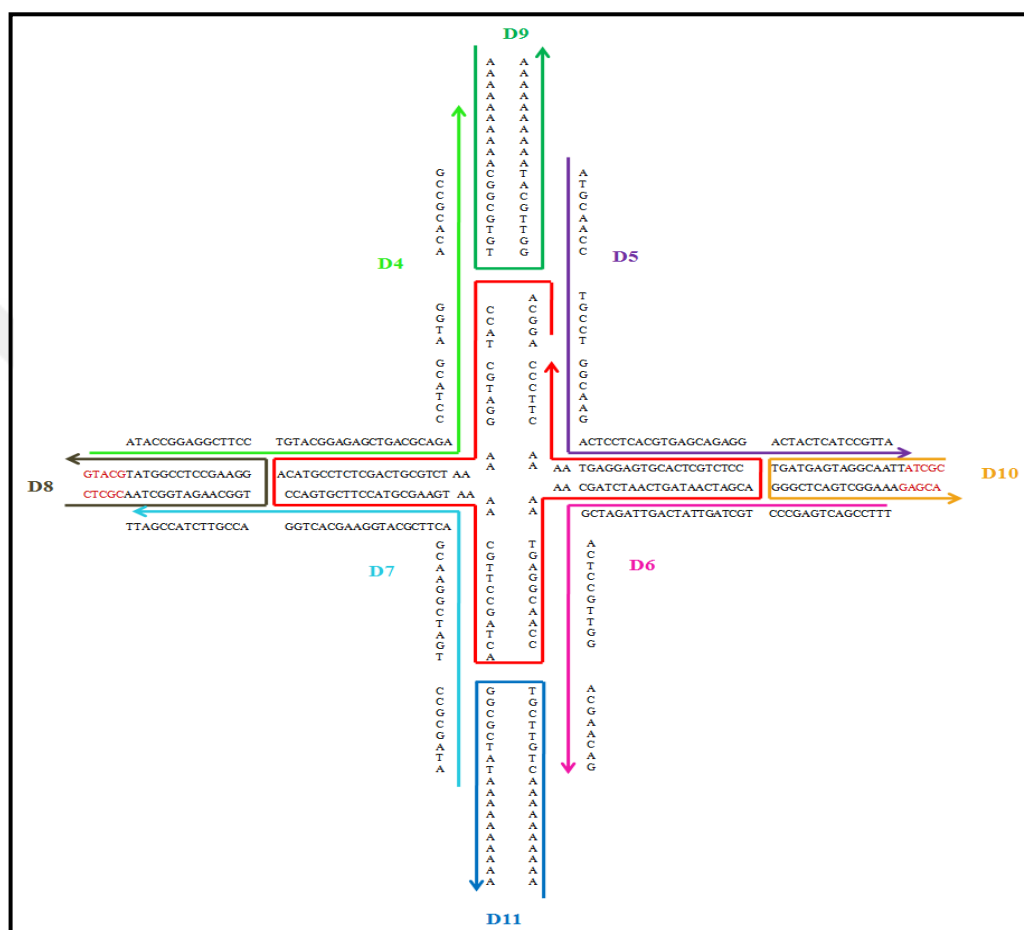
Figure 4.1. The DNA tile structure

To form the DNA tile construct, these oligonucleotides were added at 1 μM concentration to the TAE-Mg^{2+} buffer solution. The hybridization solution containing the oligonucleotide mixture was placed in a water bath heated at 95 °C. The water bath was isolated from the outside to prevent heat loss, which could cause sudden cooling. In this way, the cooling process has been extended to 24 hours. The hybridization solution containing the oligonucleotides was cooled to the room temperature for 24 hours. During this process, the oligonucleotide consisting of 140 bases folded with the aid of the short eight helper oligonucleotides to form the tile-shaped DNA structure, which has eight adhesive oligonucleotide sequences, allowing the attachment of modified oligonucleotides for

different applications, is obtained. The hybridization solution containing the newly formed DNA tile was stored at +4 °C for later use and characterization.

The characterization of DNA origami structures is generally carried out using microscopic and electrophoretic techniques [13, 20, 24, 50, 53, 235-242]. Agarose or polyacrylamide gel electrophoresis [20, 236, 237, 242], atomic force microscopy (AFM) [13, 20, 53, 240, 243], and transmission electron microscopy (TEM) [235, 238, 239, 242] are the common techniques applied for the characterization of the DNA constructs. A very detailed structural information can be obtained with these techniques. However, each technique has its own shortcomings and may not provide sufficient structural information [244]. The images obtained with AFM and TEM are important for the characterization of DNA based structures. However, these techniques do not have the resolution that can show the errors and gaps in DNA structure at base pair level and the necessity of fixing the structures on a surface during the analysis is a disadvantage [244]. It is also known that the some techniques exhibit disadvantages such as damaging the structural integrity of the DNA structures studied [13, 239, 240] and the sample requirements at high concentration and volume [24, 50, 241, 244]. Dynamic light scattering (DLS) [24, 50, 241] and fluorescence spectroscopy [26, 245-247] are also applied for the characterization of DNA based structures. However, both thechniques require high volume and concentration. Cryo-electron microscopy, which allows analysis of 3D materials, is also among the techniques that can be applied for the characterization of DNA constructs without staining or fixation [26, 248]. In this thesis, AFM, Agarose Gel Electrophoresis and DLS are the techniques used for the chracterization of the constructured structures in a suspension.

4.1.1. Agarose Gel Electrophoresis

As mentioned above, one of the most widely used DNA characterization techniques is gel electrophoresis, which is based on electrophoretic mobility of DNA fragments on polyacrylamide or agarose gel of the DNA constructs [244]. The gel electrophoresis is a technique that can be easily performed in any laboratory environment without the need for extra purification steps with a relatively small sample amount. The use of polyacrylamide gel or agarose gel electrophoresis is preferred by researchers in order to give a quick statement of the degree of DNA structure formation [20, 236]. Depending on the size of

the DNA constructs, the mobility to be exhibited on the gel will be different and this allows the separation of the DNA constructs. The gel density used in electrophoresis is selected depending on the size of the DNA structure to be investigated. For very large DNA constructs, 0.3-1% [249] and for smaller constructs 1.5-3% [34, 250] agarose gel is prepared.

The DNA tile formation, which carried out in TAE/Mg^{2+} buffer, was monitored using agarose gel electrophoresis. Figure 4.2 shows the agarose gel image indicating the formation of the DNA tile structure. Agarose gel at a density of 2 per cent was used to visualize the formation of the DNA tile structure. To demonstrate the formation of the DNA tile structure, each oligonucleotide, which is a part of the tile structure, was sequentially added into the hybridization buffer. In the agarose gel electrophoresis image given in Figure 4.2, the line 1 indicates the hybridization mixture containing a single oligonucleotide sequence and the line 3, 5, and 9 indicates the hybridization mixtures containing three, five, and nine oligonucleotide sequences, respectively. In the figure, with the sequential addition of the each oligonucleotide, it is seen that the oligonucleotides are gradually hybridized to their complementary sequence and the formation of the tile structure takes place in a controlled manner as indicated by the larger spot size.
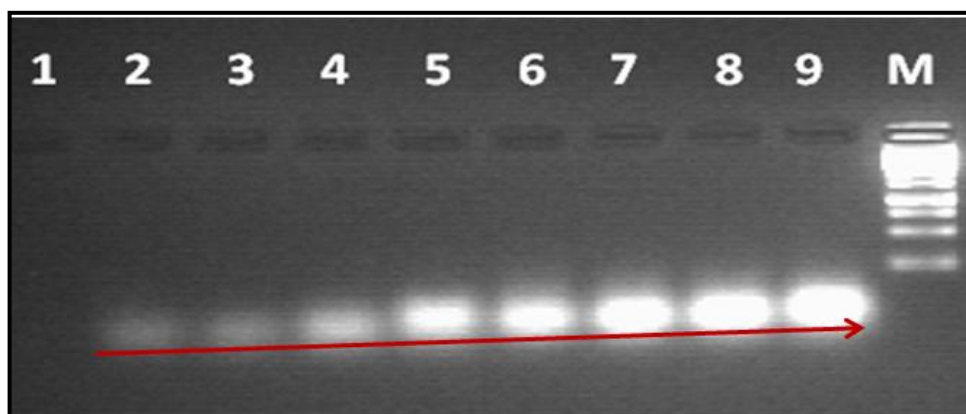
Figure 4.2. Agarose gel image of the DNA tile formation

As mentioned earlier, the tile formation was also carried out in a solution containing only Mg^{2+} ions. It was observed that the tile formation in the solution containing 12.5 mM Mg^{2+} was also successful. The agarose gel image belongs to the tile formation attempts performed in TAE/Mg^{2+} and Mg^{2+} solutions is provided in Figure 4.3. According to the gel electrophoresis image, the experiment carried out in the solution containing only Mg^{2+} ions

shown that Mg^{2+} ions provide the necessary conditions for the tile formation. However, the construct was formed with this solution will lack the buffering activity and resistance to the nuclease activity. It is important to use EDTA, which inhibits the activity of nucleases by making chelates with the bivalent cations required for the activity of the nucleases [251], to protect newly formed DNA constructs in the hybridization solution. The use of Tris-base is also obligatory for ensuring the buffering effect which is also important for subsequent applications. Due to these reasons, the use of TAE/Mg^{2+} buffer solution will be more advantageous because of the properties, which it provides, beside the solution containing only Mg^{2+}.
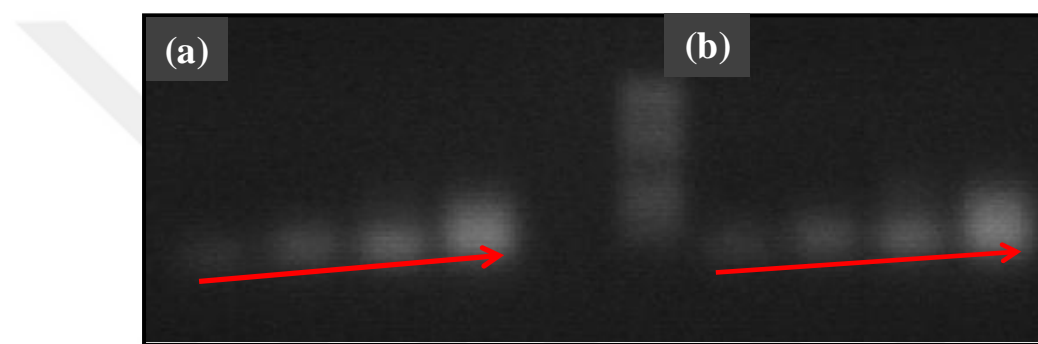
Figure 4.3. Comparison of tile formation in different buffer solutions. (a) in TAE/Mg^{2+} and (b) only Mg^{2+} solution.

4.1.2. Atomic Force Microscopy (AFM) Analysis

Atomic force microscopy is one of the most preferred techniques for the origami characterization [244]. AFM analysis, which enables DNA structures to be visualized at a resolution range of 5-5000 nm, allows for population analysis of the DNA structures examined [244]. In AFM analyses, information is collected by sensing the surface topography of a sample using a mechanical tip. However, in the analysis of 3D materials, anhydrous imaging conditions and the force of the microscopic cantilever can cause the deterioration of the image of a structure [24].

The AFM analysis was performed at non-contact mode to determine the size of the consructed tile structures and support to the observations with agarose gel electrophoresis. 2 μL of the DNA tile containing suspension was dropped onto a newly cut mica surface and allowed to dry. The droplet area on mica was imaged.

The theoretical dimentions of double helix DNA, the theoretical dimension of a DNA tile structure aimed to prepare in this thesis, and a AFM image of a droplet area on a mica surface are given in Figure 4.4. The designed DNA tile structure contains 85 bases from one end to the other. The theoretical distance between two DNA bases in the DNA helix is 0.34 nm. In the light of this information, the theoretical size of the DNA tile should be around 29 nm. On the AFM image, bright spots are the DNA tile structures and it is seen that the majority of the structures are around approximately 64 nm.

As seen in Figure 4.4, the consistent results with the theoretical values were obtained but some structures are higher than the theoretical ones. During the sample preparation for AFM analysis (drying on the mica surface), aggregation of the DNA tile structures lead us to see bigger particles than the expected size. The presence of incomplete DNA constructs and non-hybridizable oligonucleotides also led to the observation of smaller-sized structures.
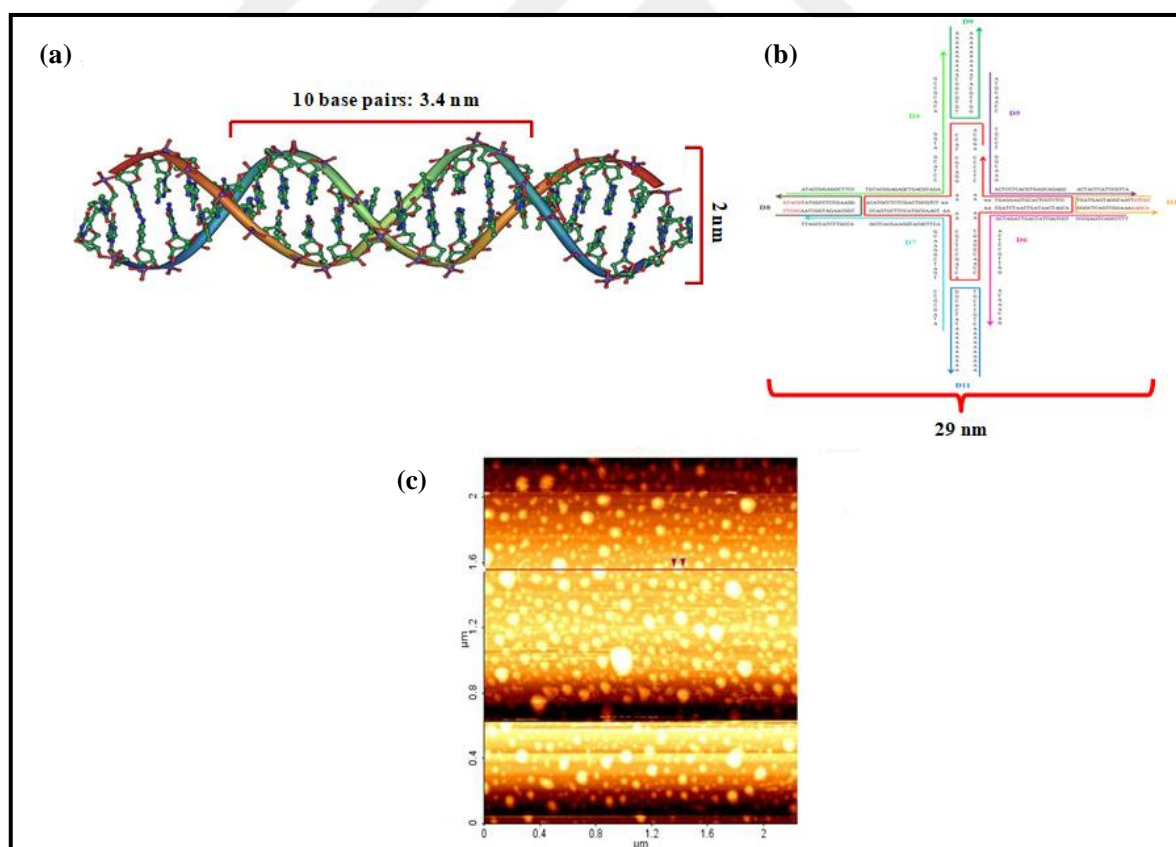
Figure 4.4. The theoretical distance between DNA bases (a), the theoretical dimension of DNA tile structure with schematic representation (b), and the AFM image of the DNA tile (Scanning area: 2x2 μm^2) (c).

4.1.3. Dynamic Light Scattering (DLS) Analysis of The DNA Tiles

Dynamic light scattering (DLS), which measures the Brownian motion of particles in a suspension, relates this movement of particles to an equivalent hydrodynamic diameter and it is often used in nanoparticle characterization [252]. The determination of the particle size is carried out taking advantage of the fluctuations on the light intensities scattered by the Brownian motion of the particles. The technique, which require high concentration and sample volume, is also used in the characterization of DNA based nanostructures [24, 50, 241].

The DNA tile structure was also characterized using DLS. Figure 4.5 shows the hydrodynamic size distribution of the DNA tile structure in its suspension obtained from a DLS measurement. The hydrodynamic size of the DNA tile structures found as approximately 60 nm, which is compareable to AFM analysis. The hydration layer surrounding the tile structure in the aqueous solution causes the analysis results to yield a larger than the expected results for the DNA tile structure.
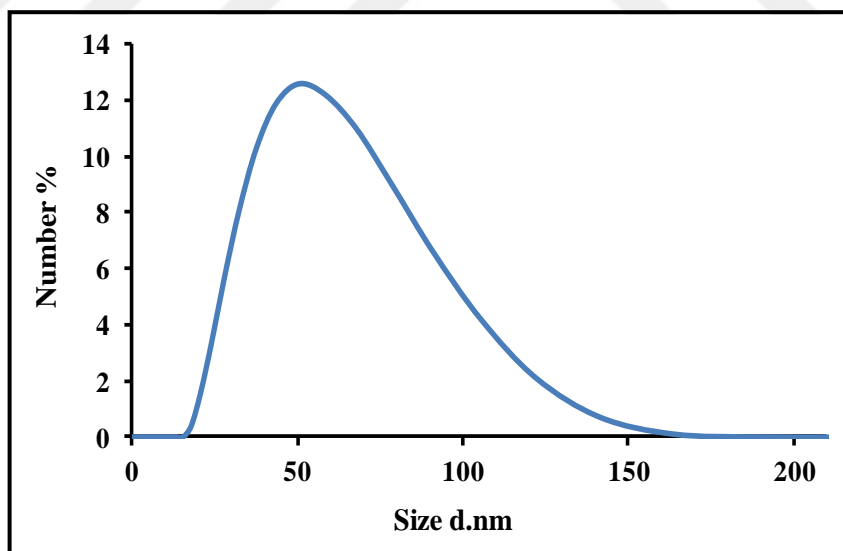
Figure 4.5. The hydrodynamic size distribution of the DNA tile

4.1.4. Stability of DNA Tile Structure

The most important problem that can be encountered in the DNA nanotechnology approach is the preservation of DNA based structures stability. DNA and RNA constructs

are open to degradation by endo- and exonuclease enzymes. This is an important challange to overcome for their *in vivo* and *in vitro* applications. The modifications, which protect such structures from nuclease activity and maintain their stability without disrupting the structure and interaction properties *in vivo*/*in vitro* applications, were extensively investigated [253-258]. The modifications at ends performed on single-stranded DNA strands contribute to the preservation of stability [259]. In this sense, there are studies showing that DNA origami structures behave differently from single-stranded double-stranded DNA constructs to nuclease attacks [242, 260]. DNA origami structures can generally maintain their integrity in ambient conditions as demonstrated in previous studies [259, 261, 262]. In a study by Mei et al., it was reported that DNA origami structures retained their stability in environments such as cell lysate unlike double-stranded DNA [262]. They showed that DNA origami structure, which maintains stability at room temperature, retains structural integrity in experiments performed with cell lysates obtained from healthy and cancer cells.

Wang et al. reported that when studying the stability of tubular DNA origami structure under different ambient conditions, the tubular DNA origami was stable between pH 5-10 and buffer solution changes such as pH and concentration did not harm the origami structure [263]. They also found that the presence of alcohol compounds such as ethanol in the environment did not interfere with the origami structure. When the effect of salt concentration on origami structure was investigated, it was seen that origami structure retained its structure in up to 3 M NaCl solution and an aggregation was observed at 4 M.

In this thesis, the stability analysis of the DNA tile was performed by incubating the DNA tile structures in fresh cell media or supernatants of cell culture for a certain period of time. After the incubation, the samples containing the control groups were loaded into two per cent agarose gel to examine whether they retained their integrity. Figure 4.6 shows the agarose gel electrophoresis image. As seen in Figure 4.6, the bands remain intact and there is not smearing suggesting that the DNA tile constructs retained their stability by preserving their size for 24 hours.
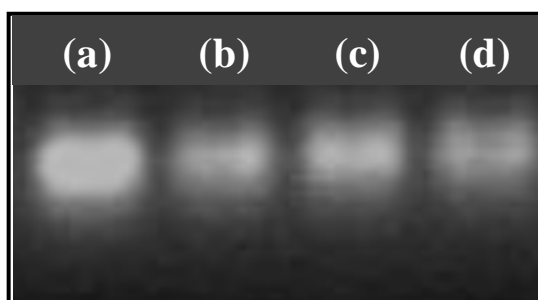
Figure 4.6. Gel electrophoresis image showing stability samples of DNA tile in the cell medium. (a) Control group, (b) 4 hours, (c) 8 hours, and (d) 24 hours sample.

DNA tile structure was also incubated with a medium containing cells, which was obtained from the supernatants of cells cultured. The examination of the stability of the DNA tile construct in the cell lysate may provide insight into the robustness of the construct prepared for *in vivo* applications. Figure 4.7 shows the agarose gel electrophoresis image of the DNA tile samples incubated in cell lysates. According to the image, tile samples found as stable for 6 hours in cell lysates. It was previously reported that the DNA nanostructures, which have more complex structural design and modified at several sites, were found to be more stable in environments such as cell lysates for longer periods [242, 262]. In the direction of the obtained results, it can be possible to perform various modifications to improve the stability of the DNA carrier for *in vivo* applications [253, 264-271]. The modifications performed in the phosphodiester bond [266, 267], sugar moiety [270, 271], and the terminal sites, particularly at the 3 'end [264, 268, 269], will provide resistance to nuclease activity and thus allows the retention of more stable DNA nanostructures *in vivo* conditions.
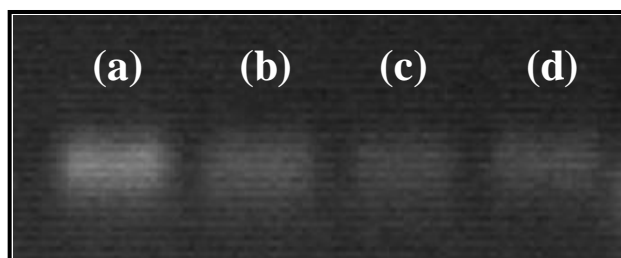
Figure 4.7. Gel electrophoresis image showing stability samples of DNA tile the in cell lysate. (a) Control group, (b) 2 hours, (c) 4 hours, and (d) 6 hours sample.

4.2. DOXORUBICIN INTERCALATION AND LOADING EFFICIENCY

As noted in Section 2.6.3, the delivery of Dox, a drug with a high toxicicity, using various nanostructures to diminish the adverse side effects and enhance cellular uptake has been investigated in many studies [215]. Dox is an anthracycline-type drug that can intercalate into the DNA [272]. Intercalation capability of Dox allows the loading of Dox into DNA-based carriers without complex reactions. Intercalation of Dox with the DNA based carrier systems, such as triangle, tube and aptamer conjugated DNA icosa has also been carried out [43, 272, 273]. In this thesis, Dox was intercalated into the DNA tile. Intercalation of Dox into the DNA tile structure was accomplished by overnight incubation of Dox with the DNA tile structure. When Dox was incubated with the DNA tile, DNA tile-Dox conjugate formed. The DNA tile-Dox conjugate was obtained as a red precipitate by centrifuging the incubation mixture and the amount of Dox intercalated into the DNA structure was calculated based on the amount of the free Dox remained in the incubation solution.

UV/Vis spectroscopy is often used to examine the interaction of nucleic acids with a variety of molecules including drugs [274]. UV-Vis spectrum of the free Dox and the DNA tile-Dox conjugates is shown in Figure 4.8. The interactions between DNA and the molecules containing chromophore groups can lead to changes in their absorption spectra, and these observed spectral changes can give information about the nature of the interaction [275]. The interaction between DNA and drug molecules can result in red shift/blue shifts and hyper/hypochromic effects [275, 276]. As seen in Figure 4.8, the max absorbance of free Dox solution is at 480 nm while doxorubicin-DNA tile-Dox conjugate has an absorbance at 496 nm. The distance between the intercalating molecule and the bases in the helix leads to the observation of spectral changes. A red shift with the decreasing absorption intensities is usually related to the intercalation involving DNA bases [277]. The coupling of π electrons of Dox and DNA and the interaction of empty π^* orbitals of the Dox with the π orbital of DNA bases cause the decrease in the π- π^* transition energy and a red shift occurs [278]. The decrease in intensity after intercalation has also been observed in fluorescence spectroscopy analysis of such molecules having a fluorophore [278, 279].
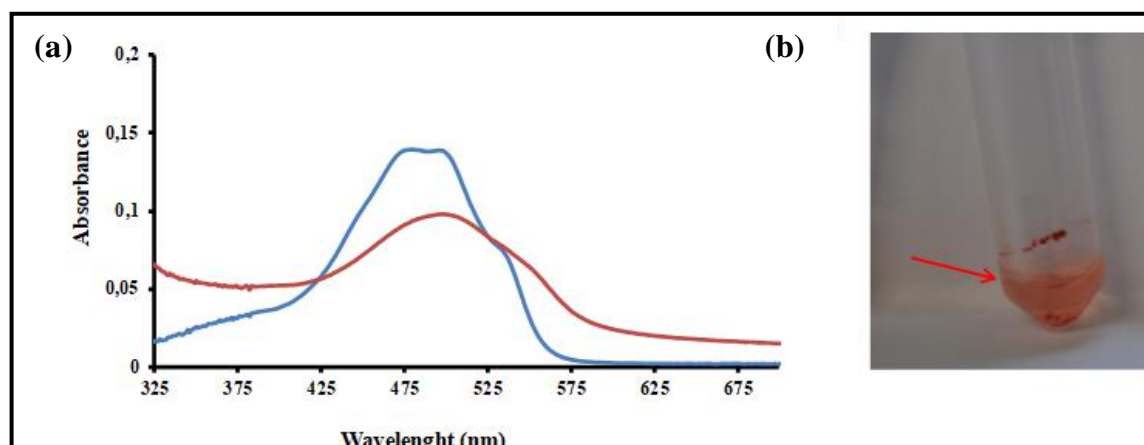
Figure 4.8. UV-visible absorption spectra of free Dox (blue line) and DNA tile-Dox complex (red line) (a) and red DNA tile-Dox precipitate (b).

Next, the doxorubicin loading efficiency was studied. For this, at a fixed doxorubicin concentration and increasing DNA tile concentrations, doxorubicin loading efficiency was determined using UV-Vis spectroscopy.

Figure 4.9 shows the doxorubicin loading efficiency with increasing DNA tile concentration obtained with UV-Vis spectroscopy. The initial doxorubicin concentration was determined as 80 µM. The origami concentration was measured as 138 ng/µL using nanodrop, which is a compact spectrophotometer that performs accurate and reproducible measurements.

In the experiment, the DNA tile structure in the range of 3.46-420,76 ng/µL was incubated in TAE buffer solution with 80 µM Dox. The DNA tile-Dox conjugate, which formed at the end of the incubation, was precipitated and the loading efficiency of Dox with increasing DNA tile construct amount was determined by UV-Vis spectroscopy at 480 nm. As seen in Figure 4.9, there is an increasing trend with the increased origami amount indicating that more Dox intercalates into the DNA tile structure.
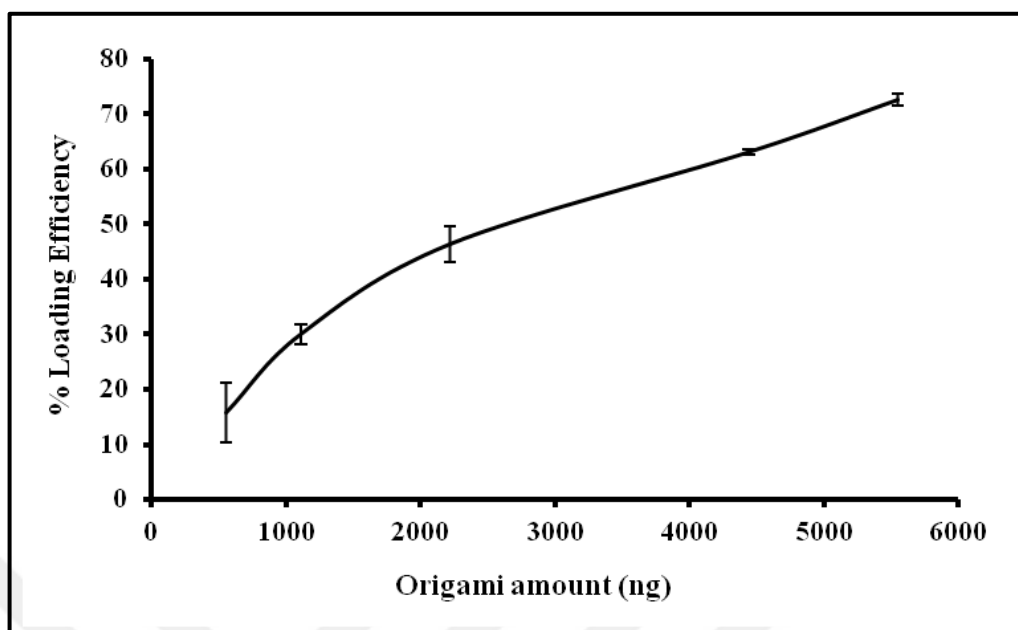
Figure 4.9. Dox loading efficiency with increasing DNA tile amount

In the second experiment to determine the Dox loading capacity of the DNA tile constructs, a constant amount of the DNA tile was incubated with the increasing concentrations of Dox. Figure 4.10 shows the Dox loading efficiency with increasing Dox amount. As shown in Figure 4.10, as the Dox concentration is increased, the number of Dox molecules intercalating into the DNA tile structure increases until a concentration around 100 μM. Then, the number of Dox intercalated decreases with the increasing concentration.

This observation brings the integrity of the origami structure into question. Thus, the stability of the DNA tile at increased Dox was investigated. It was found that the tile structure was disassembled after 300 μM of Dox concentration, which explains the observed absorbance decrease of DNA-Dox adduct at the concentrations higher than 100 μM. The experiments supporting this statement are presented in the text section. Another reason for the decreased in loading efficiency could be released Dox from the tile structure as a result of neutralization of DNA structure as Dox binds electrostatically, which is thought to be the first step of the intercalation [280].
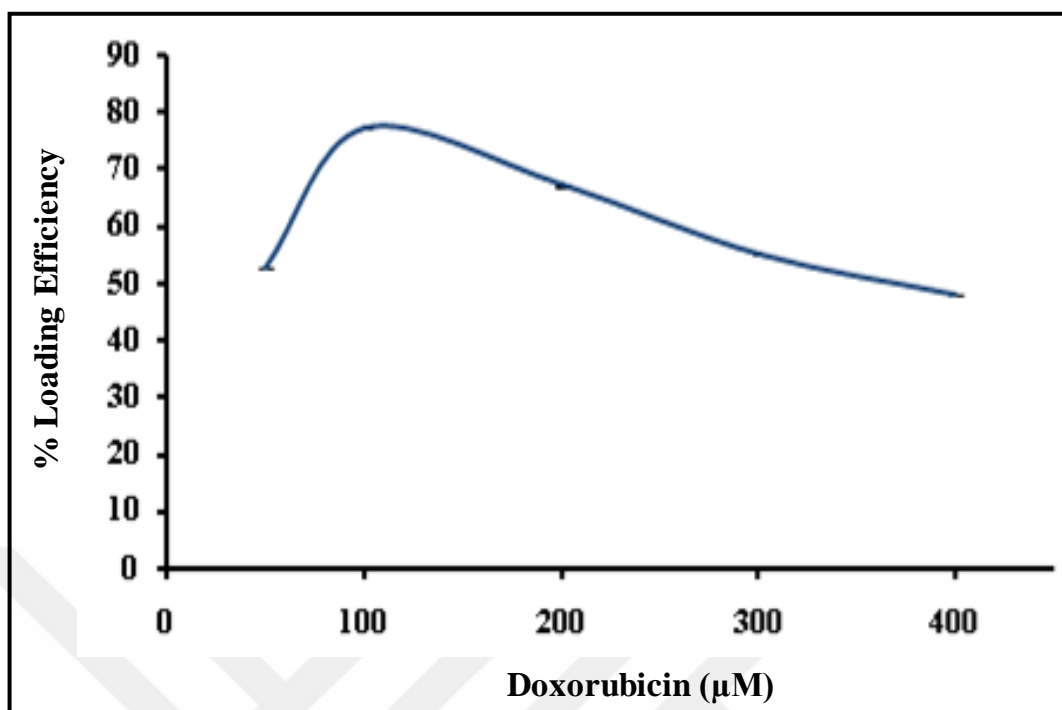
Figure 4.10. Dox loading efficiency with increasing Dox concentrations

4.3. STABILITY OF DNA TILES AT INCREASING CONCENTRATIONS OF DOXORUBICIN

The constructs can be destabilized when they are loaded with Dox. Thus, their stability after the loading was studied to assure that they could be used for the delivery purpose. The stability of the DNA tile structure was determined using agarose gel electrophoresis at increasing concentrations of Dox. DNA tile constructs were incubated with Dox for 24 hours in the range of 200-500 μM. After incubation, the DNA tile-Dox structure recovered from the incubation medium by centrifugation and was loaded on a 2 per cent agarose gel to observe possible changes in DNA tile structure. Figure 4.11 shows the agarose gel images of DNA tile constructs incubated with Dox at high concentrations. According to the agarose gel image given in Figure 4.11, the concentrations of Dox greater than 300 μM caused deterioration of the DNA tile structure. At concentrations lower than 300 μM, it was observed that the DNA tile construction retained its stability. This result shows that the concentration of 100 μM used in Dox loading is not a negative effect on DNA tile structure.
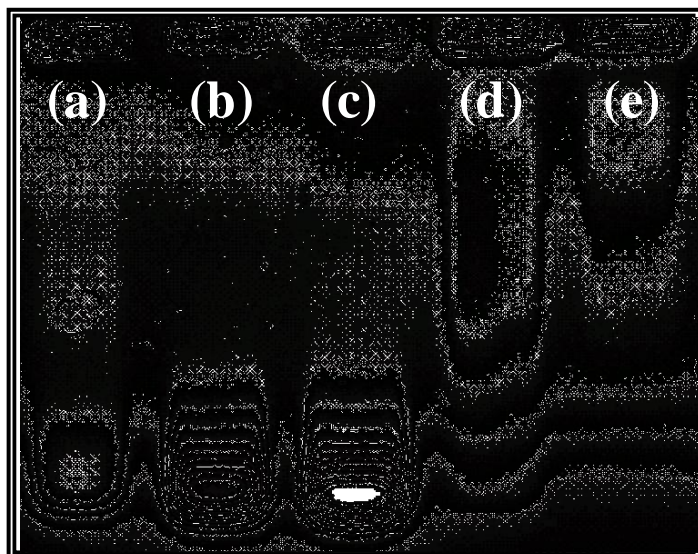
Figure 4.11. Agarose gel image of the stability analysis of the DNA tile structure at different Dox concentrations. DNA tile without Dox incubation (a), DNA tile structure incubated with 200 µM Dox (b), 300 µM Dox (c), 400 µM Dox (d), and 500 µM Dox (e).

4.4. SYNTHESIS AND CHARACTERIZATION OF MODIFIED OLIGONUCLEOTIDES

4.4.1. Carbohydrate Modification

As explained above, the attachment of a targeting moiety may increase the cellular uptake and localization of the drug loaded DNA tile structure. In this thesis, the modification of the DNA tile structure with targeting agents, lactose, folic acid, and RGD peptide is aimed. Thus, oligonucleotides complementary to the sticky ends of the DNA tile structure was modified with these targeting agents and hybridized to the DNA tile. The first targeting agent for this purpose was lactose. The synthesis of DNA-carbohydrate structures is complicated by the necessity of complex protection reactions and modifications that provide reducing end conservation [233]. The one-step reductive amination reaction, which does not require protection reactions, provides great convenience for the synthesis of the DNA-carbohydrate conjugates [233, 281]. It has been reported that aldehyde sugars can be linked by reductive amination with molecules containing amine groups [282]. The reaction rate can be modified with pH, reaction temperature, and borate ion concentration. Sodium cyanoborohydride (NaBH$_3$CN) is the most preferred hydride for reductive amination

reaction due to its stability in acidic environment and solubility in many solvents [283, 284]. However, NaBH$_3$CN is not preferred in large-scale synthesis reactions due to the formation of toxic products [285]. The covalent attachment of lactose to the end of a oligonucleotide, which is complementary to one of the sticky ends of the DNA tile, was performed applying the reductive amination procedure. For the synthesis of lactose modified oligonucleotide, lactose (20 mM), 5'-aminohexyloligonucleotide (50 μM), and sodium cyanoborohydride (250 mM) were incubated in a sodium borate buffer solution for 18 hours at 60 °C. The reductive amination reaction, which allows the direct coupling of lactose and 5'-amine modified oliogonucleotide, is shown in Figure 4.12.
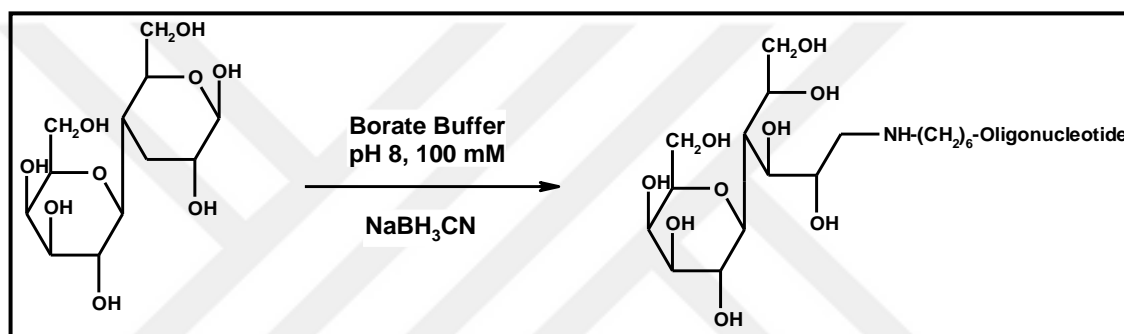
Figure 4.12. Synthesis of the lactose modified oligonucleotide

After the reaction, an ultracentrifuge column was used to remove unreacted chemicals. The samples obtained after centrifugation process was characterized with agarose gel electrophoresis and FT-IR analysis. The structure MALDI-TOF MS analysis was also tried for the characterization of the modified oligonucleotides and the results obtained are presented in the next section.

After the incubation, the reaction sample was run on 2 per cent agarose gel to monitor the molecular weight increase of modified oligonucleotides. Figure 4.13 shows the comparison of starting oligonucleotide and the carbohydrate modified oligonucleotide from the 5'-amine-oligonucleotide with the addition of carbohydrate molecule. In Figure 4.13, the line a indicates the DNA marker. The line b and c shows the pure 5'-amine-oligonucleotide and the lactose modified thymine oligonucleotide, respectively. As seen in Figure 4.13, the addition of lactose moiety to the 5'-amine-oligonucleotide caused the increase on its molecular weight and the modified oligonucleotide migrated slower than the pure oligonucleotide.
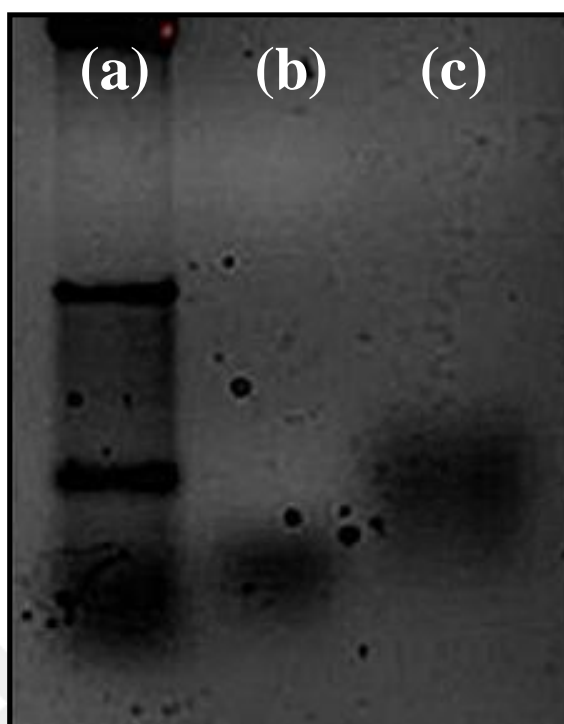
Figure 4.13. The reductive amination monitored by agarose gel electrophoresis. (a) Marker, (b) The pure 5'-amine-T14, and (c) the lactose modified-T14 oligonucleotide.

IR spectroscopy was also used for the characterization of the lactose modified oligonucleotide. The pure starting material, lactose, and the reaction products of the oligonucleotide modification reactions were analyzed using FT-IR spectroscopy (Figure 4.14). FT-IR spectra of the pure lactose and the lactose modified oligonucleotide are shown in Figure 4.14 The characteristic peaks indicated in the literature are observed in the spectra of the pure lactose and the reaction product. The C-O-C bond stretching and bending frequencies, belonging glycosidic bond, were observed around 1100 cm^{-1} and 800 cm^{-1}. The carbohydrate peaks observed between 1150-1030 cm^{-1} indicate the intermolecular stretching of C-O-C ether bond. The peaks observed around 2920 cm-1 indicates the presence of aromatic groups and methylene groups. According to the FT-IR spectra of the pure lactose and the lactose modified oligonucleotide samples given in Figure 4.14, the peak observed between 1650-1580 cm^{-1} can be attributed to N-H vibrations and the peak observed between 1250-1020 cm^{-1} can originate from the C-N vibrations.
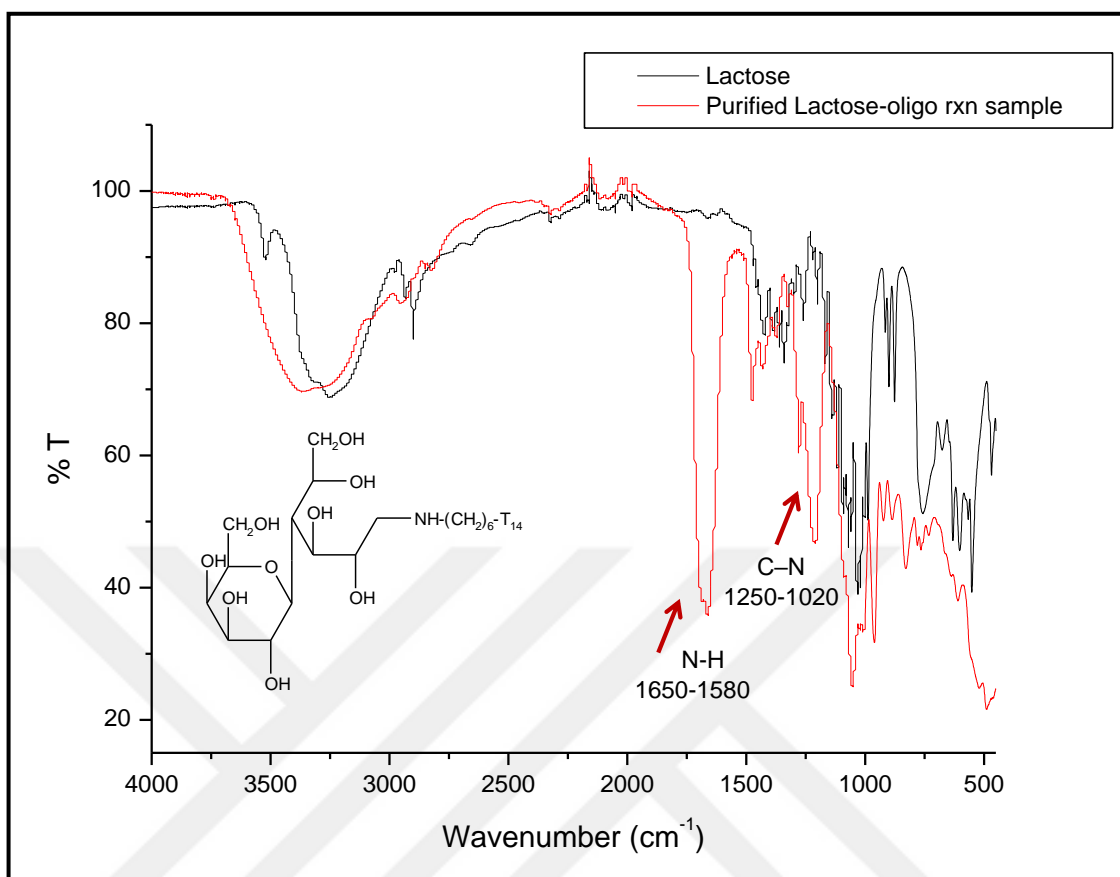
Figure 4.14. FT-IR spectra of the pure lactose and the lactose modified T_{14} oligonucleotide.

The different carbohydrate molecules were also used for the oligonucleotide modification taking into account the positive effect of the lactose modification on the cellular uptake of the drug loaded system. The carbohdyrates, glucose, maltose, and mannose, were used in the oligonucleotide modification and the modified oligonucleotides were characterized by the agarose gel electrophoresis.

The agarose gel image of the oligonucleotides modified with glucose, maltose and mannose is shown in Figure 4.15. In Figure 4.15, the line a indicates the pure 5'-amine-thymine oligonucleotide (14 mer). The line b, c, and d indicates the glucose, maltose and mannose modified thymine oligonucleotides, respectively. As shown in Figure 4.15, addition of the carbohydrate moieties to the 5'-amine-oligonucleotide caused the increase on their molecular weights and the modified oligonucleotides migrated slower than the pure oligonucleotide.
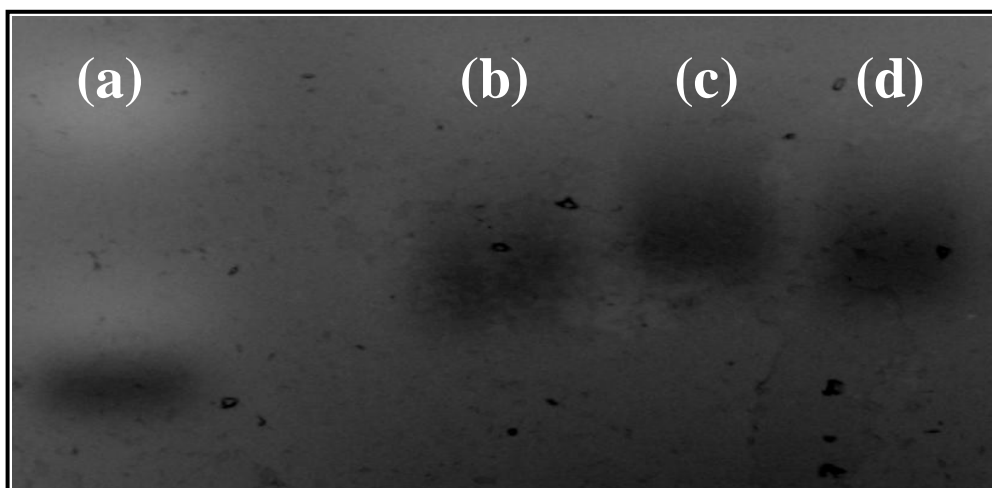
Figure 4.15. Agarose gel image of the oligonucleotides modified with sugar moieties: (a) Pure Thymine$_{14}$, (b) Glucose- Thymine$_{14}$, (c) Maltose- Thymine$_{14}$, and (d) Mannose Thymine$_{14}$.

4.4.2. Folic Acid and RGD Modification

Folic acid and RGD peptide targeting agents, frequently used in targeting studies, were covalently linked to complementary oligonucleotides of the DNA tile constructs to enhance the cellular uptake of the DNA tile construct. Modification of the oligonucleotides with folic acid and RGD peptide targeting agents was performed using DCC/NHS chemistry.

Dicyclohexyl carbodiimide is a reactant used in the cross-linking reaction of carboxylic acid compounds with amine compounds carried out in an organic solvent [286]. Insertion of NHS and Sulfo-NHS compounds to reactions carried out with EDC/DCC enhances reactivity and allows the activated molecules to be stored for further studies [287]. The carbodiimidecompound interacts with the carboxyl group to give the O-acylisourea intermediate [288, 289], which undergoes reaction with the amine compound to perform synthesis of the targeted amide compound [290]. The carboxylic acid compound activation and the coupling of amine compound reaction are shown in Figure 4.16.
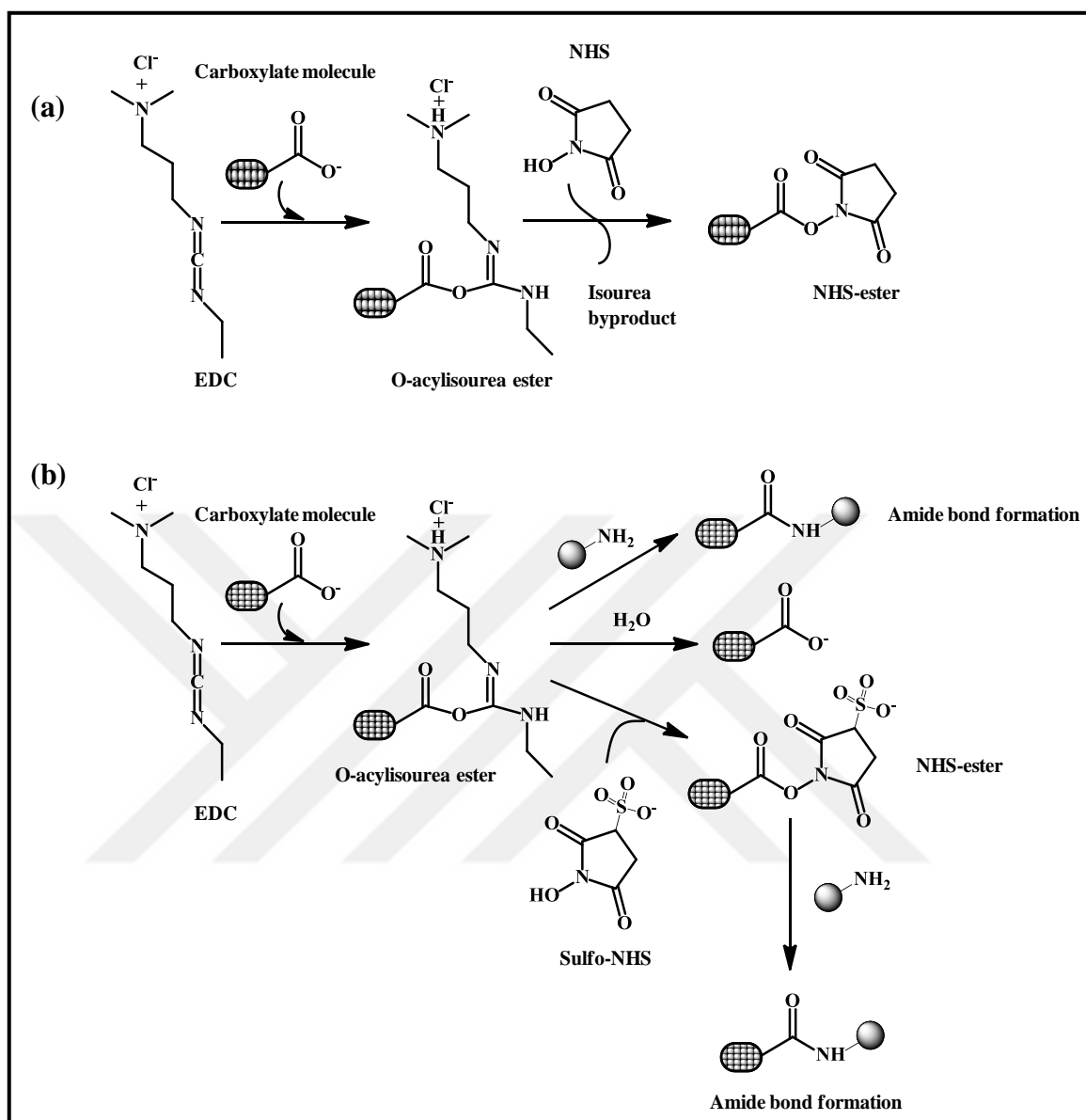
Figure 4.16. NHS ester formation with (a) NHS and (b) sulfo-NHS and coupling of amine compound.

The carboxylate groups of the folic acid and RGD peptide were activated by N-hydroxysuccimide (NHS) and dicyclohexylcarbodiimide (DCC). The activated compounds were reacted with amine-modified oligonucleotides. In Figure 4.17 and 4.18, the reaction schemes of the oligonucleotides with folic acid and RGD peptide are shown.
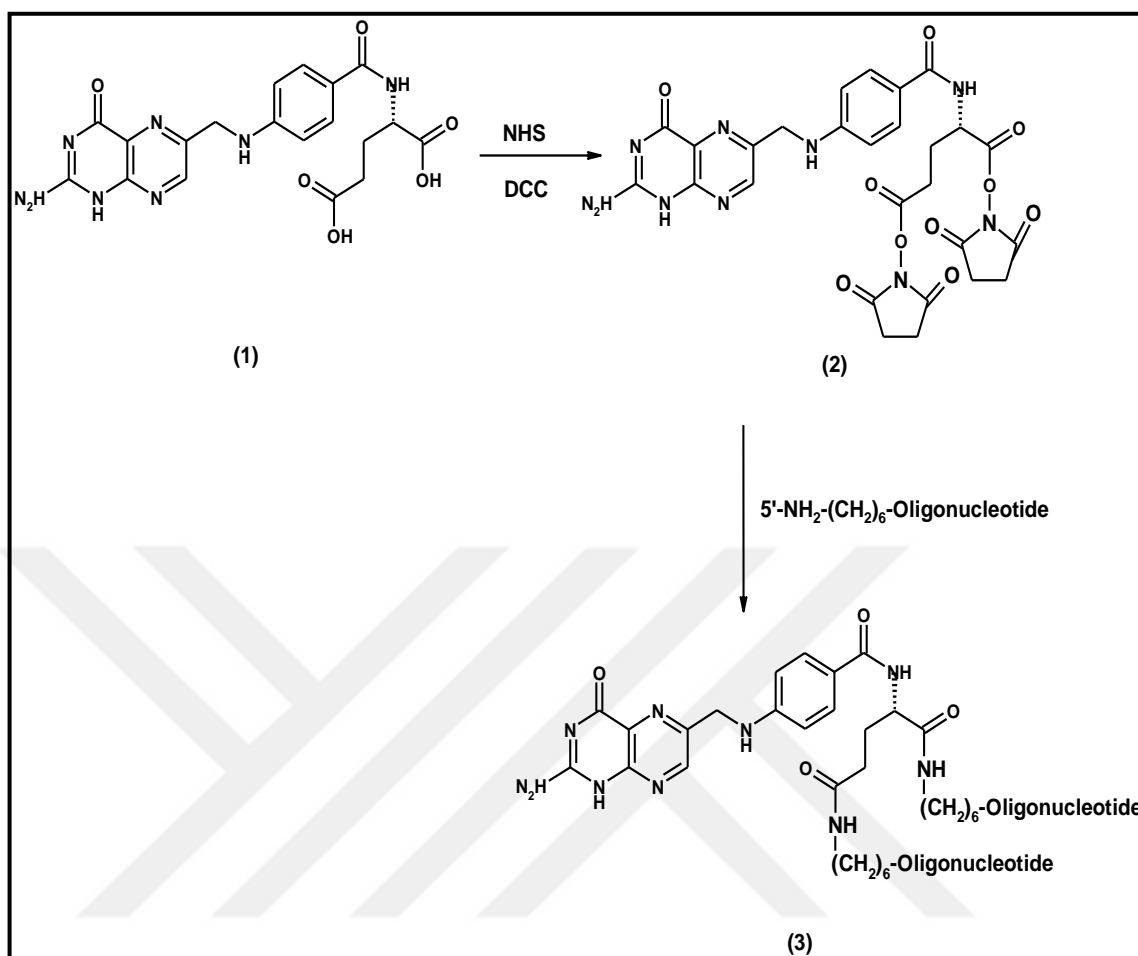
Figure 4.17. Synthesis of the folic acid modified oligonucleotide: (1) Folic acid, (2) Folic acid NHS ester, and (3) Folic acid modified oligonucleotide.
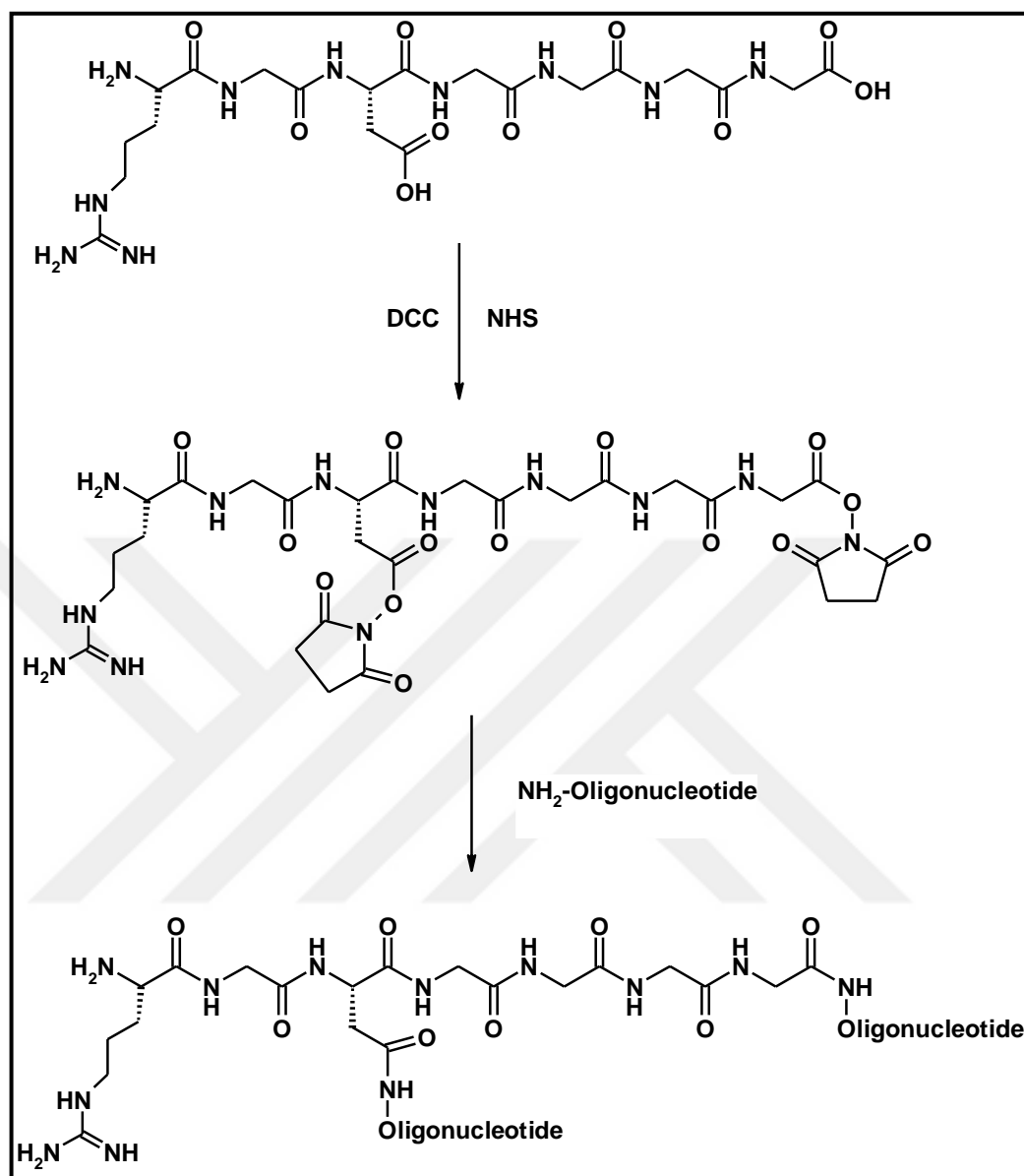
Figure 4.18. Synthesis of the RGD modified oligonucleotide.

The samples taken from the reaction mixtures were analyzed with the agarose gel electrophoresis. Agarose gel electrophoresis was carried out in 2 per cent agarose gel. Figure 4.19 shows the agarose gel image of the oligonucleotides modified with folic acid and RGD peptide. In the agarose gel electrophoresis image given in Figure 4.19, the line a indicates the pure 5'-amine-thymine oligonucleotide (14 mer), the line b and c indicate the RGD peptide and the folic acid modified thymine oligonucleotides, respectively. As shown in Figure 4.19, the addition of the folic acid and RGD peptide moieties to the 5'-amine-oligonucleotide caused an increase in their molecular weights and the modified oligonucleotides migrated slower than the pure oligonucleotide.
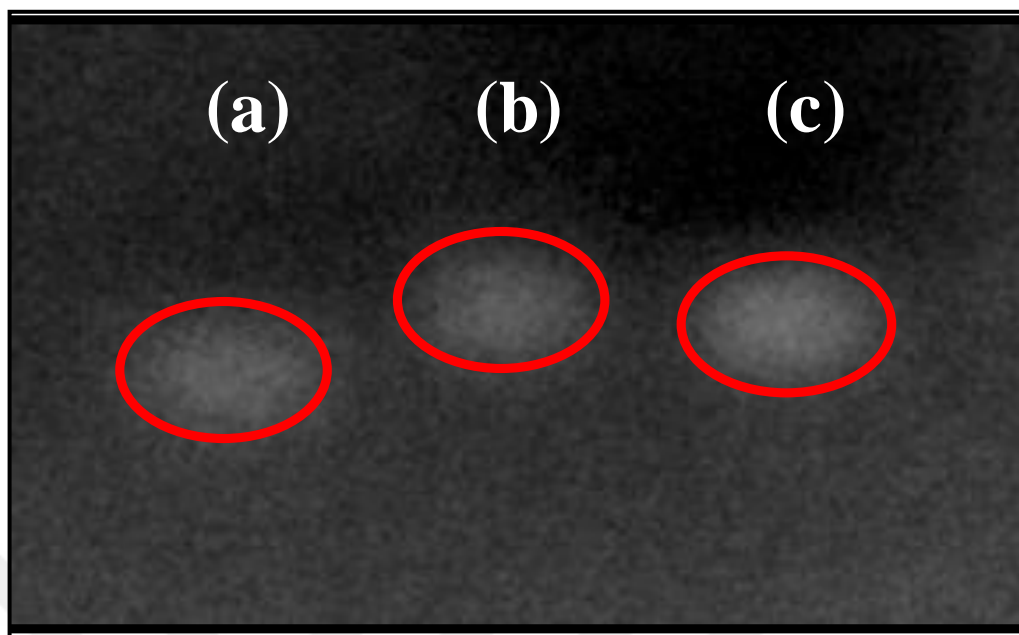
Figure 4.19. Agarose gel image of the oligonucleotides modified with folic acid and RGD peptide. (a) Pure Thymine$_{14}$, (b) RGD peptide modified Thymine$_{14}$, and (c) folic acid modified Thymine$_{14}$.

The starting materials and the reaction products of the oligonucleotide modification reactions, which were carried out using folic acid and RGD peptide, were analyzed using FT-IR spectroscopy. FT-IR spectra of the pure folic acid and RGD peptide with modified oligonucleotide structures are given in Figure 4.20.

The bands, which belong to pteroyl ring (-NH) and glutamic acid residues (-OH), of the folic acid were clearly seen in the spectrum of pure folic acid (Figure 4.20-a) between 3600-3400 cm^{-1}. The band of the C = O group was observed around 1690 cm^{-1}, while the bands were seen around 1510 to 1480 cm^{-1} were specific bands of the folic acid, which originates from the pteroyl and phenyl rings. 1670 and 1380 cm^{-1} amide bands are the characteristic bands specific to the RGD peptide and were seen in the FT-IR spectrum of the RGD peptide modification product. The sharp bands observed around 2900-2800 cm^{-1} in the spectra of folic acid and RGD peptide modification products may belong to the methylene residues in the -(CH$_2$)$_6$ linker of the oligonucleotides used in the modification reactions.
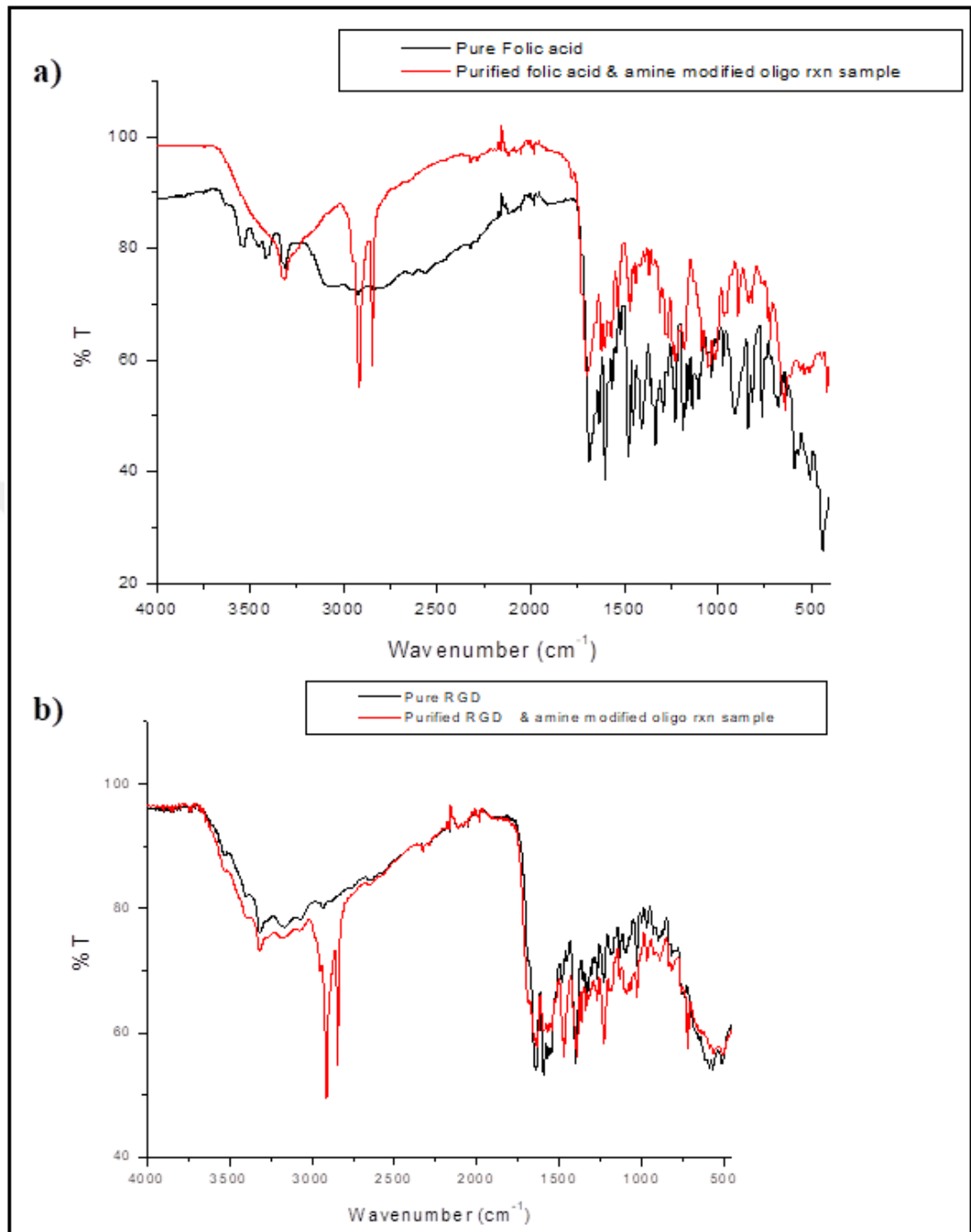
Figure 4.20. FT-IR spectrum of the pure folic acid (a) and RGD peptide (b) with modified oligonucleotide structures.

4.4.3. 5(6)-Carboxyfluorescein (5(6)-FAM) Modification

5(6)-Carboxyfluorescein is a dye, which is used in internalization or membrane permeability studies due to membrane impermeant character, containing carboxyl groups

[291, 292]. The molecular structure of the 5(6)-FAM is shown in Figure 4.21. The dye, which by itself cannot pass through the cell membrane, was used as an indicator to confirm the intracellular uptake of the DNA tile structure.
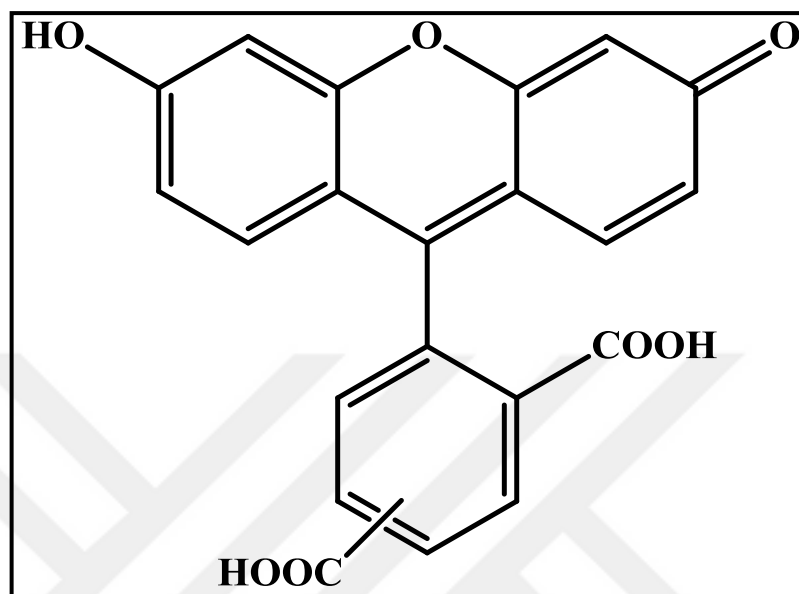
Figure 4.21. Molecular structure of the 5(6)FAM dye.

The 5(6)-Carboxyfluorescein modified oligonucleotide to be used in the internalization assay was also synthesized using the carbodiimide chemistry. The FAM modified 14 mer thymine oligonucleotide obtained at the end of the reaction was imaged by loading 2 per cent agarose gel. The pure 14 mer thymine oligonucleotide and the 5(6) FAM stain were also loaded to the gel together with the reaction product and the possible differences between the molecular weights were observed.

Figure 4.22 shows the agarose gel image of the pure thymine oligonucleotide (14 mer) (line 1), the 5(6)FAM modified oligonucleotide (line 2 and 4), and the pure 5(6)FAM dye. The agarose gel image given in Figure 4.22-a shows the pure oligonucleotide (line 1) and the 5(6)FAM modified oligonucleotide (line 2). The pure 5(6)FAM dye and (line 3) the 5(6)FAM modified oligonucleotide (line 4) are shown in Figure 4.22-b. As shown in Figure 4.22, addition of the FAM dye to the 5'-amine-oligonucleotide caused the increase on its molecular weight and the FAM modified oligonucleotide migrated slower than the pure oligonucleotide and the FAM dye.
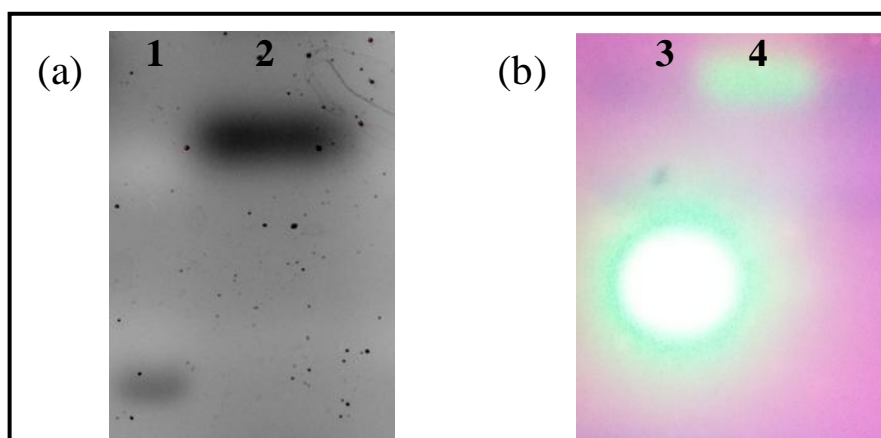
Figure 4.22. Agarose gel image of the the pure Thymine oligonucleotide (14 mer) (line 1), the 5(6)FAM modified oligonucleotide (line 2 and 4), and the pure 5(6)FAM (line 3).

4.4.4. MALDI-TOF MS Analysis

Matrix-assisted laser desorption/ionization time off flight mass spectroscopy (MALDI-TOF MS) is a frequently used analytical technique for the analysis of biomolecules due to its speed, sensitivity and reliability [293]. Thus, MALDI-TOF MS is preferred in molecular biology applications and genetic researches [294-314]. Single nucleotide polymorphism [309-314], nucleic acid sequencing [300, 302, 304-308], oligonucleotide analysis [294, 295, 297, 298, 315], etc.are the application areas of MALDI-TOF MS.

MALDI-TOF MS analysis was also performed for the characterization of the modified oligonucleotides. The analyses of oligonucleotides with MALDI-TOF MS are complicated due to the fragmentation and multi-ion production during the ionization of oligonucleotides [316]. These can prevent the exact mass determination of the samples and reduces the level of sensitivity of the analysis. The complexity of the spectra obtained and the low signal intensity are the results of the fragmentation observed during ionization.

Different compounds such as 2',4',6'-trihydroxyacetophenone [317], 6-aza-2-thiothymine (ATT) [318], picolinic [319] and anthranilic acids [320] are used as matrix materials in analysis. Determination of the proper matrices to overcome an undesired situation is important for oligonucleotide analysis. The use of such matrices leads to transfer of the only required energy for the ionization of sample and reduces the fragment formation. 3-Hydroxypicolinic acid (3-HPA) is one of the matrices with this property [316].

In addition to the appropriate matrices, the use of additives such as diammonium hydrogen citrate [321], ammonium citrate [318], and fucose [322] to improve the quality of the analysis is also available in the literature. The presence of additional compounds such as diammonium hydrogen citrate also obstructs binding of sodium and potassium ions to phosphate groups of oligonucleotides and formation of adducts. The matrix materials and the additives for the oligonucleotide analysis are given in Table 4.1.

Table 4.1. The matrix materials and the additives for the oligonucleotide analysis

Matrix for the oligonucleotide analysis	Additive	Reference
3-Hydroxypicolinic acid (3-HPA)	-	[315, 318, 323]
3-Hydroxypicolinic acid	Diammonium hydrogen citrate	[322]
Quinaldic acid	Ammonium citrate	[324]
2,4,6-Trihydroxyacetophenone (THAP)	-	[317, 318]
2,4,6-Trihydroxyacetophenone	Ammonium citrate	[317]
5-Methoxysalicylic acid	Spermine	[322]
3,4-diaminobenzophenone (DABP)	-	[325]
Ferulic acid	-	[323]
2,5-dihydroxybenzoic acid (DHB)	-	[323]
6-Aza-2-thiothymine (ATT)	-	[326]
3-Hydroxypicolinic acid	Fucose, sucrose, trehalose	[327]
3-Hydroxycoumarin (3-HC)	Diammonium hydrogen citrate	[328]
3-aminopicolinic acid (3-APA)	-	[297]
3-Hydroxypicolinic acid & picolinic acid	-	[319]

2,5-dihydroxybenzoic acid (DHB), α-cyano-4-hydroxycinnamic acid (CHCA), sinapinic acid (SA), and 3-Hydroxypicolinic acid (3-HPA) matrices were used for the determination of the exact mass of modified oligonucleotides. The low signal intensities were observed in analyzes with DHB, CHCA and SA matrices. The molecular peaks of the pure and the modified oligonucleotides could not be observed and the bands on the spectra were at the noise level.

The analysis was repeated using 3-HPA matrix recently proposed for the oligonucleotide analysis [315, 318, 323]. As previously mentioned, it was thought that better quality spectra could be obtained by using a matrix to provide adequate energy preventing the

fragmentation   such as 3-HPA. The spectra of pure and modified forms of two oligonucleotides, 5'-NH$_2$-TTTTTTTTTTTTTTT and 3'-NH$_2$-CTCGTAAAAAAAAA were obtained with MALDI-TOF MS. The theoretical ? molecular weights of these pure oligonucleotides were 4376.2 and 4452 Da, respectively. The spectra of these oligonucleotides are given in Figure 4.23 and 4.24. The use of 3-HPA as a matrix did not prevent problems such as fragmentation and low signal level in the spectra of the pure oligonucleotides that were used as standards. Figure 4.23-a shows MALDI-TOF mass spectrum of the 5'-NH$_2$-(T)$_{14}$ oligonucleotide obtained from a MALDI target preparation with 3-HPA matrix in the mass range of 4100 Da to 4600 Da. Figure 4.23-b shows the expantion of the 4370-4380 Da region of the spectra presented on Figure 4.23-a. A peak at about 4375 Da was observed but it was not possible to distinguish it from the niose.
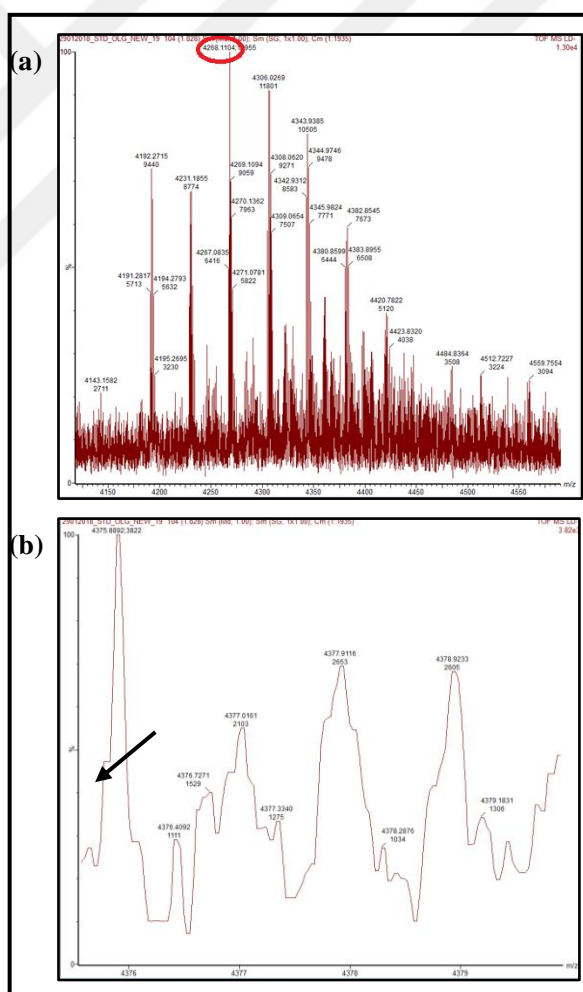
Figure 4.23. The MALDI-TOF mass spectrum of the 5'-NH$_2$-(T)$_{14}$ oligonucleotide obtained from a MALDI target preparation with 3-HPA matrix in the mass range of 4100 Da to 4600 Da (a) and 4370 Da to 4400 Da (b).

Figure 4.24-a shows MALDI-TOF mass spectrum of the 3'-NH$_2$-CTCGT(A)$_9$ perepared with 3-HPA matrix in the mass range of 4470 Da to 4780 Da. Figure 4.24-b shows the expanded portion of Figure 4.24-a. The theoretical molecular weight expected for the 3'-NH$_2$-CTCGT(A)$_9$ oligonucleotide was 4452 Da. It was seen that the adduct containing sodium and potassium ions may have formed while the expected molecule mass value was not observed. The molecular weight of Na$^+$ and K$^+$ added adduct should be 4514 Da and the observed value in the spectrum was 4517 Da.
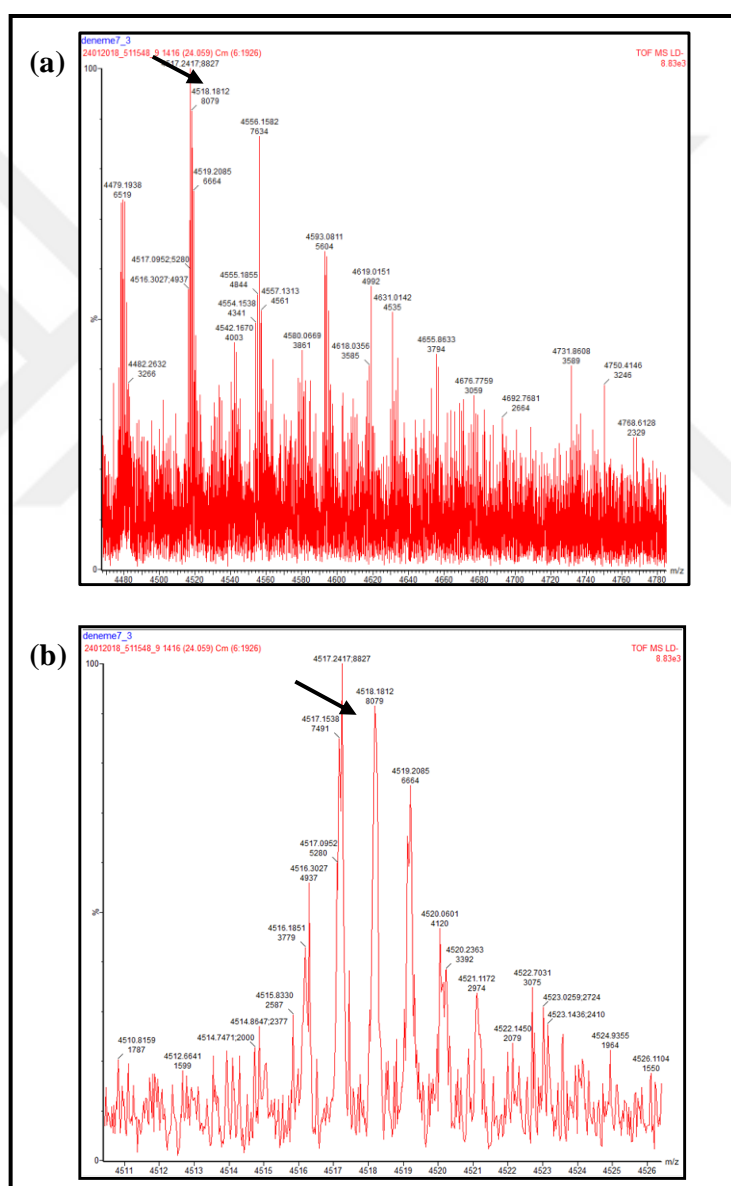
Figure 4.24. The MALDI-TOF mass spectrum of the 3'-NH$_2$ -CTCGT(A)$_9$ obtained from a MALDI target preparation with 3-HPA matrix in the mass range of 4470 Da to 4780 Da (a) 4500 Da to 4530 Da (b).

The mass spectra of monolactosylated oligonucleotides obtained by reductive amination are given in Figure 4.25 - 4.27. The spectrum of the bislactosylated oligonucleotide is given in Figure 4.28. The spectra of the monomaltosylated and bismaltosylated oligonucleotide are shown in Figure 4.29 and Figure 4.30, respectively. The monoglucosylated oligonucleotide spectrum is shown in Figure 4.31.

The theoretical molecular weight calculated for the Lac-NH-$(CH_2)_6$-$(T)_{14}$ was 4701.8 Da. This expected value in the spectrum was observed together with low signal intensities and multiple fragment formation. Figure 4.25 and Figure 4.26 shows the MALDI-TOF mass spectrum of the monolactosylated 14 mer thymine oligonucleotide.
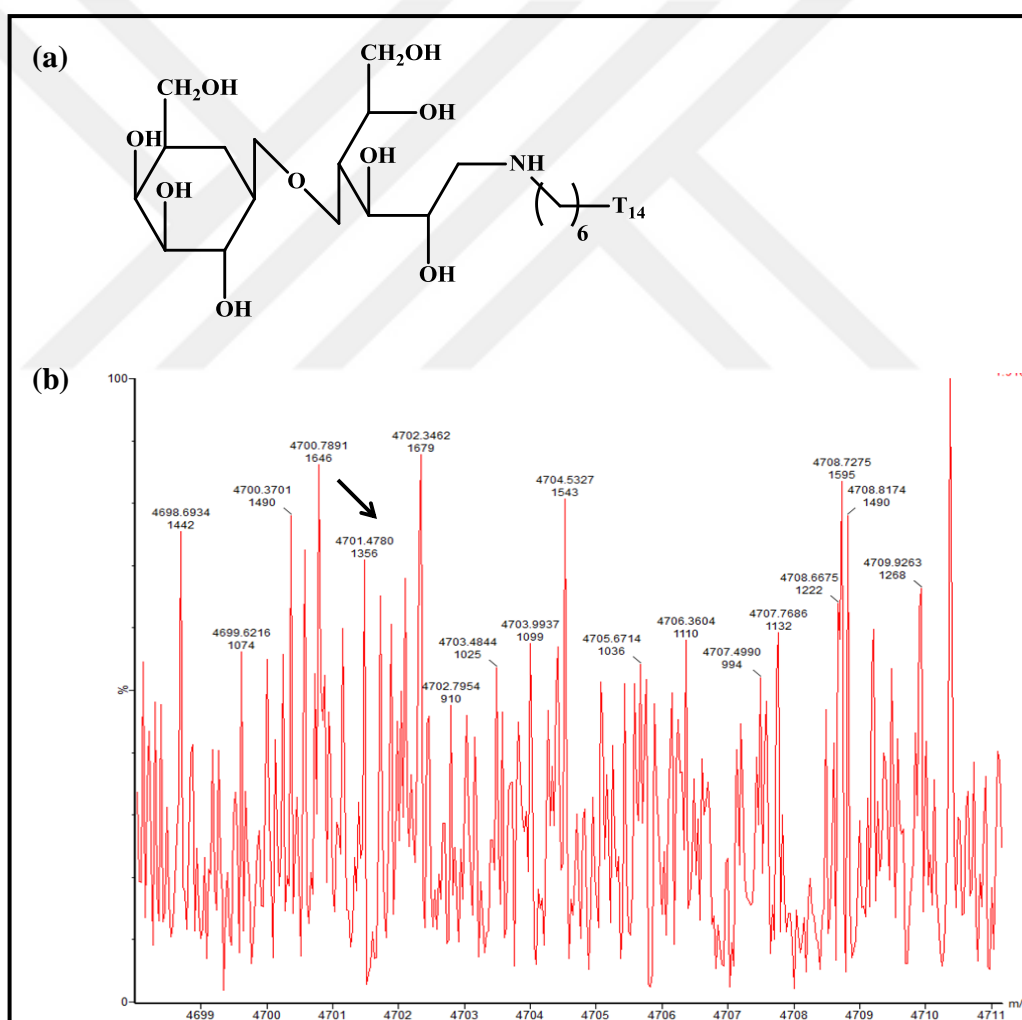
Figure 4.25. The molecular structure of the Lac-NH-$(CH_2)_6$-$(T)_{14}$ and the MALDI-TOF mass spectrum of the Lac-NH-$(CH_2)_6$-$(T)_{14}$ obtained from a MALDI target preparation with 3-HPA matrix in the mass range of 4690 Da to 4720 Da.

Theoretical value for the modified oligonucleotide was observed in mass spectrum as 4701.47 and 4701.68 Da, respectively. In Figure 4.26, it is also observed that sodium adduct (4724 Da) could have formed at the same time.
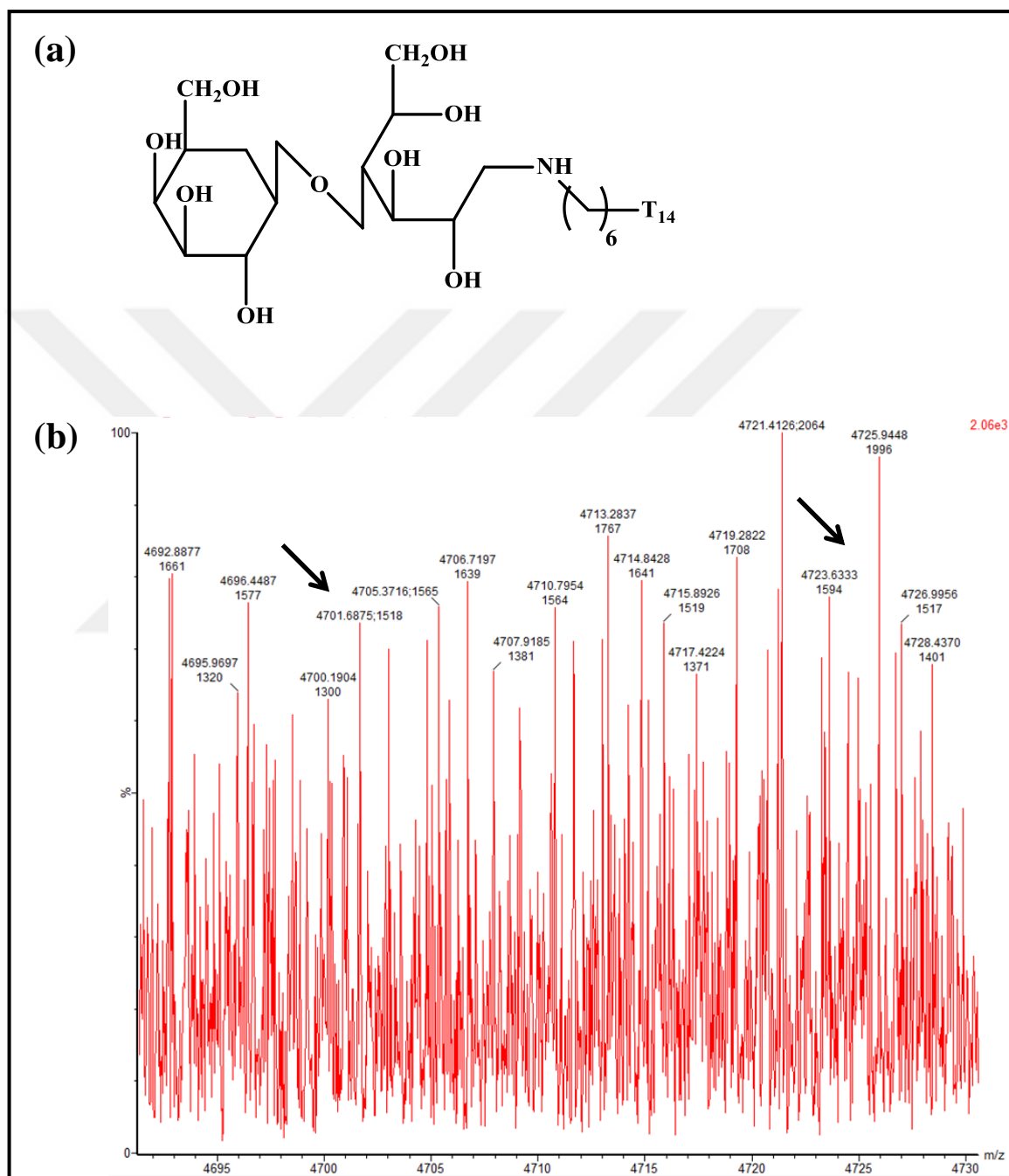
Figure 4.26. The molecular structure of the Lac-NH-(CH$_2$)$_6$-(T)$_{14}$ and the MALDI-TOF mass spectrum of the Lac-NH-(CH$_2$)$_6$-(T)$_{14}$ obtained from a MALDI target preparation with 3-HPA matrix in the mass range of 4690 Da to 4730 Da.

The theoretical molecular weight calculated for the Lac-NH-$(CH_2)_6$-CTCGT$(A)_9$ was 4778 Da. The MALDI-TOF mass spectrum of the monolactosylated CTCGT$(A)_9$ oligonucleotide is given in Figure 4.27 and the theoretical value for the modified oligonucleotide is observed in mass spectrum as 4778.96 Da.
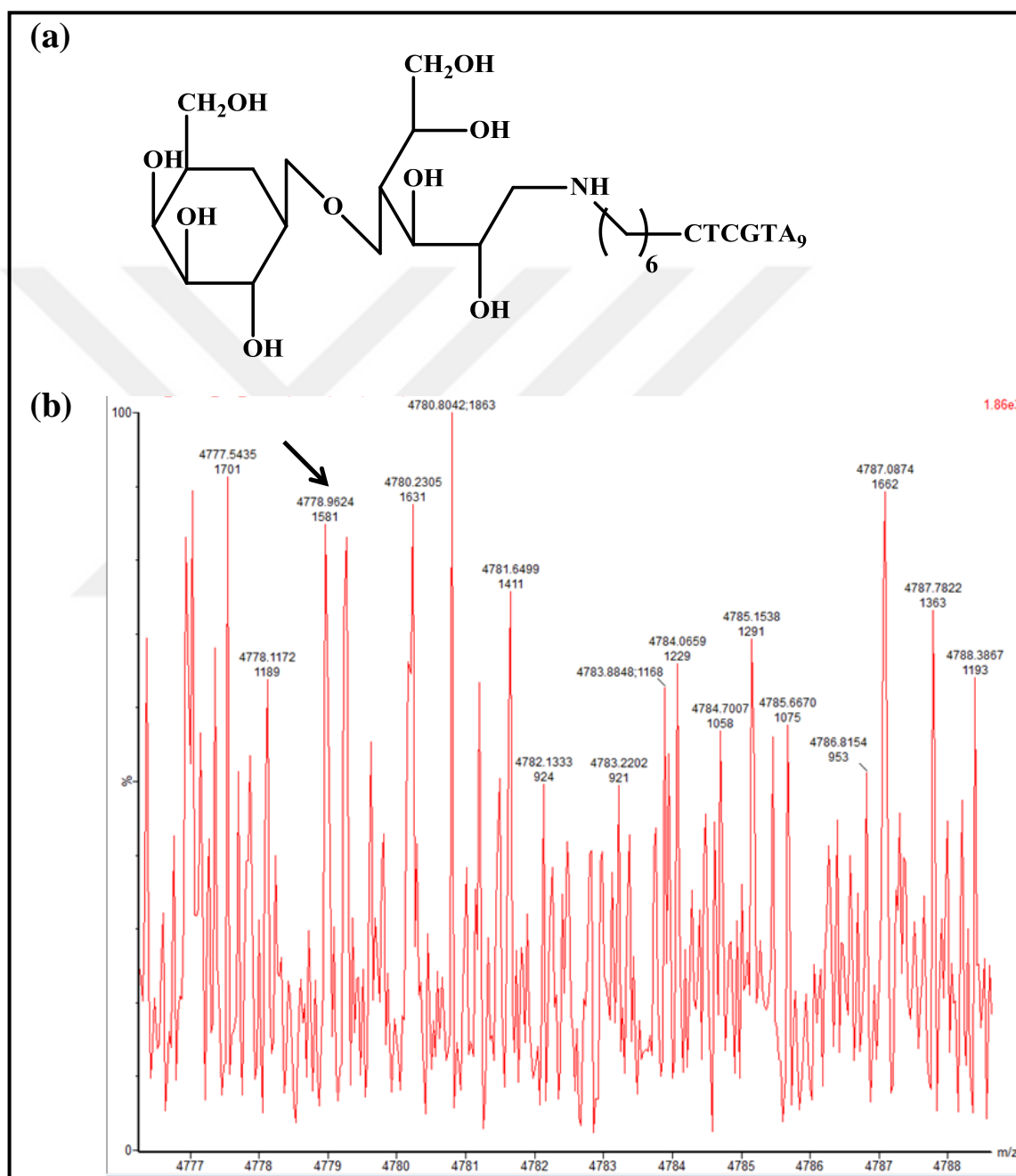
Figure 4.27. The molecular formula of the Lac-NH-CTCGT$(A)_9$ and the MALDI-TOF mass spectrum of the Lac-NH-CTCGT$(A)_9$ obtained from a MALDI target preparation with 3-HPA matrix in the mass range of 4770 Da to 4790 Da.

The theoretical molecular weight calculated for the Lac_2-N-$(CH_2)_6$-$(T)_{14}$ was 5027 Da. Figure 4.28 shows the MALDI-TOF mass spectrum of the bislactosylated 14 mer thymine oligonucleotide. Theoretical values for the modified oligonucleotide and the possible sodium adduct was observed in mass spectrum as 5026 and 5050 Da, respectively.
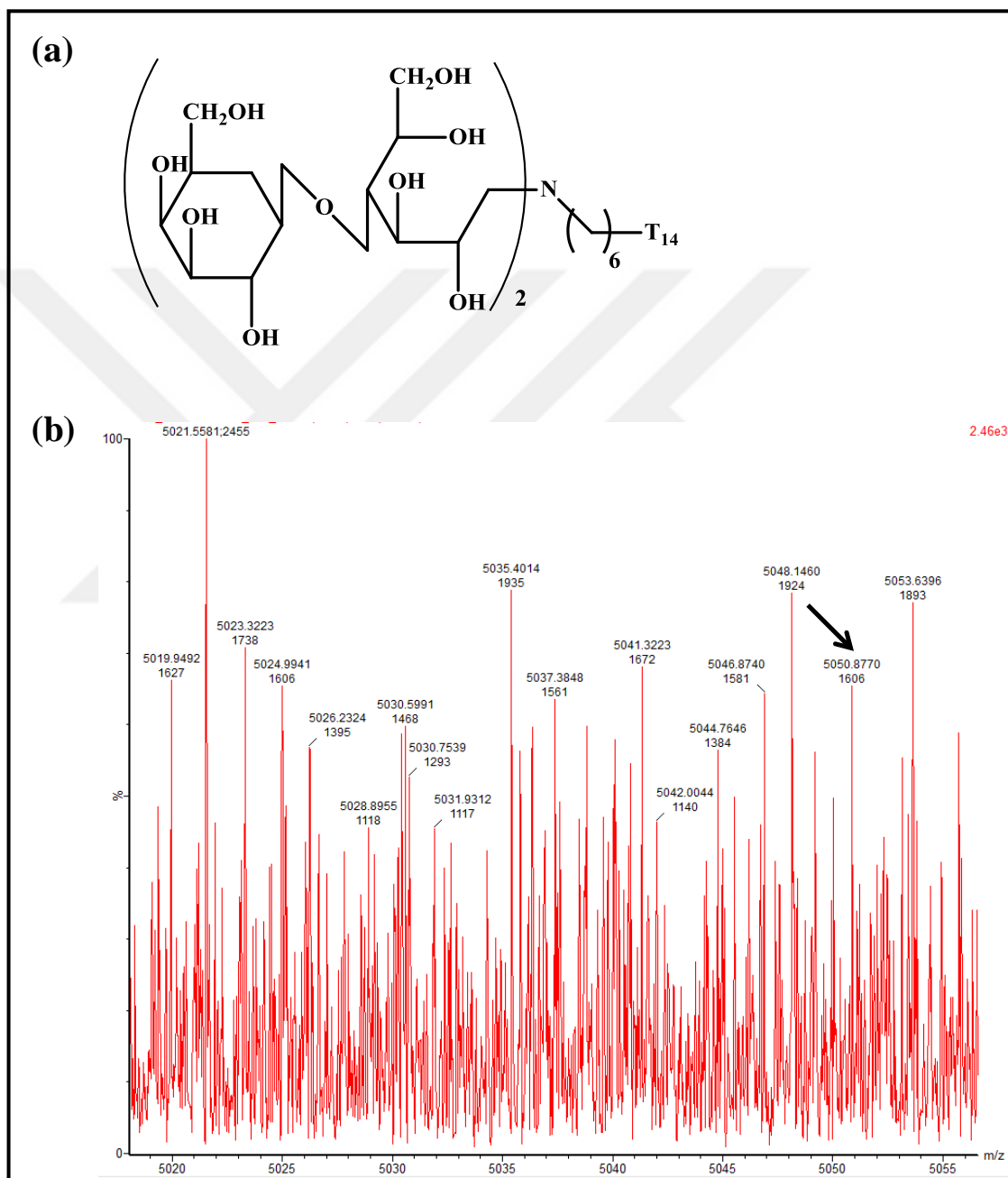
Figure 4.28. The molecular structure of the Lac_2-N-$(CH_2)_6$-$(T)_{14}$ and the MALDI-TOF mass spectrum of the Lac_2-N-$(CH_2)_6$-$(T)_{14}$ obtained from a MALDI target preparation with 3-HPA matrix in the mass range of 5000 Da to 5060 Da.

Figure 4.29 shows the MALDI-TOF mass spectrum of the monomaltosylated 14 mer thymine oligonucleotide. The theoretical molecular weight calculated for the Mal-NH-$(CH_2)_6$-$(T)_{14}$ was 4701.8 Da. This expected value was seen in the spectra as 4701.74 Da.
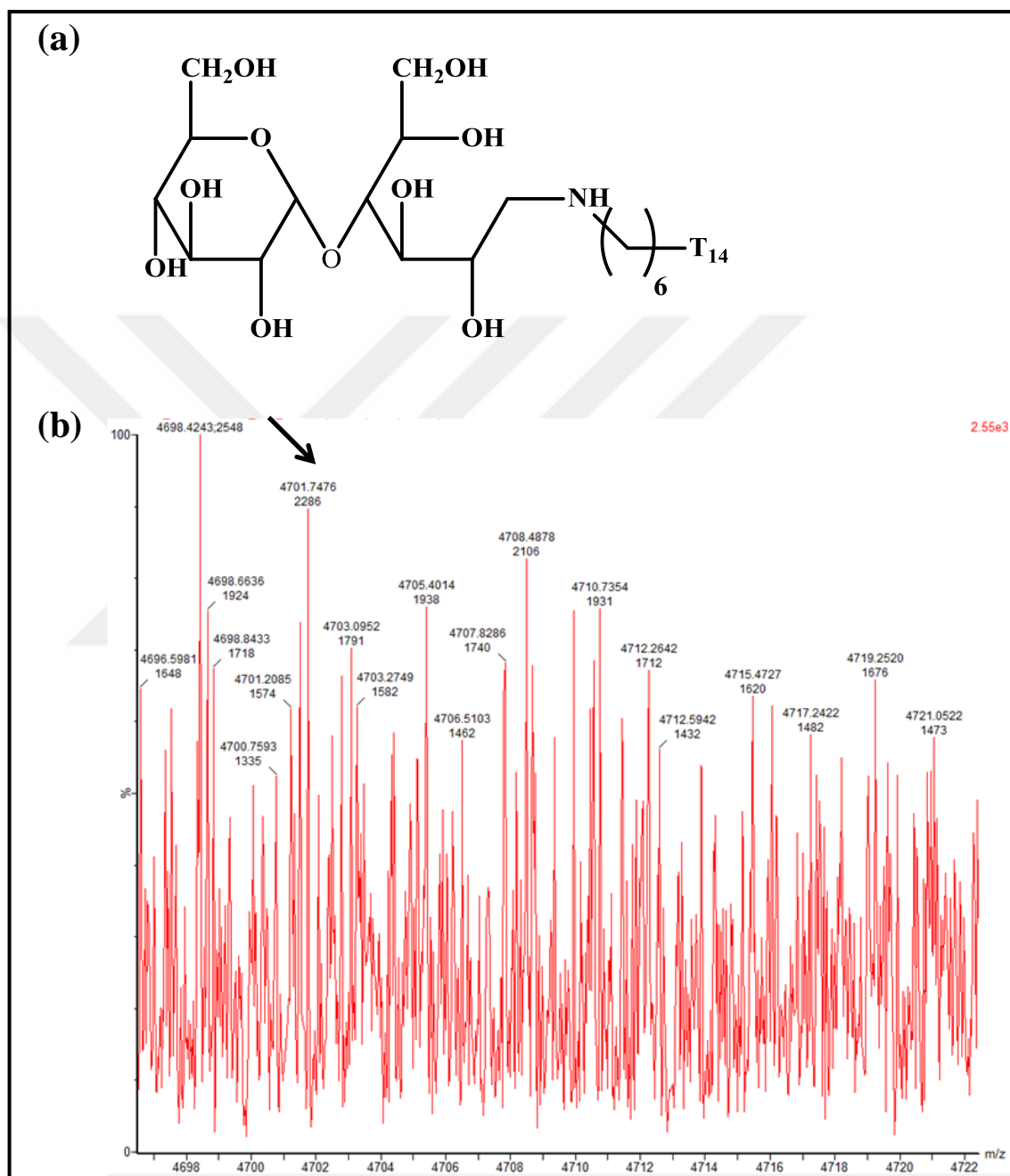
Figure 4.29. The molecular structure of the Mal-NH-$(CH_2)_6$-$(T)_{14}$ and the MALDI-TOF mass spectrum of the Mal-NH-$(CH_2)_6$-$(T)_{14}$ obtained from a MALDI target preparation with 3-HPA matrix in the mass range of 4690 Da to 4730 Da.

Figure 4.30 represents the MALDI-TOF mass spectrum of the bismaltosylated 14 mer thymine oligonucleotide. The theoretical molecular weight calculated for the Mal_2-N-$(CH_2)_6$-$(T)_{14}$ was 5027 Da. This expected value is seen in the spectra as 5027.81 Da.
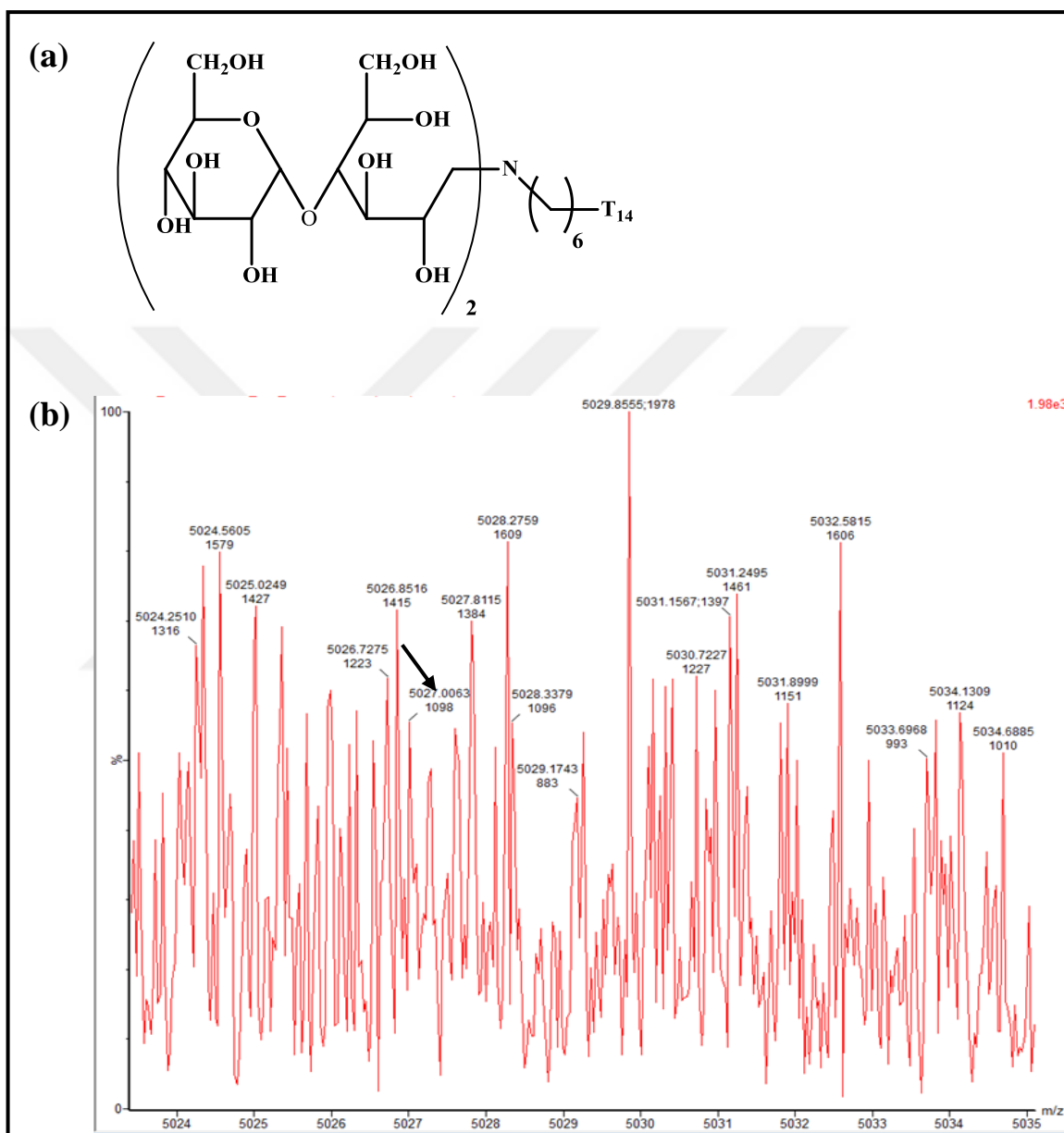
Figure 4.30. The molecular structure of the Mal_2-N-$(CH_2)_6$-$(T)_{14}$ and the MALDI-TOF mass spectrum of the Mal_2-N-$(CH_2)_6$-$(T)_{14}$ obtained from a MALDI target preparation with 3-HPA matrix in the mass range of 5020 Da to 5035 Da.

The MALDI-TOF mass spectrum of the monoglucosylated $CTCGT(A)_9$ oligonucleotide is shown in Figure 4.31. The theoretical molecular weight calculated for the Glu-NH-$(CH_2)_6$-$CTCGT(A)_9$ was 4617 Da. This expected value is seen in the spectra as 4617.32 Da.
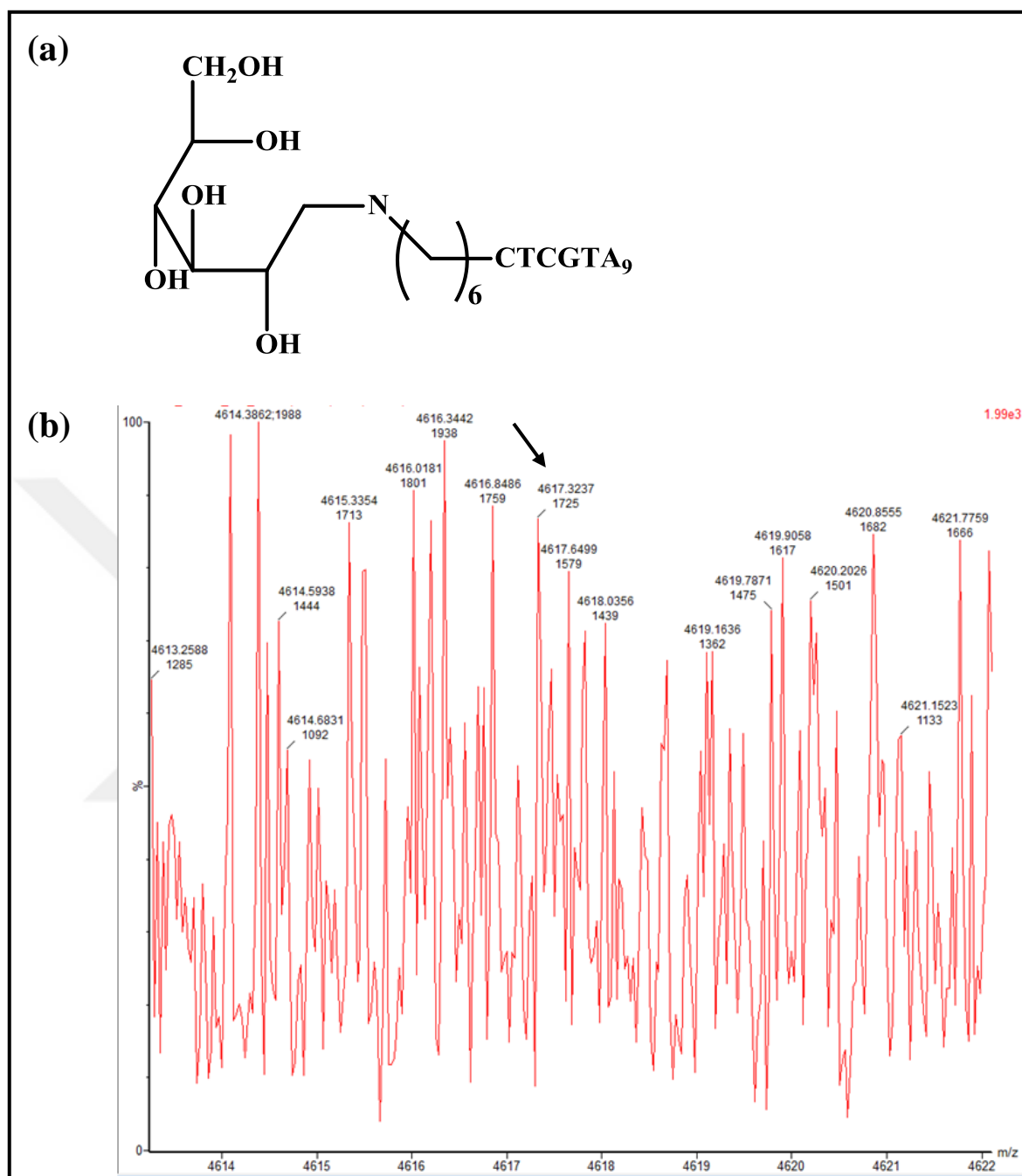
Figure 4.31. The molecular structure of the Glu-NH-CTCGT(A)$_9$ and the MALDI-TOF mass spectrum of the Glu-NH-CTCGT(A)$_9$ obtained from a MALDI target preparation with 3-HPA matrix in the mass range of 4610 Da to 4625 Da.

4.5. CYTOTOXICITY OF THE DNA TILE STRUCTURES ON CELL VIABILITY

The ideal drug delivery system should be non-toxic, biocompatible, and not immuno reactive [329]. DNA is a biomacromolecule with all these properties and therefore constructs made using DNA are expected to have these desired properties. The cytotoxicity of the DNA tile on the cell viability were determined applying WST-1 cell viability assay. The cell viability test performed with WST-1 colorimetric assay provides information about the presence of viable cells by quantifying tetrazolium salts converted by mitochondrial enzyme activity. By measuring the conversion of tetrazolium salts to formazan dye via enzyme activity and measuring the absorbance of the formed formazan dye at 450 nm, the number of metabolically active cells is determined.

The cells were incubated with free Dox and the modified and unmodified Dox loaded DNA tile (DNA tile-Dox) constructs at 37 °C in a humidified atmosphere under 5 per cent CO_2 for 24 hours. After the incubations, the WST-1 cell viability assay procedure was applied. Figure 4.32 shows the cell viability of MDA-MB-231 cells for 24 hours incubation with free drug and DNA tile-Dox samples. When the DNA tile concentration was studied at a concentration range of 50-400 nM, the DNA tile structure showed no cytotoxicity on MDA-MB-231 cells.
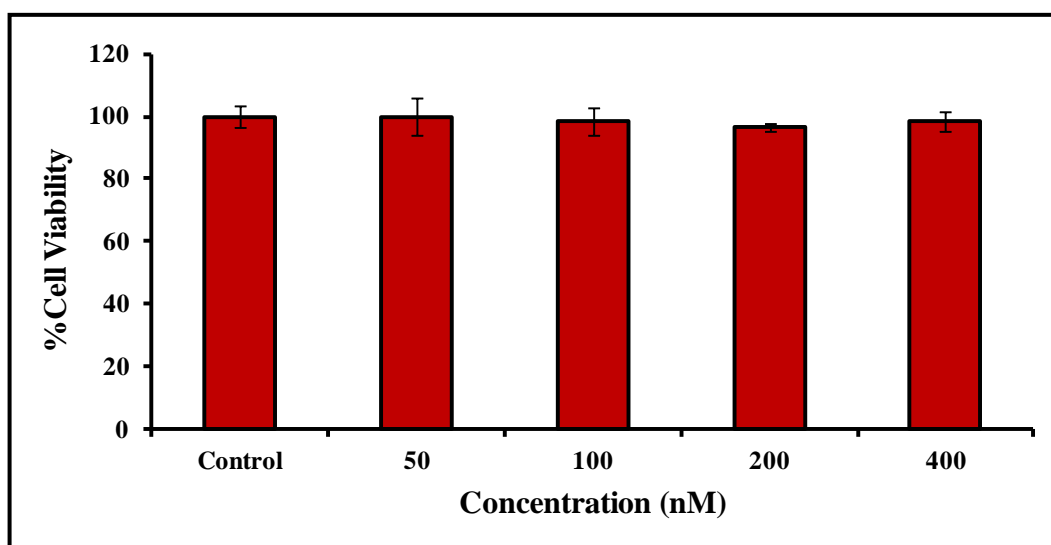
Figure 4.32. Cytotoxicity of the DNA tile structure on MDA-MB-231 cells

The cytotoxicity of Dox and the DNA tile-Dox constructs was also studied on HeLa cells. Figure 4.33 shows the cytotoxicity of free Dox and the DNA tile-Dox on HeLa cells. When

the toxicities of Dox and the DNA tile-Dox on HeLa cells were examined between 0.1-15 μM concentration range, it was observed that the DNA tile structure has less negative effect on cell viability than the free Dox at the studied concentration range. The cell viability at 15 μM Dox was found as 7 per cent for free Dox and 20 per cent for theDNA tile-Dox. It was found that at lower concentration values, the cell viability was above 50 per cent and a significant decrease on the cell viability was observed after 7.5 μM.
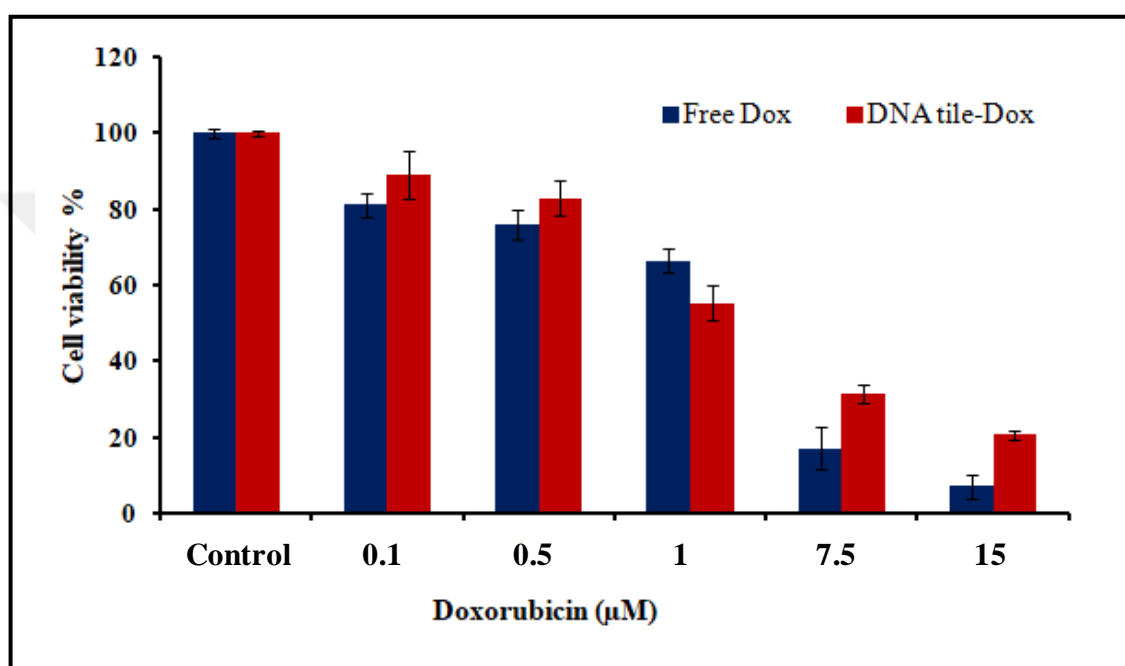
Figure 4.33. The cytotoxicity of free Dox and DNA tile-Dox on HeLa cells.

The DNA tile-Dox shows a similar cytotoxicity with free Dox. Figure 4.34 shows the comparision of the viability of MDA-MB-231 cells upon exposure to DNA tile-Dox, lactose modified doxorubicin loaded DNA tile (DNA tile-Dox-Lac) and free Dox with increasing concentrations for 24 hours incubation.

It is observed that the viability of MDA-MB-231 cells treated with free Dox and DNA tile-Dox was in the level of 53-54 per cent at 1.25-5 μM Dox. The cell viability is observed in the level of 60 per cent in cells incubated with the DNA tile-Dox-Lac at the same concentration values.
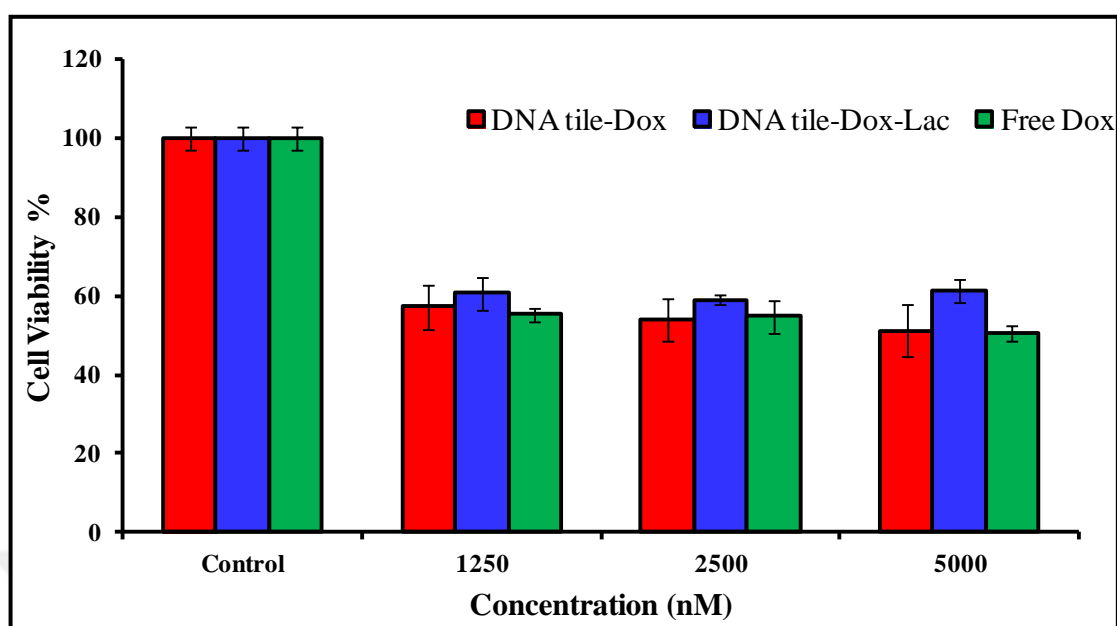
Figure 4.34. Cytotoxicity of free Dox and the DNA tile-Dox structures with/without lactose modification on MDA-MB-231 cells.

The toxicity of the DNA tile-Dox system, modified with other targeting agents RGD peptide and folic acid, was also studied on MDA-MB-231 cells. The cytotoxicity graphs of the folic acid modified Dox loaded DNA tile (DNA tile-Dox-Fol) and RGD peptide modified Dox loaded DNA tile (DNA tile-Dox-RGD) on MDA-MB-231 cells are given in Figure 4.35. The cellular viability was found as 50 per cent at 10 µM Dox concentration.
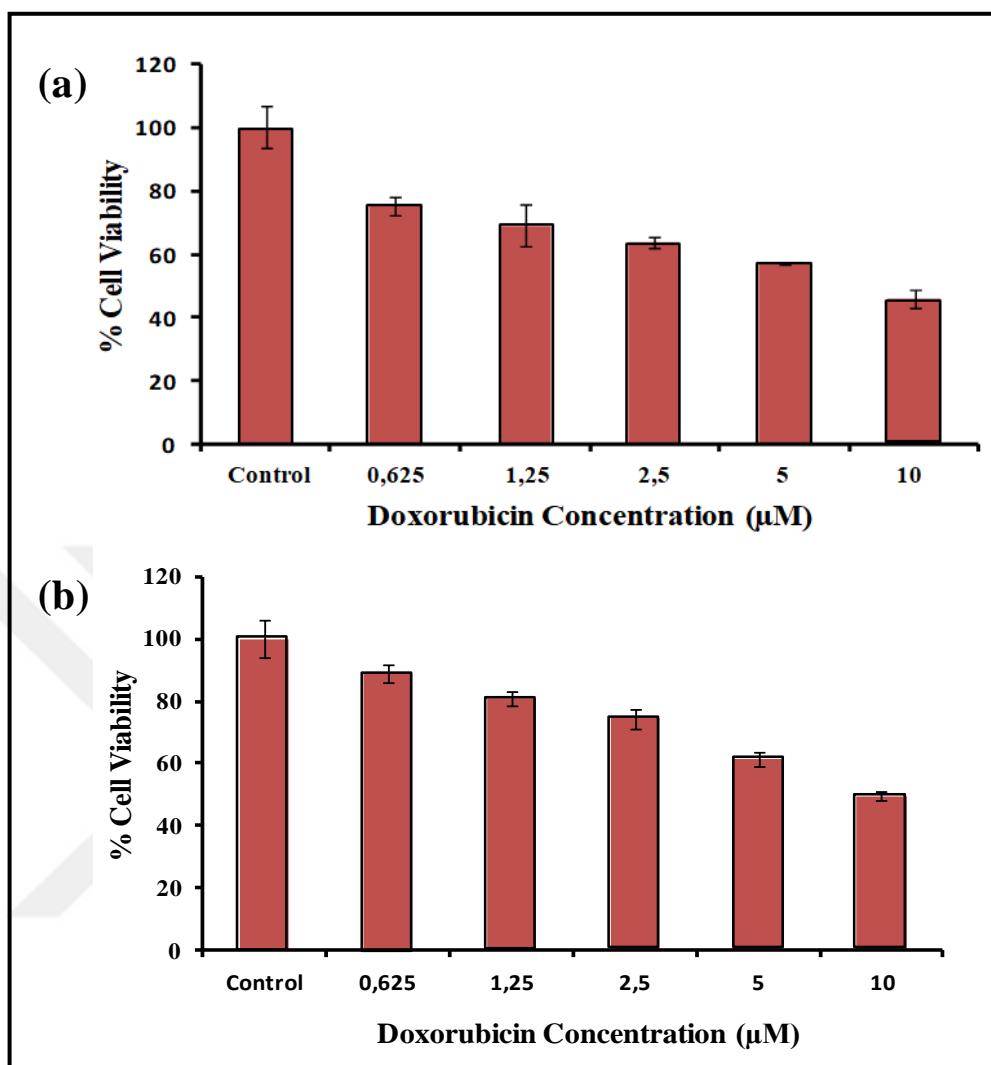
Figure 4.35. The cytotoxicity of DNA tile-Dox- Fol (a) and DNA tile-Dox-RGD (b) on MDA-MB-231 cells.

The drug retained its activity after intercalation into the DNA tile construct and modification with the lactose, biomolecule, was found to reduce the toxicity of drug to some extent.

4.6. INTERNALIZATION OF DNA TILE

Internalization of the DNA tile construct by the cells was investigated using the 5(6)-FAM dye, which normally does not pass through the membrane, with increasing incubation times. BT-474 cancer cells were seeded onto cover slips at a density of 150.000 cells/slip. After the attachment, the cells were incubated with free Dox, 5(6)-FAM, 5(6)FAM modified DNA tile (5(6)-FAM-DNA tile), and 5(6)FAM modified Dox loaded DNA tile

(5(6)-FAM -DNA tile-Dox) structures for 2-24 hours at 37 °C and 5 per cent CO_2. At the end of the incubation periods, the cells were exposed to fixation procedure, and then fixed cells were monitored by confocal microscopy. The confocal microscopy images of BT-474 cells incubated with 5(6)-FAM-DNA tile and 5(6)-FAM-DNA tile-Dox tile are shown in Figure 4.36. When BT-474 cells were incubated with 5(6)-FAM-DNA tile and 5(6)-FAM-DNA tile-Dox constructs for 2 hours, DNA tile structures were accumulated around the cell membrane.
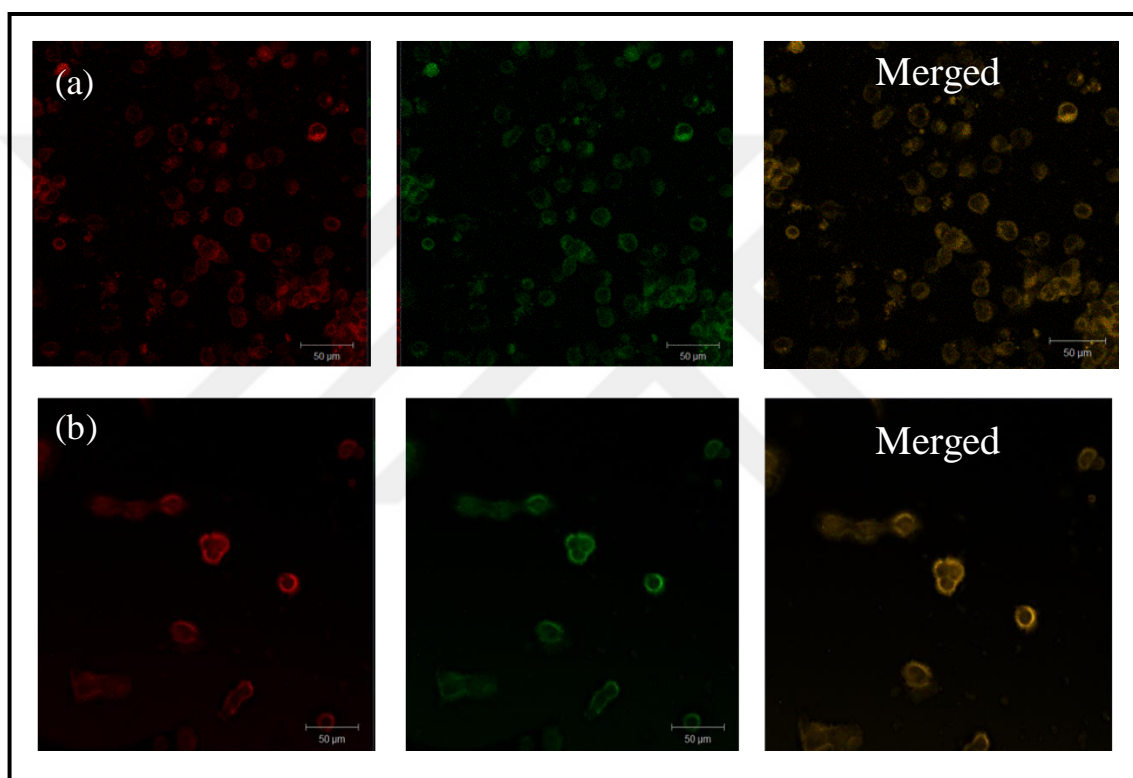
Figure 4.36. Confocal microscopy images of BT-474 cells incubated with 5(6)-FAM-DNA tile (a) and 5(6)-FAM- DNA tile-Dox for 2 hours (b).

When the incubation time was extended to 24 hours, free Dox, 5(6)-FAM-DNA tile, and 5(6)-FAM- DNA tile-Dox structures were uptaken by BT-474 cells. 5(6) FAM dye was not uptaken by the cells and continued to accumulate around the cell membrane (Figure 4.37). These results confirmed that the DNA tile structure is taken up by the cells.
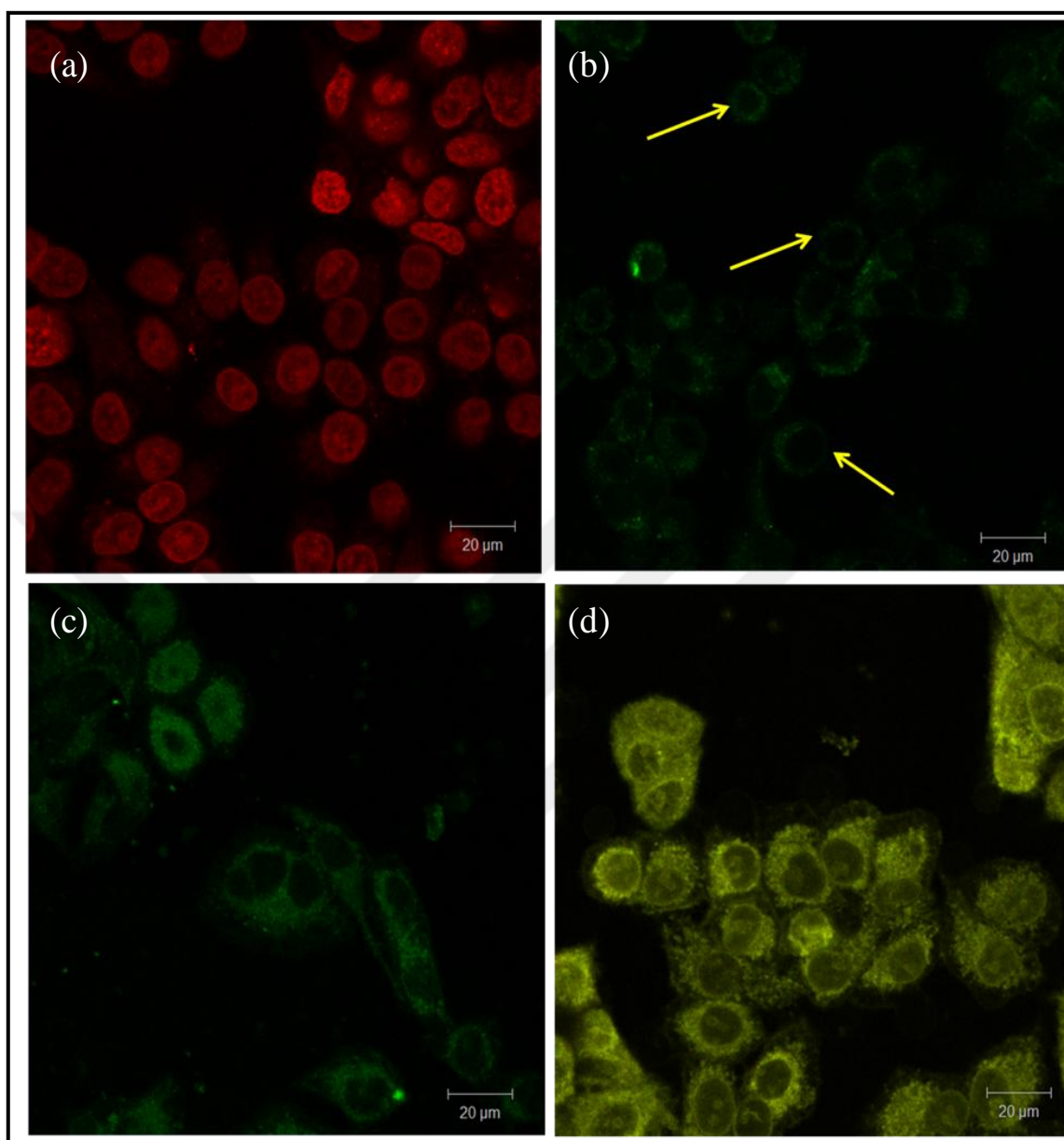
Figure 4.37. The confocal microscopy images of BT-474 cells incubated with free Dox (a), 5(6)-FAM (b), 5(6)-FAM-DNA tile (c) and 5(6)-FAM-DNA tile-Dox (d) structures for 24 hours.

4.7. CELLULAR UPTAKE OF MODIFIED DNA TILE-DOXORUBICIN

4.7.1. Fluorescence Spectroscopy Analysis

Bio- or synthetically-produced macromolecules are intensively investigated in drug delivery systems [330]. Conjugations of different ligands to these macromolecules help to reduce the potential side effects of drugs by inhibiting passive diffusion of drug molecules into the cells and provide reduced distribution and toxicity [331]. The cellular uptake pathway of a gene carrier is a determining factor in the development of carrier systems. It is clear that the carrier structures designed by considering the mechanism of cellular internalization processes will be more effective for carrier structures. Particularly, addition of a targeting molecule to the macromolecular structure enhances the efficiency of a carrier system. In this sense, carbohydrate molecules are used as effective targeting agents in drug delivery systems. Many studies have been reported showing the modification studies of carbohydrate molecules have even affected the cellular uptake and intracellular distribution of nanobased systems [332-338].

In accordance with this purpose, DNA tile-Dox system was modified with lactose molecule, and the effect of the modification on the cellular internalization was quantitatively examined by fluorescence spectroscopy. Three different cell lines, MDA-MB-231, HeLa and BT-474 cells, at the density of 200.000 cells/slip were incubated with free Dox and unmodified/modified DNA tile-Dox structures at 2 µM Dox. After the incubation, the concentration of Dox in the lysed cells was determined by fluorescence spectroscopy.

Figure 4.38. shows the Dox levels of BT-474, HeLa, and MDA-MB-231 cells incubated with free drug and unmodified/modified DNA tile-Dox structures obtained with fluorescence spectroscopy. From the results shown in Figure 4.38, when Dox levels in the cell lysates of the cells treated with Dox samples were examined by fluorescence spectroscopy in each of the three lines studied, the fluorescence signals of Dox were found to be higher in the cells treated with the DNA tile-Dox-Lac than those incubated with the unmodified DNA tile-Dox carrier and free Dox.
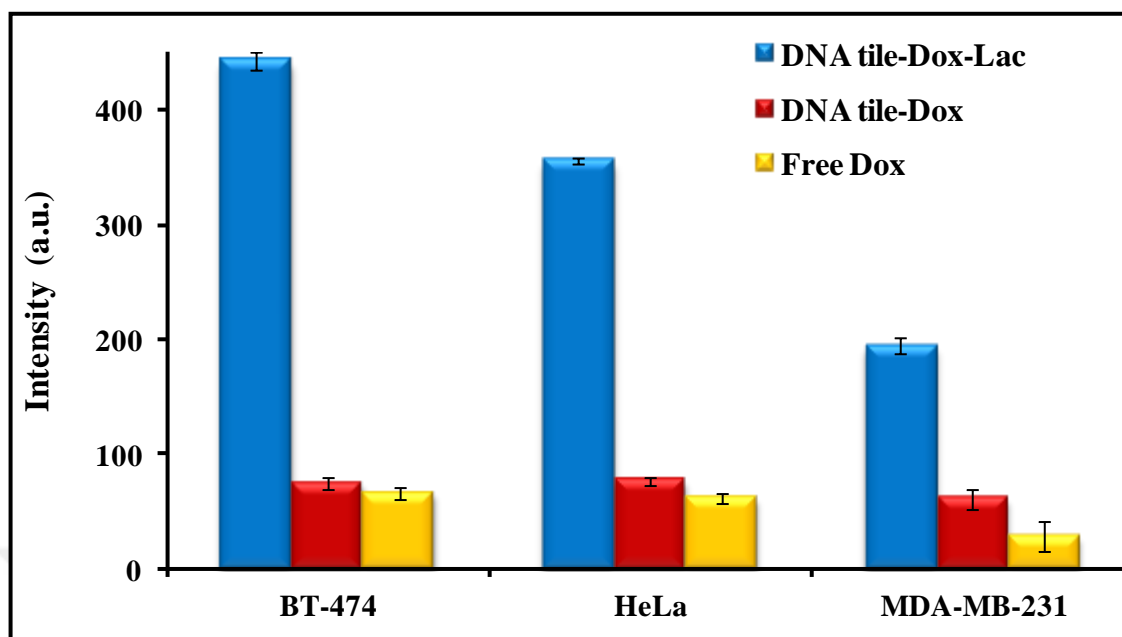
Figure 4.38. Dox levels of BT-474, HeLa, and MDA-MB-231 cells incubated with free drug and unmodified/modified DNA tile-Dox obtained with fluorescence spectroscopy.

To investigate the effect of different carbohydrates on the cellular internalization of the DNA tile-Dox structure, several experiments were performed using glucose and maltose modified structures. Glucose and maltose modified Dox loaded DNA tiles (DNA tile-Dox-Glu and DNA tile-Dox-Mal) were treated with three cancer cell lines, A549, MCF-7 and HeLa, respectively.

The Dox levels of MCF-7, HeLa, and A549 cells, which incubated with free drug and unmodified/modified DNA tile-Dox conjugates, obtained with fluorescence spectroscopy are shown in Figure 4.39. When the cells were incubated with DNA tile-Dox structures modified with glucose and maltose, an increase in the uptake of Dox by all cell lines was observed similar to effect of lactose modification. The fluorescence intensities of Dox were found to be higher in the cells treated with the carbohydrate modified DNA tile-Dox structures than those incubated with the unmodified DNA tile-Dox carrier and free Dox.
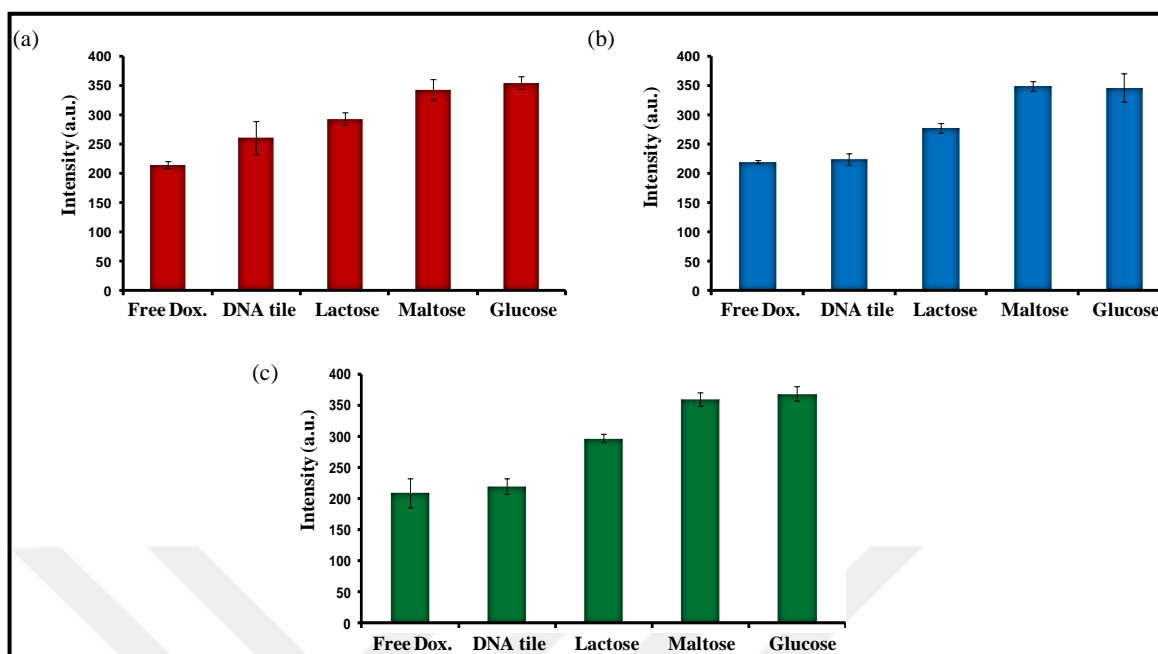
Figure 4.39. Dox levels of MCF-7 (a), HeLa (b), and A549 (c) cells incubated with free drug and unmodified/modified DNA tile-Dox obtained with fluorescence spectroscopy.

Folic acid is a natural molecule frequently used for the active targeting in drug delivery systems where nanostructures are used. Modification of the DNA origami structures with folic acid and the applications of these constructs including delivery of different therapeutics are being investigated [339]. Recently, it has been reported that the DNA tetrahedron structure modified with folic acid and SL2B aptamer increases the amount of doxorubicin taken by the cells [340]. In the study of Sun et al., it was revealed that the DNA-based carrier system designed to be able to self-degrade enhanced the activity of doxorubicin when it was modified with folic acid [341]. Folic acid modified nanocage structures in FR-positive HeLa cells have been reported to show 40-fold higher uptake than normal cells [342]. In the above-mentioned studies, the contribution of the folic acid to the DNA-based carriers for targeting and cellular uptake of the transported molecules was demonstrated clearly.

In this part of the thesis, the cellular uptake of the DNA tile-Dox system modified with folic acid (DNA tile-Dox-Fol) by FR-positive cell line HeLa cells was examined. Figure 4.40 shows the Dox levels of HeLa cells incubated with free drug and unmodified/folic acid modified DNA tile-Dox obtained with fluorescence spectroscopy. When the cellular uptake of free Dox and DNA tile-Dox-Fol system was compared in FR-positive HeLa

cells, it was seen that Dox levels of HeLa cells treated with DNA tile-Dox-Fol showed increased (Figure 4.40) similar to the previous studies performed with DNA tile-Dox-Lac.
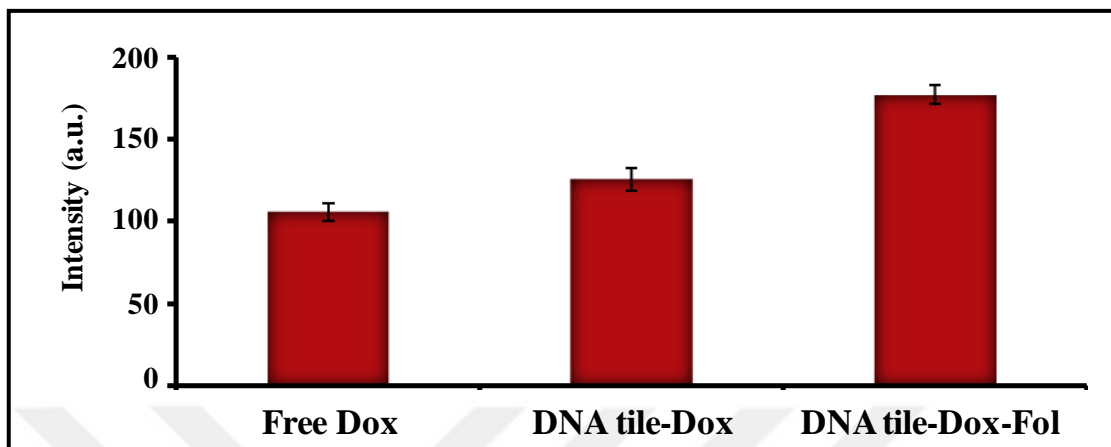
Figure 4.40. Dox levels of HeLa cells incubated with free Dox, DNA tile-Dox, and DNA tile-Dox-Fol obtained with fluorescence spectroscopy.

The application of lactose and folic acid modifications in combination has also been tried. The fluorescence spectroscopy results of the drug-loaded system modified with lactose and folic acid (DNA tile-Dox-Fol-Lac) are given in Figure 4.41. It was found that the dual modification increases the cellular uptake more than the single modification performed with the folic acid.
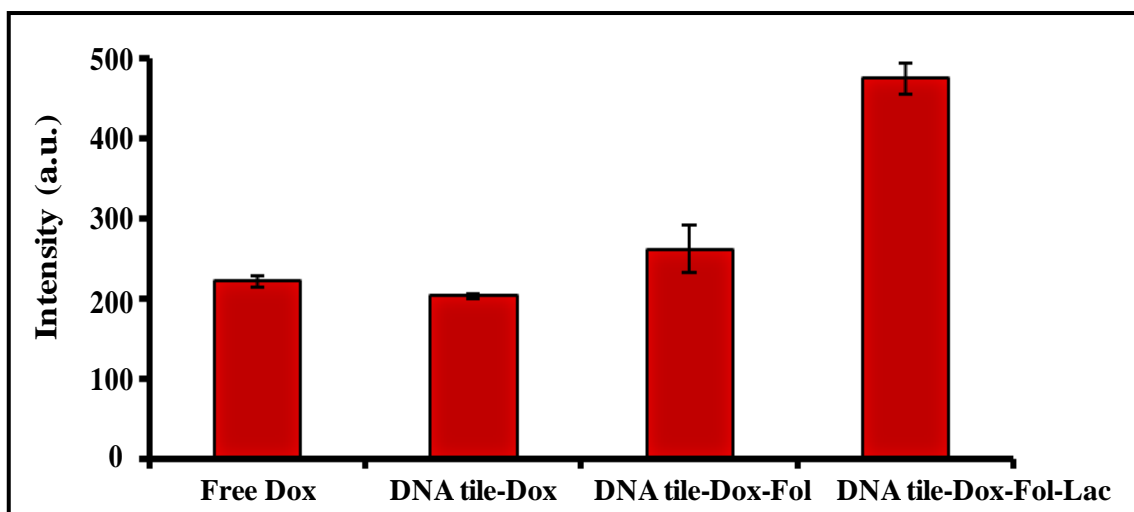
Figure 4.41. Dox levels of HeLa cells incubated with the free Dox, DNA tile-Dox, DNA tile-Dox-Fol, and DNA tile-Dox-Fol-Lac obtained with fluorescence spectroscopy.

4.7.2. Confocal Microscopy Analysis

The distribution and the cellular uptake level of the Dox in the cells were also examined using confocal microscopy. The confocal microscopy images of HeLa, BT-474, and MDA-MB-231 cells after incubation with the free drug and modified/unmodified DNA tile-Dox structures are given in Figure 4.42. The confocal microscopy images showed that doxorubicin was distributed widely in the cytosol and Dox fluorescence signals were found to be higher in the cells treated with DNA tile-Dox-Lac than the cells treated with free Dox. The results obtained by confocal microscopy analyses were consistent with the data obtained by the fluorescence spectroscopy analyses.
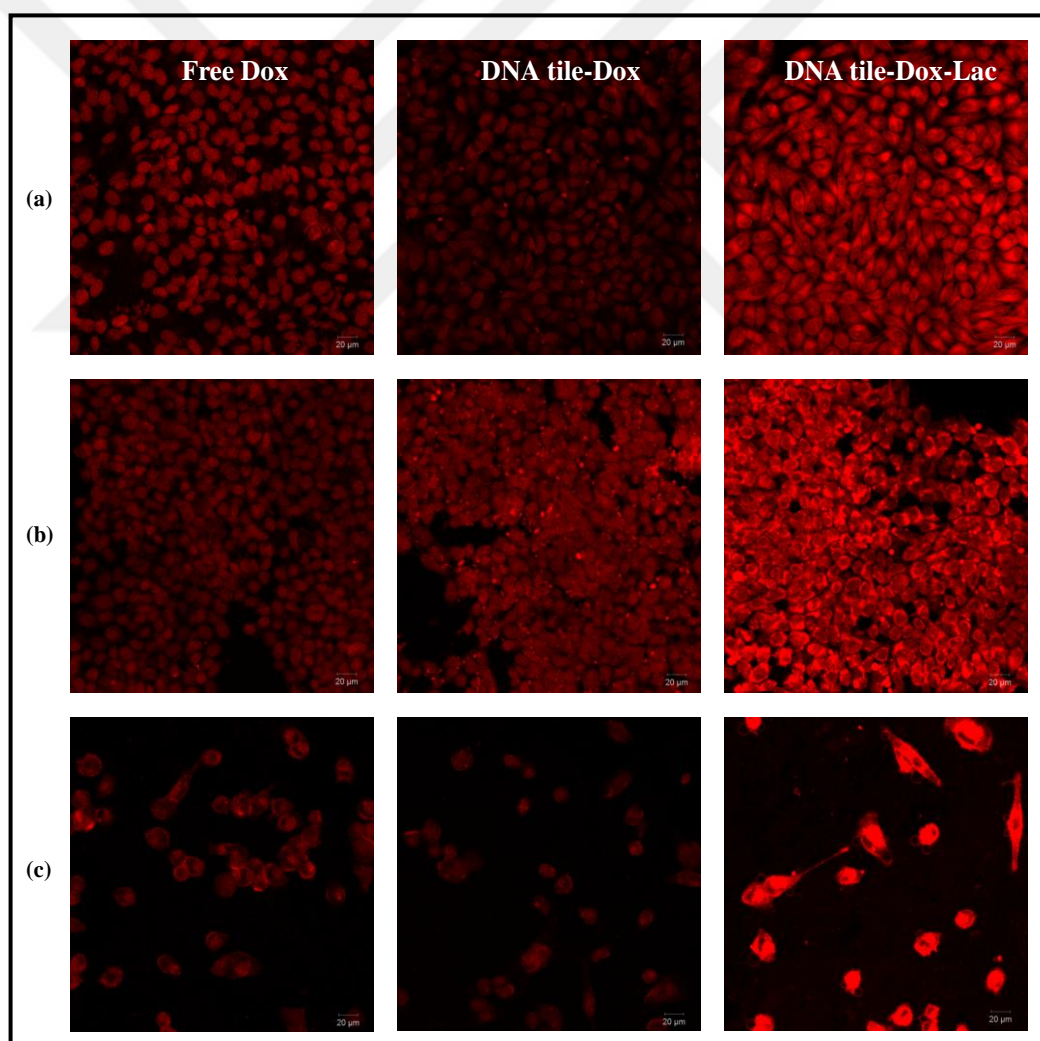
Figure 4.42. Imaging of Dox uptake levels by confocal microscopy in the cells incubated with free Dox and DNA tile-Dox with/without lactose. (a) HeLa, (b) BT-474, and (c) MDA-MB-231 cells.

The effect of the modifications performed with different carbohydrates on the cellular internalization of the DNA tile structure was also analyzed using confocal microscopy. As a result of incubation of HeLa cells with DNA tile-Dox-Glu, DNA tile-Dox-Mal, and DNA tile-Dox-Man, the fluorescence signals of Dox were found to be higher in the cells treated with the carbohydrate modified carriers than those incubated with the unmodified DNA tile-Dox carrier and free drug (Figure 4.43).
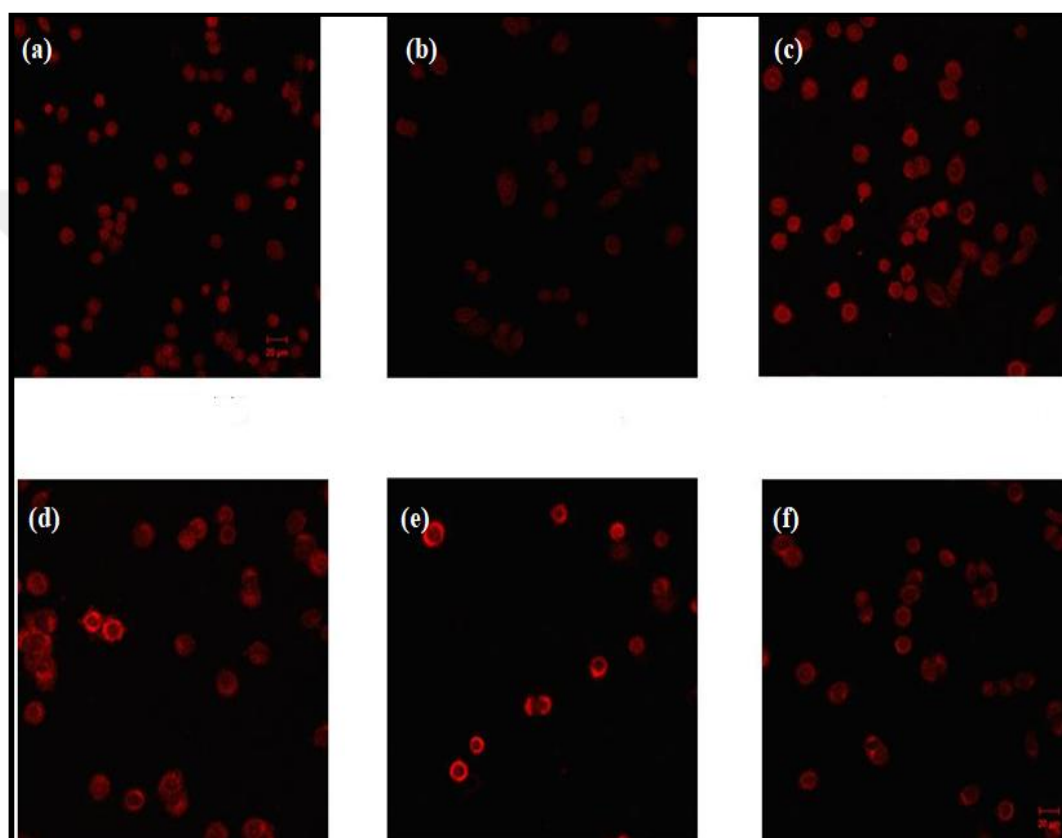
Figure 4.43. Confocal microscopy images of HeLa cells treated with free drug, unmodified/modified DNA tile-Dox with different carbohydrates by HeLa cells (20X). (a) free Dox, (b) DNA tile-Dox, (c) DNA tile-Dox-Lac, (d) DNA tile-Dox-Mal, (e) DNA tile-Dox-Glu, and (f) DNA tile-Dox-Man.

Similarly, confocal microscopy results of BT-474 cells, which were treated with carbohydrate modified DNA tile-Dox and free Dox molecule are given in Figure 4.44. The confocal microscopy images showed that the Dox fluorescence signals were found to be higher in BT-474 cells treated with carbohydrate modified DNA tile-Dox structures than BT-474 cells treated with free Dox.
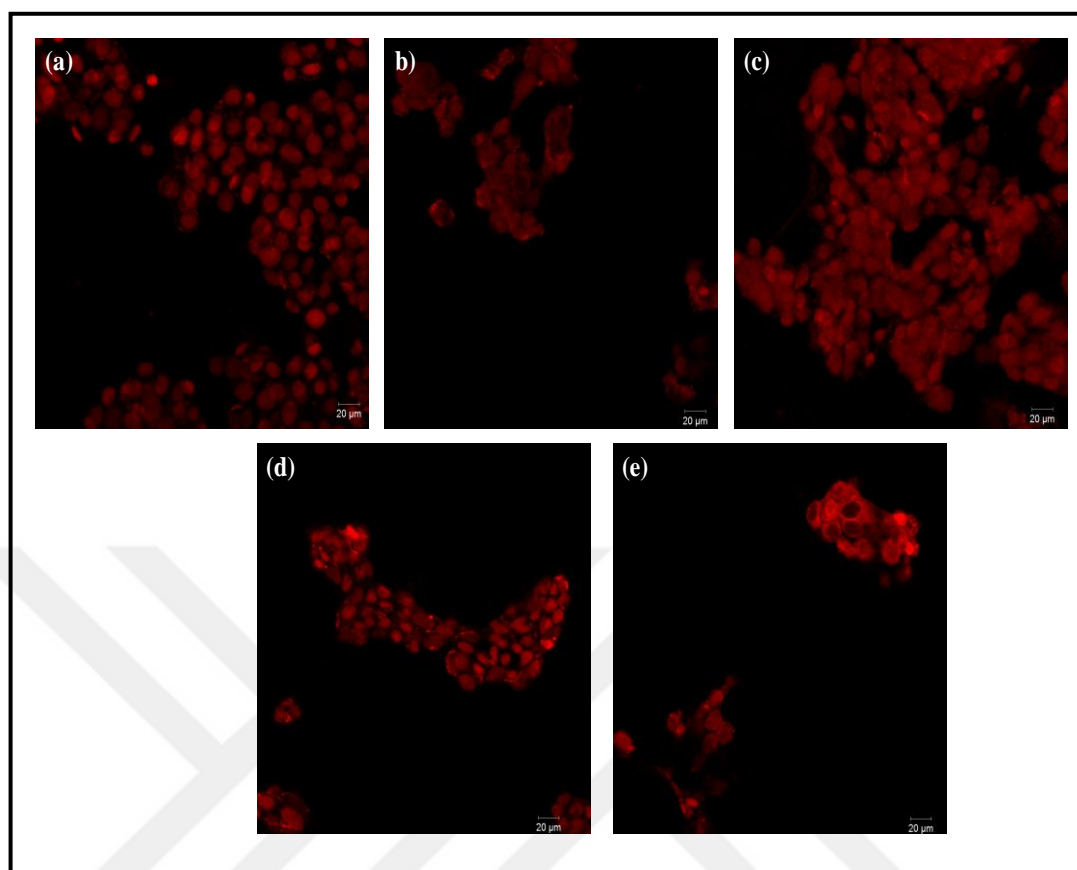
Figure 4.44. Confocal microscopy images of BT-474 cells treated with free drug, modified/unmodified DNA tile-Dox with different carbohydrates by HeLa cells (20X). (a) free Dox, (b) DNA tile-Dox, (c) DNA tile-Dox-Mal, (d) DNA tile-Dox-Lac, and (e) DNA tile-Dox-Glu.

The cellular uptake of the DNA tile-Dox-Fol was investigated using HeLa, LNCaP and PNT1A cell lines. Figure 4.45 shows the confocal microscopy images of HeLa, LNCaP, and PNT1A cells treated with free Dox, DNA tile-Dox, and DNA tile-Dox-Fol. According to the confocal microscopy analysis results, folic acid modification increased the cellular uptake of DNA tile-Dox structure in HeLa and LNCaP cancer cells. For PNT1A cells, folic acid modification didn't affect the cellular uptake of the DNA tile-Dox structure. This result can be related to low expression level of folate receptors in healthy cells.
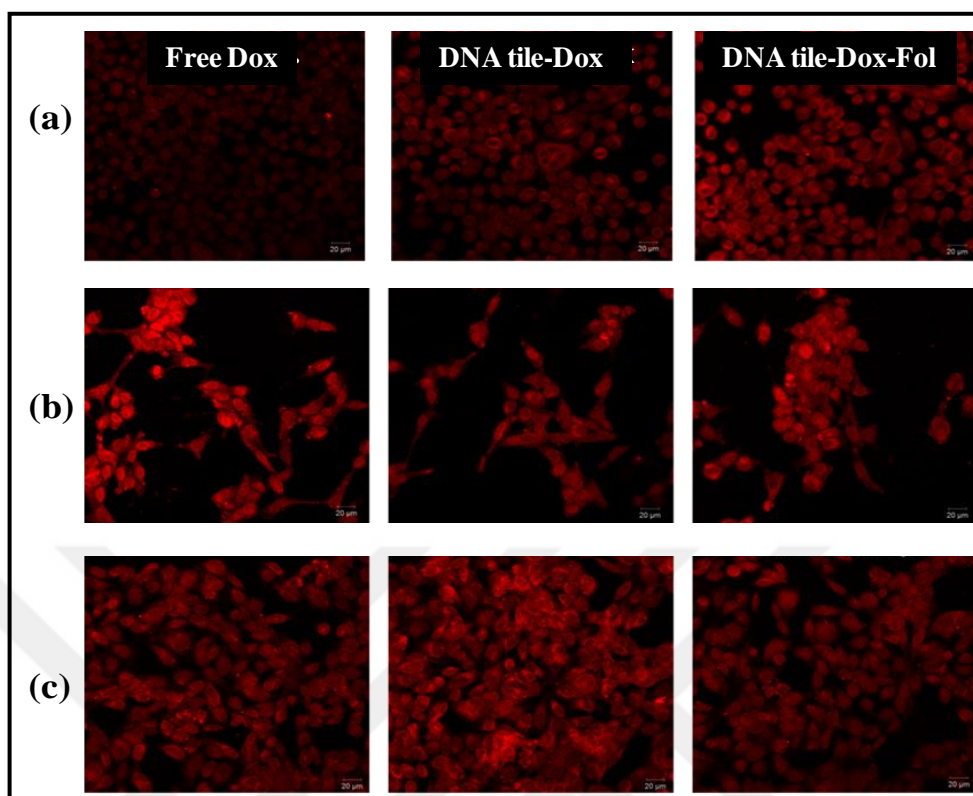
Figure 4.45. Confocal microscopy images of HeLa (a), LNCaP (b), and (c) PNT1A cells treated with free Dox, DNA tile-Dox with/without folic acid (20X).

The cellular uptake of the DNA tile-Dox-RGD by HeLa cells was also investigated using confocal microscopy. Figure 4.46 represents the confocal microscopy images of HeLa cells treated with free drug, DNA tile-Dox, and DNA tile-Dox-RGD. The results of the confocal microscopy analysis showed that the modification performed with RGD peptide contributed less to cellular uptake than the results obtained with folic acid or carbohydrate modifications.
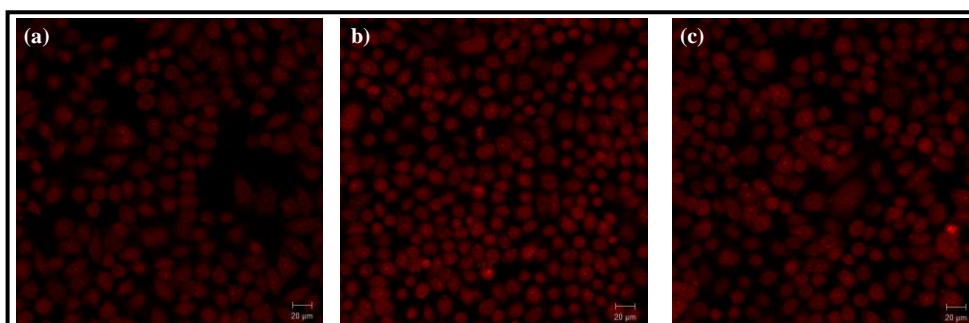
Figure 4.46. Confocal microscopy images of HeLa cells treated with free drug (a), DNA tile-Dox (b) and DNA tile-Dox-RGD.

4.7.3. Flow Cytometry Analysis

Flow cytometry, which is becoming a necessary device for the analysis of a variety of biochemical experiments such as cell cycle, cell, and apoptosis, was developed in the 1970s [343]. Flow cytometry is a high throughput technology, which can analyze thousands of cells per second. The technique uses principles of light scattering, light stimulation and emission of fluorochrome molecules to provide multi-parameter data hand from the cells [344]. During the analysis, each cell is analyzed individually and signals are detected from each cell, which is exposed to the treatment. These signals including fluorescence and light scattering, provide information about the effects of the treatments on the analyzed cells [343, 345, 346].

In a flow cytometry device, the cells or particles are carried through a fluid stream to the laser intercept and a detector, which places in front of the light beam, measures forward scatter (FS) [347]. Several detectors, which are located on the side, measure side scatter (SC). Fluorescence detectors measure the fluorescence emitted from positively stained cells or particles. While the FS informs about the size of the cell, the SS is concerned with the granularity of the cells [347]. The existence of particles in the cell causes the refractive index alterations and affects FS intensity. Therefore, the FS may not always give accurate information about cell size. SS intensity arises from the inner structure of the cells and is related to the mass and the protein content of the cells. SS is affected by the cell organelles and cytoplasm. SS gives information about the physical differences of the cells such as particle uptake and mitosis. Using flow cytometry, effects and amount of nanoparticles taken by the cells can be determined [348, 349].

The flow cytometry analyses were performed to determine the uptake levels of Dox by the cells, which were treated with free Dox and modified/unmodified DNA tile-Dox systems. Three cell lines, MDA-MB-231, HeLa and BT-474 cells, at the density of 100.000 cells/well were incubated with free Dox and modified/unmodified DNA tile-Dox structures at 2 μM Dox. After incubation, flow cytometry analysis was used to quantify the intracellular florescence of Dox in the harvested cells. Figure 4.47 shows the flow cytometry results of the MDA-MB-231, BT-474, and HeLa cells treated with free Dox and DNA tile-Dox structure with/without lactose modification. For the all three cell lines studied by flow cytometry analysis, it was seen that the DNA tile-Dox-Lac system was

taken up by a larger number of cells, and therefore the observed fluorescence was higher than the cells incubated with free Dox and unmodified DNA tile-Dox
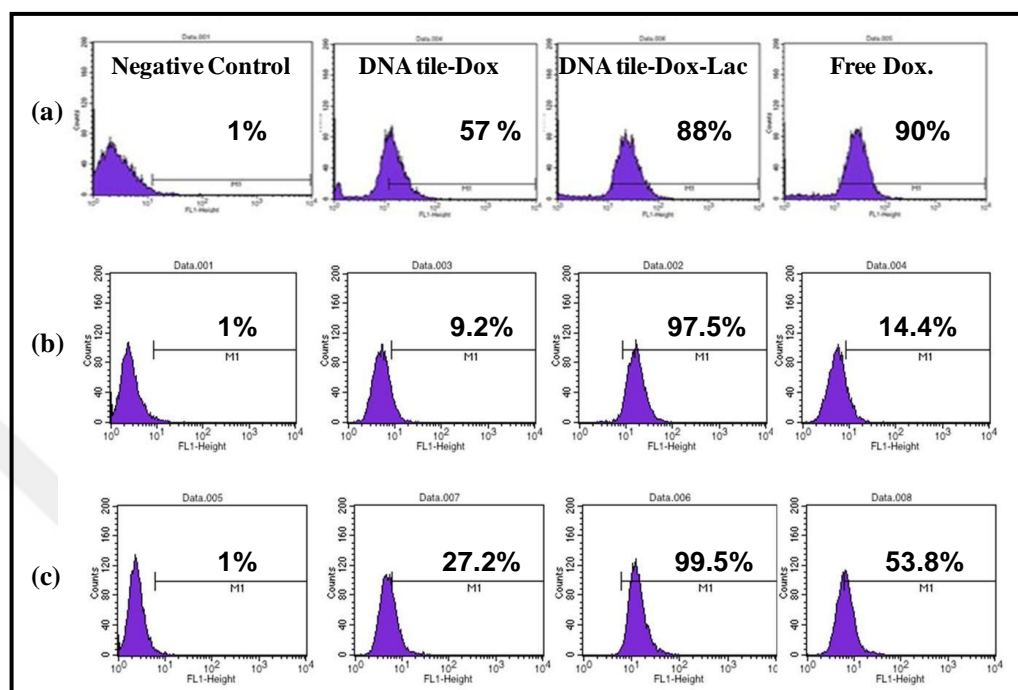
Figure 4.47. Flow cytometry results of the cells treated with free Dox and DNA tile-Dox structure with/without lactose modification. (a) MDA-MB-231, (b) BT-474, and (c) HeLa cells.

Similarly, doxorubicin uptake by the cells, which were incubated with drug-loaded DNA tile constructs modified with glucose, maltose, lactose, and mannose carbohydrates was also determined by flow cytometry analysis using MDA-MB-231, DU145, A549, MCF, and BT-474 cells. As seen in Figure 4.48, modifications performed with glucose, maltose, lactose, and mannose carbohydrates increased the number of cells, which takes the doxorubicin loaded DNA tile structures. It was shown that free drug molecule and DNA tile-Dox structure without modification are internalized by the each cancer cell line less than those of the carbohydrate modified DNA tile-Dox structures.
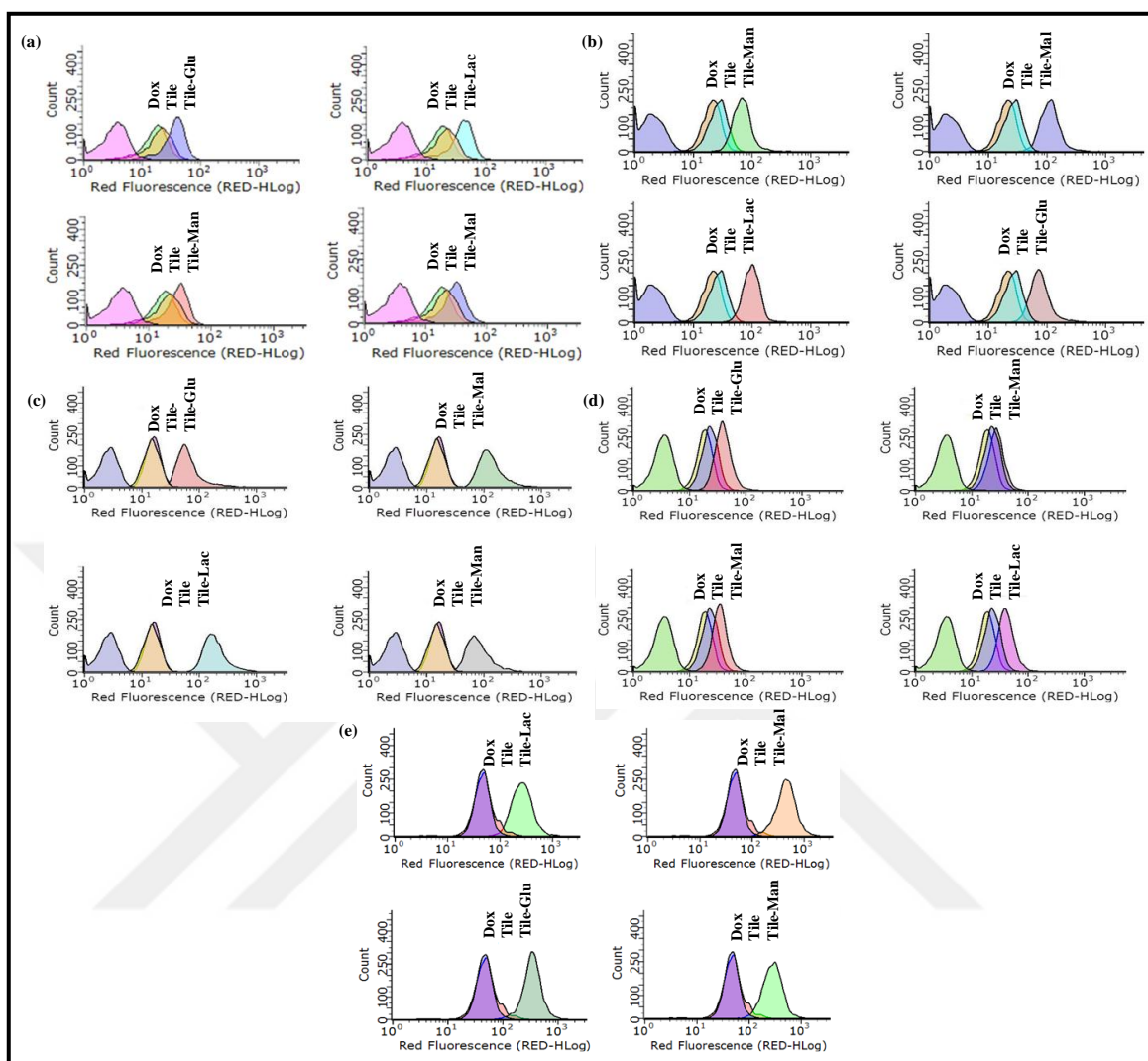
Figure 4.48. Flow cytometry results of the cells treated with free Dox and DNA tile-Dox structure with/without different carbohydrate modifications. (a) MDA-MB-231, (b) DU145, (c) A549, (d) MCF, and (e) BT-474 cells.

The cellular uptake of the folic acid and RGD peptide modified doxorubicin loaded DNA tile constructs (DNA tile-Dox-Fol and DNA tile-Dox-RGD peptide) was examined on U87 cells, which express folate receptors on the cell membranes. In order to investigate the cellular uptake of these complexes, U87 cells were exposed to free Dox, DNA tile-Dox-Fol, and DNA tile-Dox-RGD peptide. The intracellular Dox contents were determined quantitatively by using flow cytometry. Figure 4.49 shows the flow cytometric histograms of the U87 cells treated with free Dox, DNA tile-Dox-Fol, and DNA tile-Dox-RGD peptide. Flow cytometry analyses results of the U87 cells showed that when the cells were

incubated with DNA tile-Dox-Fol, and DNA tile-Dox-RGD, a shift of a histogram to the right indicates a larger amount of Dox was internalized into the U87 cells.
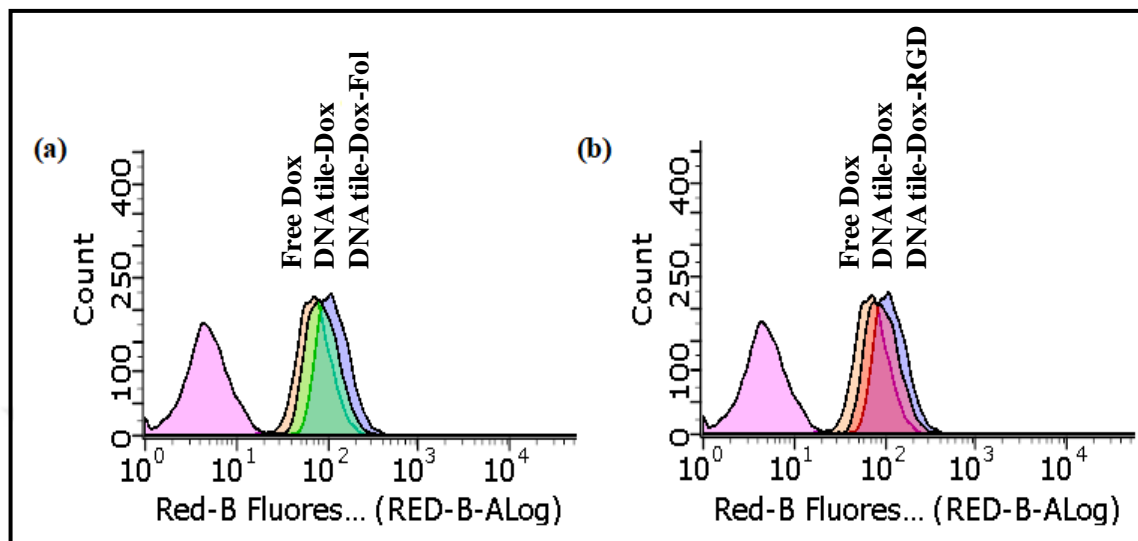
Figure 4.49. Flow cytometric histograms of the U87 cells treated with free Dox, DNA tile-Dox-Fol (a), and DNA tile-Dox-RGD (b).

As a result of the cellular uptake experiments, it was seen that the modifications made with carbohydrates increased the cellular uptake of the DNA tile-Dox constructs regardless of the cell type being studied. However, modification performed with folic acid only appears to work in cell lines that overexpress the receptors of this ligand and positive contribution to the cellular uptake of DNA carrier system only occurs in these cell types. Modification with RGD peptide has been shown to be less effective than carbohydrate modified or folic acid modified systems on the cellular uptake of the DNA tile-Dox.

4.8. INTERNALIZATION STUDIES WITH INHIBITOR MOLECULES

DNA-based structures are usually internalized into the cells through endocytic pathways such as adsorptive endocytosis, fluid phase pinocytosis etc [350, 351]. Depending on factors such as the type of cell being studied [352, 353], the composition of the gene carrier [354, 355] and the particle size [356], cellular uptake takes place via different endocytic pathways such as clathrin-dependent endocytosis (CDE) or caveolae-mediated endocytosis (CME). In clathrin mediated endocytosis, clathrin coated pit formation occurs by regulation of the clathrin coating protein inside the plasma membrane. Beside clathrin, a

number of molecules such as the adapter complex, AP2, which responsible for the connection between transported structures and clathrin, are participated in this endocytic internalization path [357, 358].

Caveolae-mediated endocytosis, which occurs by the invagination of cholesterol-rich microstructures of plasma membrane containing the coating protein, caveolin, is also one of the endocytic ingestion pathways [359]. Phagocytosis and macropinocytosis are also endocytic uptake pathways that allow the uptake of liquid and solid particles. In these ways, particle uptake occurs by the occurrence of big F-actin-coated vacuoles [360, 361].

When attempting to determine the cellular uptake pathways of carrier structures, chemicals such as chlorpromazine, sodium azide, methyl-β-cyclodextrin, which inhibits different endocytic pathways are used. Cellular uptake pathways and inhibitor molecules used in the inhibition of these pathways are shown in Figure 4.50.
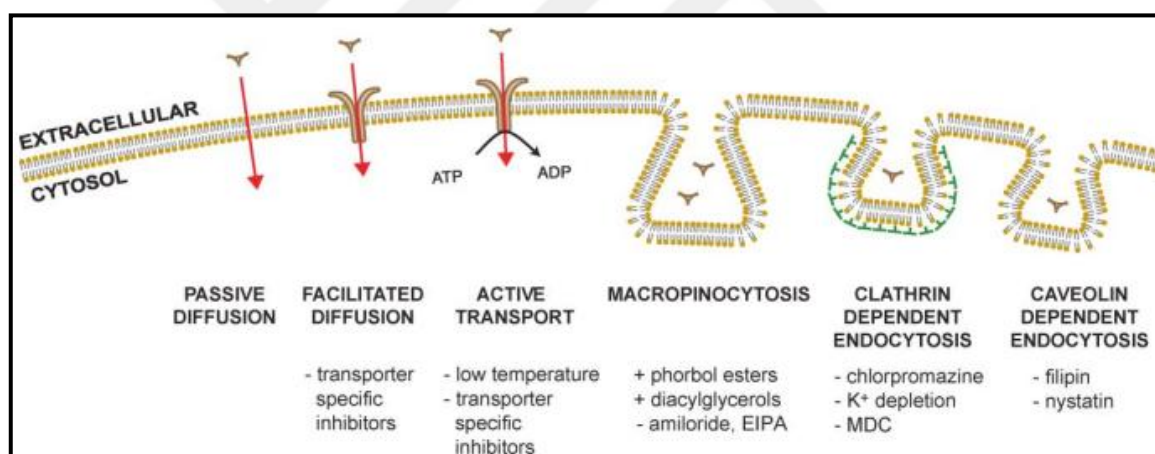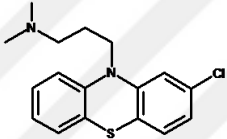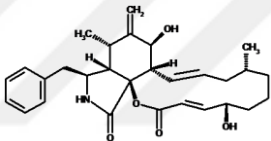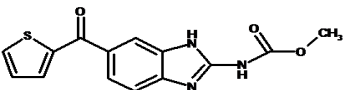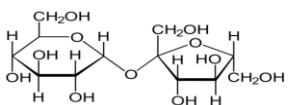
Figure 4.50. Cellular uptake pathways and inhibitor molecules used in the inhibition of these pathways [362]

As it is known, carrier structures have the ability to change drug delivery uptake routes. The presence of ligands that allow receptor interaction on the carrier molecule can seriously affect the pathway and amount of the drug is taken by the cells. According to the results of the fluorescence spectroscopy and the flow cytometry analysis, Dox is taken more by cells when given to the cells through carbohydrate modified tile structures. This situation suggests that the Dox uptake pathway could have changed and drug could have been taken up by the cell in a different way from passive diffusion.

In this part of the thesis, the uptake of the Dox molecule, which is normally taken up by passive diffusion into the cells, with the DNA tile-Dox-Lac was also investigated as mentioned before by the use of inhibitor molecules. Inhibitory molecules used in internalization of the DNA tile-Dox-Lac are listed in Table 4.2 together with their functions.

Table 4.2. Inhibitory molecules used in internalization of the DNA tile-Dox-Lac.

Inhibitor molecules	Chemical structıre	Function
Chlorpromazine		Inhibiton of Clathrin-mediated endocytosis
Cytochalasin B		Competitive inhibition of the glucose carrier action
Nocodazole		Inhibition of phagocytosis, microtubule depolymerization
Sucrose		Non-selective inhibiton of endocytosis
Sodium azide	NaN_3	Blocking ATP synthesis and endocytosis inhibition

HeLa cells were incubated with the DNA tile-Dox-Lac in the presence of the inhibitor molecules. First, HeLa cells were pretreated with medium containing inhibitor molecules for 30 minutes and then the cells were incubated with the serum free fresh medium containing samples in the presence of inhibitor molecules. All incubations were carried out

for two hours. After incubation, the cells were lysed and the cellular Dox contents were determined using the fluorescence spectroscopy.

Studies for the inhibition of the clathrin-dependent uptake pathway were first reported in the 1980s with applications such as hypertonic sucrose, potassium depletion [363, 364]. Treatment of the cells with hypertonic sucrose is one of the most common inhibition experiments. The treatment is usually carried out at a concentration of 0.4-0.5 M sucrose. With this treatment, the distribution of clathrin formations on the plasma membrane is realized [365]. It leads to inhibition by reducing the formation of clathrin-coated pits [366]. Hypertonic sucrose administration, which indicates the inhibition of clathrin-mediated endocytosis, also affects various invagination occurrences besides clathrin-mediated endocytosis.

In this study, the internalized Dox levels in Hela cells with the application of the hypertonic sucrose was determined by fluorescence spectroscopy. Figure 4.51 shows the Dox uptake levels of the cells exposed to the hypertonic sucrose treatment. As it is seen in Figure 4.51, HeLa cells were treated with sucrose at a concentration range of 0.1-0.5 M and this treatment caused to a decrease in the uptake of Dox with the modified DNA carrier structure. The hypertonic sucrose application, which is the marker of endocytosis, showed that the Dox could have been taken through CME with this carrier system.
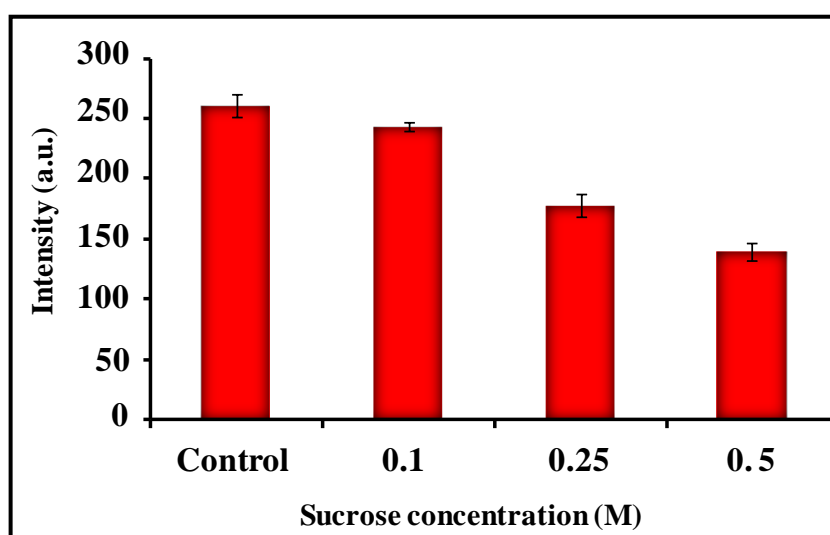
Figure 4.51. Effect of hypertonic sucrose treatment on the cells incubated with DNA tile-Dox-Lac

Chlorpromazine is an antipsychotic cationic drug molecule derived from the phenothiazine, and it is widely used in the inhibition of CDE [367, 368]. It has been reported that chlorpromazine, which interacts with clathrin and AP2 complex, affects the clathrin coated pit formation [367, 369] and also the formation of phagosome-like structures [370, 371].

Figure 4.52 shows the Dox uptake levels of the cells exposed to the chlorpromazine treatment. In the inhibition experiments performed with chlorpromazine, when working at a concentration of 5-40 µM chlorpromazine, a decrease in the level of Dox in the cells was observed with increasing chlorpromazine concentration. According to the results shown in Figure 4.52, a decrease in cellular uptake with chlorpromazine incubation showed that the drug loaded system may have been taken with clathrin-mediated endocytosis.
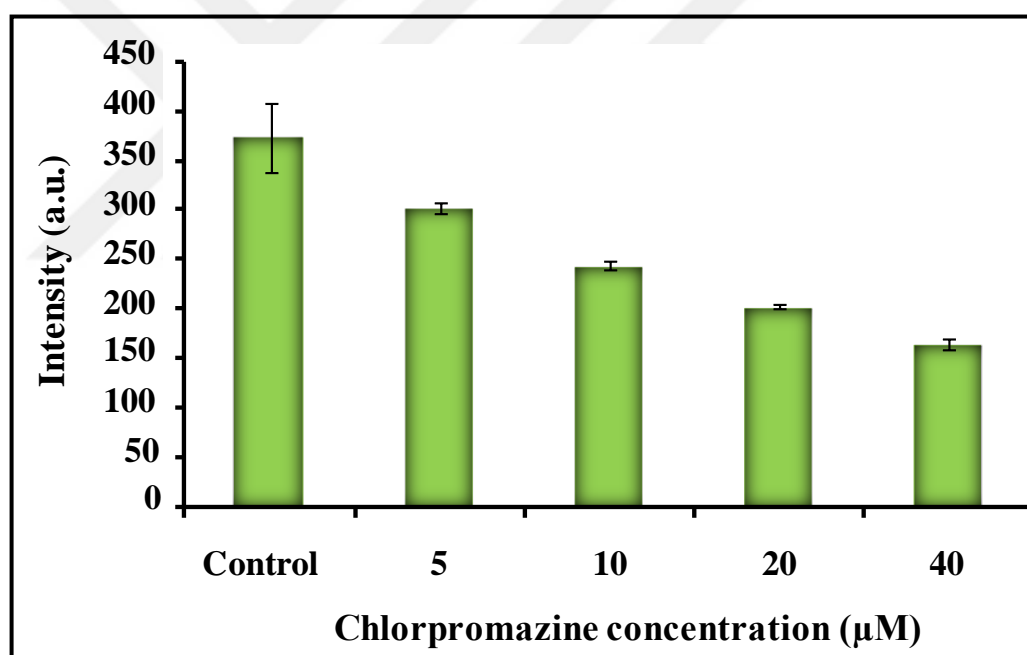
Figure 4.52. Examination of Dox uptake in cells incubated with DNA tile-Dox-lac in the presence of chlorpromazine

Energy-dependent endocytosis is a process that can be inhibited by the use of chemicals that cause ATP depletion or by reducing the cellular environment temperature [372]. Chemicals such as sodium azide (NaN_3), which inhibits ATP production, cause a decrease in the cellular uptake of different molecules when used in endocytosis inhibition assays [373].

Figure 4.53 shows the Dox uptake levels of the cells exposed to the NaN_3 treatment. The NaN_3 inhibitor, which we can identify as non-specific when compared to chlorpromazine, was studied at a concentration range of 3-48 mg/ml. It was observed that when NaN_3 was used even at 3 mg/ml concentration, the cellular uptake of Dox reduced by the DNA carrier compared to the control group. This result demonstrates that the modified DNA tile-Dox structure is taken up by the cells in an energy-dependent way and thus confirms the claim that it could have been taken by endocytosis.
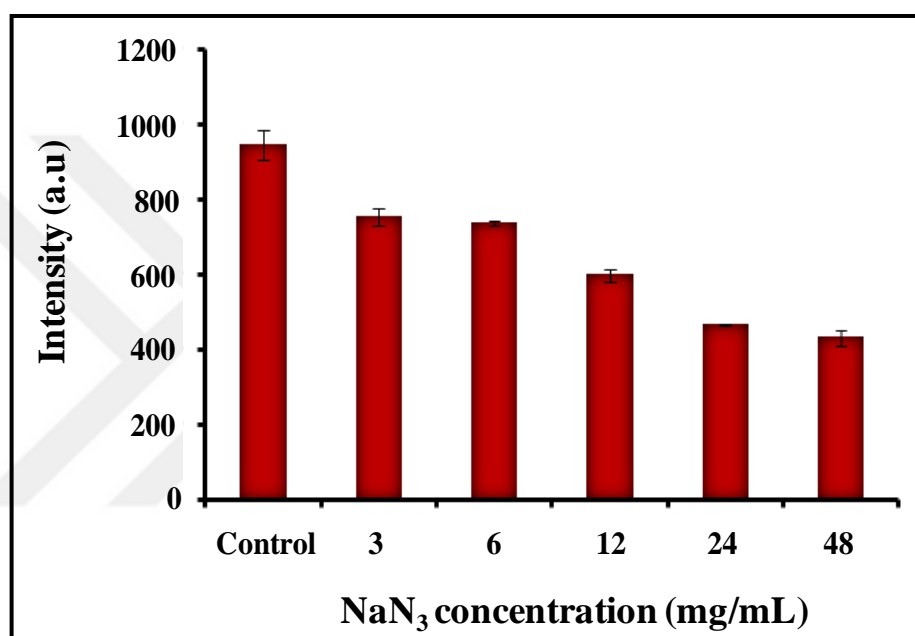
Figure 4.53. Examination of Dox uptake in cells incubated with DNA tile-Dox-lac in the presence of NaN_3

In addition to chlorpromazine and sucrose, two inhibitor molecules such as nocodazaole and cytochalasin B, which are responsible for the inhibition of different uptake pathways, have been also used in inhibition experiments. Cytochalasin blocks caveolae mediated endocytosis and macropinocytosis internalization pathways through depolymerization of actins [374]. Cytochalasin B is a competitive inhibitor molecule that blocks glucose transport [375]. Phagocytic uptake can be inhibited by the use of chemicals like nocodazole, which cause microtubule depolymerization such as colchicine [376].

In an attempt to inhibit the internalization of the DNA tile-Dox-Lac, cytochalasin B inhibitor was studied at a concentration range of 2-10 µM. Figure 4.54 shows the Dox uptake levels of the cells exposed to the cytochalasin B treatment. As shown in Figure

4.54, it was found that cytochalasin B had no inhibitory effect at any concentration value studied. This result confirmed that the DNA tile-Dox-Lac system may have been taken in a different way than the glucose transport.
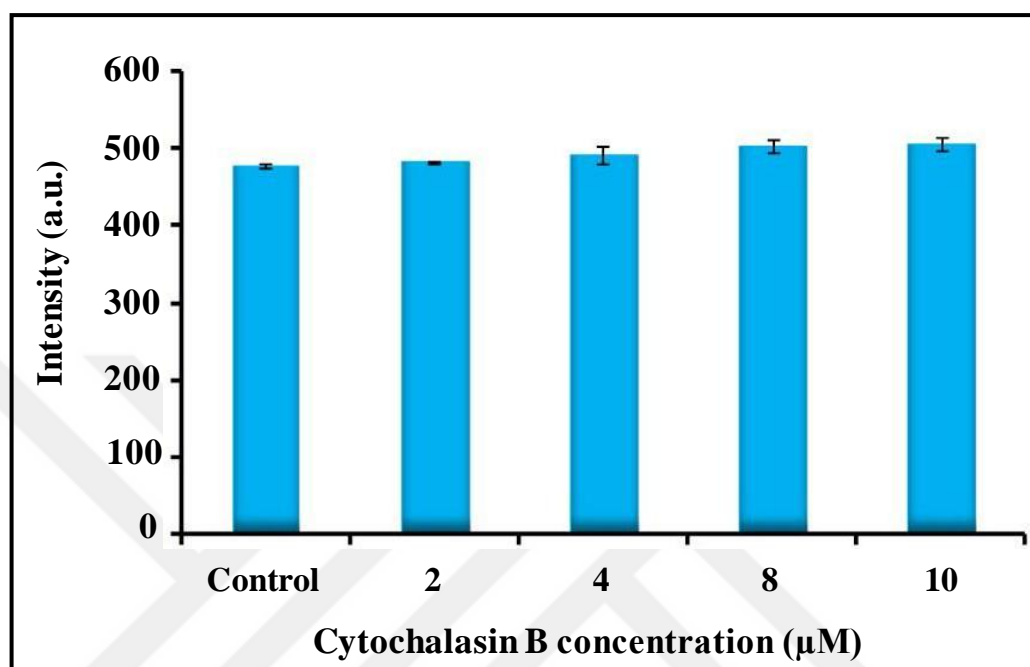
Figure 4.54. Examination of Dox uptake in cells incubated with DNA tile-Dox-lac in the presence of chlorpromazine

When chlorpromazine (15 μg/mL), nocadazole (50 μg/mL), and cytochalasin B (μg/mL) inhibitors were studied in parallel, chlorpromazine administration indicating clathrin-mediated endocytosis resulted in a decrease in the level of Dox. As can be seen in Figure 4.55, it was found that nocodazole and cytochalasin B inhibitors had no effect on Dox uptake. The experiment performed with NaN_3 showed that the DNA tile-Dox-Lac construct was taken into the cells via endocytosis. Experimental results obtained with inhibitors, which specifically characterize the uptake pathway, such as chlorpromazine, nocodazole and cytochalasin B, have shown that the uptake pathway may have been through CME.
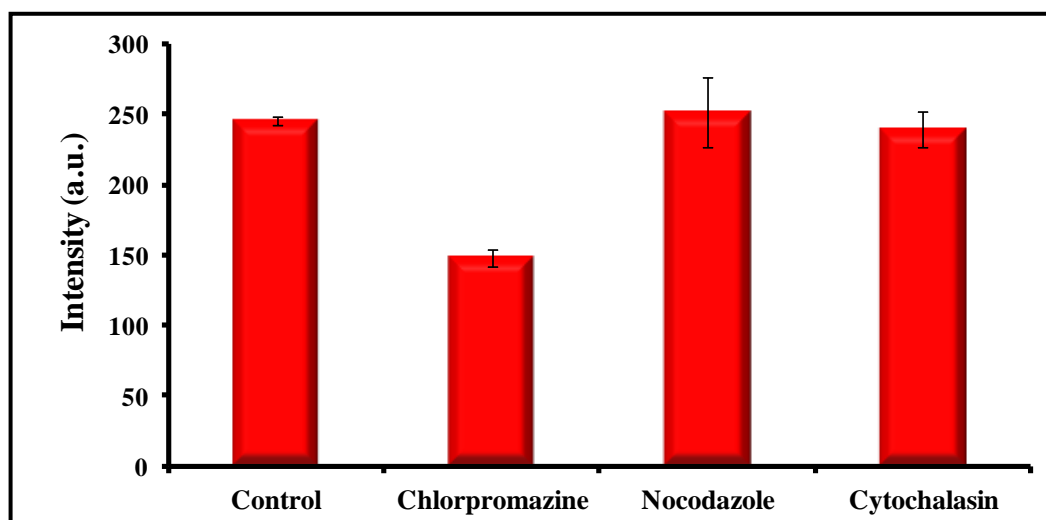
Figure 4.55. Effect of chlorpromazine (15 μg/mL), nocadazole (50 μg/mL), and cytochalasin B (1 μg/mL) treatments on the cells incubated with DNA tile-Dox-Lac

The inhibition experiments, which demonstrated with the results of fluorescence spectroscopy analysis, for the DNA tile-Dox-Lac, were also supported by confocal microscopy. Figure 4.56 shows the confocal microscopy image of the cells treated with chlorpromazine, cytochalasin B and nocadazole inhbitors. According to the confocal microscopy image given in Figure 4.56, cytochalasin B (50 μg/mL) and nocadazole (1 μg/mL) inhibitors don't affect the cellular uptake of the DNA tile-Dox-Lac. However, the reduction in the brightness of the cells treated with chlorpromazine (15 μg/mL), reiterates that this inhibitor has a negative effect on the uptake of the DNA tile-Dox-Lac construct. The confocal microscopy analysis, which performed with chlorpromazine (15 μg/mL), nocadazole (50 μg/mL), and cytochalasin B (1 μg/mL), gave consistent results with the fluorescence spectroscopy studies.
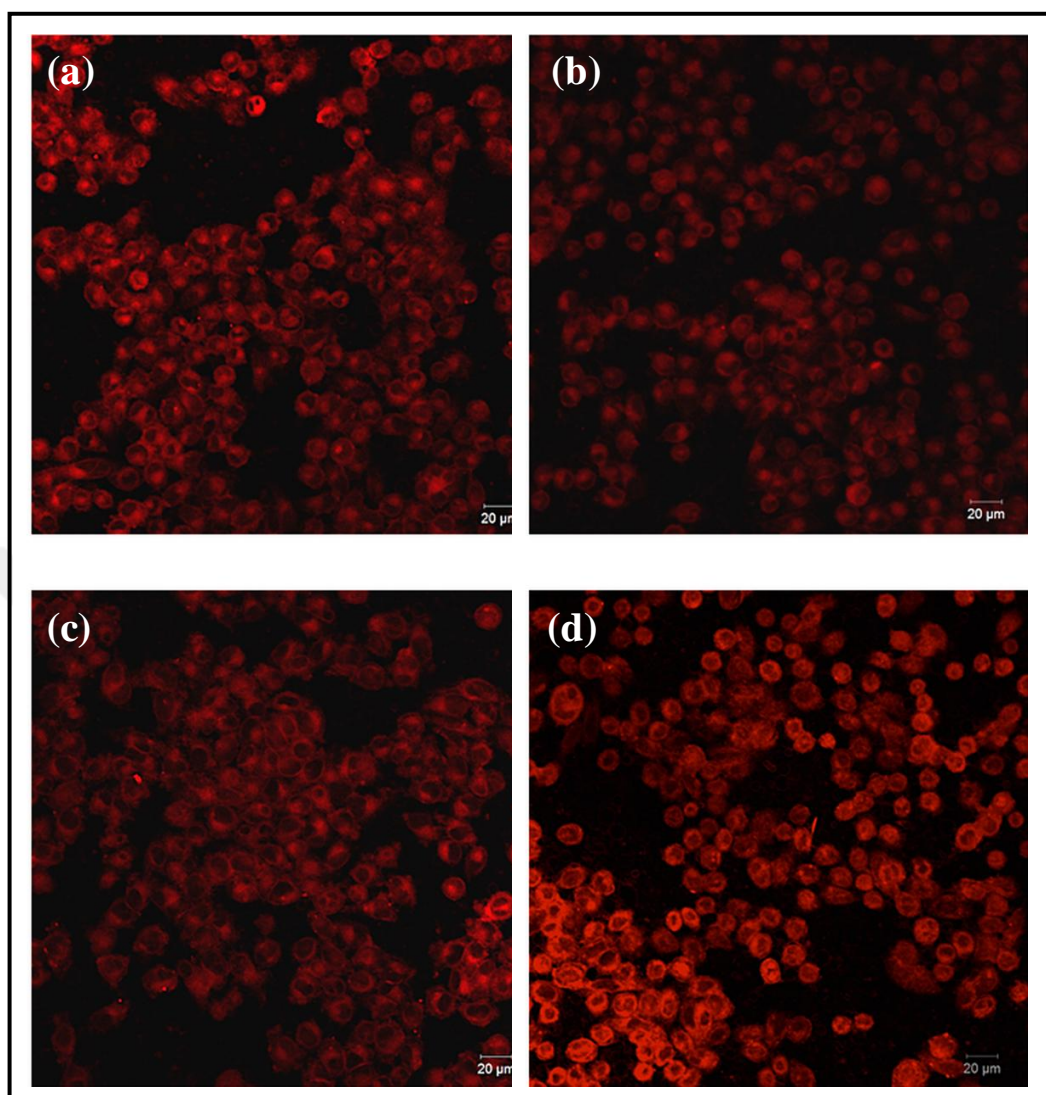
Figure 4.56. Examination of Dox uptake in cells incubated with DNA tile-Dox-lac in the presence of inhibitor molecules. (a) Control group, cells treated with (b) chlorpromazine (15 µg/mL), (c) cytochalasin B (50 µg/mL), and (d) nocadazole (1 µg/mL) inhibitors.

The effect of the targeting agent on the cellular internalization has also been studied. An excess amount of free lactose was added to the cell medium and the effect of free lactose on Dox uptake through the DNA tile-Dox-Lac was examined. Figure 4.57 shows the Dox levels of the cells incubated with increasing lactose concentrations. The similar results to the application of hypertonic sucrose showed that the lactose molecule also had an effect on the receptor-mediated endocytosis process. As it is shown in Figure 4.57, the level of cellular Dox level decreased with increasing concentration of free lactose.
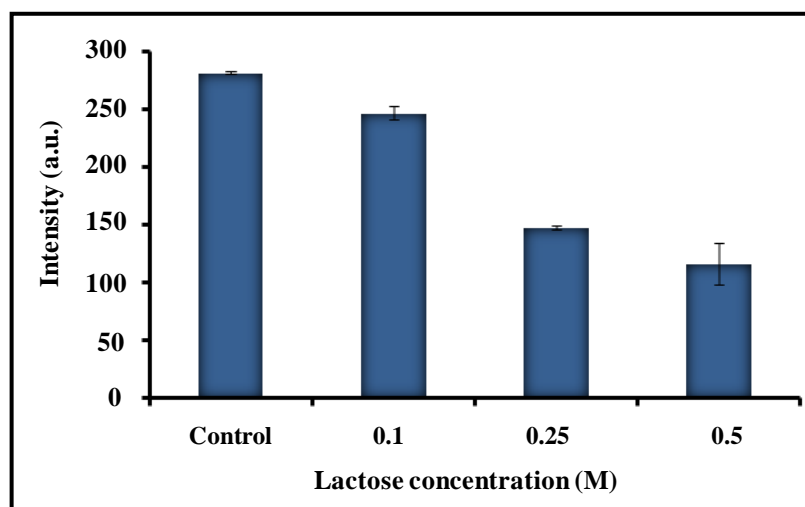
Figure 4.57. Examination of Dox uptake in cells incubated with DNA tile-Dox-lac in the presence of free lactose

The effect of inhibitor molecules on the cellular uptake of the DNA tile-Dox system and free Dox was also investigated. It is known that the uptake of Dox into the cells occurs via passive diffusion. Figure 4.58 shows the confocal microscopy image of the cells treated with free Dox in the presence of chlorpromazine (15 μg/mL), cytochalasin B (50 μg/mL), and nocadazole (1 μg/mL) inhibitors. It was observed that the inhibitory molecules studied did not influence the cellular uptake of free Dox. The absence of changes in the level of Dox in cells treated with these inhibitors confirms that Dox is taken in a different way from the uptake pathways indicated by these inhibitors.
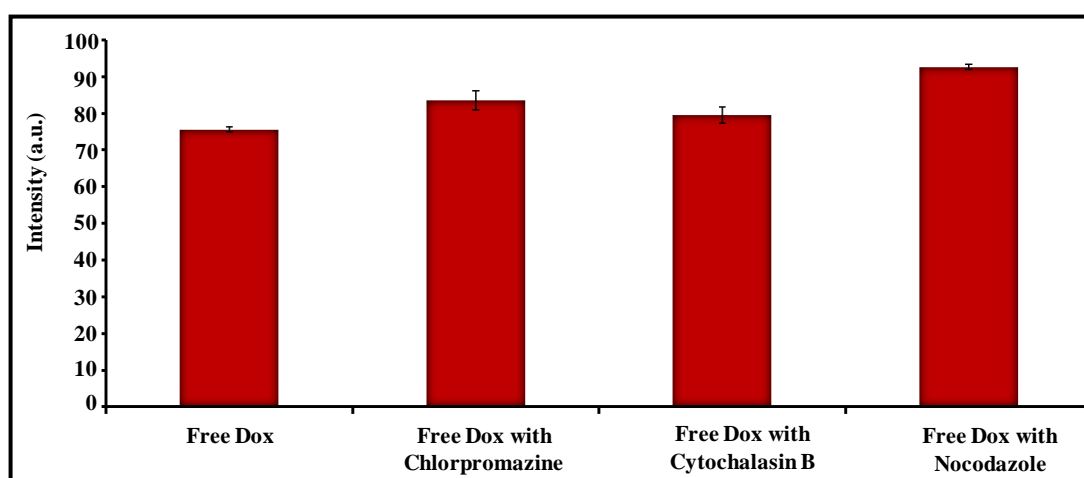
Figure 4.58. Effects of inhibitor treatments on free Dox uptake in HeLa cells.
(a) Control group, cells treated with (b) chlorpromazine (15 μg/mL), (c) cytochalasin B (50 μg/mL), and (d) nocadazole (1 μg/mL) inhibitors.

The cellular uptake of the DNA tile-Dox construct was also studied by the use of chlorpromazine and NaN$_3$ inhibitors. Figure 4.59 shows the confocal microscopy image of the cells treated with chlorpromazine (40-320 µM) and NaN$_3$ (3-12 mg/mL) inhibitors. As seen in Figure 4.59, concentrations of chlorpromazine, previously used for the DNA tile-Dox-Lac, did not show a decrease in the cellular uptake of the DNA tile-Dox construct. Similarly, the use of NaN$_3$ as an inhibitor causes a slight decrease in cellular uptake of the DNA tile-Dox
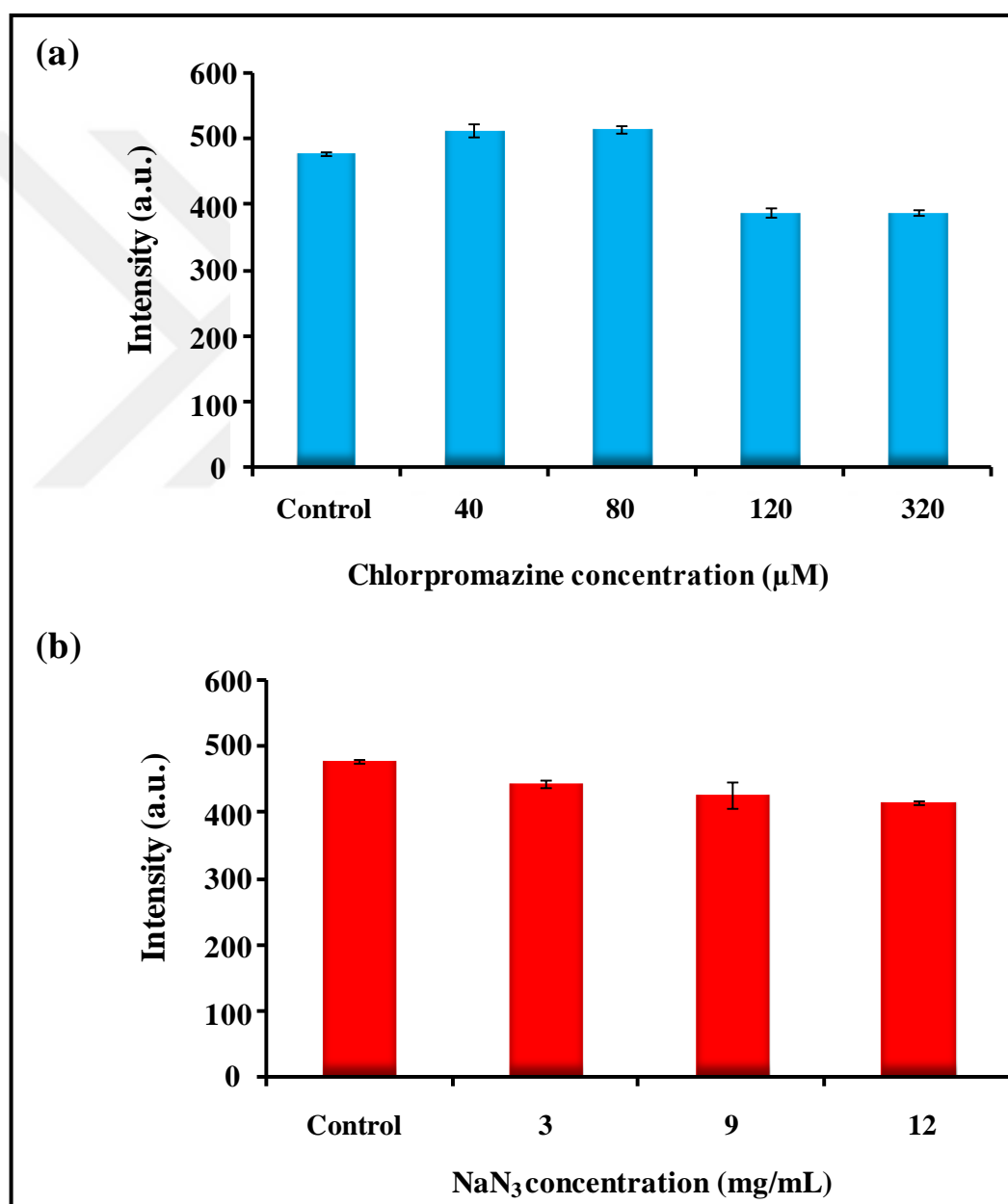
Figure 4.59. Effects of chlorpromazine (a) and NaN$_3$ (b) treatments on Dox uptake in HeLa cells incubated with DNA tile-Dox.

4.9. CELL CYCLE ANALYSIS

Cell cycle analysis allows to reveal the effects of different treatments on the cell cycle process and to determine the distribution of the cells in three basic phases of the cell cycle [377]. In the cell cycle analysis performed using a fluorescence DNA dye such as propidium iodide, the fluorescence intensity obtained in the wavelength at which the analysis is carried out will be proportional to the DNA content of the cells. It is expected that the intensities of cells in the G2/M phase (4n) will be twice that of the cells in the G0/G1 phase (2n), and this allows the determination of the amount of the cells at different phases [378].

Cancer cell dynamics were examined in real-time on live tumor tissue in the presence of a fluorescence indicator in the work of Yano et al [379]. Most of the cells in the center of tumor tissue were found to be in G0/G1 phase. In a similar manner, cancer cells distant from tumor blood vessels were reported to be in the G0/G1 phase. The study performed with the indicator molecule has shown that therapeutic agents often kill the cells mentioned above and the cells in the interior part of the tumor continue to proliferation [379].

Dox shows its effects through several ways including inhibition of the topoisomerase II acitivity, formation of free oxygen radicals and generation of a DNA-Dox intercalation product, which obstructs DNA replication [172, 380]. DNA damage is the main result of the Dox treatment. It has regulatory effects on cell proliferation and cell death pattern [179, 381]. Several cell types treated with Dox were subjected to cell cycle analysis, different results were obtained for cells. When the MCF-7 cells treated with Dox, they have arrested at G1/S and G2/M checkpoints. MDA-MB-231 cells were arrested at G2/M with Dox treatment [382].

In this part of the thesis, possible effects of the modified DNA tile-Dox structures on the cell cycle process were also tried to be determined. It was also determined whether these effects were similar to the effect of the free Dox. HeLa and U87 cells, which were exposed to Dox samples, were subjected to cell cycle analysis. In the experiment in which U87 cells were used, untreated U87 cells were used as control groups. Other cells were incubated with modified/unmodified DNA tile-Dox samples containing 2 μM Dox. Effects of the free Dox, DNA tile-Dox, DNA tile-Dox-Fol, and DNA tile-Dox-RGD on cell cycle process at 2

µM Dox concentration were investigated. Since the drug concentration used in the cellular uptake experiments was 2 µM, effect of this concentration value was investigated in the cell cycle analysis. Figure 4.60 shows the phase distribution (per cent) graph of the U87 cells treated with free Dox and modified/unmodified DNA tile-Dox. It was seen that the vast majority of control group cells that were not incubated with Dox were in phase G0/G1. As seen in flow cytometric cell cycle histograms of the U87 cells treated with Dox and DNA tile-Dox structures with/without modifications, the Dox-loaded samples caused arrest in G2/M phase similar to the effect of free Dox. In addition to this, there was an increase in the G2/M-phase population of the cells incubated with DNA tile-Dox-Fol and DNA tile-Dox-RGD compared to the cells incubated with free Dox. In parallel with this observed increase, a decrease in the cell population at the G0/G1 phase was also observed.
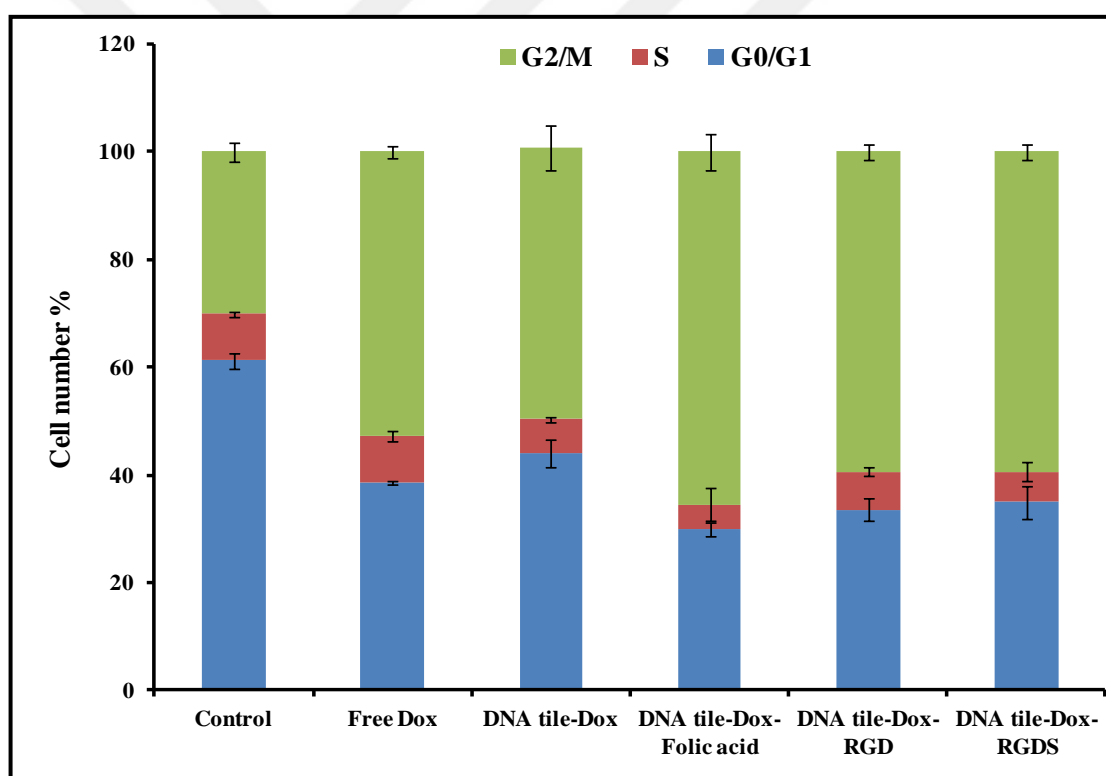
Figure 4.60. Phase distribution (per cent) graph of the U87 cells treated with free Dox and modified/unmodified DNA tile-Dox.

Effect of the DNA tile-Dox-Lac and DNA tile-Dox-Man on the cell cycle process of the HeLa cells was also studied and the phase distribution graphs are shown in Figure 4.61. When working with Hela cells, the concentration range was expanded between 0.5-10 µM. The effects of drug loaded samples on cells were examined at low and high drug

concentrations. As seen in flow cytometric cell cycle graphs of the HeLa cells, when HeLa cells were incubated DNA tile-Dox-Lac or DNA tile-Dox-Man, an increase in G0/G1 phase was observed in cells incubated with Dox at 0.5 and 1.25 μM concentrations. For both modifications, an increase in the subG1 phase indicating apoptosis was observed at these concentrations. It was observed that the decrease in the cell population of G0/G1 phase at 2.5 to 10 μM Dox concentrations was accompanied by an increase in the subG1 phase. As the concentration of Dox increases, an increase in the cell population of the subG1 phase is observed and this indicates an increase in the apoptotic cell population. This effect was observed for the cells incubated with both DNA tile-Dox-Lac and DNA tile-Dox-Man.
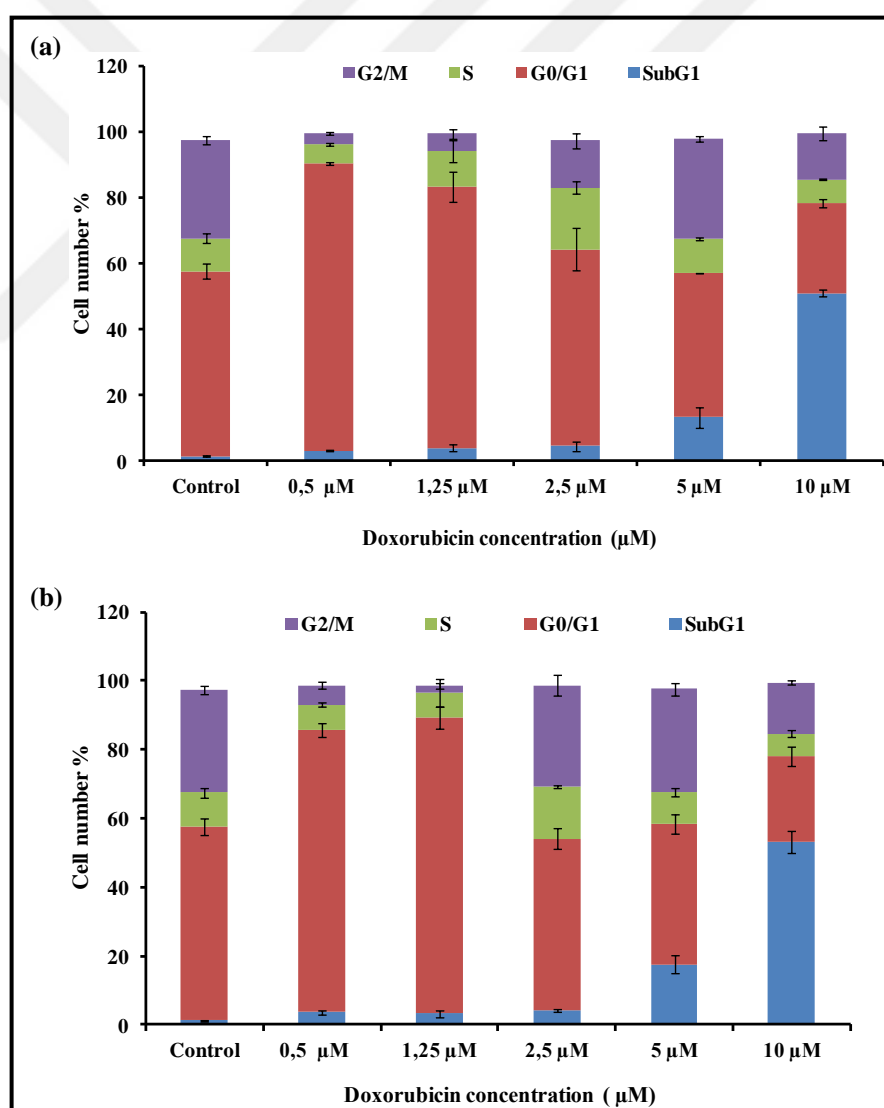
Figure 4.61. Effect of the DNA tile-Dox-Lac (a) and DNA tile-Dox-Man (b) on cell cycle process of HeLa cells.

4.10. GENE DELIVERY AND SILENCING OF LUCIFERASE

Gene therapy applications are one of the most promising strategies for the treatment of genetic diseases, although their applicability is limited by the lack of appropriate carrier systems [383]. The outcomes of the studies like human genome project revealed that the molecular level of genetic diseases is helping the development and orientation of gene therapy applications. The greatest challenge in gene therapy applications is delivery of the genetic cargo with low transfection efficiency, which is the result of the presence of biological barriers and the interaction of the genetic material, possessing polyanionic character, with biological barriers [384].

The use of viral carriers, which show high transfection efficiency with undesirable immune responses, is common in gene therapy applications [385]. However, this situation is problematic for the clinical applications, and efforts are being made to develop non-viral carrier constructs that may overcome this problem. The non-viral carriers, the vast majority of which are cationic lipids and synthetic polymers, also include several metal nanoparticles, CNTs, and synthetic liposomes [386]. However, the number of studies that were tried in the clinical stage is limited. The reason is that the toxicity and the transfection activity of the nanoparticles studied are not good enough for the clinical trials [386].

In this case, the carriers, that are formed using natural molecules, have begun to work on their transfection activities. In this regard, natural polymers such as lignin, schizophyllan, chitosan, as well as the use of nano-DNA structures, products of the structural DNA nanotechnology, are also investigated [387-390]. Ahn et al. have suggested that the wireframe DNA tetrahedra structure can be taken by endocytic pathways to human breast cancer cells without lysosomal degradation, and this structure can be used for gene and drug delivery [391]. In the study of Bermudez et al., the utility of the DNA tetrahedron structure modified with antisense oligo in gene silencing has been reported [392]. The use of the 3D DNA prism structure, designed to allow the attachment of antisense oligos at different points, was also studied by Fakhoury et al.[393]. In the study of Gang Chen et al., the use of periodic DNA ribbon constructs for siRNA delivery has been reported [394].

4.10.1. Preparation of The Luciferase Expressing Cell Lines

The most effective tools for transferring genetic information are anticipated as lentiviral expression vectors. The transfers that allow the stable expression of the effector molecules, for instance, cDNA, siRNA, are generally accomplished by the use of these vectors [395]. The lentiviral expression constructs can be packaged in psödoviral particles. The lentiviral constructions allow the transfection with high efficiency for the cells even which not prone to transfection. By transferring the lentiviral expression construct to the target organism, the desired effector molecules are expressed in a stable and prolonged manner. [395, 396]. It is thought that the most commonly used lentiviral expression constructs are HIV-based constructs [397-399] and the applications of these constructs are still biological risk factors.

In the context of the thesis, the preparation of MDA-MB-231 cells expressing luciferase, which to be used in the luciferase silencing, was carried out by the lentivirus transfection in our laboratory. The preparation of luciferase expressing MDA-MB-231 cell line began with the amplification of the required vectors. The circular pLenti-Bi-cistronic and pGL4.10.[luc.2] vectors were digested by using the restriction enzymes BamHI and KpnI. pLenti-Bi-cistronic vector consists of 8292 base pairs. pGL4.10.luc.2 vector consists of 4242 base pairs (Figure 4.62). The luciferase encoding part of the pGL4.10.[luc.2] vector was cut and transferred into the pLenti-Bi-cistronic vector.
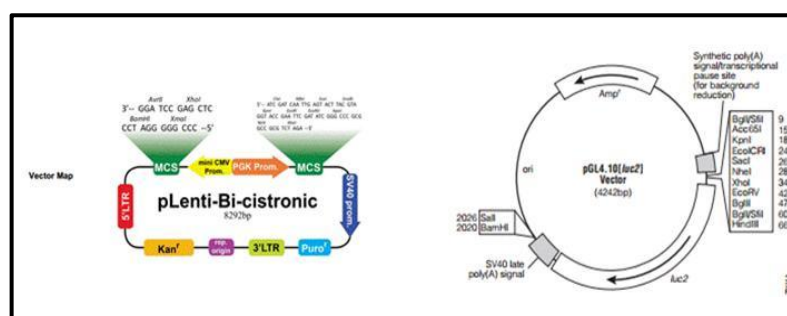
Figure 4.62**.** Map of the pLenti-Bi-cistronic and pGL4.10.[luc.2] vectors.

When pGL4.10.[luc.2] vector is digested using restriction enzymes BamHI and KpnI, pGL4.10.[luc.2] vector is divided into two fragments (2001 and 2241 bases); plenti-Bi-cistronic vector is divided into two fragments (621 and 7671 bases). In Figure 4.63, the

bands are shown in red squares indicate bands at 2001 and 7671 to be ligated to each other in the next step.
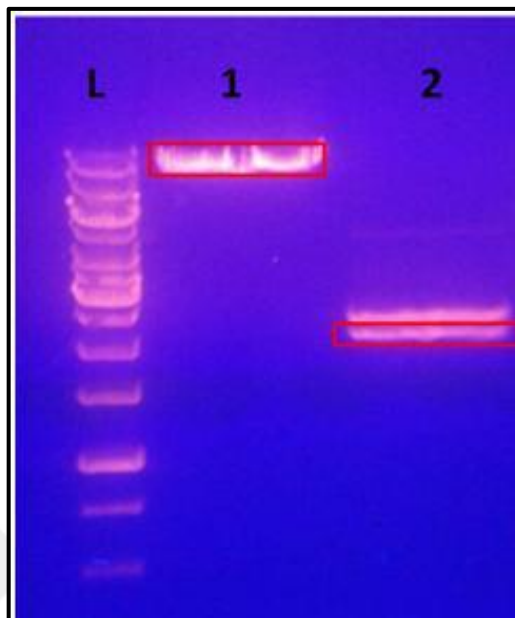
Figure 4.63. After digestion, agarose gel electrophoresis image of pLenti-Bi-cistronic and pGL4.10.[luc.2] vectors. (L) DNA marker, (1) The digestion of the pLenti-Bi-cistronic and (2) the digestion of the pGL4.10.[luc.2].

The bands at 7671 and 2001 were cut from the agarose gel using the gel extraction kit and obtained with 14.8 ng/µL and 10 ng/µL yield. The ligation of the vector components was carried out using 1:1, 1:3, and 1:5 vector/insert ratios at 22 °C in the presence of T4 DNA ligase for 18 hours. When the ligation reactions completed, transformations of the ligation reactions with different vector/insert ratios were carried out into the *E.coli* DH5α competent cells. After transformation, it was observed that the colony formation by incubation overnight at 37 °C in LB agar petri dishes with 1:5 vector/inser ratio. The single colonies were taken from the LB agar petri dishes, were amplified in LB medium and using this liquid culture, plasmid isolation was carried out using plasmid isolation kit. The new ligation product, pLenti-Bi-cistronic-[luc] vector, was isolated with 87.6 and 85.8 ng/µL yield.

To verify the ligation, the newly obtained vector was digested using BamHI and KpnI restriction enzymes. According to the gel image, when the newly obtained plasmid vector was digested, the digestion products have with the same sizes with its constituent parts. It was verified that the realization of the ligation reaction (Figure 4.64).
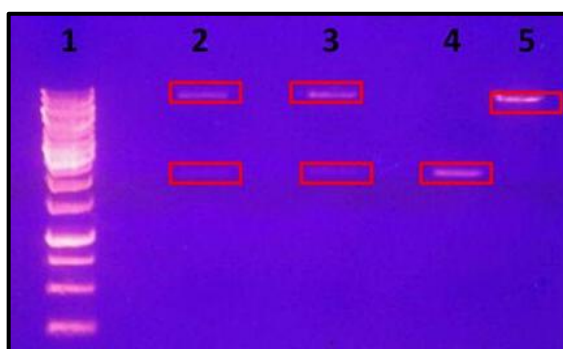
Figure 4.64. Agarose gel electrophoresis image of the digestion of the newly prepared pLenti-Bi-cistronic-[luc] vector. (1) Ladder, (2) Digestion reaction sample from isolated colony 1, (3) Digestion reaction sample from isolated colony 6, (4) The digestion products of the pGL4.10.[luc.2] vector (5) The digestion products of the pLenti-Bi-cistronic vector.

After being introduced into the HIV shell, pLenti-Bi-cistronic-[luc] vector was given into the HEK 293 packaging cells with packaging and envelope plasmids [396] used for the infection of MDA-MB-231 cancer cells. Thus obtained cell line stable and long-term luciferase expressing have been carried out.

4.10.2. Morpholino Sequence

Gene silencing experiments were performed on luciferase expressing MDA-MB-231 cells. This cell line was constructed using recombinant DNA technology in our laboratory. In silencing experiments, morpholino antisense oligonucleotide sequence, CCC AGC GCC ATT CTA CCC ACT CGA, which was designed specifically for the luciferase mRNA sequence, was used and taken part in DNA tile. Also, the scrambled form of antisense oligonucleotide, CACGACGCACCTCTCGATCTCACC, without silencing function, was used as a control (Figure 4.65).

Figure 4.65. Luciferase coding sequence and overlapping antisense morpholino sequence.

4.10.3. Characterization of The Morpholino Containing DNA Tile

4.10.3.1. Agarose Gel Electrophoresis

The morpholino containing DNA tile structure was formed using the long scaffold strand (140 base) and the short helper strands (24-66 bases) in TAE/Mg^{2+} hybridization buffer as given in method 3.1. The DNA tile formation was monitored by agarose gel electrophoresis. In Figure 4.66, the agarose gel image of the DNA hybridization sample run on gel prepared at 2 per cent agarose concentration is demonstrated. When an oligonucleotide was added in each line for the tile formation, it was observed that the growth of the structure gradually due to addition of the complementary oligonucleotides.

When agarose gel was applied (Figure 4.66-a), the tile formation was not observed well enough in 2 per cent agarose gel so that MOPS-formaldehyde gel was prepared and the structure formation was once examined in one per cent MOPS-formaldehyde gel. As seen in Figure 4.66-b tile formation is more clearly shown using the MOPS- formaldehyde gel. The increase of the molecular weights of the DNA constructs as observed from the bands on the agarose gel electrophoresis image confirmed the hybridization of oligonucleotides step by step to form the DNA tile structure.
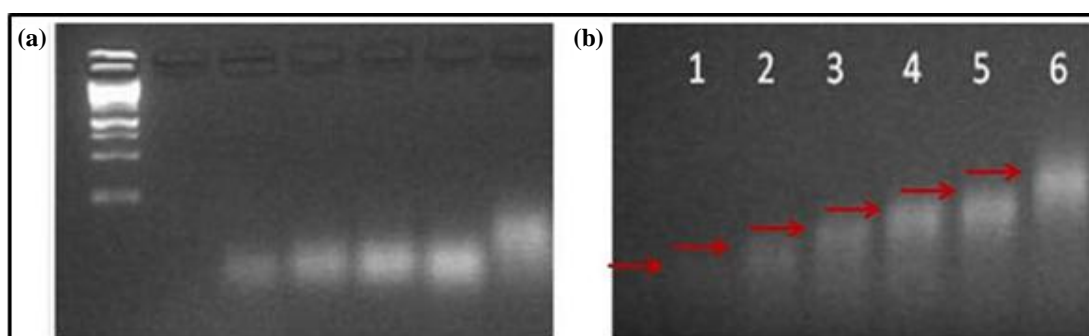
Figure 4.66. Gel images of the morpholino containing DNA tile. (a) 2 per cent agarose gel in TAE and (b) 1 per cent agarose in formaldehyde-MOPS buffer.

4.10.3.2. AFM Analysis

The formation of morpholino containing DNA tile structure was also analyzed with AFM. The AFM analysis was performed at non-contact mode to determine the sizes of tile structures and support to the observations with agarose gel electrophoresis. 2 μL of the DNA tile hybridization solution was dropped onto the newly cut mica surface, subsequently washed with deionized water and allowed to dry. The mica containing the dried sample was placed in the device and the image was taken from a droplet area where a droplet of suspension of DNA tile was placed. As mentioned earlier in the section 4.1.2, the presence of uncompleted DNA tile structures and aggregation formed they exhibited during the sample preparation, led to the observation of larger or smaller sized structures than the structures, which have expected size. The AFM image of the DNA tile is given in Figure 4.67. The DNA tile sample size was measured as 106 nm.
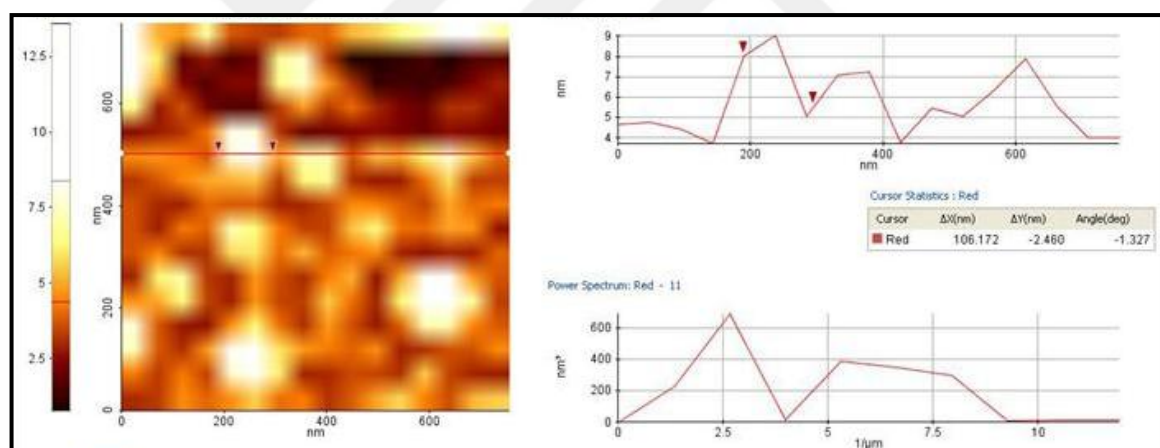
Figure 4.67. AFM image of morpholino containing DNA tile

4.10.4. Cytotoxicity of The Morpholino Containing DNA Tile

Considering the chemical structure, the morpholino oligonucleotides are not toxic molecules [400]. It has been reported that no toxicity is observed when given at 3 g/Kg doses in mice [401]. However, consideration should be given to the cytotoxicity of each sequence and possible toxic effects on the organism, taking into account the interactions that may be caused by the base pairing of the designed sequences [400]. The cytotoxicity of the DNA tile structures, which contain morpholino and scrambled morpholino sequence,

was examined on luciferase expressing MDA-MB-231 cell line at a concentration range of 0.25-1 µM. The cell viability analysis of the DNA tiles was determined applying WST-1 assay. The cell viability graphs of the morpholino sequence and the scrambled morpholino sequence containing DNA tiles are shown in Figure 4.68. As seen in Figure 4.68, the morpholino and the scrambled morpholino sequence containing DNA tile structures were found as non-toxic to MDA-MB-231 cells at studied concentrations. It was observed that the viability still remained at 80% for both constructs at 1 uM. The activation of tumor suppressor p53 and apoptosis, which is induced by their chemical toxicity of morpholino sequences, are among the off-target effects of the morpholino sequences [402-404]. This situation may be the reason for the observed cell deaths associated with increased morpholino concentration.
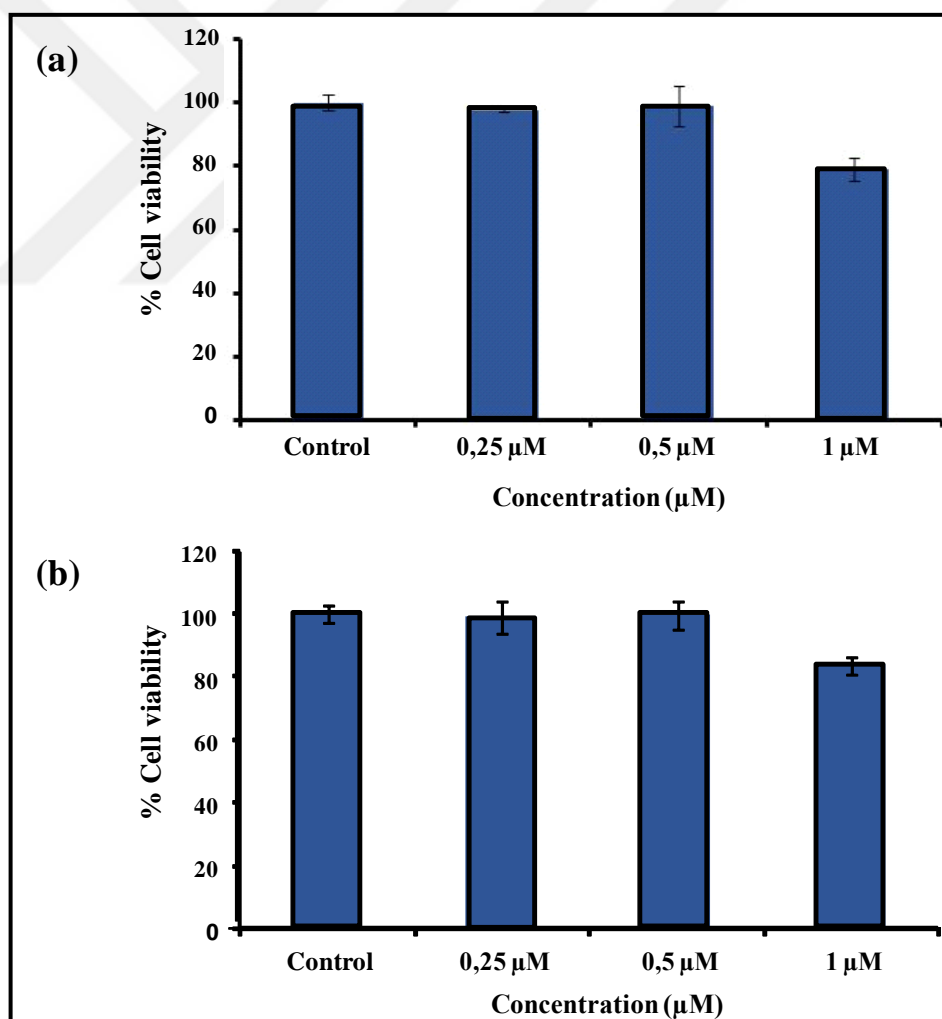
Figure 4.68. The cytotoxicity of the morpholino sequence (a) and scrambled morpholino sequence (b) containing DNA tile.

4.10.5. Western Blot Analysis of The Luciferase Silencing

Firstly, the expression of the luciferase protein by MDA-MB-231 cells was confirmed using the anti-Firefly luciferase antibody (ab181640) in Western blot analysis. Cell lysates obtained using RIPA buffer from cells expressing luciferase were used for the Western blot analysis. According to the Western blot image shown in Figure 4.69, it was seen that the preparation of the cell line expressing luciferase was successful due to the visualization of the expected protein band.
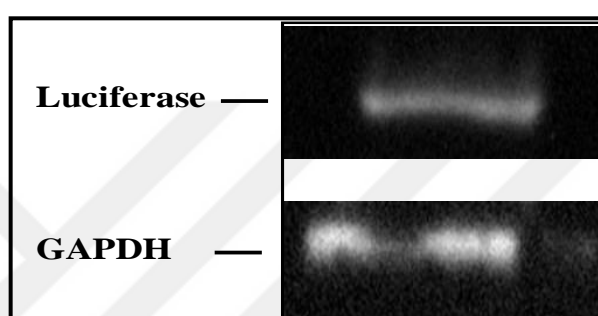
Figure 4.69. Western blot image for the confirmation of the luciferase expression

Subsequently, luciferase expressing MDA-MB-231 cells were incubated with morpholino containing DNA origami structure but significant reduction on the luciferase expression level wasn't observed. After that, same experiment was performed using commercial transfection reagent (Dream fect). The manufacturer's instructions suggest that a 2-4 μL DreamFect™ Gold transfection agent should be used for 1 μg DNA. The experiments were performed at two different DNA/transfection agent ratios 1:2 and 1:4. When the MDA-MB-231 cells were treated with morfolino/Dreamfact transfection reagent at 1:4 ratio luciferase expression showed a decrease compared to the 1:2 ratio as seen in Figure 4.70. However, when the morpholino sequence was incorporated to the DNA tile construct and given with the transfection agent, the level of luciferase expression showed a similar decrease in both DNA/transfection agent ratios.

Depending on the shape, size, and structure of the cell line, it is expected that the amount of cellular uptake of DNA nanostructures and the uptake path will vary according to oligonucleotides and plasmids [353, 405, 406]. As indicated by the work of Walsh et al., the DNA tetrahedra structure is taken more than the single and double-stranded DNAs into the cells [261]. The reduction in luciferase expression may be a consequence of increased

intracellular uptake by the addition of antisense oligonucleotide DNA to the tile construct, as well as addition to the effect of the transfection agent. Incorporation of the morpholino sequence into the DNA tile structure provided the reduction of luciferase expression using less transfection agent.
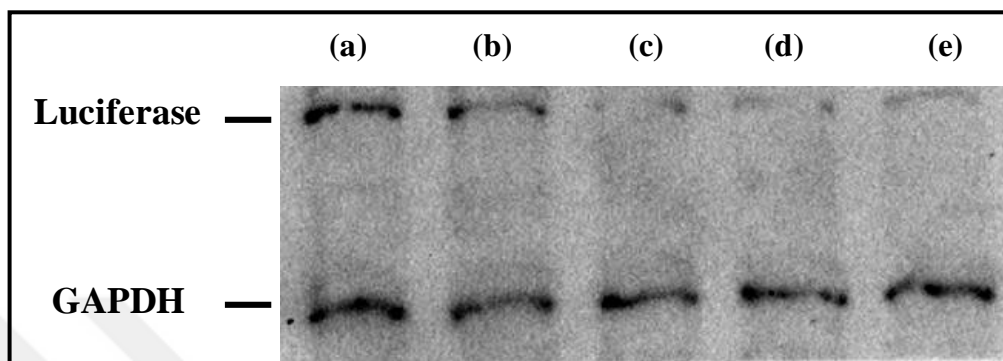
Figure 4.70. Western blot image of luciferase expression using transfection reagent with different DNA/transfection agent ratios. (a) Control, (b) Morpholino sequence with Dream fect (1:2), (c) Morpholino sequence with Dream fect (1:4), (d) Morpholino embedded DNA tile with Dream fect (1:2), and (e) Morpholino embedded DNA tile with Dream fect (1:4).

Silencing of the luciferase was studied using morpholino containing carbohydrate modified DNA tiles. Figure 4.71 shows the gel image indicates the silencing effects of the morpholino containing carbohydrate modified DNA tile structures MDA-MB-231 cells, which express luciferase, were incubated with morpholino containing DNA tile structures modified with glucose, lactose, and mannose, respectively for 48 hours. MDA-MB-231 cells, which were not treated with modified DNA tile, were used as a control group for the luciferase expression. After incubation of the cells with 0.064 μM morpholino, Western blot analysis was performed for the cell lysates. The decrease in the luciferase expression was observed for all of the cells, which were incubated with glucose, lactose, and mannose modified morpholino containing DNA tiles.
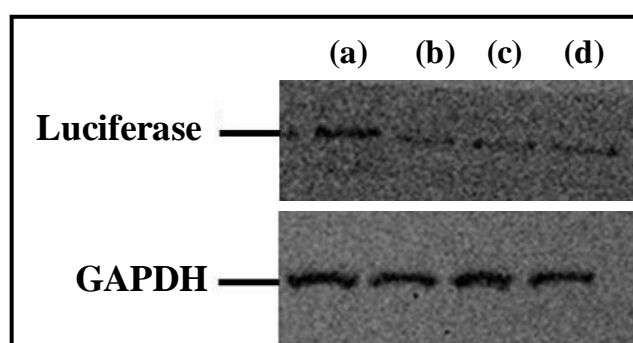
Figure 4.71. Silencing effects of the morpholino containing carbohydrate modified DNA tiles. (a) Control (without treatment), (b) glucose, (c) lactose, and (d) mannose modified morpholino containing DNA tile.

The effect of increasing amounts of morpholinos on luciferase levels of the cells was studied by studying amounts of 0.034 μM and 0.064 μM morpholino. An increase in the concentration of morpholino, as expected, will result in a decrease on the level of the lusiferase expression. A Western blot image, representing the reduction in luciferase expression due to the increase in morpholino amount is shown in Figure 4.72. When the amount of the morpholino, designed specifically for luciferase, was increased, the luciferase expression was decreased proportionally due to the increased morpholino concentration.
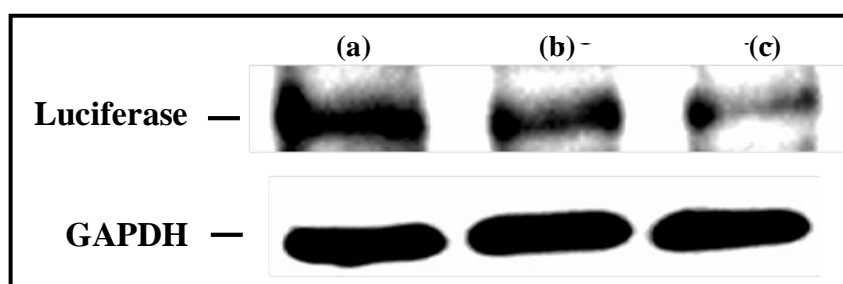
Figure 4.72. Silencing effect of the lactose modified DNA tile containing different amounts of morpholino. (a) Control, (b) 0.034 μM morpholino, and (c) 0.064 μM morpholino.

A scrambled form of the morpholino sequence, designed specifically for luciferase, was also used in the gene silencing experiments. The scrambled form is expected to have no silencing activity. The scrambled morpholino sequences do not contribute to target protein expression as they are not complementary to target protein mRNA sequences. Figure 4.73 shows the silencing effect of the lactose modified DNA tile structure and DNA tile structure containing scrambled morpholino sequence. When the cells are incubated with

the scrambled morpholino sequence, an effect on target protein expression should not be observed. There is no change in luciferase level was observed in the cells incubated with the scrambled morpholino sequence (Figure 4.73-b) as observed in MDA-MB-231 cells not incubated with morpholino sequence (Figure 4.73-c).
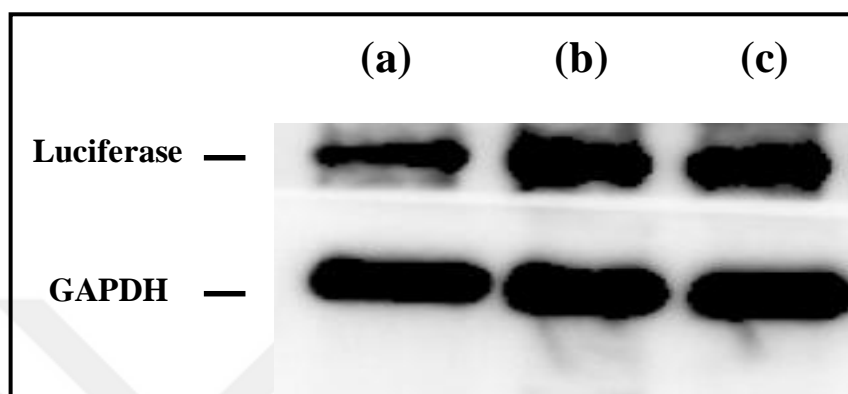
Figure 4.73. Silencing effect of the lactose modified DNA tile structure (a), DNA tile structure containing scrambled morpholino sequence (b), and the control group (c).

The use of ligands that allow the introduction of foreign genes into the cell by receptor-mediated endocytosis and the development of the carrier systems, in which these ligands are used, are being studied [407]. The use of transferrin [408], antibody molecules [409], epidermal growth factor [410], folic acid [339], and different carbohydrate molecules, such as galactose [411-414], mannose [415-417], lactose [418], etc. as ligands has been extensively investigated. Such strategies are also being applied for the delivery of gene silencing agents. The modification of oligonucleotide nanoparticles with such ligands significantly enhances the potential of efficiently transferring siRNA like agents to cancer cells [339]. It has been reported that efficient cellular uptake of the folic acid modified oligonucleotide nanoparticles by HeLa cells leads to 50 per cent decrease in target protein expression. In aforementioned study of Lee et al., when the tetrahedron structure modified with folic acid was used for the transport of 2'-OMe siRNA, the tetrahedron structure provided 50 per cent silencing of fire fly luciferase [339]. In a similar manner, the studies related with the glycotargeting strategies in which antisense oligonucleotides exhibit up to 80% cellular uptake have been reported [419].

The silencing of the luciferase was implemented with the use of DNA tile structures, modified with three different targeting agents including folic acid, lactose, and RGD peptide (Figure 4.74). When the cells treated with the modified DNA tile constructs with

different targeting agents containing the same morpholino concentration, it has been shown that the best result, among the three types of targeting agents, was obtained with the folic acid modified DNA tile system.
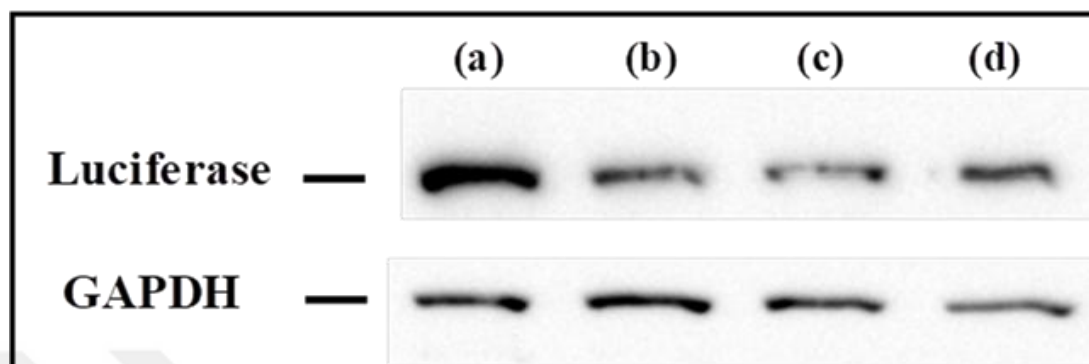
Figure 4.74. Western blot image of luciferase expression levels of reagent with different DNA/transfection agent ratios. (a) Control, (b) lactose, (c) folic acid, and (d) RGD peptide modified morpholino containing DNA tile.

The results have shown that cheap and natural molecules such as folic acid and carbohydrates can be used effectively in the transfection of DNA-based constructs as an alternative to expensive transfection agents.

5. CONCLUSION AND FUTURE PERSPECTIVE

The DNA nanotechnology idea started with the construction of simple structures at the end of the 1980s and then, developed with the formation of more complex and functional DNA based structures. It is now being used in several applications including sensing and medicine. Biocompatibility, lack of toxicity, and programmability are the features that expand the usage area of DNA and DNA-based structures. The structures developed using this technology may offer great advantage for medical applications.

In this thesis, a DNA nanostructure in the form of a tile, which can be used for the transport of drugs and other therapeutics, was built. The most important feature of the constructed DNA based carrier is its design allowing the functionalization of the system for different purposes through the adhesive oligonucleotide sequences. The tile structure has eight sticky ends and the different ligands or drugs, which may be conjugated to the complementary oligonucleotides can be bound through sticky ends to the tile system. In this way, a multi-functional system can be built.

The DNA tile structure was prepared by the slowly cooling method in TAE-Mg^{2+}, specific hybridization buffer solution. During the applied thermal annealing process, the pre-determined and synthesized oligonucleotides used to construct the DNA tile structure, found their complementary sequences in the hybridization buffer solution, they were annealed, and the formation of the desired DNA tile was ensured.

The constructed DNA tile structure was characterized using agarose gel electrophoresis, AFM and DLS. The progressive hybridization of the oligonucleotides to each other and the controlled formation of the DNA tile construct were visualized by agarose gel electrophoresis. AFM and DLS techniques were applied to determine the size of the prepared DNA tile structures. AFM and DLS measurements yielded size values that were greater than 29 nm, which determined for the DNA tile theoretically. With AFM measurements, the DNA tile structure was around 64 nm in size, while the DLS results showed that the hydrodynamic diameters of the DNA tile structures were largely above 50-60 nm.

In the thesis, it is envisaged to use the DNA tile structure for drug and antisense oligonucleotide delivery. One of the biggest problems that DNA-based systems face in

such applications is their stability, which they exhibit in the application environment. The stability experiments carried out in the cell medium showed that DNA tile structures retained their size and integrity for up to 24 hours. The stability analysis was also carried out in cell lysates obtained from the cultured cells. It's considered that stability analysis to be performed in the cell lysate may provide insight into the robustness of the construct for *in vivo* applications. The experiments performed in the cell lysates showed that the DNA tile structure retained its integrity for 6 hours.

The cytotoxicity of the newly prepared DNA tile structure was investigated on MDA-MB-231 and HeLa cells. The delivery systems used in drug delivery should be non-toxic and biocompatible. The cytotoxicity tests performed on MDA-MB-231 and HeLa cells shown that the DNA tile construct didn't exhibit a cytotoxicity or biocompatibility problem due to the natural structure of the DNA tile structure. The tile structure containing antisense oligonucleotide was also found to have no toxic effects on the cells.

The prepared DNA tile constructs were used as a carrier system for doxorubicin chemotherapy agent and an antisense morpholino oligonucleotide, a gene silencing agent. Within the scope of the thesis, lactose, folic acid, and RGD peptide were selected as targeting agents in anticipation of increasing the cellular uptake of DNA tile structure with its cargoes. For this reason, oligonucleotides, which can hybridize to the DNA tile, were functionalized with lactose, folic acid and RGD peptide targeting agents. Due to the modification with lactose giving better results in previous cellular uptake experiments, oligonucleotides modified with different carbohydrates including glucose, maltose, and mannose were also prepared. The carbohydrate modified oligonucleotides were prepared by reductive amination while oligonucleotides modified with folic acid and RGD peptide were prepared using DCC/NHS chemistry.

The synthesized functionalized oligonucleotides were characterized by agarose gel electrophoresis, FT-IR, and MALDI-TOF MS analyses. With the agarose gel electrophoresis analysis, the difference in migration rate observed between the modified oligonucleotides and the starting pure oligonucleotides, which indicates the molecular size increase, proved the success of the modifications performed. Glucose, maltose, and mannose modified oligonucleotides, which were subsequently studied for their cellular uptake effects, were also characterized by agarose gel electrophoresis. The characterization of the modified oligonucleotides was also studied by MALDI-TOF MS analysis. The

analyses did not give results which would allow precise mass determination due to fragmentation and multi-ion formation, and the results obtained were at the noise level.

The cytotoxicity and cellular uptake of the carrier tile structure with its included cargoes were investigated *in vitro*. Dox, which is used extensively in the treatment of different types of cancer, was intercalated into the DNA tile structure and used as a model drug. The stability and drug loading capacity of the DNA tile construct was also examined by agarose gel electrophoresis. It was seen that concentrations of Dox greater than 300 μM caused deterioration of the DNA tile structure while at concentrations lower than 300 μM, it was observed that the DNA tile construction retained its stability.

Due to the intercalation of Dox, the DNA tile structure has begun to exhibit toxicity to the cells, and this effect was at a similar level with the efficacy of the free drug. The modification of the DNA tile-Dox construct with natural targeting agents such as lactose, folic acid, and RGD peptide results in a slight decrease of the drug toxicity while the killing effect of the drug was preserved on the cells.

To confirm the uptake of the DNA tile structure by cells, the tile system was modified with 5(6)FAM dye, which normally cannot pass through the membrane, and the cellular uptake of the dye-DNA tile conjugate was demonstrated by confocal microscopy.

As mentioned before, lactose, folic acid, and RGD peptide molecules were used as targeting agents. The cellular uptake of the DNA tile system loaded with its cargo after modification with these targeting molecules was investigated using fluorescence spectroscopy, flow cytometry, and confocal microscopy analyses. According to the results obtained with these techniques, among the targeting agents, lactose exhibited the highest uptake effect for the drug loaded tile system. Then, the functionalization of the DNA tile structure with other carbohydrates, maltose and glucose were performed and a similar effect to the case of lactose was observed. The carrier agents based on carbohydrate molecules can be developed as an alternative to the rather expensive cationic lipid agents used to transport antisense oligonucleotides and DNA constructs into cells.

As a result of the cellular uptake experiments, it was seen that the modifications made with carbohydrates increased the cellular uptake of drug loaded DNA tile constructs regardless of the cell type being studied. However, modification performed with folic acid only appears to work in cell lines that overexpress the receptors of this ligand and positive

contribution to the cellular uptake of DNA carrier system only occurs in these cell types. The modification with RGD peptide has been shown to be less effective than carbohydrate modified or folic acid modified systems on the cellular uptake of the drug loaded DNA tile.

The carrier system and targeting agents may increase the cellular uptake of the therapeutic agent, and alter the internalization pathway of the drug by the cells as well. The presence of ligands that allow receptor interaction on the carrier molecule can seriously affect the uptake pathway and amount of the drug taken in by the cells. According to the results of the fluorescence spectroscopy and the flow cytometry analysis, Dox is taken in more by cells when given to the cells through carbohydrate modified DNA tile structures. This situation suggests that the Dox uptake pathway could have changed and Dox could have been taken up by the cell in a different pathway from passive diffusion with other DNA tile systems. To investigate the uptake pathway of the DNA tile-Dox-Lac, which exhibits the maximum cellular uptake effect, several inhibitor molecules, which are the marker of different uptake pathways were used and cellular uptake rates were examined using fuorescence spectroscopy and confocal microscopy. It was found that Dox, which is uptaken by passive diffusion into cells, internalized via endocytosis with the carbohydrate-modified DNA tile-Dox. The results of treatments performed with the markers of endocytosis such as chlorpromazine, sodium azide, and hypertonic sucrose confirmed that the DNA tile-Dox-Lac system was proved by endocytic uptake.

The effects of DNA tile-Dox-Fol, DNA tile-Dox-RGD, DNA tile-Dox-Lac, and DNA tile-Dox-Man structures on the cell cycle process were determined on HeLa and U87 cancer cells. According to the flow cytometry analysis results, it was seen that the vast majority of control group cells that were not incubated with Dox were in the G0/G1 phase. When the U87 cells incubated with free Dox and DNA tile-Dox structures with/without modifications, the Dox-loaded samples caused arrest in G2/M phase similar to the effect of free Dox. The experiments performed with DNA tile-Dox-Lac and DNA tile-Dox-Man showed that as the concentration of Dox increases up to 10 μM, an increase in subG1 phase is observed and this situation indicates an increase in an apoptotic cell population.

After the studies performed with Dox, the DNA tile system was used to carry the antisense morpholino sequence into the cells. The morpholino sequence was designed to inhibit the expression of the luciferase. The DNA tile structure containing the morpholino sequence was constructed and the newly prepared tile structure was characterized by the AFM

analysis and agarose gel electrophoresis. The formation of the DNA tile structure containing the morpholino sequence was followed by agarose gel electrophoresis and the size of the construct was found as approximately 106 nm by AFM analysis .

MDA-MB-231 cells expressing luciferase were prepared using recombinant DNA techniques. The cytotoxicity of the morpholino sequence containing DNA tile structure was investigated and the DNA tile structure was found as non-toxic to MDA-MB-231 cells expressing luciferase at the studied concentrations.

The use of modified/unmodified DNA tile constructs for morpholino delivery and their gene silencing activities were determined by Western blot analysis with observing the differences at luciferase expression levels. According to the Western blot images, when the cells were incubated with glucose, lactose, mannose, and folic acid modified morpholino containing DNA tiles, a decrease in the luciferase expression was observed. Also, the increase in morpholino amount applied resulted in a decrease in the level of luciferase expression. It was shown that the best result, among the three types of targeting agents, was obtained with the lactose modified DNA tile system. The scrambled morpholino sequence didn't show an effect on the luciferase expression level. Briefly, the results have shown that cheap and natural molecules such as folic acid and carbohydrates can be used effectively in the transfection of DNA-based constructs as an alternative to expensive transfection agents

As mentioned above, the tile structure is designed to be clearly functional and adjustable. In line with the obtained favorable outcomes, the effort to utilize the DNA tile structure as a nanocarrier should continue. The use of anti-cancer drugs such as Dox, which can easily intercalate into DNA structure, and other therapeutics can be incorporated into the tile structure and used for the treatment of various diseases *in vitro* and *in vivo*. The therapeutic efficacy of drugs whose therapeutic activities are restricted by the presence of biological barriers can be increased with the use of the tile system. To increase the *in vivo* applicability of the system, the tile structure can be made more resistant to nuclease activity with different end point modifications. Apart from medical applications, it is also possible to use a DNA tile system in various assemblies and microarray-like formations due to its design.

REFERENCES

1. Bamrungsap S, Zhao Z, Chen T, Wang L, Li C, Fu T, et al. Nanotechnology in therapeutics: a focus on nanoparticles as a drug delivery system. *Nanomedicine*. 2012;7(8):1253-1271.

2. Junghanns J-UA, Müller RH. Nanocrystal technology, drug delivery and clinical applications. *International Journal of Nanomedicine*. 2008;3(3):295-310.

3. Davidson R, Scott A, Maini M, Bryceson A, Croft S. Liposomal amphotericin B in drug-resistant visceral leishmaniasis. *The Lancet*. 1991;337(8749):1061-1062.

4. Rivera E. Current status of liposomal anthracycline therapy in metastatic breast cancer. *Clinical Breast Cancer*. 2003;4:76-83.

5. Guaglianone P, Chan K, DelaFlor-Weiss E, Hanisch R, Jeffers S, Sharma D, et al. Phase I and pharmacologie study of liposomal daunorubicin (DaunoXome). *Investigational New Drugs*. 1994;12(2):103-110.

6. Bellott R, Auvrignon A, Leblanc T, Pérel Y, Gandemer V, Bertrand Y, et al. Pharmacokinetics of liposomal daunorubicin (DaunoXome) during a phase I-II study in children with relapsed acute lymphoblastic leukaemia. *Cancer Chemotherapy and Pharmacology*. 2001;47(1):15-21.

7. Bory C, Boulieu R, Souillet G, Chantin C, Guibaud P, Hershfield M. Effect of polyethylene glycol-modified adenosine deaminase (PEG-ADA) therapy in two ADA-deficient children: measurement of erythrocyte deoxyadenosine triphosphate as a useful tool. *Advances in Experimental Medicine* and *Biology*. 1991;309A:173-176.

8. Kim T-Y, Kim D-W, Chung J-Y, Shin SG, Kim S-C, Heo DS, et al. Phase I and pharmacokinetic study of Genexol-PM, a cremophor-free, polymeric micelle-formulated paclitaxel, in patients with advanced malignancies. *Clinical Cancer Research*. 2004;10(11):3708-3716.

9.   Nyman DW, Campbell KJ, Hersh E, Long K, Richardson K, Trieu V, et al. Phase I and pharmacokinetics trial of ABI-007, a novel nanoparticle formulation of paclitaxel in patients with advanced nonhematologic malignancies. *Journal of Clinical Oncology*. 2005;23(31):7785-7793.

10.   Alberts B, Johnson A, Lewis J, Raff M, Roberts K, Walter P. *Molecular Biology of The Cell*. New York: NCBI-Garland Science; 2002.

11.   Niemeyer CM. Self-assembled nanostructures based on DNA: towards the development of nanobiotechnology. *Current Opinion in Chemical Biology*. 2000;4(6):609-618.

12.   Lo PK, Metera KL, Sleiman HF. Self-assembly of three-dimensional DNA nanostructures and potential biological applications. *Current Opinion in Chemical Biology*. 2010;14(5):597-607.

13.   Rothemund PW. Folding DNA to create nanoscale shapes and patterns. *Nature*. 2006;440(7082):297-302.

14.   Seeman NC. Nucleic acid junctions and lattices. *Journal of Theoretical Biology*. 1982;99(2):237-247.

15.   Fu T-J, Tse-Dinh Y-C, Seeman NC. Holliday junction crossover topology. *Journal of Molecular Biology*. 1994;236(1):91-105.

16.   Seeman NC. Construction of three-dimensional stick figures from branched DNA. *DNA and Cell Biology*. 1991;10(7):475-486.

17.   Seeman NC. The design and engineering of nucleic acid nanoscale assemblies. *Current Opinion in Structural Biology*. 1996;6(4):519-526.

18.   Zadegan RM, Norton ML. Structural DNA nanotechnology: from design to applications. *International Journal of Molecular Sciences*. 2012;13(6):7149-7162.

19.	Kershner RJ, Bozano LD, Micheel CM, Hung AM, Fornof AR, Cha JN, et al. Placement and orientation of individual DNA shapes on lithographically patterned surfaces. *Nature Nanotechnology*. 2009;4(9):557-561.

20.	Winfree E, Liu F, Wenzler LA, Seeman NC. Design and self-assembly of two-dimensional DNA crystals. *Nature*. 1998;394(6693):539-544.

21.	Chen J, Seeman NC. Synthesis from DNA of a molecule with the connectivity of a cube. *Nature*. 1991;350(6319):631-633.

22.	Shih WM, Quispe JD, Joyce GF. A 1.7-kilobase single-stranded DNA that folds into a nanoscale octahedron. *Nature*. 2004;427(6975):618-621.

23.	Yan H, LaBean TH, Feng L, Reif JH. Directed nucleation assembly of DNA tile complexes for barcode-patterned lattices. *Proceedings of The National Academy of Sciences*. 2003;100(14):8103-8108.

24.	Ke Y, Sharma J, Liu M, Jahn K, Liu Y, Yan H. Scaffolded DNA origami of a DNA tetrahedron molecular container. *Nano Letters*. 2009;9(6):2445-2447.

25.	Endo M, Hidaka K, Kato T, Namba K, Sugiyama H. DNA prism structures constructed by folding of multiple rectangular arms. *Journal of The American Chemical Society*. 2009;131(43):15570-15571.

26.	Andersen ES, Dong M, Nielsen MM, Jahn K, Subramani R, Mamdouh W, et al. Self-assembly of a nanoscale DNA box with a controllable lid. *Nature*. 2009;459(7243):73-76.

27.	Saccà B, Niemeyer CM. DNA origami: the art of folding DNA. *Angewandte Chemie International Edition*. 2012;51(1):58-66.

28.   Rothemund PW, editor. Design of DNA origami. *Proceedings of the IEEE/ACM International Conference on Computer-aided Design, 2005 IEEE International Conference on Computer-aided Design*; 2005: IEEE.

29.   Zadeh JN, Steenberg CD, Bois JS, Wolfe BR, Pierce MB, Khan AR, et al. NUPACK: analysis and design of nucleic acid systems. *Journal of Computational Chemistry*. 2011;32(1):170-173.

30.   Zuker M. Mfold web server for nucleic acid folding and hybridization prediction. *Nucleic Acids Research*. 2003;31(13):3406-3415.

31.   Seeman NC. De novo design of sequences for nucleic acid structural engineering. *Journal of Biomolecular Structure and Dynamics*. 1990;8(3):573-581.

32.   Zhu J, Wei B, Yuan Y, Mi Y. UNIQUIMER 3D, a software system for structural DNA nanotechnology design, analysis and evaluation. *Nucleic Acids Research*. 2009;37(7):2164-2175.

33.   Rothemund PW, Papadakis N, Winfree E. Algorithmic self-assembly of DNA Sierpinski triangles. *PLoS Biology*. 2004;2(12):e424.

34.   Douglas SM, Marblestone AH, Teerapittayanon S, Vazquez A, Church GM, Shih WM. Rapid prototyping of 3D DNA-origami shapes with caDNAno. *Nucleic Acids Research*. 2009;37(15):5001-5006.

35.   Mirkin CA, Letsinger RL, Mucic RC, Storhoff JJ. A DNA-based method for rationally assembling nanoparticles into macroscopic materials. *Nature*. 1996;382(6592):607-609.

36.   Ding B, Deng Z, Yan H, Cabrini S, Zuckermann RN, Bokor J. Gold nanoparticle self-similar chain structure organized by DNA origami. *Journal of The American Chemical Society*. 2010;132(10):3248-3249.

37. Schreiber R, Do J, Roller E-M, Zhang T, Schüller VJ, Nickels PC, et al. Hierarchical assembly of metal nanoparticles, quantum dots and organic dyes using DNA origami scaffolds. *Nature Nanotechnology*. 2014;9(1):74-78.

38. Pal S, Deng Z, Ding B, Yan H, Liu Y. DNA-origami-directed self-assembly of discrete silver-nanoparticle architectures. *Angewandte Chemie International Edition*. 2010;49(15):2700-2704.

39. Kuzuya A, Kimura M, Numajiri K, Koshi N, Ohnishi T, Okada F, et al. Precisely programmed and robust 2D streptavidin nanoarrays by using periodical nanometer-scale wells embedded in DNA origami assembly. *ChemBioChem*. 2009;10(11):1811-1815.

40. Kuzyk A, Laitinen KT, Törmä P. DNA origami as a nanoscale template for protein assembly. *Nanotechnology*. 2009;20(23):235305.

41. Schüller V, Heidegger S, Sandholzer N, Nickels P, Suhartha N, Endres S, et al. ACS Nano, 2011, 5, 9696–9702; Q. *Mei, X Wei, F Su, Y Liu, C Youngbull, R Johnson, S Lindsay, H Yan and D Meldrum, Nano Lett*. 2011;11:1477-1482.

42. Halley PD, Lucas CR, McWilliams EM, Webber MJ, Patton RA, Kural C, et al. Daunorubicin-loaded DNA origami nanostructures circumvent drug-resistance mechanisms in a leukemia model. *Small*. 2016;12(3):308-320.

43. Jiang Q, Song C, Nangreave J, Liu X, Lin L, Qiu D, et al. DNA origami as a carrier for circumvention of drug resistance. *Journal of The American Chemical Society*. 2012;134(32):13396-13403.

44. Alivisatos AP, Johnsson KP, Peng X, Wilson TE, Loweth CJ, Bruchez Jr MP, et al. Organization of'nanocrystal molecules' using DNA. *Nature*. 1996;382(6592):609-611.

45. Maune HT, Han S-p, Barish RD, Bockrath M, Goddard III WA, Rothemund PW, et al. Self-assembly of carbon nanotubes into two-dimensional geometries using DNA origami templates. *Nature Nanotechnology*. 2009;5(1):61-66.

46. Pal S, Deng Z, Ding B, Yan H, Liu Y. DNA-Origami-Directed Self-Assembly of Discrete Silver-Nanoparticle Architectures. *Angewandte Chemie*. 2010;122(15):2760-2764.

47. Douglas SM, Bachelet I, Church GM. A logic-gated nanorobot for targeted transport of molecular payloads. *Science*. 2012;335(6070):831-834.

48. Schuller V, Heidegger S, Sandholzer N, Nickels P, Suhartha N, Endres S. Cellular immunostimulation by CPG-sequence-coated DNA origami structures. *ACS Nano*. 2011; 5(12):9696-9702.

49. Jiang Q, Shi Y, Zhang Q, Li N, Zhan P, Song L, et al. A self-assembled DNA origami-gold nanorod complex for cancer theranostics. *Small*. 2015;11(38):5134-41.

50. Kuzuya A, Komiyama M. Design and construction of a box-shaped 3D-DNA origami. *Chemical Communications*. 2009(28):4182-4184.

51. Nangreave J, Han D, Liu Y, Yan H. DNA origami: a history and current perspective. *Current Opinion in Chemical Biology*. 2010;14(5):608-615.

52. Zhang Z, Song J, Besenbacher F, Dong M, Gothelf KV. Self-Assembly of DNA Origami and Single-Stranded Tile Structures at Room Temperature. *Angewandte Chemie*. 2013;125(35):9389-9393.

53. Endo M, Katsuda Y, Hidaka K, Sugiyama H. Regulation of DNA methylation using different tensions of double strands constructed in a defined DNA nanostructure. *Journal of The American Chemical Society*. 2010;132(5):1592-1597.

54. Suzuki Y, Endo M, Cañas C, Ayora S, Alonso JC, Sugiyama H, et al. Direct analysis of Holliday junction resolving enzyme in a DNA origami nanostructure. *Nucleic Acids Research*. 2014;42(11):7421-7428.

55.   Okholm AH, Aslan H, Besenbacher F, Dong M, Kjems J. Monitoring patterned enzymatic polymerization on DNA origami at single-molecule level. *Nanoscale*. 2015;7(25):10970-10973.

56.   Takeuchi Y, Endo M, Suzuki Y, Hidaka K, Durand G, Dausse E, et al. Single-molecule observations of RNA–RNA kissing interactions in a DNA nanostructure. *Biomaterials Science*. 2016;4(1):130-135.

57.   Zhang Z, Wang Y, Fan C, Li C, Li Y, Qian L, et al. Asymmetric DNA Origami for Spatially Addressable and Index-Free Solution-Phase DNA Chips. *Advanced Materials*. 2010;22(24):2672-2675.

58.   Yurke B, Turberfield AJ, Mills Jr AP, Simmel FC, Neumann JL. A DNA-fuelled molecular machine made of DNA. *Nature*. 2000;406(6796):605.

59.   Zhang Z, Zeng D, Ma H, Feng G, Hu J, He L, et al. A DNA-Origami Chip Platform for Label-Free SNP Genotyping Using Toehold-Mediated Strand Displacement. *Small*. 2010;6(17):1854-1858.

60.   Subramanian HK, Chakraborty B, Sha R, Seeman NC. The label-free unambiguous detection and symbolic display of single nucleotide polymorphisms on DNA origami. *Nano Letters*. 2011;11(2):910-913.

61.   Kuzuya A, Watanabe R, Yamanaka Y, Tamaki T, Kaino M, Ohya Y. Nanomechanical DNA origami pH sensors. *Sensors*. 2014;14(10):19329-19335.

62.   Douglas SM, Chou JJ, Shih WM. DNA-nanotube-induced alignment of membrane proteins for NMR structure determination. *Proceedings of The National Academy of Sciences*. 2007;104(16):6644-6648.

63.   Cho K, Wang X, Nie S, Shin DM. Therapeutic nanoparticles for drug delivery in cancer. *Clinical Cancer Research*. 2008;14(5):1310-1316.

64.   Sudimack J, Lee RJ. Targeted drug delivery via the folate receptor. *Advanced Drug Delivery Reviews*. 2000;41(2):147-162.

65.   Arap W, Pasqualini R, Ruoslahti E. Cancer treatment by targeted drug delivery to tumor vasculature in a mouse model. *Science*. 1998;279(5349):377-380.

66.   Wu Y, Sefah K, Liu H, Wang R, Tan W. DNA aptamer–micelle as an efficient detection/delivery vehicle toward cancer cells. *Proceedings of The National Academy of Sciences*. 2010;107(1):5-10.

67.   Leamon CP, Reddy JA. Folate-targeted chemotherapy. *Advanced Drug Delivery Reviews*. 2004;56(8):1127-1141.

68.   Brannon-Peppas L, Blanchette JO. Nanoparticle and targeted systems for cancer therapy. *Advanced Drug Delivery Reviews*. 2004;56(11):1649-1659.

69.   Ehrlich P, Hata S. *Die experimentelle Chemotherapie der Spirillosen*. New York: Springer-Verlag Press; 1910.

70.   Sinha R, Kim GJ, Nie S, Shin DM. Nanotechnology in cancer therapeutics: bioconjugated nanoparticles for drug delivery. *Molecular Cancer Therapeutics*. 2006;5(8):1909-1917.

71.   Mok H, Park JW, Park TG. Enhanced intracellular delivery of quantum dot and adenovirus nanoparticles triggered by acidic pH via surface charge reversal. *Bioconjugate Chemistry*. 2008;19(4):797-801.

72.   Min KH, Kim J-H, Bae SM, Shin H, Kim MS, Park S, et al. Tumoral acidic pH-responsive MPEG-poly (β-amino ester) polymeric micelles for cancer targeting therapy. *Journal of Controlled Release*. 2010;144(2):259-266.

73.   Sethuraman VA, Na K, Bae YH. pH-responsive sulfonamide/PEI system for tumor specific gene delivery: an in vitro study. *Biomacromolecules*. 2006;7(1):64-70.

74.   Kumar Khanna V. Targeted delivery of nanomedicines. *ISRN Pharmacology*. 2012;2012:1-9.

75.   Sledge G, Miller K. Exploiting the hallmarks of cancer: the future conquest of breast cancer. *European Journal of Cancer*. 2003;39(12):1668-75.

76.   Teicher BA. Molecular targets and cancer therapeutics: discovery, development and clinical validation. *Drug Resistance Updates*. 2000;3(2):67-73.

77.   Moulari B, Beduneau A, Pellequer Y, Lamprecht A. Nanoparticle targeting to inflamed tissues of the gastrointestinal tract. *Current Drug Delivery*. 2013;10(1):9-17.

78.   Mongelard F, Bouvet P. AS-1411, a guanosine-rich oligonucleotide aptamer targeting nucleolin for the potential treatment of cancer, including acute myeloid leukemia. *Current Opinion in Molecular Therapeutics*. 2010;12(1):107-114.

79.   Gao X, Cui Y, Levenson RM, Chung LW, Nie S. In vivo cancer targeting and imaging with semiconductor quantum dots. *Nature Biotechnology*. 2004;22(8):969-976.

80.   Hadjipanayis CG, Machaidze R, Kaluzova M, Wang L, Schuette AJ, Chen H, et al. EGFRvIII antibody–conjugated iron oxide nanoparticles for magnetic resonance imaging–guided convection-enhanced delivery and targeted therapy of glioblastoma. *Cancer Research*. 2010;70(15):6303-6312.

81.   Albanell J, Baselga J. Trastuzumab, a humanized anti-HER2 monoclonal antibody, for the treatment of breast cancer. *Drugs Today (Barc)*. 1999;35(12):931-946.

82.   Wente MN, Jain A, Kono E, Berberat PO, Giese T, Reber HA, et al. Prostate stem cell antigen is a putative target for immunotherapy in pancreatic cancer. *Pancreas*. 2005;31(2):119-125.

83.   Chen G, Chen W, Wu Z, Yuan R, Li H, Gao J, et al. MRI-visible polymeric vector bearing CD3 single chain antibody for gene delivery to T cells for immunosuppression. *Biomaterials*. 2009;30(10):1962-1970.

84.   Beekman KW, Colevas AD, Cooney K, DiPaola R, Dunn RL, Gross M, et al. Phase II evaluations of cilengitide in asymptomatic patients with androgen-independent prostate cancer: scientific rationale and study design. *Clinical Genitourinary Cancer*. 2006;4(4):299-302.

85.   Veiseh O, Sun C, Fang C, Bhattarai N, Gunn J, Kievit F, et al. Specific targeting of brain tumors with an optical/magnetic resonance imaging nanoprobe across the blood-brain barrier. *Cancer Research*. 2009;69(15):6200-6207.

86.   He X, Na M-H, Kim J-S, Lee G-Y, Park JY, Hoffman AS, et al. A novel peptide probe for imaging and targeted delivery of liposomal doxorubicin to lung tumor. *Molecular Pharmaceutics*. 2011;8(2):430-438.

87.   Dvorak H, Senger DR, Dvorak A, Harvey V, McDonagh J. Regulation of extravascular coagulation by microvascular permeability. *Science*. 1985;227(4690):1059-1061.

88.   Abe K, Shoji M, Chen J, Bierhaus A, Danave I, Micko C, et al. Regulation of vascular endothelial growth factor production and angiogenesis by the cytoplasmic tail of tissue factor. *Proceedings of The National Academy of Sciences*. 1999;96(15):8663-8668.

89.   Pilch J, Brown DM, Komatsu M, Järvinen TA, Yang M, Peters D, et al. Peptides selected for binding to clotted plasma accumulate in tumor stroma and wounds. *Proceedings of the National Academy of Sciences of The United States of America*. 2006;103(8):2800-2804.

90.   Davis ME, Zuckerman JE, Choi CHJ, Seligson D, Tolcher A, Alabi CA, et al. Evidence of RNAi in humans from systemically administered siRNA via targeted nanoparticles. *Nature*. 2010;464(7291):1067-1070.

91.   Platt VM, Szoka Jr FC. Anticancer therapeutics: targeting macromolecules and nanocarriers to hyaluronan or CD44, a hyaluronan receptor. *Molecular Pharmaceutics*. 2008;5(4):474-486.

92.   Bhang SH, Won N, Lee T-J, Jin H, Nam J, Park J, et al. Hyaluronic acid− quantum dot conjugates for in vivo lymphatic vessel imaging. *ACS Nano*. 2009;3(6):1389-1398.

93.   Wu W, Shen J, Banerjee P, Zhou S. Core–shell hybrid nanogels for integration of optical temperature-sensing, targeted tumor cell imaging, and combined chemo-photothermal treatment. *Biomaterials*. 2010;31(29):7555-7566.

94.   Lee RJ, Low PS. Folate-mediated tumor cell targeting of liposome-entrapped doxorubicin in vitro. *Biochimica et Biophysica Acta (BBA)-Biomembranes*. 1995;1233(2):134-144.

95.   Pan X, Lee RJ. Tumour-selective drug delivery via folate receptor-targeted liposomes. *Expert Opinion on Drug Delivery*. 2004;1(1):7-17.

96.   Zhao XB, Lee RJ. Tumor-selective targeted delivery of genes and antisense oligodeoxyribonucleotides via the folate receptor. *Advanced Drug Delivery Reviews*. 2004;56(8):1193-1204.

97.   Elnakat H, Ratnam M. Distribution, functionality and gene regulation of folate receptor isoforms: implications in targeted therapy. *Advanced Drug Delivery Reviews*. 2004;56(8):1067-1084.

98.   Shmeeda H, Mak L, Tzemach D, Astrahan P, Tarshish M, Gabizon A. Intracellular uptake and intracavitary targeting of folate-conjugated liposomes in a mouse lymphoma model with up-regulated folate receptors. *Molecular Cancer Therapeutics*. 2006;5(4):818-824.

99.   Low PS, Antony AC. Folate receptor-targeted drugs for cancer and inflammatory diseases. *Advanced Drug Delivery Reviews*. 2004;56(8):1055-1058.

100.   Zhao R, Diop-Bove N, Visentin M, Goldman ID. Mechanisms of membrane transport of folates into cells and across epithelia. *Annual Review of Nutrition*. 2011;31:177-201.

101.   Citro G, Szczylik C, Ginobbi P, Zupi G, Calabretta B. Inhibition of leukaemia cell proliferation by folic acid–polylysine-mediated introduction of c-myb antisense oligodeoxynucleotides into HL-60 cells. *British Journal of Cancer*. 1994;69(3):463-467.

102.   Leamon CP, Cooper SR, Hardee GE. Folate-liposome-mediated antisense oligodeoxynucleotide targeting to cancer cells: evaluation in vitro and in vivo. *Bioconjugate Chemistry*. 2003;14(4):738-747.

103.   Zhou W, Yuan X, Wilson A, Yang L, Mokotoff M, Pitt B, et al. Efficient intracellular delivery of oligonucleotides formulated in folate receptor-targeted lipid vesicles. *Bioconjugate Chemistry*. 2002;13(6):1220-1225.

104.   Li S, Huang L. Targeted delivery of antisense oligodeoxynucleotides by LPDII. *Journal of Liposome research*. 1997;7(1):63-75.

105.   Konda SD, Aref M, Brechbiel M, Wiener EC. Development of a tumor-targeting MR contrast agent using the high-affinity folate receptor: work in progress. *Investigative Radiology*. 2000;35(1):50-57.

106.   Gottschalk S, Cristiano R, Smith L, Woo S. Folate receptor mediated DNA delivery into tumor cells: potosomal disruption results in enhanced gene expression. *Gene Therapy*. 1994;1(3):185-191.

107.   Mislick KA, Baldeschwieler JD, Kayyem JF, Meade TJ. Transfection of folate-polylysine DNA complexes: evidence for lysosomal delivery. *Bioconjugate Chemistry*. 1995;6(5):512-515.

108.   Leamon CP, Weigl D, Hendren RW. Folate copolymer-mediated transfection of cultured cells. *Bioconjugate Chemistry*. 1999;10(6):947-957.

109.   Guo W, Lee RJ. Efficient gene delivery via non-covalent complexes of folic acid and polyethylenimine. *Journal of Controlled Release*. 2001;77(1-2):131-138.

110.   Reddy JA, Dean D, Kennedy MD, Low PS. Optimization of folate-conjugated liposomal vectors for folate receptor-mediated gene therapy. *Journal of Pharmaceutical Sciences*. 1999;88(11):1112-1118.

111.   Shi G, Guo W, Stephenson SM, Lee RJ. Efficient intracellular drug and gene delivery using folate receptor-targeted pH-sensitive liposomes composed of cationic/anionic lipid combinations. *Journal of Controlled Release*. 2002;80(1-3):309-319.

112.   Steinberg G, Borch RF. Synthesis and evaluation of pteroic acid-conjugated nitroheterocyclic phosphoramidates as folate receptor-targeted alkylating agents. *Journal of Medicinal Chemistry*. 2001;44(1):69-73.

113.   Aronov O, Horowitz AT, Gabizon A, Gibson D. Folate-targeted PEG as a potential carrier for carboplatin analogs. Synthesis and in vitro studies. *Bioconjugate Chemistry*. 2003;14(3):563-574.

114.   Liu J, Kolar C, Lawson TA, Gmeiner WH. Targeted drug delivery to chemoresistant cells: folic acid derivatization of FdUMP [10] enhances cytotoxicity toward 5-FU-resistant human colorectal tumor cells. *The Journal of Organic Chemistry*. 2001;66(17):5655-5663.

115.   Reddy JA, Low PS. Folate-mediated targeting of therapeutic and imaging agents to cancers. *Critical Reviews™ in Therapeutic Drug Carrier Systems*. 1998;15(6):568-627.

116.   Hilgenbrink AR, Low PS. Folate receptor-mediated drug targeting: from therapeutics to diagnostics. *Journal of Pharmaceutical Sciences*. 2005;94(10):2135-2146.

117.   Leamon CP, Low PS. Folate-mediated targeting: from diagnostics to drug and gene delivery. *Drug Discovery Today*. 2001;6(1):44-51.

118. Dosio F, Milla P, Cattel L. EC-145, a folate-targeted Vinca alkaloid conjugate for the potential treatment of folate receptor-expressing cancers. *Current Opinion in Investigational Drugs (London, England: 2000)*. 2010;11(12):1424-1433.

119. Leamon CP, Reddy JA, Vlahov IR, Westrick E, Dawson A, Dorton R, et al. Preclinical antitumor activity of a novel folate-targeted dual drug conjugate. *Molecular Pharmaceutics*. 2007;4(5):659-667.

120. Leamon CP, Low P. Cytotoxicity of momordin-folate conjugates in cultured human cells. *Journal of Biological Chemistry*. 1992;267(35):24966-24971.

121. Leamon CP, Pastan I, Low P. Cytotoxicity of folate-Pseudomonas exotoxin conjugates toward tumor cells. Contribution of translocation domain. *Journal of Biological Chemistry*. 1993;268(33):24847-24854.

122. Leamon C, Low P. Selective targeting of malignant cells with cytotoxin-folate conjugates. *Journal of Drug Targeting*. 1994;2(2):101-112.

123. Lee RJ, Low PS. Delivery of liposomes into cultured KB cells via folate receptor-mediated endocytosis. *Journal of Biological Chemistry*. 1994;269(5):3198-3204.

124. Zhang Y, Zhang J. Surface modification of monodisperse magnetite nanoparticles for improved intracellular uptake to breast cancer cells. *Journal of Colloid and Interface Science*. 2005;283(2):352-357.

125. Mittal V, Patel S, Sheth S. Development and characterization of folate targeted nanoparticle drug delivery system. *Int J Pharm Bio Sci*. 2010;1:1-2.

126. Nisato RE, Tille J-C, Jonczyk A, Goodman SL, Pepper MS. αvβ3 and αvβ5 integrin antagonists inhibit angiogenesis in vitro. *Angiogenesis*. 2003;6(2):105-119.

127. Nasongkla N, Shuai X, Ai H, Weinberg BD, Pink J, Boothman DA, et al. cRGD-functionalized polymer micelles for targeted doxorubicin delivery. *Angewandte Chemie*. 2004;116(46):6483-6487.

128. Hood JD, Bednarski M, Frausto R, Guccione S, Reisfeld RA, Xiang R, et al. Tumor regression by targeted gene delivery to the neovasculature. *Science*. 2002;296(5577):2404-2407.

129. Pasqualini R, Koivunen E, Ruoslahti E. αv integrins as receptors for tumor targeting by circulating ligands. *Nature Biotechnology*. 1997;15(6):542-546.

130. Wickham TJ, Tzeng E, Shears L, Roelvink PW, Li Y, Lee GM, et al. Increased in vitro and in vivo gene transfer by adenovirus vectors containing chimeric fiber proteins. *Journal of Virology*. 1997;71(11):8221-8229.

131. Erbacher P, Remy J, Behr J. Gene transfer with synthetic virus-like particles via the integrin-mediated endocytosis pathway. *Gene Therapy*. 1999;6(1):138-145.

132. Müller K, Nahde T, Fahr A, Müller R, Brüsselbach S. Highly efficient transduction of endothelial cells by targeted artificial virus-like particles. *Cancer Gene Therapy*. 2001;8(2):107-117.

133. Janssen ML, Oyen WJ, Dijkgraaf I, Massuger LF, Frielink C, Edwards DS, et al. Tumor targeting with radiolabeled αvβ3 integrin binding peptides in a nude mouse model. *Cancer Research*. 2002;62(21):6146-6151.

134. Schraa AJ, Kok RJ, Moorlag HE, Bos EJ, Proost JH, Meijer DK, et al. Targeting of RGD-modified proteins to tumor vasculature: A pharmacokinetic and cellular distribution study. *International Journal of Cancer*. 2002;102(5):469-475.

135. Warburg O, Wind F, Negelein E. The metabolism of tumors in the body. *The Journal of General Physiology*. 1927;8(6):519-530.

136.   Warburg O. On the origin of cancer. *Science*. 1956;123(3191):309-314.

137.   Hanahan D, Weinberg RA. Hallmarks of cancer: the next generation. *Cell*. 2011;144(5):646-674.

138.   Granchi C, Minutolo F. Anticancer agents that counteract tumor glycolysis. *ChemMedChem*. 2012;7(8):1318-1350.

139.   Vander Heiden MG. Targeting cancer metabolism: a therapeutic window opens. *Nature Reviews Drug Discovery*. 2011;10(9):671-684.

140.   Herrmann K, Benz M, Krause B, Pomykala K, Buck A, Czernin J. (18)F-FDG-PET/CT in evaluating response to therapy in solid tumors: where we are and where we can go. *The Quarterly Journal of Nuclear Medicine and Molecular Imaging*. 2011;55(6):620-632.

141.   Ben-Haim S, Ell P. 18F-FDG PET and PET/CT in the evaluation of cancer treatment response. *Journal of Nuclear Medicine*. 2009;50(1):88-99.

142.   Calvaresi EC, Hergenrother PJ. Glucose conjugation for the specific targeting and treatment of cancer. *Chemical Science*. 2013;4(6):2319-2333.

143.   Yan H, Tram K. Glycotargeting to improve cellular delivery efficiency of nucleic acids. *Glycoconjugate Journal*. 2007;24(2-3):107-123.

144.   Mandai T, Okumoto H, Oshitari T. Synthesis and Biological Evaluation of Water Soluble Taxoids Bearing Sugar Moleties. *Heterocycles*. 2001;54(2):561-566.

145.   Mikuni K, Nakanishi K, Hara K, Hara K, Iwatani W, Amano T, et al. In vivo antitumor activity of novel water-soluble taxoids. *Biological and Pharmaceutical Bulletin*. 2008;31(6):1155-1158.

146. Lin Y-S, Tungpradit R, Sinchaikul S, An F-M, Liu D-Z, Phutrakul S, et al. Targeting the delivery of glycan-based paclitaxel prodrugs to cancer cells via glucose transporters. *Journal of Medicinal Chemistry*. 2008;51(23):7428-7441.

147. Halmos T, Santarromana M, Antonakis K, Scherman D. Synthesis of glucose-chlorambucil derivatives and their recognition by the human GLUT1 glucose transporter. *European Journal of Pharmacology*. 1996;318(2):477-484.

148. Halmos T, Santarromana M, Antonakis K, Scherman D. Synthesis of O-methylsulfonyl derivatives of D-glucose as potential alkylating agents for targeted drug delivery to the brain. Evaluation of their interaction with the human erythrocyte GLUT1 hexose transporter. *Carbohydrate Research*. 1997;299(1-2):15-21.

149. Reux B, Weber V, Galmier M-J, Borel M, Madesclaire M, Madelmont J-C, et al. Synthesis and cytotoxic properties of new fluorodeoxyglucose-coupled chlorambucil derivatives. *Bioorganic & Medicinal Chemistry*. 2008;16(9):5004-5020.

150. Miot-Noirault E, Reux B, Debiton E, Madelmont J-C, Chezal J-M, Coudert P, et al. Preclinical investigation of tolerance and antitumour activity of new fluorodeoxyglucose-coupled chlorambucil alkylating agents. *Investigational New Drugs*. 2011;29(3):424-433.

151. Goff RD, Thorson JS. Assessment of chemoselective neoglycosylation methods using chlorambucil as a model. *Journal of Medicinal Chemistry*. 2010;53(22):8129-8139.

152. Chesnoy S, Huang L. Structure and function of lipid-DNA complexes for gene delivery. *Annual Review of Biophysics and Biomolecular Structure*. 2000;29(1):27-47.

153. Hirko A, Tang F, Hughes JA. Cationic lipid vectors for plasmid DNA delivery. *Current Medicinal Chemistry*. 2003;10(14):1185-1193.

154. Liu D, Ren T, Gao X. Cationic transfection lipids. *Current Medicinal Chemistry*. 2003;10(14):1307-1315.

155.   Graham FL, van der Eb AJ. A new technique for the assay of infectivity of human adenovirus 5 DNA. *Virology*. 1973;52(2):456-467.

156.   Sorgi F, Bhattacharya S, Huang L. Protamine sulfate enhances lipid-mediated gene transfer. *Gene Therapy*. 1997;4(9):961-968.

157.   Schwartz B, Ivanov M, Pitard B, Escriou V, Rangara R, Byk G, et al. Synthetic DNA-compacting peptides derived from human sequence enhance cationic lipid-mediated gene transfer in vitro and in vivo. *Gene Therapy*. 1999;6(2):282-292.

158.   Karak N, Maiti S. Dendritic polymers: A class of novel material. *Journal of Polymer Materials*. 1997;14(2):107-122.

159.   Tang MX, Redemann CT, Szoka FC. In vitro gene delivery by degraded polyamidoamine dendrimers. *Bioconjugate Chemistry*. 1996;7(6):703-714.

160.   Yang N-S, Burkholder J, Roberts B, Martinell B, McCabe D. In vivo and in vitro gene transfer to mammalian somatic cells by particle bombardment. *Proceedings of The National Academy of Sciences*. 1990;87(24):9568-9572.

161.   Yang N-S, Sun WH. Gene gun and other non-viral approaches for cancer gene therapy. *Nature Medicine*. 1995;1(5):481-483.

162.   Ye G-N, Daniell H, Sanford JC. Optimization of delivery of foreign DNA into higher-plant chloroplasts. *Plant Molecular Biology*. 1990;15(6):809-819.

163.   Wong T-K, Neumann E. Electric field mediated gene transfer. *Biochemical and Biophysical Research Communications*. 1982;107(2):584-587.

164.   Neumann E, Schaefer-Ridder M, Wang Y, Hofschneider P. Gene transfer into mouse lyoma cells by electroporation in high electric fields. *The EMBO Journal*. 1982;1(7):841-845.

165. Monsigny M, Midoux P, Mayer R, Roche A-C. Glycotargeting: influence of the sugar moiety on both the uptake and the intracellular trafficking of nucleic acid carried by glycosylated polymers. *Bioscience Reports*. 1999;19(2):125-132.

166. Nishikawa M, Takemura S, Yamashita F, Takakura Y, Meijer D, Hashida M, et al. Pharmacokinetics and in vivo gene transfer of plasmid DNA complexed with mannosylated poly (L-lysine) in mice. *Journal of Drug Targeting*. 2000;8(1):29-38.

167. Hasegawa T, Umeda M, Matsumoto T, Numata M, Mizu M, Koumoto K, et al. Lactose-appended schizophyllan is a potential candidate as a hepatocyte-targeted antisense carrier. *Chemical Communications*. 2004(4):382-383.

168. Koumoto K, Mizu M, Sakurai K, Kunitake T, Shinkai S. Polysaccharide/polynucleotide complexes. *Chemistry&Biodiversity*. 2004;1(3):520-529.

169. Mumper R, Wang J, Claspell J, Rolland A. Novel polymeric condensing carriers for gene delivery. *Proceedings of The Controlled Release Society*. 1995(22):178-179.

170. Tacar O, Sriamornsak P, Dass CR. Doxorubicin: an update on anticancer molecular action, toxicity and novel drug delivery systems. *Journal of Pharmacy and Pharmacology*. 2013;65(2):157-170.

171. González ID, Saez RS, Rodilla EM, Yges E, Toledano F. Hypersensitivity reactions to chemotherapy drugs. *Alergol Immunol Clin*. 2000;15:161-181.

172. Minotti G, Menna P, Salvatorelli E, Cairo G, Gianni L. Anthracyclines: molecular advances and pharmacologic developments in antitumor activity and cardiotoxicity. *Pharmacological Reviews*. 2004;56(2):185-229.

173. Biganzoli L, Minisini A, Aapro M, Di Leo A. Chemotherapy for metastatic breast cancer. *Current Opinion in Obstetrics and Gynecology*. 2004;16(1):37-41.

174.   Humber C, Tierney J, Symonds P, Collingwood M, Kirwan J, Williams C, et al. Chemotherapy for advanced, recurrent or metastatic endometrial carcinoma. *Cochrane Database Syst Rev*. 2005;4:1-56.

175.   Suzuki F, Hashimoto K, Kikuchi H, Nishikawa H, Matsumoto H, Shimada J, et al. Induction of tumor-specific cytotoxicity and apoptosis by doxorubicin. *Anticancer Research*. 2005;25(2A):887-893.

176.   Cutts SM, Nudelman A, Rephaeli A, Phillips DR. The power and potential of doxorubicin-DNA adducts. *IUBMB Life*. 2005;57(2):73-81.

177.   Zheng Z, Pavlidis P, Chua S, D'agati VD, Gharavi AG. An ancestral haplotype defines susceptibility to doxorubicin nephropathy in the laboratory mouse. *Journal of the American Society of Nephrology*. 2006;17(7):1796-1800.

178.   Lerman L. Structural considerations in the interaction of DNA and acridines. *Journal of Molecular Biology*. 1961;3(1):18-IN4.

179.   Gewirtz D. A critical evaluation of the mechanisms of action proposed for the antitumor effects of the anthracycline antibiotics adriamycin and daunorubicin. *Biochemical Pharmacology*. 1999;57(7):727-741.

180.   Shen Z, Li Y, Kohama K, Oneill B, Bi J. Improved drug targeting of cancer cells by utilizing actively targetable folic acid-conjugated albumin nanospheres. *Pharmacological Research*. 2011;63(1):51-58.

181.   Fornari FA, Randolph JK, Yalowich JC, Ritke MK, Gewirtz DA. Interference by doxorubicin with DNA unwinding in MCF-7 breast tumor cells. *Molecular Pharmacology*. 1994;45(4):649-656.

182.   Momparler RL, Karon M, Siegel SE, Avila F. Effect of adriamycin on DNA, RNA, and protein synthesis in cell-free systems and intact cells. *Cancer Research*. 1976;36(8):2891-2895.

183. De Graaf H, Dolsma W, Willemse P, Van Der Graaf W, Sleijfer D, De Vries E, et al. Cardiotoxicity from intensive chemotherapy combined with radiotherapy in breast cancer. *British Journal of Cancer*. 1997;76(7):943-945.

184. Suzuki T, Hayashi D, Yamazaki T, Mizuno T, Kanda Y, Komuro I, et al. Elevated B-type natriuretic peptide levels after anthracycline administration. *American Heart Journal*. 1998;136(2):362-363.

185. Mobaraki M, Faraji A, Zare M, Dolati P, Ataei M, Manshadi HD. Molecular Mechanisms of Cardiotoxicity: A Review on Major Side-effect of Doxorubicin. *Indian Journal of Pharmaceutical Sciences*. 2017;79(3):335-344.

186. Buchholz TA, Stivers DN, Stec J, Ayers M, Clark E, Bolt A, et al. Global gene expression changes during neoadjuvant chemotherapy for human breast cancer. *The Cancer Journal*. 2002;8(6):461-468.

187. Lal S, Mahajan A, Ning Chen W, Chowbay B. Pharmacogenetics of target genes across doxorubicin disposition pathway: a review. *Current Drug Metabolism*. 2010;11(1):115-128.

188. Minotti G, Mancuso C, Frustaci A, Mordente A, Santini SA, Calafiore AM, et al. Paradoxical inhibition of cardiac lipid peroxidation in cancer patients treated with doxorubicin. Pharmacologic and molecular reappraisal of anthracycline cardiotoxicity. *Journal of Clinical Investigation*. 1996;98(3):650-661.

189. Gianni L, Zweier JL, Levy A, Myers C. Characterization of the cycle of iron-mediated electron transfer from Adriamycin to molecular oxygen. *Journal of Biological Chemistry*. 1985;260(11):6820-6826.

190. Olson RD, Mushlin PS. Doxorubicin cardiotoxicity: analysis of prevailing hypotheses. *The FASEB Journal*. 1990;4(13):3076-3086.

191.   Doroshow JH. Role of hydrogen peroxide and hydroxyl radical formation in the killing of Ehrlich tumor cells by anticancer quinones. *Proceedings of The National Academy of Sciences*. 1986;83(12):4514-4518.

192.   Alderton PM, Gross J, Green MD. Comparative study of doxorubicin, mitoxantrone, and epirubicin in combination with ICRF-187 (ADR-529) in a chronic cardiotoxicity animal model. *Cancer Research*. 1992;52(1):194-201.

193.   Rossi F, Filippelli W, Russo S, Filippelli A, Berrino L. Cardiotoxicity of doxorubicin: effects of drugs inhibiting the release of vasoactive substances. *Basic & Clinical Pharmacology & Toxicology*. 1994;75(2):99-107.

194.   Vásquez-Vivar J, Martasek P, Hogg N, Masters BSS, Pritchard KA, Kalyanaraman B. Endothelial nitric oxide synthase-dependent superoxide generation from adriamycin. *Biochemistry*. 1997;36(38):11293-11297.

195.   Rajagopalan S, Politi PM, Sinha BK, Myers CE. Adriamycin-induced free radical formation in the perfused rat heart: implications for cardiotoxicity. *Cancer Research*. 1988;48(17):4766-4769.

196.   Keizer H, Pinedo HM, Schuurhuis GJ, Joenje H. Doxorubicin (adriamycin): a critical review of free radical-dependent mechanisms of cytotoxicity. *Pharmacology & Therapeutics*. 1990;47(2):219-231.

197.   Zhou S, Starkov A, Froberg MK, Leino RL, Wallace KB. Cumulative and irreversible cardiac mitochondrial dysfunction induced by doxorubicin. *Cancer Research*. 2001;61(2):771-777.

198.   Halestrap A. Calcium, mitochondria and reperfusion injury: a pore way to die. *Biochemical Society Transactions*. 2006;34(2):232-237.

199. Kashfi K, Israel M, Sweatman TW, Seshadri R, Cook GA. Inhibition of mitochondrial carnitine palmitoyltransferases by adriamycin and adriamycin analogues. *Biochemical Pharmacology*. 1990;40(7):1441-1448.

200. Immordino ML, Dosio F, Cattel L. Stealth liposomes: review of the basic science, rationale, and clinical applications, existing and potential. *International Journal of Nanomedicine*. 2006;1(3):297-315.

201. Park JW. Liposome-based drug delivery in breast cancer treatment. *Breast Cancer Research*. 2002;4(3):95-99.

202. Hoarau D, Delmas P, Roux E, Leroux J-C. Novel long-circulating lipid nanocapsules. *Pharmaceutical Research*. 2004;21(10):1783-1789.

203. Hong R-L. Liposomal Anti-Cancer Drug Researches-The Myth of Long Circulation. *Chinese Journal of Clinical Oncology*. 2004;20(2):10-21.

204. Gardikis K, Tsimplouli C, Dimas K, Micha-Screttas M, Demetzos C. New chimeric advanced Drug Delivery nano Systems (chi-aDDnSs) as doxorubicin carriers. *International Journal of Pharmaceutics*. 2010;402(1):231-237.

205. Yarmolenko PS, Zhao Y, Landon C, Spasojevic I, Yuan F, Needham D, et al. Comparative effects of thermosensitive doxorubicin-containing liposomes and hyperthermia in human and murine tumours. *International Journal of Hyperthermia*. 2010;26(5):485-498.

206. Dromi S, Frenkel V, Luk A, Traughber B, Angstadt M, Bur M, et al. Pulsed-high intensity focused ultrasound and low temperature–sensitive liposomes for enhanced targeted drug delivery and antitumor effect. *Clinical Cancer Research*. 2007;13(9):2722-2727.

207. Barenholz YC. Doxil®—the first FDA-approved nano-drug: lessons learned. *Journal of Controlled Release*. 2012;160(2):117-134.

208. Gabizon A, Catane R, Uziely B, Kaufman B, Safra T, Cohen R, et al. Prolonged circulation time and enhanced accumulation in malignant exudates of doxorubicin encapsulated in polyethylene-glycol coated liposomes. *Cancer Research*. 1994;54(4):987-992.

209. Symon Z, Peyser A, Tzemach D, Lyass O, Sucher E, Shezen E, et al. Selective delivery of doxorubicin to patients with breast carcinoma metastases by stealth liposomes. *Cancer*. 1999;86(1):72-78.

210. Janes KA, Fresneau MP, Marazuela A, Fabra A, Alonso MaJ. Chitosan nanoparticles as delivery systems for doxorubicin. *Journal of Controlled Release*. 2001;73(2-3):255-267.

211. Ta HT, Dass CR, Larson I, Choong PF, Dunstan DE. A chitosan–dipotassium orthophosphate hydrogel for the delivery of Doxorubicin in the treatment of osteosarcoma. *Biomaterials*. 2009;30(21):3605-3613.

212. Mitra S, Gaur U, Ghosh P, Maitra A. Tumour targeted delivery of encapsulated dextran–doxorubicin conjugate using chitosan nanoparticles as carrier. *Journal of Controlled Release*. 2001;74(1-3):317-323.

213. Unsoy G, Khodadust R, Yalcin S, Mutlu P, Gunduz U. Synthesis of Doxorubicin loaded magnetic chitosan nanoparticles for pH responsive targeted drug delivery. *European Journal of Pharmaceutical Sciences*. 2014;62:243-250.

214. Zhang J, Tao W, Chen Y, Chang D, Wang T, Zhang X, et al. Doxorubicin-loaded star-shaped copolymer PLGA-vitamin E TPGS nanoparticles for lung cancer therapy. *Journal of Materials Science: Materials in Medicine*. 2015;26(4):165-177.

215. Kanwal U, Irfan Bukhari N, Ovais M, Abass N, Hussain K, Raza A. Advances in Nano-delivery Systems for Doxorubicin: An updated insight. *Journal of Drug Targeting*. 2017:1-15.

216. Summerton JE. Morpholino, siRNA, and S-DNA compared: impact of structure and mechanism of action on off-target effects and sequence specificity. *Current Topics in Medicinal Chemistry*. 2007;7(7):651-660.

217. Miller PS, Yano J, Yano E, Carroll C, Jayaraman K, Ts'o PO. Nonionic nucleic acid analogs. Synthesis and characterization of dideoxyribonucleoside methylphosphonates. *Biochemistry*. 1979;18(23):5134-5143.

218. Zamecnik PC, Stephenson ML. Inhibition of Rous sarcoma virus replication and cell transformation by a specific oligodeoxynucleotide. *Proceedings of The National Academy of Sciences*. 1978;75(1):280-284.

219. Summerton J, Bartlett PA. Sequence-specific crosslinking agents for nucleic acids: Use of 6-bromo-5, 5-dimethoxyhexanohydrazide for crosslinking cytidine to guanosine and crosslinking RNA to complementary sequences of DNA. *Journal of Molecular Biology*. 1978;122(2):145-162.

220. Summerton J. Intracellular inactivation of specific nucleotide sequences: a general approach to the treatment of viral diseases and virally-mediated cancers. *Journal of Theoretical Biology*. 1979;78(1):77-99.

221. Campbell JM, Bacon TA, Wickstrom E. Oligodeoxynucleoside phosphorothioate stability in subcellular extracts, culture media, sera and cerebrospinal fluid. *Journal of Biochemical and Biophysical methods*. 1990;20(3):259-267.

222. Wickstrom E. Oligodeoxynucleotide stability in subcellular extracts and culture media. *Journal of Biochemical and Biophysical Methods*. 1986;13(2):97-102.

223. Hudziak RM, Barofsky E, Barofsky DF, Weller DL, Huang S-B, Weller DD. Resistance of morpholino phosphorodiamidate oligomers to enzymatic degradation. *Antisense and Nucleic Acid Drug Development*. 1996;6(4):267-272.

224. Summerton J, Weller D. Morpholino antisense oligomers: design, preparation, and properties. *Antisense and Nucleic Acid Drug Development*. 1997;7(3):187-195.

225. Summerton J. Morpholino antisense oligomers: the case for an RNase H-independent structural type. *Biochimica et Biophysica Acta (BBA)-Gene Structure and Expression*. 1999;1489(1):141-158.

226. Summerton JE. Endo-Porter: A Novel Reagent for Safe, Effective Delivery of Substances into Cells. *Annals of The New York Academy of Sciences*. 2005;1058(1):62-75.

227. Summerton JE. *Peptide Nucleic Acids, Morpholinos and Related Antisense Biomolecules*. New York: Springer; 2006.

228. Moulton JD, Yan YL. Using Morpholinos to control gene expression. *Current Protocols in Molecular Biology*. 2008;26(8):1-9.

229. Deluca M, McElroy W. [1] Purification and properties of firefly luciferase. *Methods in Enzymology*. 1978;57(1):3-15.

230. De Wet JR, Wood KV, Helinski DR, DeLuca M. Cloning of firefly luciferase cDNA and the expression of active luciferase in Escherichia coli. *Proceedings of The National Academy of Sciences*. 1985;82(23):7870-7873.

231. Seliger H, McElroy W. The colors of firefly bioluminescence: enzyme configuration and species specificity. *Proceedings of The National Academy of Sciences*. 1964;52(1):75-81.

232. Seliger HH, McElroy WD. Spectral emission and quantum yield of firefly bioluminescence. *Archives of Biochemistry and Biophysics*. 1960;88(1):136-141.

233. Sando S, Matsui K, Niinomi Y, Sato N, Aoyama Y. Facile preparation of DNA-tagged carbohydrates. *Bioorganic & Medicinal Chemistry Letters*. 2003;13(16):2633-2636.

234.   Bradford MM. A rapid and sensitive method for the quantitation of microgram quantities of protein utilizing the principle of protein-dye binding. *Analytical Biochemistry*. 1976;72(1-2):248-254.

235.   Han D, Pal S, Nangreave J, Deng Z, Liu Y, Yan H. DNA origami with complex curvatures in three-dimensional space. *Science*. 2011;332(6027):342-346.

236.   He Y, Ye T, Su M, Zhang C, Ribbe AE, Jiang W, et al. Hierarchical self-assembly of DNA into symmetric supramolecular polyhedra. *Nature*. 2008;452(7184):198-201.

237.   Ke Y, Ong LL, Shih WM, Yin P. Three-dimensional structures self-assembled from DNA bricks. *Science*. 2012;338(6111):1177-1183.

238.   Nickels PC, Høiberg HC, Simmel SS, Holzmeister P, Tinnefeld P, Liedl T. DNA origami seesaws as comparative binding assay. *ChemBioChem*. 2016;17(12):1093-6.

239.   Mathur D, Henderson ER. Programmable DNA Nanosystem for Molecular Interrogation. *Scientific reports*. 2016;6:27413:1-9.

240.   Kuzuya A, Sakai Y, Yamazaki T, Xu Y, Komiyama M. Nanomechanical DNA origami'single-molecule beacons' directly imaged by atomic force microscopy. *Nature Communications*. 2011;2:449:1-8.

241.   Burns JR, Göpfrich K, Wood JW, Thacker VV, Stulz E, Keyser UF, et al. Lipid-bilayer-spanning DNA nanopores with a bifunctional porphyrin anchor. *Angewandte Chemie International Edition*. 2013;52(46):12069-12072.

242.   Castro CE, Kilchherr F, Kim D-N, Shiao EL, Wauer T, Wortmann P, et al. A primer to scaffolded DNA origami. *Nature Methods*. 2011;8(3):221-229.

243.   Dunn KE, Dannenberg F, Ouldridge TE, Kwiatkowska M, Turberfield AJ, Bath J. Guiding the folding pathway of DNA origami. *Nature*. 2015;525(7567):82-86.

244.   Mathur D, Medintz IL. Analyzing DNA nanotechnology: a call to arms for the analytical chemistry community. *Anal. Chem*. 2017;89 (5):2646-2663.

245.   Sobczak J-PJ, Martin TG, Gerling T, Dietz H. Rapid folding of DNA into nanoscale shapes at constant temperature. *Science*. 2012;338(6113):1458-1461.

246.   Goodman RP, Heilemann M, Doose S, Erben CM, Kapanidis AN, Turberfield AJ. Reconfigurable, braced, three-dimensional DNA nanostructures. *Nature Nanotechnology*. 2008;3(2):93-96.

247.   Saccà B, Meyer R, Feldkamp U, Schroeder H, Niemeyer CM. High-Throughput, Real-Time Monitoring of the Self-Assembly of DNA Nanostructures by FRET Spectroscopy. *Angewandte Chemie International Edition*. 2008;47(11):2135-2137.

248.   Bai X-c, Martin TG, Scheres SH, Dietz H. Cryo-EM structure of a 3D DNA-origami object. *Proceedings of The National Academy of Sciences*. 2012;109(49):20012-20017.

249.   Zhao Z, Yan H, Liu Y. A route to scale up DNA origami using DNA tiles as folding staples. *Angewandte Chemie International Edition*. 2010;49(8):1414-1417.

250.   Stein IH, Schüller V, Böhm P, Tinnefeld P, Liedl T. Single-Molecule FRET Ruler Based on Rigid DNA Origami Blocks. *ChemPhysChem*. 2011;12(3):689-695.

251.   Eyler E. Nuclease protection assays. *Methods in Enzymology*. 2013;530:89-97.

252.   Frisken BJ. Revisiting the method of cumulants for the analysis of dynamic light-scattering data. *Applied Optics*. 2001;40(24):4087-4091.

253.   Shaw J-P, Kent K, Bird J, Fishback J, Froehler B. Modified deoxyoligonucleotides stable to exonuclease degradation in serum. *Nucleic Acids Research*. 1991;19(4):747-750.

254. Czauderna F, Fechtner M, Dames S, AyguÈn H, Klippel A, Pronk GJ, et al. Structural variations and stabilising modifications of synthetic siRNAs in mammalian cells. *Nucleic Acids Research*. 2003;31(11):2705-2716.

255. Crooke ST, Lebleu B. *Antisense research and applications*. Florida: Taylor & Francis-CRC Press; 1993.

256. Haginoya N, Ono A, Nomura Y, Ueno Y, Matsuda A. Synthesis of oligodeoxyribonucleotides containing 5-(N-aminoalkyl) carbamoyl-2′-deoxyuridines by a new postsynthetic modification method and theri thermal stability and nuclease-resistance properties. *Bioconjug Chem*. 1997;8:271-280.

257. Inoue H, Hayase Y, Imura A, Iwai S, Miura K, Ohtsuka E. Synthesis and hybridization studies on two complementary nona (2'-O-methyl) ribonucleotides. *Nucleic Acids Research*. 1987;15(15):6131-6148.

258. Ito T, Ueno Y, Komatsu Y, Matsuda A. Synthesis, thermal stability and resistance to enzymatic hydrolysis of the oligonucleotides containing 5-(N-aminohexyl) carbamoyl-2′-O-methyluridines. *Nucleic Acids Research*. 2003;31(10):2514-2523.

259. Conway JW, McLaughlin CK, Castor KJ, Sleiman H. DNA nanostructure serum stability: greater than the sum of its parts. *Chemical Communications*. 2013;49(12):1172-1174.

260. Wei B, Dai M, Yin P. Complex shapes self-assembled from single-stranded DNA tiles. *Nature*. 2012;485(7400):623-626.

261. Walsh AS, Yin H, Erben CM, Wood MJ, Turberfield AJ. DNA cage delivery to mammalian cells. *ACS Nano*. 2011;5(7):5427-5432.

262. Mei Q, Wei X, Su F, Liu Y, Youngbull C, Johnson R, et al. Stability of DNA origami nanoarrays in cell lysate. *Nano Letters*. 2011;11(4):1477-1482.

263. Wang D, Da Z, Zhang B, Isbell MA, Dong Y, Zhou X, et al. Stability study of tubular DNA origami in the presence of protein crystallisation buffer. *RSC Advances*. 2015;5(72):58734-58737.

264. Ortigao JR, Rösch H, Montenarh M, Fröhlich A, Seliger H. Oligonucleotide analogs with terminal 3′, 3′-and 5′, 5′-internucleotidic linkages as antisense inhibitors of viral replication. *Antisense Research and Development*. 1991;1(4):380.

265. Shum KT, Tanner JA. Differential inhibitory activities and stabilisation of DNA aptamers against the SARS coronavirus helicase. *Chembiochem*. 2008;9(18):3037-3045.

266. Zaitseva M, Kaluzhny D, Shchyolkina A, Borisova O, Smirnov I, Pozmogova G. Conformation and thermostability of oligonucleotide d (GGTTGGTGTGGTTGG) containing thiophosphoryl internucleotide bonds at different positions. *Biophysical Chemistry*. 2010;146(1):1-6.

267. Pozmogova G, Zaitseva M, Smirnov I, Shvachko A, Murina M, Sergeenko V. Anticoagulant effects of thioanalogs of thrombin-binding DNA-aptamer and their stability in the plasma. *Bulletin of Experimental Biology and Medicine*. 2010;150(2):180-184.

268. Dougan H, Lyster DM, Vo CV, Stafford A, Weitz JI, Hobbs JB. Extending the lifetime of anticoagulant oligodeoxynucleotide aptamers in blood. *Nuclear Medicine and Biology*. 2000;27(3):289-297.

269. Gupta S, Hirota M, Waugh SM, Murakami I, Suzuki T, Muraguchi M, et al. Chemically modified DNA aptamers bind interleukin-6 with high affinity and inhibit signaling by blocking its interaction with interleukin-6 receptor. *Journal of Biological Chemistry*. 2014;289(12):8706-8719.

270. Maier KE, Levy M. From selection hits to clinical leads: Progress in aptamer discovery. *Molecular Therapy-Methods & Clinical Development*. 2016;3:1-10.

271.   Peng CG, Damha MJ. G-quadruplex induced stabilization by 2′-deoxy-2′-fluoro-D-arabinonucleic acids (2′ F-ANA). *Nucleic Acids Research*. 2007;35(15):4977-4988.

272.   Zhao Y-X, Shaw A, Zeng X, Benson E, Nyström AM, Högberg Br. DNA origami delivery system for cancer therapy with tunable release properties. *ACS Nano*. 2012;6(10):8684-8691.

273.   Chang M, Yang C-S, Huang D-M. Aptamer-conjugated DNA icosahedral nanoparticles as a carrier of doxorubicin for cancer therapy. *ACS Nano*. 2011;5(8):6156-6163.

274.   Sirajuddin M, Ali S, Badshah A. Drug–DNA interactions and their study by UV–Visible, fluorescence spectroscopies and cyclic voltametry. *Journal of Photochemistry and Photobiology B: Biology*. 2013;124:1-19.

275.   Hajian R, Guan Huat T. Spectrophotometric studies on the thermodynamics of the ds-DNA interaction with irinotecan for a better understanding of anticancer drug-DNA interactions. *Journal of Spectroscopy*. 2012;2013:1-9.

276.   Yang P, Zhou C. Study on the interaction between calcein and herring sperm DNA by spectrometry. *Acta Chimica Sinica*. 2003;61(1):1455-1460.

277.   Long EC, Barton JK. On demonstrating DNA intercalation. *Accounts of Chemical Research*. 1990;23(9):271-273.

278.   Hajian R, Shams N, Parvin A. DNA-binding Studies of Daunorubicin in the Presence of Methylene Blue by Spectroscopy and Voltammetry Techniques. *Chinese Journal of Chemistry*. 2009;27(6):1055-1060.

279.   Chaires JB, Dattagupta N, Crothers DM. Studies on interaction of anthracycline antibiotics and deoxyribonucleic acid: equilibrium binding studies on the interaction of daunomycin with deoxyribonucleic acid. *Biochemistry*. 1982;21(17):3933-3940.

280. Akkus Sut P, Tunc CU, Culha M. Lactose-modified DNA tile nanostructures as drug carriers. *Journal of Drug Targeting*. 2016;24(8):709-719.

281. Maruyama A, Watanabe H, Ferdous A, Katoh M, Ishihara T, Akaike T. Characterization of interpolyelectrolyte complexes between double-stranded DNA and polylysine comb-type copolymers having hydrophilic side chains. *Bioconjugate Chemistry*. 1998;9(2):292-299.

282. Roy R, Katzenellenbogen E, Jennings HJ. Improved procedures for the conjugation of oligosaccharides to protein by reductive amination. *Canadian Journal of Biochemistry and Cell Biology*. 1984;62(5):270-275.

283. Lane C. Sodium cyanoborohydride-a highly effective reducing agent for organic functional compounds. *Synthesis*. 1975;135:1-12.

284. Borch RF, Bernstein MD, Durst HD. Cyanohydridoborate anion as a selective reducing agent. *Journal of The American Chemical Society*. 1971;93(12):2897-2904.

285. Cosenza VA, Navarro DA, Stortz CA. Usage of α-picoline borane for the reductive amination of carbohydrates. *ARKIVOC: Online Journal of Organic Chemistry*. 2011:182-194.

286. Sheehan JC, Hess GP. A new method of forming peptide bonds. *Journal of The American Chemical Society*. 1955;77(4):1067-1068.

287. Weetall HH. Covalent coupling methods for inorganic support materials. *Methods in Enzymology*. 1976;44:134-148.

288. DeTar DF, Silverstein R. Reactions of carbodiimides. *Journal of The American Chemical Society*. 1966;88(5):1013-1019.

289. Khorana H. The Chemistry of Carbodiimides. *Chemical Reviews*. 1953;53(2):145-166.

290.   DeTar DF, Silverstein R. Reactions of Carbodiimides. *Journal of The American Chemical Society*. 1966;88(5):1020-1023.

291.   Ferdani R, Li R, Pajewski R, Pajewska J, Winter RK, Gokel GW. Transport of chloride and carboxyfluorescein through phospholipid vesicle membranes by heptapeptide amphiphiles. *Organic & Biomolecular Chemistry*. 2007;5(15):2423-2432.

292.   Fischer R, Mader O, Jung G, Brock R. Extending the applicability of carboxyfluorescein in solid-phase synthesis. *Bioconjugate Chemistry*. 2003;14(3):653-660.

293.   Garcia BA, Heaney PJ, Tang K. Improvement of the MALDI-TOF analysis of DNA with thin-layer matrix preparation. *Analytical Chemistry*. 2002;74(9):2083-2091.

294.   Spengler B, Pan Y, Cotter RJ, Kan LS. Molecular weight determination of underivatized oligodeoxyribonucleotides by positive-ion matrix-assisted ultraviolet laser-desorption mass spectrometry. *Rapid Communications in Mass Spectrometry*. 1990;4(4):99-102.

295.   Tang K, Taranenko N, Allman S, Chen C, Chág L, Jacobson K. Picolinic acid as a matrix for laser mass spectrometry of nucleic acids and proteins. *Rapid Communications in Mass Spectrometry*. 1994;8(9):673-677.

296.   Nordhoff E, Kirpekar F, Karas M, Cramer R, Hahner S, Hillenkamp F, et al. Comparison of IR-and UV-matrix-assisted laser desorption/ionization mass spectrometry of oligodeoxynucleotides. *Nucleic Acids Research*. 1994;22(13):2460-2465.

297.   Taranenko N, Tang K, Allman S, Ch'ang L, Chen C. 3-aminopicolinic aid as a matrix for laser desorption mass spectrometry of biopolymers. *Rapid Communications in Mass Spectrometry*. 1994;8(12):1001-1006.

298.   Juhasz P, Roskey MT, Smirnov IP, Haff LA, Vestal ML, Martin SA. Applications of delayed extraction matrix-assisted laser desorption ionization time-of-flight mass spectrometry to oligonucleotide analysis. *Analytical Chemistry*. 1996;68(6):941-946.

299.	Roskey MT, Juhasz P, Smirnov IP, Takach EJ, Martin SA, Haff LA. DNA sequencing by delayed extraction-matrix-assisted laser desorption/ionization time of flight mass spectrometry. *Proceedings of The National Academy of Sciences*. 1996;93(10):4724-4729.

300.	Köster H, Tang K, Fu D-J, Braun A, Van Den Boom D, Smith CL, et al. A strategy for rapid and efficient DNA sequencing by mass spectrometry. *Nature Biotechnology*. 1996;14(9):1123-1128.

301.	Zhu Y, Taranenko N, Allman S, Taranenko N, Martin S, Haff L, et al. Oligonucleotide Sequencing by Fragmentation in Matrix-assisted Laser Desorption/Ionization Time-of-flight Mass Spectrometry. *Rapid Communications in Mass Spectrometry*. 1997;11(8):897-903.

302.	Polo LM, McCarley TD, Limbach PA. Chemical sequencing of phosphorothioate oligonucleotides using matrix-assisted laser desorption/ionization time-of-flight mass spectrometry. *Analytical Chemistry*. 1997;69(6):1107-1112.

303.	Faulstich K, Wörner K, Brill H, Engels JW. A sequencing method for RNA oligonucleotides based on mass spectrometry. *Analytical Chemistry*. 1997;69(21):4349-4353.

304.	Kirpekar F, Nordhoff E, Larsen LK, Kristiansen K, Roepstorff P, Hillenkamp F. DNA sequence analysis by MALDI mass spectrometry. *Nucleic Acids Research*. 1998;26(11):2554-2559.

305.	Fu D-J, Tang K, Braun A, Reuter D, Iverson BL, Darnhofer-Demar B, et al. Sequencing exons 5 to 8 of the p53 gene by MALDI-TOF mass spectrometry. *Nature Biotechnology*. 1998;16(4):381-384.

306.	Tolson D, Nicholson N. Sequencing RNA by a combination of exonuclease digestion and uridine specific chemical cleavage using MALDI-TOF. *Nucleic Acids Research*. 1998;26(2):446-451.

307.   Taranenko N, Allman S, Golovlev V, Taranenko N, Isola N, Chen C. Sequencing DNA using mass spectrometry for ladder detection. *Nucleic Acids Research*. 1998;26(10):2488-2490.

308.   Nordhoff E, Luebbert C, Thiele G, Heiser V, Lehrach H. Rapid determination of short DNA sequences by the use of MALDI-MS. *Nucleic Acids Research*. 2000;28(20):e86-e.

309.   Braun A, Little DP, Köster H. Detecting CFTR gene mutations by using primer oligo base extension and mass spectrometry. *Clinical Chemistry*. 1997;43(7):1151-1158.

310.   Haff LA, Smirnov IP. Single-nucleotide polymorphism identification assays using a thermostable DNA polymerase and delayed extraction MALDI-TOF mass spectrometry. *Genome Research*. 1997;7(4):378-388.

311.   Ross P, Hall L, Smirnov I, Haff L. High level multiplex genotyping by MALDI-TOF mass spectrometry. *Nature Biotechnology*. 1998;16(13):1347-1351.

312.   Fei Z, Ono T, Smith LM. MALDI-TOF mass spectrometric typing of single nucleotide polymorphisms with mass-tagged ddNTPs. *Nucleic Acids Research*. 1998;26(11):2827-2828.

313.   Tang K, Fu D-J, Julien D, Braun A, Cantor CR, Köster H. Chip-based genotyping by mass spectrometry. *Proceedings of The National Academy of Sciences*. 1999;96(18):10016-10020.

314.   Sun X, Ding H, Hung K, Guo B. A new MALDI-TOF based mini-sequencing assay for genotyping of SNPS. *Nucleic Acids Research*. 2000;28(12):e68-e.

315.   Wu KJ, Shaler TA, Becker CH. Time-of-flight mass spectrometry of underivatized single-stranded DNA oligomers by matrix-assisted laser desorption. *Analytical Chemistry*. 1994;66(10):1637-1645.

316.   Haff L, Juhasz P, Martin S, Roskey M, Smirnov I, Stanick W, et al. Oligonucleotide analysis by MALDI-MS. *Analysis*. 1998;26(10):26-30.

317.   Zhu Y, Chung C, Taranenko N, Allman S, Martin S, Haff L, et al. The Study of 2, 3, 4-Trihydroxyacetophenone and 2, 4, 6-Trihydroxyacetophenone as Matrices for. *Rapid Communications in Mass Spectrometry*. 1996;10(3):383-388.

318.   Lecchi P, Le H, Pannell LK. 6-Aza-2-thiothymine: a matrix for MALDI spectra of oligonucleotides. *Nucleic Acids Research*. 1995;23(7):1276-1277.

319.   Tang K, Taranenko N, Allman S, Chang L, Chen C, Lubman D. Detection of 500-nucleotide DNA by laser desorption mass spectrometry. *Rapid Communications in Mass Spectrometry*. 1994;8(9):727-730.

320.   Stemmler E, Buchanan M, Hurst G, Hettich R. Analysis of modified oligonucleotides by matrix-assisted laser desorption/ionization Fourier transform mass spectrometry. *Analytical Chemistry*. 1995;67(17):2924-2930.

321.   Zhang L-K, Gross ML. Matrix-assisted laser desorption/ionization mass spectrometry methods for oligodeoxynucleotides: improvements in matrix, detection limits, quantification, and sequencing. *Journal of The American Society for Mass Spectrometry*. 2000;11(10):854-865.

322.   Distler AM, Allison J. 5-Methoxysalicylic acid and spermine: A new matrix for the matrix-assisted laser desorption/ionization mass spectrometry analysis of oligonucleotides. *Journal of The American Society for Mass Spectrometry*. 2001;12(4):456-462.

323.   Tang K, Allman S, Chen C. Matrix-assisted laser desorption ionization of oligonucleotides with various matrices. *Rapid Communications in Mass Spectrometry*. 1993;7(10):943-948.

324. Song F. Quinaldic acid as a new matrix for matrix-assisted laser desorption/ionization of nucleic acids. *Rapid Communications in Mass Spectrometry*. 2003;17(15):1802-1807.

325. Fu Y, Xu S, Pan C, Ye M, Zou H, Guo B. A matrix of 3, 4-diaminobenzophenone for the analysis of oligonucleotides by matrix-assisted laser desorption/ionization time-of-flight mass spectrometry. *NucleicAcids Research*. 2006;34(13):e94-e.

326. Lecchi P, Pannell LK. The detection of intact double-stranded DNA by MALDI. *Journal of The American Society for Mass Spectrometry*. 1995;6(10):972-975.

327. Shahgholi M, Garcia BA, Chiu NH, Heaney PJ, Tang K. Sugar additives for MALDI matrices improve signal allowing the smallest nucleotide change (A: T) in a DNA sequence to be resolved. *Nucleic Acids Research*. 2001;29(19):e91-e.

328. Zhang Z, Zhou L, Zhao S, Deng H, Deng Q. 3-Hydroxycoumarin as a new matrix for matrix-assisted laser desorption/ionization time-of-flight mass spectrometry of DNA. *Journal of The American Society for Mass Spectrometry*. 2006;17(12):1665-1668.

329. Rani K, Paliwal S. A review on targeted drug delivery: Its entire focus on advanced therapeutics and diagnostics. *Sch J App Med Sci*. 2014;2(1C):328-331.

330. Juliano RL, Astriab-Fisher A, Falke D. Macromolecular therapeutics. *Molecular Interventions*. 2001;1(1):40-53.

331. Danhier F, Feron O, Préat V. To exploit the tumor microenvironment: passive and active tumor targeting of nanocarriers for anti-cancer drug delivery. *Journal of Controlled Release*. 2010;148(2):135-146.

332. Sur I, Cam D, Kahraman M, Baysal A, Culha M. Interaction of multi-functional silver nanoparticles with living cells. *Nanotechnology*. 2010;21(17):175104-175115.

333. Moros M, Hernáez B, Garet E, Dias JT, Sáez B, Grazú V, et al. Monosaccharides versus PEG-functionalized NPs: influence in the cellular uptake. *ACS Nano*. 2012;6(2):1565-1577.

334. Marradi M, Martín-Lomas M, PenadÉs S. Glyconanoparticles: polyvalent tools to study carbohydrate-based interactions. *Advances in Carbohydrate Chemistry and Biochemistry*. 2010;64:211-290.

335. Kikkeri R, Lepenies B, Adibekian A, Laurino P, Seeberger PH. In vitro imaging and in vivo liver targeting with carbohydrate capped quantum dots. *Journal of The American Chemical Society*. 2009;131(6):2110-2112.

336. Kennedy DC, Grünstein D, Lai CH, Seeberger PH. Glycosylated Nanoscale Surfaces: Preparation and Applications in Medicine and Molecular Biology. *Chemistry-A European Journal*. 2013;19(12):3794-3800.

337. David A. Carbohydrate-based Biomedical Copolymers for Targeted Delivery of Anticancer Drugs. *Israel Journal of Chemistry*. 2010;50(2):204-219.

338. Benito-Alifonso D, Tremel S, Hou B, Lockyear H, Mantell J, Fermin DJ, et al. Lactose as a "trojan horse" for quantum dot cell transport. *Angewandte Chemie*. 2014;126(3):829-833.

339. Lee H, Lytton-Jean AK, Chen Y, Love KT, Park AI, Karagiannis ED, et al. Molecularly self-assembled nucleic acid nanoparticles for targeted in vivo siRNA delivery. *Nature Nanotechnology*. 2012;7(6):389.

340. Sun P, Zhang N, Tang Y, Yang Y, Chu X, Zhao Y. Sl2b aptamer and folic acid dual-targeting DNA nanostructures for synergic biological effect with chemotherapy to combat colorectal cancer. *International Journal of Nanomedicine*. 2017;12:2657-2672.

341. Sun W, Jiang T, Lu Y, Reiff M, Mo R, Gu Z. Cocoon-like self-degradable DNA nanoclew for anticancer drug delivery. *Journal of The American Chemical Society*. 2014;136(42):14722-14725.

342. Raniolo S, Vindigni G, Ottaviani A, Unida V, Iacovelli F, Manetto A, et al. Selective targeting and degradation of doxorubicin-loaded folate-functionalized DNA nanocages. *Nanomedicine: Nanotechnology, Biology and Medicine*. 2018:1181-1190.

343. Shapiro HM. *Practical flow cytometry*. New Jersey: John Wiley & Sons; 2005.

344. Ibrahim SF, van den Engh G. High-speed cell sorting: fundamentals and recent advances. *Current Opinion in Biotechnology*. 2003;14(1):5-12.

345. Orfao A, Ruiz-Arguelles A, Lacombe F, Ault K, Basso G, Danova M. Flow cytometry: its applications in hematology. *Haematologica*. 1995;80(1):69-81.

346. Recktenwald DJ. Introduction to flow cytometry: principles, fluorochromes, instrument set-up, calibration. *Journal of Hematotherapy*. 1993;2(3):387-394.

347. Gival AL. *Flow cytometry: First principles*. New York: Wiley-Liss; 2001.

348. Ibuki Y, Toyooka T. Nanoparticle uptake measured by flow cytometry. *Methods in Molecular Biology*. 2012;926:157-166

349. Dos Santos T, Varela J, Lynch I, Salvati A, Dawson KA. Quantitative assessment of the comparative nanoparticle-uptake efficiency of a range of cell lines. *Small*. 2011;7(23):3341-3349.

350. Medina-Kauwe L, Xie J, Hamm-Alvarez S. Intracellular trafficking of nonviral vectors. *Gene Therapy*. 2005;12(24):1734-1751.

351.   Khalil IA, Kogure K, Akita H, Harashima H. Uptake pathways and subsequent intracellular trafficking in nonviral gene delivery. *Pharmacological Reviews*. 2006;58(1):32-45.

352.   Von Gersdorff K, Sanders NN, Vandenbroucke R, De Smedt SC, Wagner E, Ogris M. The internalization route resulting in successful gene expression depends on both cell line and polyethylenimine polyplex type. *Molecular Therapy*. 2006;14(5):745-753.

353.   Douglas KL, Piccirillo CA, Tabrizian M. Cell line-dependent internalization pathways and intracellular trafficking determine transfection efficiency of nanoparticle vectors. *European Journal of Pharmaceutics and Biopharmaceutics*. 2008;68(3):676-687.

354.   Wong AW, Scales SJ, Reilly DE. DNA internalized via caveolae requires microtubule-dependent, Rab7-independent transport to the late endocytic pathway for delivery to the nucleus. *Journal of Biological Chemistry*. 2007;282(31):22953-22963.

355.   Gabrielson NP, Pack DW. Efficient polyethylenimine-mediated gene delivery proceeds via a caveolar pathway in HeLa cells. *Journal of Controlled Release*. 2009;136(1):54-61.

356.   Rejman J, Oberle V, Zuhorn IS, Hoekstra D. Size-dependent internalization of particles via the pathways of clathrin-and caveolae-mediated endocytosis. *Biochemical Journal*. 2004;377(1):159-169.

357.   Conner SD, Schmid SL. Regulated portals of entry into the cell. *Nature*. 2003;422(6927):37-44.

358.   Marsh M, McMahon H. The structural era of endocytosis. *Science*. 1999;285(5425):215-220.

359.   Parton RG, Richards AA. Lipid rafts and caveolae as portals for endocytosis: new insights and common mechanisms. *Traffic*. 2003;4(11):724-738.

360.   Amyere M, Mettlen M, Van Der Smissen P, Platek A, Payrastre B, Veithen A, et al. Origin, originality, functions, subversions and molecular signalling of macropinocytosis. *International Journal of Medical Microbiology*. 2001;291(6-7):487-494.

361.   Niedergang F, Chavrier P. Signaling and membrane dynamics during phagocytosis: many roads lead to the phagos (R) ome. *Current Opinion in Cell Biology*. 2004;16(4):422-428.

362.   Puckett CA, Ernst RJ, Barton JK. Exploring the cellular accumulation of metal complexes. *Dalton Transactions*. 2010;39(5):1159-170.

363.   Larkin JM, Brown MS, Goldstein JL, Anderson RG. Depletion of intracellular potassium arrests coated pit formation and receptor-mediated endocytosis in fibroblasts. *Cell*. 1983;33(1):273-85.

364.   Daukas G, Zigmond SH. Inhibition of receptor-mediated but not fluid-phase endocytosis in polymorphonuclear leukocytes. *The Journal of Cell Biology*. 1985;101(5):1673-1679.

365.   Hansen SH, Sandvig K, Van Deurs B. Clathrin and HA2 adaptors: effects of potassium depletion, hypertonic medium, and cytosol acidification. *The Journal of Cell Biology*. 1993;121(1):61-72.

366.   Carpentier JL, Sawano F, Geiger D, Gorden P, Perrelet A, Orci L. Potassium depletion and hypertonic medium reduce "non-coated" and clathrin-coated pit formation, as well as endocytosis through these two gates. *Journal of Cellular Physiology*. 1989;138(3):519-526.

367.   Wang L-H, Rothberg KG, Anderson R. Mis-assembly of clathrin lattices on endosomes reveals a regulatory switch for coated pit formation. *The Journal of Cell Biology*. 1993;123(5):1107-1117.

368.   Daniel JA, Chau N, Abdel-Hamid MK, Hu L, von Kleist L, Whiting A, et al. Phenothiazine-Derived Antipsychotic Drugs Inhibit Dynamin and Clathrin-Mediated Endocytosis. *Traffic*. 2015;16(6):635-654.

369.   Yao D, Ehrlich M, Henis YI, Leof EB. Transforming growth factor-β receptors interact with AP2 by direct binding to β2 subunit. *Molecular Biology of The Cell*. 2002;13(11):4001-4012.

370.   Elferink J. Chlorpromazine inhibits phagocytosis and exocytosis in rabbit polymorphonuclear leukocytes. *Biochemical Pharmacology*. 1979;28(7):965-968.

371.   Watanabe S, Hirose M, Miyazaki A, Tomono M, Takeuchi M, Kitamura T, et al. Calmodulin antagonists inhibit the phagocytic activity of cultured Kupffer cells. *Laboratory Investigation; A Journal of Technical Methods and Pathology*. 1988;59(2):214-218.

372.   Saraste J, Palade GE, Farquhar MG. Temperature-sensitive steps in the transport of secretory proteins through the Golgi complex in exocrine pancreatic cells. *Proceedings of the National Academy of Sciences*. 1986;83(17):6425-6429.

373.   Yang H, Lou C, Xu M, Wu C, Miyoshi H, Liu Y. Investigation of folate-conjugated fluorescent silica nanoparticles for targeting delivery to folate receptor-positive tumors and their internalization mechanism. *International Journal of Nanomedicine*. 2011;6:2023-2032.

374.   Parton RG, Joggerst B, Simons K. Regulated internalization of caveolae. *The Journal of Cell Biology*. 1994;127(5):1199-1215.

375.   Jung C, Rampal A. Cytochalasin B binding sites and glucose transport carrier in human erythrocyte ghosts. *Journal of Biological Chemistry*. 1977;252(15):5456-5463.

376.   Peterson JR, Mitchison TJ. Small molecules, big impact: a history of chemical inhibitors and the cytoskeleton. *Chemistry & Biology*. 2002;9(12):1275-1285.

377.   Pozarowski P, Darzynkiewicz Z. Analysis of cell cycle by flow cytometry. Checkpoint Controls and Cancer. *Methods In Molecular Biology*. 2004;281:301-311

378.   Darzynkiewicz Z, Huang X, Zhao H. Analysis of cellular DNA content by flow cytometry. *Current Protocols in Immunology*. 2017;119(1):5.7. 1-5.7. 20.

379.   Yano S, Zhang Y, Miwa S, Tome Y, Hiroshima Y, Uehara F, et al. Spatial–temporal FUCCI imaging of each cell in a tumor demonstrates locational dependence of cell cycle dynamics and chemoresponsiveness. *Cell Cycle*. 2014;13(13):2110-2119.

380.   Swift LP, Rephaeli A, Nudelman A, Phillips DR, Cutts SM. Doxorubicin-DNA adducts induce a non-topoisomerase II–mediated form of cell death. *Cancer Research*. 2006;66(9):4863-4871.

381.   Hortobagyi G. Anthracyclines in the treatment of cancer. *Drugs*. 1997;54(4):1-7.

382.   Bar-On O, Shapira Ma, Hershko DD. Differential effects of doxorubicin treatment on cell cycle arrest and Skp2 expression in breast cancer cells. *Anti-cancer Drugs*. 2007;18(10):1113-1121.

383.   Young LS, Searle PF, Onion D, Mautner V. Viral gene therapy strategies: from basic science to clinical application. *The Journal of Pathology*. 2006;208(2):299-318.

384.   Dalby B, Cates S, Harris A, Ohki EC, Tilkins ML, Price PJ, et al. Advanced transfection with Lipofectamine 2000 reagent: primary neurons, siRNA, and high-throughput applications. *Methods*. 2004;33(2):95-103.

385.   Larocca C, Schlom J. Viral Vector–based Therapeutic Cancer Vaccines. *Cancer Journal*. 2011;17(5):359-371.

386.   Mintzer MA, Simanek EE. Nonviral vectors for gene delivery. *Chemical Reviews*. 2008;109(2):259-302.

387. Ten E, Ling C, Wang Y, Srivastava A, Dempere LA, Vermerris W. Lignin nanotubes as vehicles for gene delivery into human cells. *Biomacromolecules*. 2013;15(1):327-38.

388. Mizu M, Koumoto K, Anada T, Matsumoto T, Numata M, Shinkai S, et al. A polysaccharide carrier for immunostimulatory CpG DNAs to enhance cytokine secretion. *Journal of The American Chemical Society*. 2004;126(27):8372-8373.

389. Shimada N, Ishii KJ, Takeda Y, Coban C, Torii Y, Shinkai S, et al. Synthesis and in vitro characterization of antigen-conjugated polysaccharide as a CpG DNA carrier. *Bioconjugate Chemistry*. 2006;17(5):1136-1140.

390. Liu WG, Zhang X, Sun SJ, Sun GJ, Yao KD, Liang DC, et al. N-alkylated chitosan as a potential nonviral vector for gene transfection. *Bioconjugate Chemistry*. 2003;14(4):782-789.

391. Kim K-R, Kim D-R, Lee T, Yhee JY, Kim B-S, Kwon IC, et al. Drug delivery by a self-assembled DNA tetrahedron for overcoming drug resistance in breast cancer cells. *Chemical Communications*. 2013;49(20):2010-2012.

392. Keum JW, Ahn JH, Bermudez H. Design, assembly, and activity of antisense DNA nanostructures. *Small*. 2011;7(24):3529-3535.

393. Fakhoury JJ, McLaughlin CK, Edwardson TW, Conway JW, Sleiman HF. Development and characterization of gene silencing DNA cages. *Biomacromolecules*. 2013;15(1):276-282.

394. Chen G, Liu D, He C, Gannett TR, Lin W, Weizmann Y. Enzymatic synthesis of periodic DNA nanoribbons for intracellular pH sensing and gene silencing. *Journal of The American Chemical Society*. 2015;137(11):3844-3851.

395. Cann AJ. *RNA viruses. A practical approach*. Oxford: Oxford University Press; 2000.

396.   Kalpana GV. Retroviral vectors for liver-directed gene therapy. *Semin Liver Disease*. 1999;19(1):27-37.

397.   Federico M. *Lentivirus gene engineering protocols*. New York: Springer; 2003.

398.   Heiser WC. *Gene delivery to mammalian cells: Volume 2: Viral gene transfer techniques. Methods in Molecular Biology*. New York: Springer; 2004.

399.   Machida CA. Viral vectors for gene therapy: methods and protocols. New York: Springer-Science & Business Media; 2003.

400.   Moulton J. Guide for morpholino users: toward therapeutics. *Journal* of *Drug Discovery*, *Development* and *Delivery*. 2016;3(2):1023-1036.

401.   Wu B, Lu P, Benrashid E, Malik S, Ashar J, Doran T, et al. Dose-dependent restoration of dystrophin expression in cardiac muscle of dystrophic mice by systemically delivered morpholino. *Gene Therapy*. 2010;17(1):132-140.

402.   Cheng R, Ford B, O'Neal P, Mathews C, Bradford C, Thongtan T, et al. Zebrafish (Danio rerio) p53 tumor suppressor gene: cDNA sequence and expression during embryogenesis. *Molecular Marine Biology and Biotechnology*. 1997;6(2):88-97.

403.   Vogelstein B, Lane D, Levine AJ. Surfing the p53 network. *Nature*. 2000;408(6810):307-310.

404.   Vousden KH, Prives C. Blinded by the light: the growing complexity of p53. *Cell*. 2009;137(3):413-431.

405.   Zhao F, Zhao Y, Liu Y, Chang X, Chen C, Zhao Y. Cellular uptake, intracellular trafficking, and cytotoxicity of nanomaterials. *Small*. 2011;7(10):1322-1337.

406. Koppelhus U, Awasthi SK, Zachar V, Holst HU, Ebbesen P, Nielsen PE. Cell-dependent differential cellular uptake of PNA, peptides, and PNA-peptide conjugates. *Antisense and Nucleic Acid Drug Development*. 2002;12(2):51-63.

407. Hashida M, Nishikawa M, Yamashita F, Takakura Y. Cell-specific delivery of genes with glycosylated carriers. *Advanced Drug Delivery Reviews*. 2001;52(3):187-196.

408. Kircheis R, Kichler A, Wallner G, Kursa M, Ogris M, Felzmann T, et al. Coupling of cell-binding ligands to polyethylenimine for targeted gene delivery. *Gene Therapy*. 1997;4(5):409-418.

409. Ferkol T, Kaetzel CS, Davis PB. Gene transfer into respiratory epithelial cells by targeting the polymeric immunoglobulin receptor. *The Journal of Clinical Investigation*. 1993;92(5):2394-2400.

410. Chen J, Gamou S, Takayanagi A, Shimizu N. A novel gene delivery system using EGF receptor-mediated endocytosis. *FEBS Letters*. 1994;338(2):167-169.

411. Hara T, Aramaki Y, Takada S, Koike K, Tsuchiya S. Receptor-mediated transfer of pSV2CAT DNA to a human hepatoblastoma cell line HepG2 using asialofetuin-labeled cationic liposomes. *Gene*. 1995;159(2):167-174.

412. Wu GY, Wu CH. Receptor-mediated gene delivery and expression in vivo. *Journal of Biological Chemistry*. 1988;263(29):14621-14624.

413. Remy J-S, Kichler A, Mordvinov V, Schuber F, Behr J-P. Targeted gene transfer into hepatoma cells with lipopolyamine-condensed DNA particles presenting galactose ligands: a stage toward artificial viruses. *Proceedings of The National Academy of Sciences*. 1995;92(5):1744-1748.

414. Mahato RI, Takemura S, Akamatsu K, Nishikawa M, Takakura Y, Hashida M. Physicochemical and disposition characteristics of antisense oligonucleotides complexed with glycosylated poly (L-lysine). *Biochemical Pharmacology*. 1997;53(6):887-895.

415.   Erbacher P, Bousser M-T, Raimond J, Monsigny M, Midoux P, Roche AC. Gene transfer by DNA/glycosylated polylysine complexes into human blood monocyte-derived macrophages. *Human Gene Therapy*. 1996;7(6):721-729.

416.   Kawakami S, Sato A, Nishikawa M, Yamashita F, Hashida M. Mannose receptor-mediated gene transfer into macrophages using novel mannosylated cationic liposomes. *Gene Therapy*. 2000;7(4):292-299.

417.   Sato A, Kawakami S, Yamada M, Yamashita F, Hashida M. Enhanced gene transfection in macrophages using mannosylated cationic liposome-polyethylenimine-plasmid DNA complexes. *Journal of Drug Targeting*. 2001;9(3):201-207.

418.   Choi YH, Liu F, Park JS, Kim SW. Lactose-poly (ethylene glycol)-grafted poly-L-lysine as hepatoma cell-targeted gene carrier. *Bioconjugate Chemistry*. 1998;9(6):708-718.

419.   Biessen E, Vietsch H, Rump ET, Fluiter K, Kuiper J, Bijsterbosch MK, et al. Targeted delivery of oligodeoxynucleotides to parenchymal liver cells in vivo. *Biochemical Journal*. 1999;340(3):783-792.